Novel RNA-based adjuvants with strong immunostimulatory activities improve the efficacy of VLP-based cancer vaccines

Dissertation
zur Erlangung des Grades
“Doktor der Naturwissenschaften”

Am Fachbereich Biologie
Der Johannes Gutenberg-Universität
in Mainz

Mahjoub Bihi
Geb. am 07.11.1979 in Casablanca

Mainz, 2018

(Dissertation Universität Mainz)

Summary

Target specific induction of adaptive immune responses against tumor-associated antigens (TAAs) is an already established strategy to fight cancer diseases. Furthermore, chimeric TAA-presenting *virus-like particle* (VLP)-based vaccines have been shown to be an attractive modality for inducing target specific immune responses after active immunization. However, the therapeutically successful application of such type of vaccines often depends on co-administration of adjuvants, enhancing the vaccine induced adaptive immune responses.

Toll-like receptor (TLR) agonists have been shown to improve the quality and quantity of host adaptive immune responses when used in vaccine formulations against infectious diseases or cancer. Based on an iterative fragmentation strategy in combination with *in silico* predictions, we were able to identify novel, small immunostimulatory RNA sequences (isRNAs) derived from Influenza A virus nucleoprotein (NP) with high specificity for TLR7 and/or TLR8. The identified isRNAs could be *in vitro* transcribed and purified in large scale and were potent IFN type I, but only very weak TNF-α inducers. Liposomally formulated isRNAs in particular NP71-Seq45 co-administered with chimeric HBcAg-VLP based anti-cancer vaccines profoundly increased the immunogenicity of the VLP-based vaccine and elicited high-titer antibody responses against the target molecule, characterized by a balanced Th1/Th2 profile. Furthermore, the co-administration of formulated isRNAs with chimeric HBcAg-VLPs elicited antibodies recognizing the target molecule in its native conformation and exerting potent cytocidal effector functions like complement dependent cytotoxicity (CDC). A direct comparison of the identified isRNAs with CpG-ODN1826 and more than seven other classes of adjuvants (e.g. MPLA, poly(I:C), R848, CFA/IFA, Addavax, and aluminum hydroxide) revealed a superior efficacy of the novel isRNA-based adjuvants to enhance a strong target molecule specific B cell response. Moreover, only the immunization of liposomally formulated isRNAs in combination with HBcAg-CLDN6 VLPs was capable to elicit significant target-epitope specific CD4+ T cell responses as determined by *ex vivo* IFN-γ ELISpot.

Preclinical data shown for three different, syngeneic mouse tumor models demonstrated that the isRNA adjuvant can significantly increase the anti-tumoral potency of HBcAg-CLDN6 VLPs as a prophylactic and also therapeutic cancer vaccine. Complete immune protection against s.c. or i.v. challenge with syngeneic tumor cells could be achieved only by prophylactic vaccination with isRNA adjuvanted HBcAg-#A79 VLPs in Balb/c mice indicating the strong effects of the induced CLDN6-specific B responses. This work revealed for the first time that the combination of HBcAg-CLDN6 VLP vaccines with a liposomally formulated TLR7 agonist based on small isRNAs induced therapeutically active anti-tumoral immune responses and may result in the development of a novel vaccine format for active cancer immunotherapy.

Zusammenfassung

Die Induktion von zielgerichteten, adaptiven Immunantworten gegen tumorassoziierte Antigene (TAAs) ist eine bereits etablierte Strategie zur Bekämpfung von Krebserkrankungen. Darüber hinaus wurde gezeigt, dass Vakzine, basierend auf chimären, TAA-präsentierenden Virus-ähnlichen Partikeln (*virus-like particles*, VLP) eine attraktive Modalität zur Induktion zielspezifischer Immunantworten nach aktiver Immunisierung darstellen. Die erfolgreiche, therapeutisch wirksame Anwendung protein-basierter Vakzine hängt jedoch oftmals von co-applizierten Adjuvantien ab, die die Impfstoff-induzierten adaptiven Immunantworten verstärken. Für Adjuvantien aus der Klasse der *Toll-like* Rezeptor (TLR) Agonisten konnte gezeigt werden, dass sie die Qualität und Quantität der adaptiven Immunantworten signifikant verbessern, wenn sie mit Vakzinen gegen Infektionskrankheiten oder Krebs co-appliziert werden. Durch die Entwicklung und Anwendung einer iterativen Fragmentierungsstrategie in Kombination mit *in silico* Prädiktionen konnten wir neuartige, kleine immunostimulatorische RNA-Sequenzen (isRNAs) identifizieren, die aus dem Influenza A-Virus-Nukleoprotein (NP) abgeleitet wurden und spezifisch TLR7 und/oder TLR8 aktivieren. Die identifizierten isRNAs konnten *in vitro* transkribiert und in großem Maßstab gereinigt werden und fungierten als potente Interferon Typ-I, aber nur als sehr schwache TNF-α Induktoren. Liposomal formulierte isRNA-Adjuvantien, insbesondere isRNA NP71-Seq45, führten zu einer drastischen Verstärkung der Immunogenität der verwendeten, chimären HBcAg-CLDN6 VLP-Impfstoffe und induzierten eine CLDN6 Antigen-spezifische humorale Immunantwort, die durch ein balanciertes Th1/Th2 Profil gekennzeichnet war. Die induzierten Antikörper erkannten hochspezifisch CLDN6 in seiner nativen Konformation auf der Oberfläche lebender Zellen und vermittelten zytotoxische Effektorfunktionen, wie eine komplementabhängige Zytotoxizität (CDC). Ein direkter Vergleich der identifizierten isRNAs mit CpG-ODN1826 und mehr als sieben anderen Klassen von Adjuvantien zeigte eine überlegene Wirksamkeit der neuartigen isRNA-basierten Adjuvantien in Bezug auf die Induktion zielmolekülspezifischer B-Zell-Antwort. Darüber hinaus war nur die Immunisierung von liposomal formulierten isRNAs in Kombination HBcAg-CLDN6 VLPs in der Lage, signifikante CLDN6 Epitop-spezifische CD4+ T-Zellreaktionen hervorzurufen. Präklinische Daten für drei verschiedene, syngene Maus-Tumormodelle zeigten, dass das isRNA-Adjuvans die antitumorale Potenz von HBcAg-CLDN6 VLPs als prophylaktisches und auch therapeutisches Krebsvakzin signifikant erhöhen kann. Ein vollständiger Schutz gegen s.c. oder i.v. inokulierte, syngene Tumorzellen konnte jedoch nur durch prophylaktische Impfung mit isRNA-adjuvantierten HBcAg-#A79 VLPs von Balb/c Mäusen erreicht werden, was die starke Effekt von der induzierten CLDN6-spezifischen B Zellreaktionen vermuten lässt. Die vorliegende Arbeit zeigt erstmals, dass die Kombination von HBcAg-CLDN6 VLP-Vakzinen mit einem liposomalen formulierten TLR7-Agonisten auf der Basis von kleinen isRNAs therapeutisch aktive antitumorale Immunantworten induzieren kann und die nachfolgende Entwicklung eines neuartigen Impfstoffformats für die aktive Krebsimmuntherapie zur Folge haben könnte.

Liste of Abbreviations

%	Procent	**Inj.**	Injection
µ	Micro	**is**	Immunostimulatory
Δ	Trancuted varient	**Insol.**	Insoluble
aa	amino acid	**Ig**	Immunoglobulin
Ab	Antibody	**IRAK**	IL-1R-associated kinase
AF4	Asymmetrical flow field-flow fractionation	**kDa**	Kilodalton
AMS	Amonium sulfate	**L**	Liter
ADCC	Antibody-dependent cell-mediated cytotoxicity	**LB**	Luria-Bertani Medium
AG	Working group	**IKK complex**	inhibitor of nuclear factor-κB (IκB)-kinase complex
AIM	Auto-induction medium	**LRR**	Leucine rich repeats
ATP	Adenosine triphosphate	**LS**	light scattering
bp	Base pair	**LPX**	Lipoplexe
BSA	Bovine serum albumin	**LCMV**	Lymphocytic chroiomeningitis virus
BCIP	5-Bromo-4-chloro-3-indolyl phosphate	**m**	Meter
APCs	Antigen presenting cells	**M**	Molar
°C	Grad celsius	**MDA-5**	Melanoma differentiation-associated protein 5
C	Concentration	**MHC**	Major histocompatibility complex
CD	Cluster of Differentiation	**MACS**	Magnetic-activated cell sorting
CDC	Complement-dependent cytotoxicity	**MyD88**	Myeloid differentiation primary response protein 88
CTL	Cytotoxic T lymphocyte	**MAMPs**	Microorganism-associated molecular patterns
CLDN	Claudin	**NP**	Nucleoprotein
CHO	Chinese hamster ovary cells	**MFI**	Mean fluorescence intensity
CFA	Complete Freund`s Adjuvant	**MALS**	Multi-Angle Light Scattering
ConA	Concanavalin A	**MPLA**	Monophosphoryl Lipid A
cm	Centimeter	**mm**	Millimeter
cDC	conventional dendritic cells	***mm***	Mus musculus
CCR7	C-C chemokine receptor type 7	**mRNA**	Messenger RNA
DTR	diphtheria toxin receptor	**MIR**	Major immunodominante region
DCs	Dendritic cells	**Min**	Minute
dH2O	Distilled water	**mAbs**	Monoclpnal antibody
DMSO	Dimethyl sulfoxide	**MW**	Molecular wieght
DMEM	Dulbecco's Modified Eagle Medium	**Nr.**	Number
DNAs	Deoxyribonucleoic acid	**NCBI**	National Center for Biotechnology Information
ds	double strang	**nm**	Nanometer
DAMPs	Damage-associated molecular pattern	**ng**	nanogramm
EDTA	Ethylenediaminetetraacetic acid	**NK**	natural killer cells
ECD	Extracellular domain	**ns**	non significant
EE	Glutamic acid linker	**NEAA**	Non essential amino acids
ELISpot	Enzyme-linked immunospot	**NS**	Non structural protein
EMA	European medicines agency	**NBD**	nucleotid binding domain

ELISA	Enzyme linked immune sorbens assay	**OD**	optical density
E. coli	Escherichia coli	**ON**	Overnight
FACS	fluorescence-activated cell sorting	**ODN**	Unmethylated CpG oligodeoxynucleotides
FoxA2	Forkhead box A2	**PBS**	Phosphate saline buffer
FBS	Foetal bovine serum	**PAGE**	Polyacrylamid gel electrophoresis
FSC	Forward Scatter	**PBMC**	Peripheral Blood Mononuclear Cell
Fc	Fragment crystallizable region	**PKR**	Protein kinase RNA-activated also known as protein kinase R
G4SG4	Glycin (x 4)-Serin (x1)-Glycin (x 4) Linker	**PAMPs**	Pathogen-associated molecular pattern
Grp.	Group	**PRR**	Pattern recognition receptors
GMP	Good Manufacturing Practice	**Poly I:C**	Polyriboinosinic acid-polyribocytidylic acid
g-α-h	Goat anti human	**rpm**	revolutions per minute
g-α-m	Goat anti mouse	**pDCs**	Plasmacytoid dendritic cells
g	Gramm	**R848**	Resiquimod
HA	Hemagglutinin	**RPMI**	Roswell Park Memorial Institute
h	Hour	**RIG-I**	retinoic acid inducible gene I
HEPES	4-(2-hydroxyethyl)-1-piperazineethanesulfonic acid	**R.T.**	Room temperature
HPLC	High-performance liquid chromatography	**rDNA**	Ribosomale DANN
HCP	Host cell protein	**Sol**	Soluble
HBV	Hepatits B virus	**s.c.**	Subcutaneous
HPV	Human papillomavirus	**s.e.m**	Standard error of the mean
HBcAg	Hepatitis B Virus core Antigen	**SDS**	Sodium dodecyl sulfate
FDA	U S Food and Drug Administration	**SSC**	Side Scatter
HFF	Human Foreskin Fibroblast Cell Lines	**ssRNA**	single strand RNA
HEK293	Human embryonic kidney cells 293	**TAAs**	Tumor associated antigens
H + L	Heavy + light	**Tab.**	Table
His	Hexahistin	**TNF**	Tumor necrosis factor
HRP	Horseredish peroxidase	**TCR**	T cell receptor
HBV	Hepatitis B virus	**TFF-1**	Thyroid transcription factor 1
hs	Homo sapiens	**TU182**	HBcAg Del 79-80 with inserted CLDN81.2 epitope
IVT	in vitro transcribed.	**TRAF6**	Tumour-necrosis-factor-receptor-associated factor 6
IL6	Interleucin 6	**TAK1**	Transforming growth factor-β-activated kinase
IRF	Interferon regulatory factor 3	**TAB1**	TAK1-binding protein 1
IRF	Interferon regulatory factor 7	**TLR**	Toll like receptors
IF	Immunofluorescence	**v/v**	Volume per volume
IFA	Incomplete Freund`s Adjuvant	**vs.**	Versus
IFN	Interferon	**VLPs**	Virus-like particles
Luc	Firefly Luciferase	**UBC13**	ubiquitin conjugating enzyme 13
IL	Interleukin	**U**	Unit
i.m.	Intramuscularly	**UEV1A**	ubiquitin-conjugating enzyme E2 variant 1
i.v.	Intravenous	**w/v**	Weight per volume
iMAB	Monoclonal antibody	**WT**	Wild type

Liste of figures

Liste of Tables

Table of contents

1 Introduction

1.1 Cancer Vaccines

Vaccination is the most successful health intervention to achieve immune protection against infectious diseases. Furthermore, vaccine approaches can also be used in general to enable the host immune system to fight against non-pathogenic diseases like cancer and others [1, 2]. Currently, live-attenuated or completely inactivated pathogens are still presenting essential parts of successful and clinically approved vaccines against infectious diseases [3]. Based on the same principle, the first cancer vaccine that has been attracting attention for several years, also consisted of whole tumor cells that were previously inactivated or irradiated [4-6]. Preclinical studies using this kind of vaccination strategy in mouse models demonstrated the effective eradication of solid tumors [5]. In addition, these studies indicated that tumor cells are immunogenic and that the host immune system is in general capable to detect and potently attack solid tumors [5]. However, the usage of irradiated cancer cells as a vaccine modality bears tremendous risks hindering their entry for routine clinical usage [7]. Therefore, modern cancer vaccines are focussing either on tumor specific antigens (like neo-antigens) or on tumor-associated antigens (TAAs) [6].

TAAs have been defined as antigenic molecules that are correlated and overexpressed in specifc tumor cells and mostly occur due to the genetic instability of cancer cells [8]. Furthermore, TAAs can be classified according to their restriction for B cells [9], T cells [10] or those that are recognized by both immune cell types [11]. Numerous preclinical and clinical studies have demonstrated that passive (using preformed immune effectors like monoclonal antibodies (mAbs) or genetically modified T cells etc.) or active immunization (formats activating the own immune system of the host) directed against defined TAAs could induce an effective anti-tumoral response by triggering a potent and target specific humoral and/or cellular adaptive immune response [12, 13]. Examples of well-characterized TAAs recognized by T and/or B cells and their categorization are given in Table 1.1.

Table 1.1: General categories, cancer histology and examples of TAAs. BRCA = breast cancer antigen; CDK4 = cyclin-dependent kinase-4; CEA = carcino-embryonic antigen; CT= cancer testis; HPV = human papilloma virus; Ep-CAM = epithelial cell adhesion molecule; MART-1/-2 = melanoma antigen recognized by T cells-1/-2; TAG-72 = tumor antigen-72; TRP = tyrosinase-related protein. Adapted from Zarour, HM et al., Holland-Frei Cancer Medicine, 6th edition, 2003. [14]

Category	Example Antigen	Cancer Histology
Oncofetal	CEA	Colorectal carcinoma
	Immature laminin receptor	RCC
	TAG-72	Prostate carcinoma
Oncoviral	HPV E6, E7	Cervical carcinoma
Overexpressed/accumulated	BING-4	Melanoma
	Cyclin-B1	Multi
	9D7	RCC
	Ep-CAM	Breast carcinoma
	EphA3	Multi
	Her2/neu	Multi
	Telomerase	Multi
	Mesothelin	Ductal pancreatic carcinoma
	SAP-1	Colorectal carcinoma
	Survivin	Multi
Cancer-Testis	BAGE, CAGE, GAGE, MAGE family	Multi
	SAGE, XAGE family	Multi
	NY-ESO-1/LAGE-1	Multi
	PRAME	Multi
	SSX-2	Melanoma, Multi
Lineage Restricted	Melan-A/MART-1	Melanoma
	Gp100/pmel17	Melanoma
	Tyrosinase	Melanoma
	TRP-1/-2	Melanoma
	P.polypeptide	Melanoma
	MC1R	Melanoma
	Prostate-pecific antigen	Prostate
Mutated	β-catenin	Melanoma, Prostate, HCC
	BRCA1/2	Breast, ovarian carcinoma
	CDK4	Multi
	CML66	CML
	Fibronectin	Multi
	MART-2	Melanoma
	p53	Multi
	Ras	Multi
	TGF-βRII	Colorectal carcinoma

Furthermore, the application format of TAA-based cancer vaccines seems to have a critical impact on the induction of a potent and specific immune response resulting in the eradication of tumors or the control of tumor growth [8].

1.2 Categories of active cancer vaccines utilizing TAAs

Active anti-cancer vaccine strategies utilizing TAAs can be classified in principle into four different categories [15]: 1) recombinant viral or bacterial vaccines, 2) dendritic cell (DC)-

based vaccines, 3) nucleic acid-based vaccines and 4) peptide- or protein-based vaccines [8, 16]. The promising clinical outcomes of active immunization strategies using such types of vaccines have become evident by the approval of the first therapeutic cancer vaccine by the US Food and Drug Administration (FDA), namely the Sipuleucel-T (Provenge™) for the treatment of asymptomatic metastatic castrate-resistant prostate cancer [8, 17]. Table 1.2 summarizes ongoing or completed clinical Phase III trials of therapeutic cancer vaccines based on active immunization.

Table 1.2: Ongoing or completed phase III trials of therapeutic cancer vaccines. EOC, epithelial ovarian cancer; GBM, glioblastoma; RCC, renal cell carcinoma; SCCHN, squamous cell cancer of the head and neck; NSCLC, non-small cell lung cancer; NCT, ClinicalTrials.gov Identifier. Adapted from Guo, C et al., Adv Cancer Res. 2013; 119: 421–475 [8] and was actualized using ClinicalTrials.gov [18].

Vaccines		Description	Cancer type	Status
DC/APCs	AGS-003	autologous DCs transfected with tumor and CD40L RNAs	RCC	Ongoing
	DCVax®-L	autologous DCs loaded with tumor lysate	GBM	Ongoing
	Cvac	autologous DCs pulsed with MUC1-mannan fusion protein	EOC	Completed
Virus vectors	PROSTVAC	recombinant fowlpox/vaccinia virus encoding hPSA and TRICOM	Metastatic Prostate Cancer	Ongoing
	CG0070	oncolytic adenovirus encoding GM-CSF	Bladder Cancer	Completed
	TG4010	modified vaccinia virus encoding human MUC1 and IL-2	NSCLC	Completed
Peptides/proteins	NeuVax™	HER2/neu peptide combined with GM-CSF	Breast Cancer	Completed
	Stimuvax	liposome-encapsulated synthetic peptide derived from MUC-1	NSCLC	Completed
	Rindopepimut	hEGFR variant III specific peptide conjugated to KLH	GBM	Completed
	POL-103A	protein antigens from 3 melanoma cell lines with alum adjuvant	Melanoma	Ongoing

Several of the clinical trials listed above are using adoptive transfer technologies of autologous, modified DCs. However, the dependency of autologous cancer vaccines, including whole tumor or DC/Antigen-presenting cell (APC) vaccines, on the availability of patient samples and the complicated process of preparing such kind of individualized vaccines are limiting their widespread clinical use [8, 19]. Other strategies, like genetic vaccination comprising DNA/RNA-based cancer vaccines are still under clinical investigation [20]. Although nucleic acid-based vaccines and oncolytic viral and bacterial vaccines have shown good and promising preclinical results, the clinical outcomes have been unsatisfactory so far [8, 19, 21].

Recombinant peptide- or protein-based vaccines representing defined TAAs, which are usually administrated in combination with an adjuvant or immune modulator, are able not only to induce transient effects but also long-lasting antitumoral effects by inducing immunological memory [8, 16, 22]. Furthermore, peptide- or protein-based vaccines are

more cost effective than individualized or autologous cancer vaccines [8] and accordingly may be an attractive platform for usage in cancer vaccine development.

1.2.1 Peptide- or protein-based vaccines

Most of the currently approved cancer vaccines against specific tumor antigens and those in clinical trials are made up of TAA-derived peptides or highly purified recombinant TAA proteins [1, 23]. The first TAA-derived peptide vaccination was tested in melanoma patients in 1995 [24]. Various clinical studies could demonstrate a specific immune response after immunization with this peptide-based vaccine [25, 26]. Despite the induction of a desired immune response, the clinical outcomes have been unsatisfactorily limited [27, 28]. However, the invention of peptide-conjugated nanoparticles and a better understanding of the immunoproteasome function, both critically affecting the MHC class I antigen presentation pathway, opened up new modalities for the treatment of cancer by peptide vaccination. Furthermore, targeting of multiple epitopes to fight the heterogeneity of cancers resulted in an improvement of peptide-based vaccines to provide clinical benefits. In this context, the glioblastoma multiforme multipeptide vaccine IMA950 (Immatics Biotechnologies GmbH) that displays 13 synthetically tumor-associated peptides (TUMAPs) for the treatment of colorectal cancer, successfully completed a phase II clinical study in 2010 [29]. The clinical data revealed a correlation between the induced specific immune responses against the TUMAPs in IM910 treated patients and the overall survival [29].
In addition to peptide-based vaccines, protein-based vaccinations, in particular monoclonal antibody (mAb)-based cancer immunotherapies, although representing a passive immunization strategy, could achieve good clinical results and have entered successfully routine clinical usage [16, 30]. Rituximab, Herceptin, Cetuximab, and Catumaxomab are examples of mAbs that were approved by the European Medicines Agency (EMA) and the FDA for cancer immunotherapy [31]. Complement-dependent cytotoxicity (CDC) and antibody-dependent cell-mediated cytotoxicity (ADCC) present the main effector functions of mAbs, which are responsible for their anti-tumoral efficacy [32]. However, passive immunization with mAbs, in which a continued and a large amount of antibody has to be administrated to maintain a high antibody level titer in the body and thus achieve clinical efficacy, does not lead to a memory immune response. In addition, potential undesired anti-mAb immune responses and high costs of mAb production [33] illustrate disadvantages of the clinical use of mAbs.
An antibody response, which is induced by active immunization, could be used as an alternative to passive immunization. Self-induced antibodies or autoantibody responses with memory qualities would ensure a long-term immune response and protection [34, 35]. Such immune responses could be induced and generated *in vivo* by immunization with virus-like particles (VLPs) [34, 36].

1.3 Virus-like particle-based vaccines

1.3.1 Virus-like particles in vaccine development

Despite the progress that has been made in understanding the immune mechanisms leading to anti-tumor immunity, the successful translation of therapeutic approaches into effective cancer immunotherapies is prevented by several immunological barriers such as immunosuppression and immune tolerance [37]. Natural virus-like particles (VLPs) have been shown to enhance a specific immune response and therefore might be an attractive and novel approach to overcome immunosuppression by tumors [38].

VLPs consist of viral surface or capsid proteins with the intrinsic capacity to self-assemble into macromolecular structures. VLPs are highly immunogenic due to several biophysical characteristics like their size and shape, but especially due to the highly repetitive, dense display and spacing of viral surface proteins. Due to a lack of viral genomic material, VLP vaccines are neither infectious nor able to replicate. Hence, VLP-based vaccines against the virus from which they originated have demonstrated excellent safety [39, 40].

Various VLP-based vaccines against their origin virus have been already approved or are in clinical trials (see Figure 1.1.). Among these are vaccines against human hepatitis B virus (HBV) such as Recombivax (Merck; approved by the FDA as the worlds first recombinant vaccine in July 1986) [41] and against human papilloma virus (HPV), like Cervarix (GlaxoSmithKline group; approved by the FDA in October 2009) and Gardasil (Merck; first approved by FDA in June 2006) [42]. HBV and HPV are each responsible for approximately 5% of cancers worldwide [39]. Furthermore, HPV infection is directly associated with many types of mucocutaneous diseases in humans including cervical, vulvar and vaginal cancer [39, 43]. Thus, Cervarix protects against HPV infection and accordingly prevents the appearance of HPV-related cancer. Thus, HBV and HPV vaccines are protecting prophylactically against virus infection and only indirectly against viral induced tumors, but can’t be used for therapeutic cancer immunotherapy.

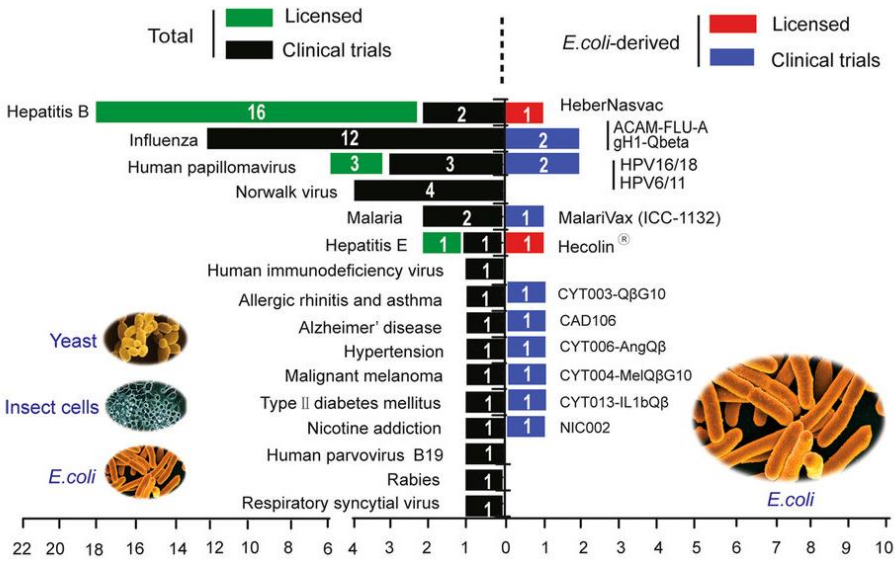

Figure 1.1: VLP-based vaccines or vaccine candidates that were approved or are in clinical studies from 1986 to 2015. On the left side the total number of VLP-based vaccines in clinical use (black) or in clinical trials (green) derived from different expression systems including *E. coli*, Insect cells or yeast are presented. On the right side of the figure only approved VLP-based vaccines (red) or vaccine candidates (blue) that are produced in *E. coli* are illustrated. Adapted from Huang X et al., Vaccines 2, Article number: 3 (2017) [44].

As shown in Figure 1.1, 16 vaccines based on HBV-derived VLPs have been licensed so far and most of them have been used to prevent HBV infections. Currently, HBV vaccination has been used routinely in programs in 179 countries [45], which indicates the widespread and accordingly the successful and safe application of VLP-based vaccines.

Most of the VLP-based vaccines already approved or in clinical trials are intended as prophylactic vaccines against the virus from which their originate. However, in recent years VLPs of different origins have been used as carriers for heterologous epitopes derived from pathogens or from self-antigens, including TAAs [36, 46]. The display of foreign peptides on the surface of these so-called chimeric VLPs efficiently transfers the high intrinsic immunogenicity of VLPs to the presented antigen-peptides [36]. The induced immune response upon vaccination with chimeric VLPs displaying self-antigens can even break the pre-existing self-tolerance against self-antigens in the host. Therefore, chimeric VLPs represent an attractive vaccine format for active immunization in the field of cancer immunotherapy [36, 46].

1.3.2 HBcAg-VLPs as a carrier for heterologous epitopes

Prophylactic vaccination based on VLPs has been shown to enhance effective antibody responses und successfully prevent viral infections which are responsible for emerging of virally related cancers such as cervical cancer [46]. However, no therapeutic efficacy has been achieved against pre-existing viral infections and accordingly viral-related lesions [39]. Therefore, therapeutic VLP-based vaccines, which aim to generate target specific humoral and cellular immune responses and are able to selectively kill target positive cancer cells, are

imperatively required. When using HBcAg-VLPs as a carrier for heterologous epitopes is it possible to trigger target specific B and T cell responses [36, 46, 47]. The first preclinical studies have demonstrated that the hepatitis viral proteins, particularly HBcAg, are extremely immunogenic and could be used as a carrier for tumor antigens [36, 48]. A partial protection against Claudin 18 isoform 2 (CLDN 18.2) expressing tumors using chimeric HBcAg-CLDN18.2 VLP vaccines could be demonstrated in mice by Klamp et al. [36].

HBcAg monomers consist of 183 to 185 amino acids (aa) depending on the viral subtype and contain at the C-terminus an arginine-rich domain that is involved as a nucleic acid binding domain (NBD) for the attachment of the viral genome (Figure 1.2 b). It was demonstrated that a truncated HBcAg-variant (HBcAg aa 1-140) also called HBcAgΔ, in which the C-terminally located 43-45 aa are missing, is able to assemble into capsid particles in different expression systems such as *E. coli* and insect cells (Figure 1.2 a and b). Furthermore, there was no morphological difference between full length and truncated HBcAg-VLPs. Hence, the NBD is not essential for self-assembly of the HBV capsid [49, 50]. During the self-assembly of HBcAg monomers, two types of VLPs can occur. The two types differ in their size and the number of HBcAg monomers. Whereas the larger particles with a diameter of 28-30 nm have an icosahedral symmetry of T=4 and consist of 240 HBcAg monomers, the smaller particles are made up of 180 HBcAg monomers with a size of 25 nm and present an icosahedral symmetry of T=3 [51-53].
Each HBcAg monomer consists of five alpha-helices (α1 to 5). The α1 and α2 simultaneously present two forms α1a/α1b and α2a/α2b (Figure 1.2 a). It should be emphasized that the smallerT=3 particles represent the main population of self-assembled HBcAg-VLPs if *E.coli* is used as expression system [50].

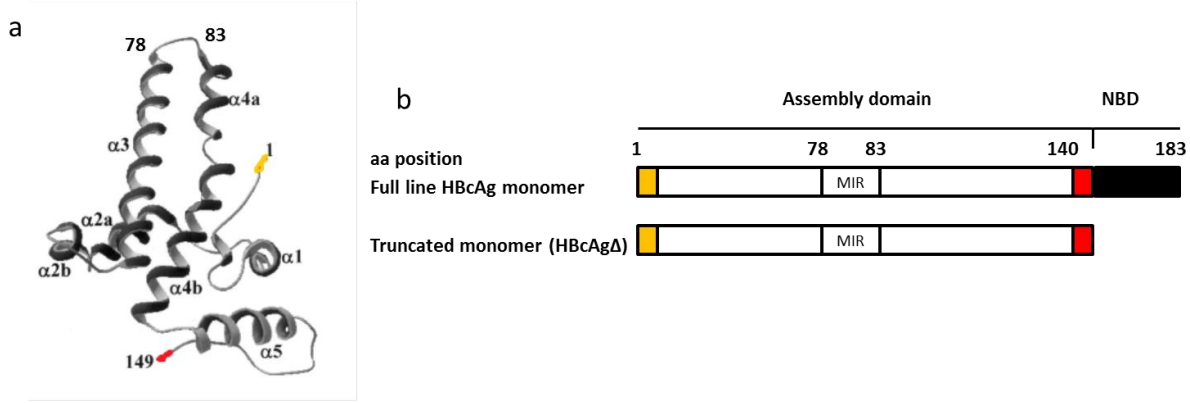

Figure 1.2: Ribbon representation of a truncated HBcAg monomer (a) and schematic sequence comparison between full length and truncated HBcAg monomers (b). Orange: N-Terminus; Red: C-Terminus. NBD = nucleic acid binding domain. MIR = major immunodominant region. Adapted from Newmann M. et al., J Virol. 2003 Dec;77(24):12950-60 [54].

HBcAg-VLPs as a carrier for heterologous epitopes have already been reported [36, 46, 55]. It was demonstrated that the major immunodominant region (MIR) at the tip of the viral nanoparticle is the preferable insertion site of heterologous sequences to provoke high immunogenicity [56]. The addition of glycine-rich linkers on both ends of the epitope inserted into the MIR provides higher flexibility and minimizes steric constraints, leading to a

higher proportion of correctly assembled chimeric HBcAg-VLP generation in *E. coli* or other expression systems [36, 56]. The ability of VLPs to be generated in *E. coli* or in other expression systems has also been investigated when the heterologous epitopes were inserted at the N or C terminus of HBcAg monomers [48, 57]. Thereby, a linker might be also required for correct particle formation [48, 57, 58].

Whereas the MIR region of HBcAg capsids is mostly used for the insertion of heterologous B-cell epitopes [59], the C-terminus was used preferentially for T cell epitopes [48, 58]. Nevertheless, other studies have demonstrated that the insertion of T cell epitopes in the MIR can also result in strong T cell responses [58]. Ruedl et al. reported that HBcAg-VLPs carrying the p33 T cell epitope at the C-terminus could induce a p33-specific $CD8^+$ T cell response and at the same time VLP-specific antibodies [48]. Interestingly, the induced VLP-specific antibodies did not negatively affect the antigen presentation on APCs by a so called carrier-induced epitopic suppression effect (CIES) in a substantial way. However, the T cell priming by APCs was slightly reduced [48]. Nevertheless, a protective T cell response against lymphocytic choriomeningitis virus (LMCV) infection, the origin of p33, in mice could be demonstrated [48].

Besides the possibility to use the HBcAg carrier molecule to induce B and T cell responses simultaneously by insertion of B and T cell epitopes, a T cell independent B cell response could be also enhanced especially by insertion of B cell epitopes in the MIR region of HBcAg monomer [36, 60]. The strong T cell independent B cell response against epitopes in MIR is caused by the direct activation of B cells which is mainly due to the high degree of repetitiveness and the close spacing of HBcAg MIRs in the context of VLPs leading to B cell receptor cross-linking [58].

In general, HBcAg-VLPs are representing promising and versatile carrierrs for antigen display and induce a very strong antigen-specific B and/or T cell immunity. However, the successful development of a chimeric HBcg-based cancer vaccine is critically depending on an appropiate, ideal TAA with restricted expression patterns in healthy tissues. One promising TAA fulfilling these specifications is Claudin 6 (CLDN6), which has been identified as an overexpressed TAA in many tumor types [61-63].

1.4 The tight junction protein Claudin 6 as a potential target for cancer immunotherapy

Tight junctions are intracellular junctional structures that present one form of cell-cell adhesion in epithelial and endothelial cells [64, 65]. It was estimated that 90% of malignant tumors are originated from the epithelium [66]. Furthermore, it was repeatedly reported that the loss of such cell-cell adhesion represents one of the important steps in the progression of cancer to metastasis [65, 66]. As known so far, the main types of the tight junction protein family are occludins and claudins [67].

The down- or upregulation of claudins has been observed in several epithelial-derived cancers [66, 68]. In particular, the altered expression of Claudin proteins such as CLDN1, -3

and -4 caused the development of several types of cancer [68]. In addition, Claudin proteins, such as CLDN4 or 18.2, were identified as promising TAAs and could be recognized by *in vivo* generated polyclonal autoantibodies after immunization with the according protein-based vaccine [36, 69].

Claudins are tetraspanin transmembrane proteins that have a molecular mass of approximately 23 kDa [70]. They consist of four transmembrane domains and two extracellular domains (ECD1 and ECD2). Both, the N- and C-Terminus are located in the cytoplasm (Figure 1.3). The phosphorylation site is displayed by the C-terminal region and might be involved in protein-protein interactions and signal transduction [71].

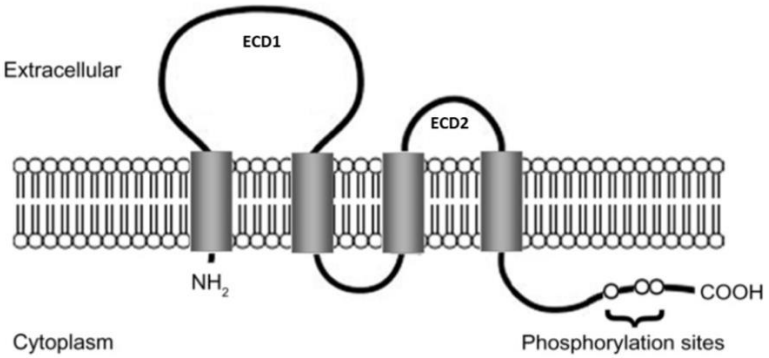

Figure 1.3: Schematic structure of Claudin proteins. All Claudin proteins are made up of four transmembrane domains and two ECDs. ECD1 consists of about 53 aa whereas ECD2 is much smaller with only about 24 aa. The intracellularly located N-terminal region is very short with approximately 4 to 10 aa; the C-Terminus is also located in the intracellular space but much longer and displayed an aa content of 21 to 63. Adapted and modified from Ding L et al., Cancer Manag Res. 2013 Nov 8;5:367-75 [71].

One of the most promising Claudin proteins that has been identified as a TAA is CLDN6 [38, 72]. CLDN6 expression in healthy tissue is mostly restricted to embryonic and fetal cells and CLDN6 is the only pluripotent-specific Claudin [38, 72]. Ben-David et al. found that CLDN6 is highly expressed in human embryonic stem cells and human induced pluripotent stem cells and also in human embryonic carcinoma cell lines, but is completely absent in over 250 somatic tissue samples [72]. TTF1, Gata-6, and FoxA2 are transcription factors that regulate critical genes during the pulmonary epithelial cell differentiation within lung morphogenesis. Accordingly, these transcription factors have been found to regulate CLDN6 expression during pulmonary development [73-75]. Furthermode, it has been reported that CLDN6 is aberrantly activated in several types of cancer including ovarian, gastric, breast and pediatric cancers [61]. Currently, IMAB027, an humanized IgG1 immune effector mAb that selectively binds to CLDN6, is under clinical investigation [61]. A first-in-human dose escalation and dose-finding phase I trial of IMAB027 in patients with advanced ovarian cancer is currrently taking place (NCT02054351). Thus, CLDN6 seems to be a promising TAA for treatment with antibody-based cancer immunotherapy approaches.

Therefore, the use of chimeric HBcAg-VLPs carrying a specific CLDN6 epitope may be a new path for the treatment of CLDN6 positive cells in many types of cancer. However, it is known that the successful application of most protein-based vaccines, including VLPs, is dependent

on so-called adjuvants that substantially increase the immunogenicity and efficacy of such types of vaccines.

1.5 Vaccine Adjuvants

1.5.1 Used adjuvants in protein-based vaccines and their mode of action

Milich et al. reported that nanogram amounts of wildtype HBcAg-VLPs are sufficient to induce an HBcAg-specific antibody response in mice [76]. The structural analysis of HBcAg-nanoparticles revealed their ability to bind specifically to the antigen-specific membrane immunoglobulin (mIg) of B cells and subsequently leads to upregulation of the costimulatory molecules B7.1 and B7.2. Hence, B cells could take up, process and then present HBcAg to T helper cells (Th) cells *in vivo* [34]. However, the induced humoral and cellular immune response could be significantly increased if the HBcAg-VLPs were co-administered with an adjuvant such as the saponin-based ISCOMATRIX [77].

Adjuvants (a word that originates from the latin word *adjuvare* that means help or support) are known as a group of compounds that sustain or modulate the antigenicity or immunogenicity of poorly immunogenic protein- or peptide-based vaccines. The induction of specific B and T cell immune responses, as part of adaptive immunity, could be significantly increased if the innate immune system is also included in an induced immune response upon vaccination. Therefore, the role of the innate immune system in stimulating adaptive immunity presents the basis for the mode of action and accordingly the key role of the adjuvant as an important part of protein- or peptide-based vaccines.

Ramon et al. discovered that horses that developed an abscess at the inoculation site of diphtheria toxoid generated higher specific antibody titers [78, 79]. Subsequently, he and others found other compounds such as tapioca, agar, lecithin, saponin and aluminum that could also strongly enhance antibody titers [78, 80]. In addition, Freund et al. discovered that the combination of mineral oil and water along with killed mycobacteria could be used as a good and potent adjuvant [81]. These discoveries demonstrated the basic concept of the adjuvant and denote the beginning phase of rationally based vaccine adjuvant development.

Actually, the history of vaccines containing adjuvants began even earlier, namely in the year 1885, and started with natural adjuvants and followed in the coming years with more defined adjuvants (Table 1.3).

Table 1.3: The history of adjuvant development. Adjuvant development can be subdivided into two main phases. In the first phase undefined structures in live attenuated or inactivated vaccines have been used whereas the second phase is characterized by usage of defined adjuvants in combination with a well-known and studied protein or peptide-based vaccine. All types of adjuvants affect its contribution in the vaccine by induction and stimulation of pathogen recognition receptors (PRRs). ssRNA = single stranded RNA, TLR = Toll-like receptor, LPS = lipopolysaccharide. Adapted from Reed, SG et al., Nature Medicine 2013, 19, 1597–1608. [82].

Year	Vaccine	Adjuvant and mechanism	Scientific findings
1885	Rabies	ssRNA TLRs 7 and 8	
1886			Briegen describes endotoxin
1889			Coley shows tumor necrosis with bacterial extracts
1911	Typhoid	LPS, DNA TLRs 1, 2, 4, 5, 6 and 9	
1916		Lipovaccine	More durable immune response to typhoid vaccine
1921	BCG for TB	DNA, lipoprotein TLRs 1, 2, 6 and 9	
1926		Aluminum salts	Enhanced antibody responses to diphtheria vaccine
1937		Incomplete Freund's adjuvant (IFA) (water-in-oil emulsion)	Enhanced cellular and antibody responses to TB
1942	Diphtheria, pertussis and tetanus	LPS, DNA TLRs 1, 2, 4, 5, 6 and 9	
1949	Whole-cell influenza	ssRNA TLRs 7 and 8	
1955	Inactivated polio vaccine	ssRNA TLRs 7 and 8	
1966			LPS structure determined
1979			Ribi makes detoxified endotoxin MPL
1991	Hepatitis A		MPL tested in clinic
1996			TLRs discovered
1997	Fluad	MF59 (oil-in-water emulsion)	
1997	Epaxal (for hepatitis A) Inflexal (for influenza)	Virosome	
1998			LPS shown to be TLR ligand
2004	Invivac (for influenza; Europe)	Virosome	
2005	Fendrix (for hepatitis B; Europe)	MPL Defined TLR4	
2007–2009	Pandemic influenza vaccines (Europe)	MF59, AS03 (oil-in-water emulsion)	
2009	Cervarix (for HPV16 and HPV18; USA)	MPL Defined TLR4	

The natural adjuvant in live attenuated or inactivated vaccines, such as rabies vaccine, is heterogeneous and may include particulate forms of proteins, lipids and oligonucleotides, while modern adjuvants consist of well-defined molecules, formulations or both [82]. As known and illustrated in Table 1.3. most adjuvants applied their mode of action via pattern recognition receptors (PRRs), which represent an essential part of the innate immune system. Actually, PRRs play a crucial role by recognizing foreign pathogens. They are able to recognize conserved structures or pathogen-associated molecular patterns (PAMPs) in pathogenic molecules [83]. They can bind also so called damage-associated molecular patterns (DAMPs) and microorganism-associated molecular patterns (MAMPs) [83] and include Toll-like receptors (TLRs), RIG-I-like receptors (RLRs), NOD-like receptors (NLRs), and C-type lectin receptors (CLRs) [84]. The capture of extracellular or endosomal antigens by PRRs in the context of APCs such as DCs, upregulates the surface expression of co-stimulatory molecules like B7.1 and B7.2 and MHC-class II molecules. Furthermore, the stimulation of PRRs results in cytokine and chemokine induction including the upregulation of their receptors and maturation of DCs into APCs. The nature of ligands influences the type

of PRRs that bind specifically to it. This leads to the induction of a defined cytokine secretion pattern, which contributes to the phenotype of differentiated T helper cells and the pattern of adaptive immune responses [85].

1.5.2 TLR-based immune adjuvants

Several TLR ligands are currently being developed as vaccine adjuvants for human use [86]. The stimulation of defined TLRs through TLR based adjuvants triggers the release of defined proinflammatory cytokines, which could significantly increase the specific immune response against an antigen used in a model vaccine. As an example, Monophosphoryl Lipid A from *Salmonalla minnesota* R595 (MPLA) adjuvant, a TLR4 ligand, is approved by the FDA and EMA for human use in HPV and HBV vaccines. Other TLR ligands such as Pam3CSK4 (TLR2 ligand) and R848 (TLR7/8 ligand) are under clinical investigation (see section 1.5.4). However, there are also other adjuvant classes that are already approved in human vaccines and provide their immunostimulatory activities by stimulation of other types of PRRs. The most common of them are the aluminum salts [87] (see Table 1.4 in section 1.5.3).
Several TLRs are located on the plasma membrane (TLR1, 2, 4, 5, 6 and 11) while others like TLR3, TLR7, TLR8 and TLR9 are located in the endosomal compartment. Whereas the endosomally located TLRs are responsible for the recognition of nucleic-acid-like structures and small molecules such as Imidazoquinoline, membrane-bound TLRs can recognize a wide range of ligands that can originate from bacteria, fungi, protozoa or viruses (Figure 1.4).

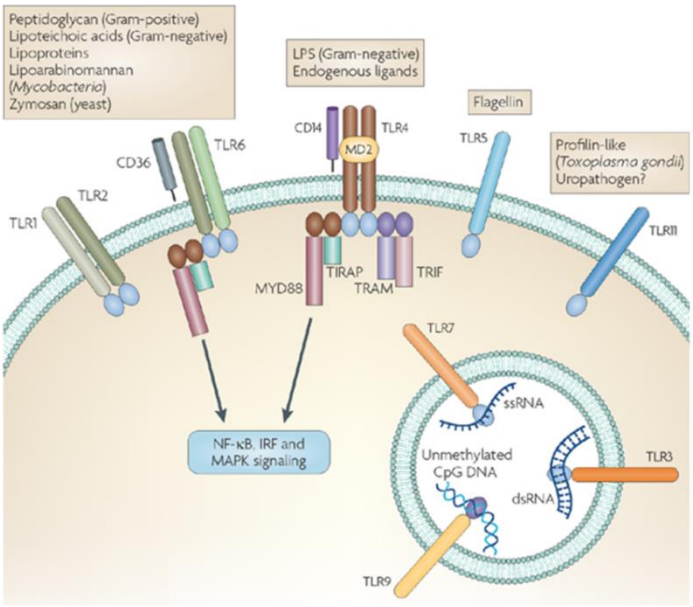

Figure 1.4: Toll-like receptors (TLRs) and their ligands. Most TLRs are located at the plasma membrane with the exception of the endosomally located TLR3, TLR7, TLR8, and TLR9. The endosomal TLRs are responsible for the recognition of microbial and endogenously derived PAMPs. After specific binding of ligands with or without the help of additional molecules such as CD14, MD2, and CD36, TLRs undergo a dimerisation stage followed by the transmission of signals in immune cells using a complex of adaptor molecules such as MYD88 and TRIF. This leads to upregulation of transcription factors such as NF-κB or IRFs which resulted in the release of defined cytokines. Adapted from Rakoff-Nahoum, S et al., Nature Reviews Cancer 9, 57-63 (January 2009) [88].

As reported by Cervantes et al., TLRs can be found as homo- or heterodimers such as TLR1/2 and TLR2/6 [88]. After recognition and specific binding of ligands by TLRs, several types of adaptor proteins could be recruited and bound to the conformationally changed TLR (see Figure 1.5).

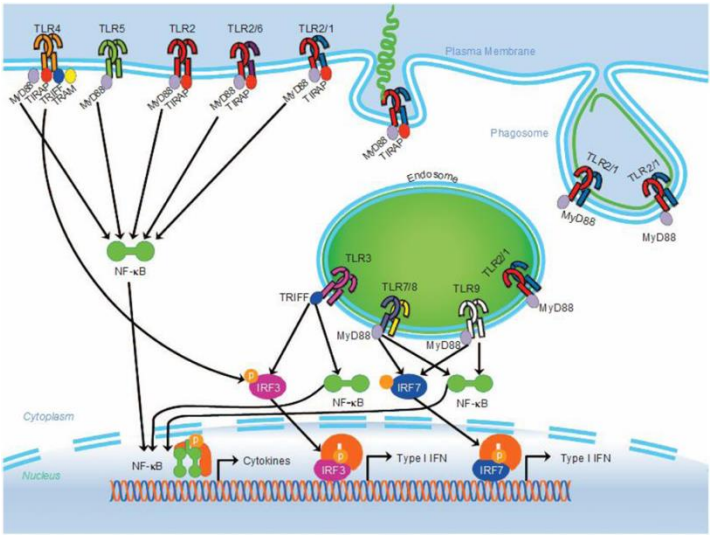

Figure 1.5: Signaling pathways of TLRs. MyD88 as an adapter protein is involved in all TLR signal transduction pathways except for TLR3 in which the TRIFF adapter protein is important by upregulation of TLR3-IFR3 signaling pathway. Adapted from Cervantes et al., Cell Mol Immunol. 2012 Nov; 9(6): 434–438. [89].

The cell surface TLRs including the heterodimers TLR1/2 and 2/6 recruit MyD88 and TIRAP as adaptor proteins. The resulting upregulated NF-κB signaling pathway results in the induction of NF-κB -mediated cytokines. Otherwise than MyD88, TLR4 uses other mediator proteins (TRIF and TRAM), which results in the induction of type I IFNs through the IRF3 pathway. All endosomal TLRs except TLR3 apply MyD88 as an adaptor protein to trigger a signal through NF-κB and IRF7 pathways. Finally, TLR3 recruits TRIF protein to elicit type I IFN and NF-κB regulated cytokines through IRF3 and NF-κB pathways (Figure 1.5) [89]. The importance of understanding and discovering the TLR signaling and the involved mechanisms was highlighted by the 2011 Nobel Prize in Physiology or Medicine, which was awarded to Bruce A. Beutler, Jules A. Hoffmann and Ralph M. Steinmann for their work on the TLRs as an important part of the innate but also the adaptive immune system [90].

1.5.3 Adjuvants approved for human vaccines

So far, the mostly used adjuvants in human vaccines are aluminum salts (alum), which have been approved for use with human vaccines even though their mechanisms of action are poorly understood. It is widely believed that alum creates a depot effect that prolongs antigen presentation and facilitates the antigen uptake by APCs. However, many recent studies are trying to uncover the mode of action of alum. They indicate that alum could activate caspase I through the inflammasome containing cytosolic NLRP1 receptor [91].

These studies agree with older observations that suggested that Alum triggers IL-1ß production via activation of the cytosolic inflammasome [92]. Nevertheless, it was recently reported that alum induces a release of DAMPs, such as DNA, from dying host cells, which then indirectly activate the TLR9 and cGAS-STING signaling pathway [93].
Only a few other adjuvant classes (see Table 1.4) such as adjuvant system 04 (AS04) and MF59 have been used in clinical practice. AS04 combines hydroxide aluminum and monophosphoryl lipid-A as a TLR4 ligand. The obtained clinical results indicated that the induced anti-HPV 16/18 antibody responses by the Cervarix vaccine were greater with an AS04 adjuvant than with an aluminum salt alone. MF59 is an oil in water squalene nanoemulsion that found use as a vaccine adjuvant in the infectious disease setting. Both adjuvant classes, MF59 and AS04, are injected into skeletal muscle tissue, which may trigger a defined cytokine-chemokine milieu and help to uptake antigen by APCs and recruitment of specific T and B cells to the lymph node [82, 94]. Another squalene-based emulsion is AS03, which has been demonstrated to enhance the efficacy of pandemic influenza vaccines [94]. The latest adjuvant that was approved in the human vaccine setting are virosomes [95]. Virosomes were further developed as a carrier for subunit vaccines, in particular for synthetic peptides [95]. Virosomes display viral envelopes, which are made up of membrane lipids and viral glycoproteins without any viral genetic material [87, 96]. The virosome adjuvant is approved in Europe with Influenza and Hepatitis A virus vaccines. The vaccination with virosome vaccines assures a high quality and long-lasting antibody responses and induces a strong cellular immune response by presenting antigen via MHC-I and MHC-II [95]. Due to an excellent safety profile, virosomes can be used for infants, immunocompromised patients and the elderly.

Table 1.4: Licensed vaccine adjuvants: All listed adjuvants have been used as parts of the vaccines against infectious diseases except for AS04 that has been applied in combination with HPV types 16 and 18 vaccines (Cervarix) against HPV infection and indirectly against cervical cancer. Adapted from Lee, S et al., Immune Netw. 2015 Apr; 15(2): 51–57. [87].

Adjuvant name (year licensed)	Class	Manufacturer	Description
Alum (1926)	Mineral Salt	Various	Improves humoral immune responses and antigen stability. Antigens are adsorbed to the surface. The adjuvant in >80% of vaccines licensed for human use. Th2 type immune responses.
MF59 (1997)	Oil-in-water emulsion	Novartis	Improves humoral and cell-mediated immunity. Used in influenza vaccines. Antigen delivery.
AS03 (2009)	Oil-in-water emulsion	GSK	Improves humoral and cell-mediated immunity. Used in influenza vaccine during 2009 H1N1 pandemic.
Virosome (2000)	Liposome	Berna Biotech (Crucell)	Improves humoral and cell-mediated immunity. A virosome is the reconstituted membrane of an enveloped virus. The vaccines for influenza and for Hepatitis A are approved products
AS04 (2005)	Alum-adsorbed TLR4 agonist	GSK	Improves humoral and cell-mediated immunity. Combination of aluminum adjuvant with monophosphoryl lipid A (MPL) co-adsorbed. Used for HPV and HBV vaccine.

1.5.4 Adjuvants in clinical trails

Most adjuvants that are being tested in clinical trials are TLR agonists (see Table 1.4). The most advanced one is the TLR9 ligand unmethylated CpG oligodeoxynucleotide (CpG-ODN). This TLR9 agonist is able to enhance antigen-specific immune responses and induce proinflammatory cytokines such as TNF-α, IL-1, IL-6 and IFN-γ secretion [95]. The company Dynavax started phase 1/2 clinical studies using CpG-ODN immunotherapy in B cell lymphoma in 2014. Besides CpG-ODNs, there are other TLR ligands like Polyriboinosinic acid-polyribocytidylic acid (Poly I:C) which is a promising candidate as a vaccine adjuvant against many types of diseases. Poly I:C, a TLR3 ligand, can induce potent type I IFN secretion and specific cellular immune response [95]. The clinical results of Poly I:C and its derivative Poly-ICLC (Poly I:C in combination with poly-lysine) indicated a good adjuvant efficacy, which contributed to tumor elimination in both animal tumor models and patients [97]. Therefore, the compound Poly-ICLC is currrently being extensively studied in ongoing cancer vaccine clinical trials. Another example of a TLR based adjuvant is flagellin. Flagellin is a TLR5 ligand that is known to induce high antibody titer and a mixed Th1 and Th2 response. The D1 part of flagellin, which binds specifically to TLR5, could be expressed as a fusion protein in combination with a selected antigen vaccine [87]. Thus, the antigen and the TLR5 adjuvant could be targeted to the same APCs and this is considered as an advantage for using flagellin as an adjuvant. Flagellin adjuvant, which is conjugated with matrix protein 2 ectodomain, has been in clinical trials as a vaccine adjuvant against Influenza (NCT01172054). AS01 and AS02 are two further adjuvants that are currently under clinical investigation. Both adjuvants are developed for T cell-based vaccines against malaria and Mycobacterium tuberculosis [98]. The clinical trials revealed that AS01 adjuvant in combination with RTS,S and M27 antigens for malaria and tuberculosis respectively induce Th1 responses against both antigens [99, 100].

There are also other adjuvant classes that are non TLR-based and are currently undergoing clinical trials, such as the immunostimulating complex (ISCOMs). ISCOMs are cage-like particles that are about 40 nm in size, which consist of a mix of saponin, cholesterol, and phospholipid. These lipid-based particles have been shown to induce a very strong and long-lasting antibody titer, a balanced Th1 and Th2 response and a strong cellular immune response [101]. The human data from clinical studies have revealed the good tolerability of ISCOMATRIX as an adjuvant. Currently, ISCOMATRIX is being tested as an adjuvant in combination with several vaccine candidates against hepatitis C virus, influenza, and cancer [102-105].

Table 1.5: Example of adjuvants that are under clinical investigations: Adapted from Lee, S et al., Immune Netw. 2015 Apr; 15(2): 51–57. [87].

Adjuvant name	Class	Description	Clinical phase
CpG	TLR 9 agonist	Enhances antibody titer, Th1 type immunity and CD8 T cell-mediated immunity. CpG oligonucleotides.	Phase 3
Flagellin	TLR 5 agonist	Enhances antibody titer, Th1 and Th2 type immunity. Flagellin linked to antigen.	Phase 1
PolyI:C	TLR3 agonist	Enhances antibody titer, Th1 type immunity and CD8 T cell-mediated immunity. Double-stranded RNA analogues	Phase 1
AS01	Combination	Enhances antibody titer, Th1 type immunity and CD8 T cell-mediated immunity. Combined with MPL, QS21 and liposomes.	Phase 3
AS02	Combination	Enhances antibody titer and Th1 type immunity. Combined with MPL, QS21 and emulsion.	Phase 3
ISCOMs and ISCOMMATRIX	Combination	Enhances antibody titer, Th1 and Th2 type immunity and CD8 T cell-mediated immunity. Combined with saponin and phospholipid.	Phase 2

1.6 RNA-based vaccine adjuvants

1.6.1 RNA as a ligand for the innate immune system

It is well known that virus-derived single stranded RNA (ssRNA) can be recognized by human TLR7/8 and murine TLR7 [106, 107]. Diebold et al. reported that plasmacytoid dendritic cells (pDCs) are the main APCs that trigger an immune response against wild-type Influenza virus by secretion of IFN-α. Therefore, an endosomal recognition of influenza genomic RNA by means of TLR7-MyD88 signaling is required [106]. A similar immune response could be investigated by using non-viral ssRNA, which indicates the central role of the TLR7 receptor in the recognition and binding of ssRNA [106]. In addition, Savarese et al. and Vollmer et al. demonstrated that TLR7 and TLR8 are the receptors involved in the recognition of self-RNA in systemic lupus erythematosus as autoimmune disorders [108, 109]. Furthermore, Heil et al. discovered in 2004 the ability of TLR7/8 receptors in DCs and macrophages to bind specific GU-rich small ssRNA (ssRNA40) [110]. The TLR7 agonist ssRNA40 consists of GU-rich, small phosphothioate-protected ssRNAs that originate from human immunodeficiency virus–1 (HIV-1). The two derivates ssRNA41 and ssRNA42, in which all U or G nucleotides were substituted with adenosine, could not be recognized by TLR7 in pDCs, and therefore did not result in the induction of proinflammatory cytokine secretion [110]. In fact, as reported by many groups, the TLR7/8 stimulation by ssRNA depends on ssRNA bearing defined sequence motifs [110-114]. Interestingly, double-stranded small interfering RNAs (siRNAs), which are known as TLR3 ligands, can be also recognized by TLR7 [111]. Two years later after its discovery, Diebold et al. investigated whether uridine and ribose, the two defined features of RNA, are both essential for TLR7 stimulation [115]. Recently, Zhang et al. determined the tertiary structure of TLR7 and accordingly revealed the mode of action of TLR7 stimulation by ssRNA (Figure 1.6) [53].

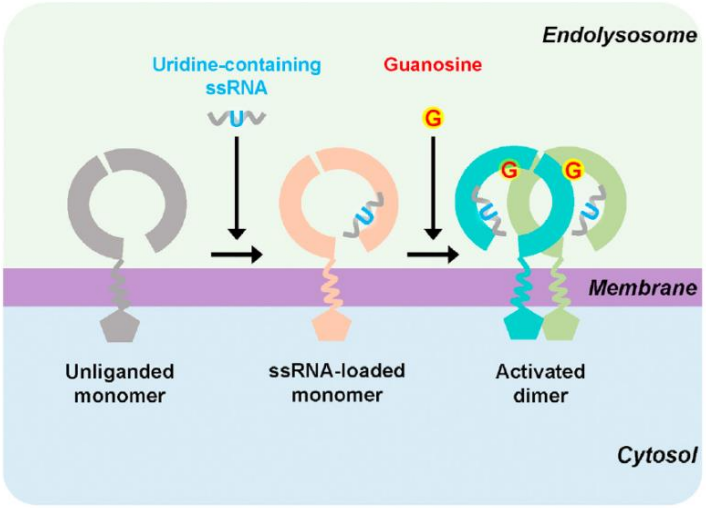

Figure 1.6: Activation mechanism of TLR7. Structural, biochemical and mutagenesis studies revealed that TLR7 has two binding sites. One binding site for guanosine and the second binding site for uridine-containing ssRNA. The double binding lets the activated TLR7 monomers undergo a dimerisation and this leads to their activation. Adapted from Zhang, Z et al., Immunity. 2016 Oct 18;45(4):737-748 [53].

Other researchers demonstrated that not only the sequence or primary structure but also the secondary structure of ssRNA contributes to the stimulation of the innate immune system by specific binding of TLR7 or TLR8 [116]. Confirming this finding, Gantier et al. revealed that the position of uridine in stem-loop structures of ssRNA also plays a role in the TLR7 stimulation and found that the introduction of a micro-RNA (miRNA)-like, non-pairing uridine-bulge in the passenger strand strongly enhanced the innate induction on human immune cells, especially through TLR8 [117]. Interestingly, the GU in a duplex region of a weakly stable RNA secondary structure stimulates specific the TLR7 receptor and a single GU-rich sequence seems to be sufficient to bind and stimulate TLR7 [108]. In summary, ssRNA and non-modified mRNA are characterized by a potent immunostimulatory activity by inducing PRRs including TLR7 and therefore may be good candidates for a new class of adjuvant.

1.6.2 Intravenous application of isRNA-LPX adjuvant

Currently, several RNA-based therapies are being under investigation in clinical trials. Two companies have successfully marketed RNA-based therapies -NeXstar and Ionis Pharmaceuticals. Based on obtained clinical data, the RNA therapeutics market seems to be more promising and efficient than the market for DNA therapeutics [20]. However, the successful application of RNA vaccines is dependent on several critical parameters, among these are the immunization route and whether they should be used as a stand-alone therapy, or in combination with another component such as checkpoint inhibitors. Furthermore, intravenous (i.v.) application could be seen also as an alternative immunization route for RNA-based immunotherapy to induce very strong and specific immune responses, which are able to control tumor growth. Thus, BioNTech RNA Pharmaceuticals initiated in 2015 the first clinical trial evaluating the i.v. administration of an mRNA-based cancer

vaccine using liposomes as a carrier material. This new therapeutic approach, which based on i.v. administration of RNA formulated liposomes and described by Kranz et al [118], could open a new strategy in the field of cancer immunotherapies. The first published clinical results indicated that the systemic RNA delivery was well-tolerated and the vaccine is able to induce very potent T cell responses [118].

1.6.3 Non-coding immunostimulatory oligonucleotide RNA-based adjuvants

The use of non-coding immunostimulatory (is)RNA as a defined adjuvant in combination with protein vaccines, such as rabies vaccine, was already tested in the clinical setting [119]. Preclinical data, which was published by Heidenreich et al., showed a beneficial use of an RNA-based adjuvant in combination with several model antigens such as TC-1 and HPV-16 E7. The RNA adjuvant acted locally without any systemic cytokine release, displayed an excellent safety profile and proved to be superior to Poly I:C with regard to adjuvant and anti-tumoral efficacy [120]. The RNA-based adjuvant used in these studies consisted of a long synthetic RNA and a polymeric carrier [120].
It is important for RNA as an adjuvant to use a carrier, which is needed for the targeting, as well as protecting the RNA against degradation and improving the uptake by APCs. Ziegler et al. could demonstrate that two types of PRRs have to be targeted to become a good adjuvant and accordingly the RNA adjuvant led to upregulation of two signaling platforms, TLR and RIG-I-like RNA helicases (RLH) [121].
Nguyen et al. described the possibility of using lipid-derived nanoparticles for RNA adjuvant delivery [122]. Thereby, a specific isRNA, which was firstly described by Hornung et al. [111] and several types of lipid-like materials, termed lipidoids, were mixed in defined ratios and tested for their adjuvant activity [122]. Subcutaneous (s.c.) injection of lipidoid-isRNA nanoparticles showed functionality and led to high IFN-α responses in mice. These nanoparticles triggered a strong antiviral activity and enhanced the anti-ovalbumin humoral and cellular immune responses in a MyD88-dependent manner when used as a vaccine adjuvant [122]. It was also investigated whether the biological activity of lipidoid-isRNA nanoparticles was TLR dependent, but also TLR7 independent [122]. Thus, Bourquin et al. could demonstrate that isRNA oligonucleotides formulated with 1,2-dioleoyl-3-trimethylammonium-propane (DOTAP) could induce a strong adjuvant activity and accordingly a potent antigen-specific cytotoxic T cell and IgG2a response, when the adjuvant was combined with ovalbumin as a model antigen [123]. In this study, a synthetic DOTAP formulated isRNA was used as a specific TLR7 ligand and used to trigger an immune response against ovalbumin in a sequence-dependent manner [123]. Another study from Bourquin et al. revealed that the i.v. injection of DOTAP formulated small isRNA led to a beneficial anti-tumoral NK cell responses *in vivo* mediated by TLR7 activation [124]. In addition, Hamm et. al. described the safety of the RNA adjuvant [125]. Stimulation with isRNA did not provoke splenomegaly, a known phenomenon and potentially harmful side effect of CpG-DNA-induced immune activation in mice [125].

Given that immune cells targeted by such formulations play a crucial role in the nature of the secreted cytokine pattern and accordingly in the type of the induced immune reponse, the formulation is reported to be an important parameter along with the ligands that are used. Thus, Rettig et al. and others reported that the type of the carriers as a delivery vehicle for isRNAs and the subsequent engineered particle size affects directly the type of the targeted immune cells and accordingly the nature of the induced cytokines. Thus, they found that nanoparticles, but not microparticles, are selectively taken up and phagocytosed by pDCs, which then produce IFN-α [126]. Besides pDCs, monocytes and blood dendritic cell antigens 1+ (BDCA-1^{+}) DCs are the main cell types that highly and invariably express TLR7 in mice. In turn, human pDCs are the main cell type in which TLR7 is highly and invariably expressed (Figure 1.7) [127].

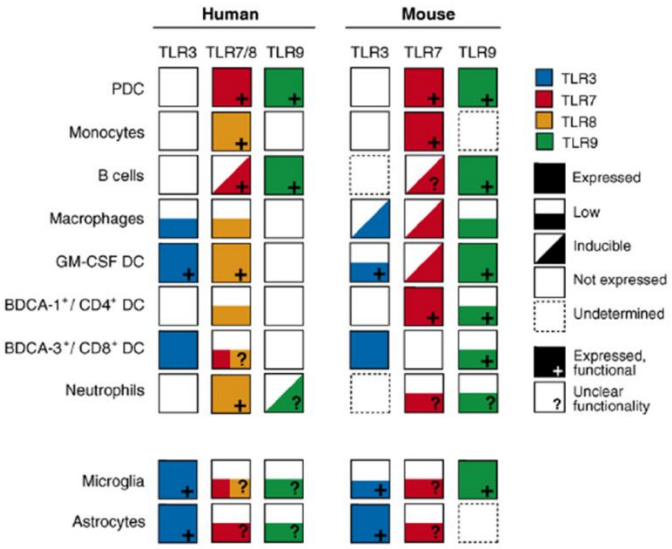

Figure 1.7: The expression level of endosomal TLR3, TLR7, TLR8 and TLR9 in APCs. Adapted from Barchet W et al., Curr Opin Immunol. 2008 Aug;20(4):389-95 [127].

1.7 Purpose of the thesis

BioNTech Protein Therapeutics GmbH (BPT) has developed the SAPHIR® technology platform for cancer immunotherapy based on chimeric, truncated HBcAg-VLPs as a carrier for heterologous TAAs or TAA- derived epitopes. The inherent biophysical and biological properties of these chimeric VLPs enables the inserted TAA epitope to be displayed in a conformation specific, highly repetitive and ordered manner on the VLP surface [36]. The chimeric HBcg-VLPs do not contain any genetic material and therefore, are neither infectious nor able to replicate, leading to an excellent safety profile. Over the last years, BPT was able to establish a high-throughput platform for chimeric VLP-generation and screening as well as a GMP-compatible production platform to express and purify chimeric HBcAg-VLPs. Thus, a level of purification of >95% was achieved routinely in a research and development (R&D) environment. Neither host cell proteins (HCP), nor endotoxin or residual DNA (rDNA) could

be detected in the highly pure chimeric VLP end-product using standard quality control assays. However, it became obvious that a potent immune response against the displayed TAA epitope (and the TAA in its native conformation) elicited upon chimeric HBcAg-VLP immunization was highly dependent on the co-administration of adjuvants. Furthermore, most of the adjuvants tested succesfully in immunization studies using these chimeric HBcAg-VLPs were only for R&D purposes or patent protected by other companies. Therefore, BPT decided to develop an own adjuvant optimized (but not exclusively) for VLP vaccination.

The ratio behind this development that is presented in this thesis, was to develop a patent protected isRNA based adjuvant with freedom-to-operate (FTO) that potently enhances the anti-tumoral efficacy of VLP-based vaccines and fulfilling the following criteria: a) the isRNA should originate from viral RNAs known to activate the innate immune system, b) the isRNA has to be small and with a defined primary and secondary structure, c) the isRNA should have a high specificity for TLR7, as the primary APCs for VLPs are B cells (and/or pDCs) in which TLR7 expression occurs constitutively or can be induced, d) the isRNA should induce a defined cytokine pattern charaterized by high IFN-α and low TNF-α secretion, e) the overall cytokine pattern should promote a Th1-biased immune response leading to an antibody response with cytotoxic effector functions, f) the isRNA should be formulated in such a way that it reaches the same immune compartment when co-administered with chimeric HBcAg-VLPs, g) the isRNA adjuvant should have a good safety profile and h) it should enable a cost effecive production, purification and formulation using pre-established protocols from BioNTech AG.

For the achievement of this goals and criteria this doctoral thesis was subdivided into the following parts:

1. Perform an adjuvant screening for HBcAg-based vaccines

2. Develop a novel RNA-based adjuvant with strong immunostimulatory activities, which can be applied using different immunization routes, including i.v. application.

    a) Establish a new and valid discovery platform based on an easy sequential fragmentation strategy of Influenza nucleoprotein (NP) encoding RNA for identifying small isRNA sequences that could induce a defined cytokine profile in human and mouse immune cells.
    b) Define the *in vitro* and *in vivo* functionality of these RNA-based adjuvants.
    c) Investigate the tolerability of these RNA adjuvants after i.v. administration.

3. Assess *in vivo* induced antigen-specific immune responses of HBcAg based vaccines with and without adjuvant.

a) Investigate the tolerability and *in vivo* functionality after co-administration of the RNA-based adjuvant and the co-administered HBcAg-based vaccine.
b) Provide the preclinical proof-of-concept (POC) that the RNA adjuvant can increase the immunogenicity or antigenicity of the HBcAg-based vaccine including induction of antigen-specific B and T cell responses.
c) Characterize the immunological features of the induced antibody responses including their capability to bind the native target antigen and to trigger target specific cytocidal effector functions such as CDC.

4. Assess the antitumoral effects of HBcAg-based vaccines with and without adjuvant

a) Investigate the prophylactic and therapeutic efficacy of the induced antigen-specific immune response in a mouse tumor model using CT26-mmCLDN6 and E0771 tumor cell line after co-administration of the RNA adjuvant and the HBcAg-based vaccine.
b) Identify the main effector cells that are responsible for the antitumoral effects.

2 Material and Methods

2.1 Material

2.1.1 Buffer and Cell Culture Media

FACS-buffer

DPBS	
FBS	5% (v/v)
EDTA	5 mM

Erythrycyte lysis buffer

NH_4Cl	8.25 g
$KHCO_3$	1 g
EDTA	100 µM
dH_2O	fill up to 1 l

Freezing medium

FBS	10% (v/v)
DMSO	

MACS-buffer

DPBS	
Human AB Serum	5% (v/v)
EDTA	5 mM

Fekete's solution

Ethanol, 70 %	5 ml
Formalin, 37 %	0,5 ml
Acetic acid, 100 %	0,25 ml

ELISA blocking solution

DPBS	
FBS	2% (v/v)

ELISA Washing solution

DPBS	
Tween 20	0,05 % (v/v)

Coomassie staining buffer

Coomassie	0,25 % (w/v)
Ethanol	40% (v/v)
Acetic acid	10 % (v/v)

DC Medium

RPMI 1640 GlutaMAX™	
FBS	10 % (v/v)
NEAA	1 % (v/v)
Sodium pyruvate	1 % (v/v)
Penicilline/Streptomycin	0.5 % (v/v)

CHO-K1-WT medium

DMEMF12 Glutamax	
FBS	10 % (v/v)
Penicillin Streptomycin	0,5 % (v/v)

CHO-K1-hsCLDN6 medium

DMEMF12 Glutamax	
FBS	10 % (v/v)
G418	1mg/ml
Penicillin Streptomycin	0,5 % (v/v)

CHO-K1-hsCLDN9 medium

DMEMF12 Glutamax	
FBS	10 % (v/v)
Blasticidin	1µg/ml

CT26 WT medium

RPMI 1640 GlutaMAX™	
FBS	10 % (v/v)

CT26-mmCLDN6 medium

RPMI 1640 GlutaMAX™	
FBS	10 % (v/v)
Hygromycin	300µg/ml

E0771-mmCLDN6 medium

DMEMF12 Glutamax	
FBS	10 % (v/v)
Hygromycin	400µg/ml

MC38-mmCLDN6 medium

DMEMF12 Glutamax	
FBS	10 % (v/v)
Hygromycin	400µg/ml

HEK 293 hu TLR3, 8, 7, 9_Luc. miRNA 81 medium

DMEMF12 Glutamax	
FBS	10 % (v/v)
HEPES	1 % (v/v)
NEAA	1 % (v/v)
Sodium pyruvate	1 % (v/v)
Penicilline/Streptomycin	0.5 % (v/v)
Blasticidin	10µg/ml
Zeocin	100µg/ml
G418	250µg/ml

(Only for HEK 293 hu TLR7,8 ,9)

Disassembly buffer (pH = 9)

dH2O	
Urea	3,5 M
Tris/HCl	50 mM
Glycerin	20% (v/v)

Lysis Buffer (pH = 8)

dH2O	
Na2HPO4	50 mM
NaCl	300 mM
Tween20	0,25 % (v/v)

Reassembly Buffer (pH = 7)

dH2O	
Tris	50 mM
NaCl	800 mM NaCl

VLP formulation buffer

dH2O	
Tris	50 mM
NaCl	100 mM NaCl

SDS-Page

Acrylamid Mix (40%)	12,5 % (v/v)
Tris (pH = 6,8)	13,5 % (v/v)
Sodiumdocecylsulfat (SDS)	1 % (v/v)
Ammoniumpersulfat (APS)	1 % (v/v)
Tetramethylethylendiamin (TEMED)	0,1 % (v/v)
Mixing	
Poymerisation for 30min	

1X Laemmli SDS-PAGE buffer

dH2O	
Glycerin	192 mM
Tris	25 mM
SDS	0,1 % (w/v)

2.1.2 Hardware

Name	Company
AF4 MALS (Eclipse®, miniDAWN™ TREOS® MALS-Detector)	Wyatt Technology, Dernbach, Germany
Agilent HPLC 1260 Infinity	Agilent Technologies, Waldbronn, Germany
Äkta Avant 25	GE Healthcare, München, Germany
Automated cell counter Vi-Cell XR	Beckman Coulter, Krefeld, Germany
Anesthetic system, UniVet Porta	Groppler, Deggendorf, Germany
Avanti J-26XP Series High-Speed Centrifuges	Beckman Counter, Krefeld, Germany
BD FACS CantoTM II	Becton Dickinson, Heidelberg, Germany
Centrifuge 5810R	Eppendorf, Hamburg, Germany
Clean bench, Biobase, Safety Cabinet	Envair, Emmendingen, Germany
Clean bench, HeraSafe® HS18	Heraeus, Hanau, Germany
CO2 incubators HERAcell 150	Heraeus, Hanau, Germany
CTL-ImmunoSpot® S6 Macro Analyzer	CTL, Shaker Heights, OH
Eppendorf® Thermomixer Compact	Eppendorf, Hamburg, Germany
Electroporation System ECM 830	BTX, Holliston, MA
ELIspot reader Bioreader 6000-Eg	BIO-SYS, Karben, Germany
Freezer, -80°C	Heraeus, Hanau, Germany
Mr. Frosty™ Freezing Container	Thermo Fisher Scientific, Schwerte, Germany
Heraeus™ Pico™ 17 Microcentrifuge	ThermoFisher, Schwerte, Germany
Heraeus Pico 17 Microcentrifuge	Heraeus, Hanau, Germany
Heraeus Multifuge X3 Centrifuge	Hettich, Tuttlingen, Germany
INFORS HT - Incubation Shakers	Infors HT, Einsbach, Germany
Inverter Convection Microwave Oven	Sharp, Cologne , Germany
Incubators, INCU-Line®, IL 53	VWR, Darmstadt, Germany
ImageQuant LAS 4000	GE Healthcare, Munich, Germany
Laminar flow bench HERAsafe 2020	Heraeus, Hanau, Germany
Microscope CKX31	Olympus, Hamburg, Germany
pH-Meter inolab®, pH730 set	WTW, Weilheim, Germany
Precision balance Kern KB	Kern und Sohn, Balingen, Germany
Restrainer, mouse	LabArt, Waldbüttelbrunn, Germany
Semi Dry Blotter	CTI Idstein, Germany
Sartorius CPA225D semi micro balance	Sartorius, Göttingen, Germany
Tecan 96 microplate washer	Tecan, Männedorf, Switzerland
Tecan NanoQuant Infinite M200Pro	Tecan, Männedorf, Switzerland
Thermocycler T3	Fermentas, St. Leon-Roth, Germany
Thermomixer comfort	Eppendorf, Hamburg, Germany
UV-Transilluminator	Intas, Göttingen, Germany
Vortex mixer	IKA, Staufen, Germany
Water bath	Heraeus, Hanau, Germany
Wide Mini-Sub Cell GT electrophoresis Cell	BIO-RAD, munich, Germany

2.1.3 Cell Culture Media

Name	Company
Dulbecco's Modified Eagle Medium (DMEM)	Thermo Fisher Scientific, Schwerte, Germany
Roswell Park Memorial Institute (RPMI), 1640 GlutaMAX™	Thermo Fisher Scientific, Schwerte, Germany
X-VIVO™ 20	Lonza, Basel, Switzerland

2.1.4 Consumables

Name	Company
6-well cell culture plates	Nunc, Wiesbaden, Germany
12-well cell culture plates	Nunc, Wiesbaden, Germany
96-Well-Plates, Maxisorp™	Nunc, Wiesbaden, Germany
96-Well-Plates, Streptavidin Microtiterplates	Nunc, Wiesbaden, Germany
96-Well-Plates, U-Form, flach	Nunc, Wiesbaden, Germany
96 well plate, polystyrene, white round bottom wells	Merck Millipore, Darmstadt, Germany
BioTrace™ NT Nitrocellulose Transfer Membrane	Pall Corp. Pensacola, USA
Discofix® 3-way Stopcock	Braun, Mesungen, Germany
CELLSTAR®Cell Culture Flasks 25, 75 and 175 cm2	Greiner, Frickenhausen, Germany
Cryogenic vial, 1.8 mL, round bottom	Nunc, Wiesbaden, Germany
Eppendorf Safe-Lock Tubes 0.5, 1.5, 2 and 5 ml	Eppendorf, Hamburg, Germany
Electroporation Cuvette	VWR, Darmstadt, Germany
Elispot plate, MSIPS45 clear	Millipore, Darmstadt, Germany
Ep Dualfilter T.I.P.S. Filterspitzen (10, 20, 100, 200, 1000 µl)	Eppendorf, Hamburg, Germany
EASYstrainer™	Greiner, Frickenhausen, Germany
FACS tubes, polystyrene, 5ml	BD Biosciences, Heidelberg, Germany
Falcon tubes 15 and 50 ml	BD Biosciences, Heidelberg, Germany
Greiner CELLSTAR® serological pipette 5, 10, 25, 50 ml	Greiner, Frickenhausen, Germany
Heparin-containing micro tube (1.3ml, Lithium Heparin)	Sarstedt, Nümbrecht, Germany
Microhematocrit Capillary Tubes	Brand, Wertheim, Germany
MACS cell separation columns LS	Miltenyi Biotec, Bergisch-Gladbach, Germany
Microlance 19 G canula	BD Biosciences, Heidelberg, Germany
Millex-VV 0,1 µm	Merck Millipore, Darmstadt, Germany
Minisart®Syringe Filters 0.2 µM	Sartorius, Goettingen, Germany
Microscope Slide Coverslips	Thermo Fisher Scientific, Schwerte, Germany
Protein LoBind DeepWell 96/2000 µL	Eppendorf, Hamburg, Germany
Protein LoBind tubes 0.5, 1.5, 2.0 mL	Eppendorf, Hamburg, Germany
ProteinA Magnetic Beads (Dynabeads®)	Life Technologies, Paisley, UK
Sterican canula 20 G and 27 G	Braun, Mesungen, Germany
Slide-A-Lyzer™ Dialysis Cassettes	Thermo Fisher Scientific, Schwerte, Germany
Reagenzien-Reservoirs 25, 100 ml	Thermo Fisher Scientific, Schwerte, Germany
RNA/DNA LoBind tubes 0.5, 1.5, 2.0 mL	Eppendorf, Hamburg, Germany
Syringes 5 ml, 1 ml, 0.5 ml	BD Biosciences, Heidelberg, Germany
Superfrost Plus Slides	Thermo Fisher Scientific, Schwerte, Germany
Petri dish,100 x 20 mm,	Greiner, Frickenhausen, Germany
Whatman Papier 3 mm CHR	Carl-Roth, Karlsruhe, Germany
Ultra-Fine Syringes 0.3, 0.5, 1 ml	BD Biosciences, Heidelberg, Germany

2.1.5 Mice

Mice were female and 6 to 10 weeks of age at the onset of experiments. They were maintained under specific-pathogen free conditions at the University of Mainz or BioNTech AG Mainz.

Mice	Company
BALB/c	Janvier Labs, Saint-Berthevin, France
C57BL/6	Janvier Labs, Saint-Berthevin, France
BDCA2-DTR C57BL/6	The Jackson Laboratory, Bar Harbor ,USA

2.1.6 Antibodies

Name	Company
Anti PKR Rabbit polyclonal antibody	Abcam, Cambridge, UK
Anti p-PKR Rabbit polyclonal antibody	Abcam, Cambridge, UK
anti- ßactin mouse monoclonal antibody	Sigma-Aldrich, Schnelldorf, Germany
Goat anti-mouse F(ab')2 ALEXA Fluor 647	BD Biosciences, Heidelberg, Germany
Goat anti-human F(ab')2 ALEXA Fluor 647	BD Biosciences, Heidelberg, Germany
APC-Cy™7 Mouse Anti-Human CD14 Clone MϕP9	BD Biosciences, Heidelberg, Germany
Alexa Fluor® 647 F(ab')2 Fragment, g α-m IgG (H+L)	Life Technologies, Paisley, UK
Brilliant Violet 421™ anti-human CD19 Antibody	Biolegend, Koblenz, Germany
CD16, Fc Gamma Receptor III_FITC (Clone DJ130c)	Agilent, Waldbronn, Germany
CD141 (BDCA-3) antibodies, human (clone: AD5-14H12)	Miltenyi Biotec, Bergisch Gladbach, Germany
CD303 (BDCA-2) antibodies, human (clone: AC144)	Miltenyi Biotec, Bergisch Gladbach, Germany
HRP-conjugated, goat anti-mouse IgG isotype-specific secondary antibodies	Thermo Fisher Scientific, Schwerte, Germany
HRP-IgG (H+L) g-α-m	Jackson ImmunoResearch Europe Ltd, Suffolk, UK
HRP Rat Anti-Mouse IgG2a	BD Biosciences, Heidelberg, Germany
HRP Rat Anti-Mouse IgG1	BD Biosciences, Heidelberg, Germany
IgG1κ α-HBcAg Maus monoklonal (10E11); aa2-8	Merck Millipore, Darmstadt, Deutschland
IgG2a α-HBcAg Maus monoklonal (3120; determ. β)	Institute of Immunology, Tokio, Japan
IMAB027 Maus monoklonal, α-CLDN6	Ganymed Pharmaceuticals, Mainz, Deutschland
J2 antibody	scicons, Budapest, Hungary
FITC rat anti-mouse CD4, clone GK1.5	BD Biosciences, Heidelberg, Germany
PerCP Mouse Anti-Human CD69 Clone L78	BD Biosciences, Heidelberg, Germany
Rat anti-mouse IFN-γ, clone AN18	Mabtech, Nacka Strand, Sweden
V500 Mouse Anti-Human CD3 Clone UCHT1	BD Biosciences, Heidelberg, Germany

2.1.7 Kits

Mice	Company
Agilent RNA 6000 Nano Kit	Agilent Technologies, Waldbronn, Germany
Bio-Plex Pro assays, Kits, and Reagents (Human and mouse)	BioRad, Munich, Germany
CD304 (BDCA-4/Neuropilin-1) MicroBead Kit, human	Miltenyibiotec, Bergisch Gladbach, Germany
Compensation particles set anti-rat and anti-hamster	BD Biosciences, Heidelberg, Germany
Dynabeads MyOne Carboxylic Acid	Invitrogen, Karlsruhe, Germany
EZ-Link™Sulfo-NHS-Biotinylation Kit	Thermo Fisher Scientific, Schwerte, Germany
IFN alpha Mouse ELISA Kit	Thermo Fisher Scientific, Schwerte, Germany
High Pure PCR Product Purification Kit	Roche, Basel, Schweiz
High Pure Plasmid Isolation Kit	Roche, Basel, Schweiz
Human TNF-alpha Platinum ELISA Kit	eBioscience, Frankfurt am Main, Germany
Human IFN-alpha Platinum ELISA Kit	eBioscience, Frankfurt am Main, Germany
QiaQuick Gel Extraction Kit	Qiagen, Hilden, Germany
MelonGel IgG Spin Purification	Thermo Fisher Scientific, Schwerte, Germany
eBioscience™ Mouse TNF-alpha Platinum ELISA Kit	Thermo Fisher Scientific, Schwerte, Germany
NucleoBond Xtra Midi	Machery&Nagel, Düren, Germany
Plasmacytoid Dendritic Cell Isolation Kit, mouse	Miltenyibiotec, Bergisch Gladbach, Germany
Rneasy Mini Kit	Qiagen, Hilden, Germany
TNF alpha Mouse ELISA Kit	Thermo scientific, Dreieich, Deutschland
XTT-Proliferations assay	Roche, Basel, Schweiz

2.1.8 Reagents, Chemicals and Stimuli

Name	Company
6 x DNA Loading Dye	Sigma-Aldrich, Saint Louis, MO
10 x Casein-Puffer	Sigma-Aldrich, Steinheim, Germany
7AAD	Beckman coulter, Krefeld, Germany
2-Mercaptoethanol	Sigma-Aldrich, Saint Louis, MO
4-(2-hydroxyethyl)-1-piperazineethanesulfonic acid (HEPES)	Thermo Fisher Scientific, Schwerte, Germany
5-Bromo-4-chloro-3-indolyl phosphate (BCIP) / nitro blue tetrazolium chloride (NBT) solution"	Sigma-Aldrich, Saint Louis, MO
Gerbu Adjuvant LQ	Gerbu Biotechnik, Heidelberg, Germany
Accutase soluition	Sigma-Aldrich, Saint Louis, MO
Acetic acid, 100 %	Sigma-Aldrich, Saint Louis, MO
Alhydrogel® adjuvant 2%	Invivogen, Toulouse, France
Ammonium chloride (NH4Cl)	Sigma-Aldrich, Saint Louis, MO
Aceton (C3H6O)	AppliChem, Darmstadt, Germany
Acrylamid 40 % (37,5:1) (C3H5NO)	Carl Roth, Karlsruhe, Germany
AddaVax™	Invivogen, Toulouse, France
Alkaline phosphatase	Fermentas, St. Leon-Rot, Germany
Ammoniumperoxodisulfat (APS) ((NH4)2S2O8)	Carl Roth, Karlsruhe, Germany
Ammoniumsulfat (AMS) (NH4)2SO4	Carl Roth, Karlsruhe, Germany
Bovine serum albumin (BSA)	Sigma-Aldrich, Saint Louis, MO
BioTrace™ NT Nitrozellulose-Membran (0,2 µm)	Pall, Dreieich, Deutschland
Bafilomycin A1	Invivogen, Toulouse, France
Carbenicillin	Sigma-Aldrich, Steinheim, Deutschland
CL097	Invivogen, Toulouse, France
Concanavalin A (ConA)	Sigma-Aldrich, Saint Louis, MO
Coomassie® Brilliantblau R 250	AppliChem, Darmstadt, Deutschland
Diphtheria Toxin	Sigma-Aldrich, Saint Louis, MO
Dimethyl sulfoxide (DMSO)	Applichem, Darmstadt, Germany
Dynabeads MyOne Carboxylic Acid	Invitrogen, Karlsruhe, Germany
Dithiothreitol (DTT)	AppliChem, Darmstadt, Deutschland
Ethanol, 98%	Carl Roth, Karlsruhe, Germany
Ethylenediaminetetraacetic acid (EDTA), 0.5M	Sigma-Aldrich, Saint Louis, MO
Ethidiumbromid	Sigma-Aldrich, Saint Louis, MO
Kanamycin	Sigma-Aldrich, Saint Louis, MO
Fc Blocking reagent	Miltenyi Biotec, Bergisch Gladbach, Germany
FACS clean	BD Biosciences, Heidelberg, Germany
FACS flow	BD Biosciences, Heidelberg, Germany
FACS Lysing Solution (10X)	BD Biosciences, Heidelberg, Germany
FACS rinse	BD Biosciences, Heidelberg, Germany
Fetal bovine serum (FBS)	PAA Laboratories, Pasching, Austria
Ficoll-Paque PREMIUM 1,084	Thermo Fisher Scientific, Schwerte, Germany
Ficoll-Paque PLUS	Thermo Fisher Scientific, Schwerte, Germany
Formaldehyde, 37%	Carl Roth, Karlsruhe, Germany
Fixation-Buffer	BD Biosciences, Heidelberg, Germany
G418, Geneticin	Life Technology, Carlsbad, USA
Glycerin (C3H8O3)	AppliChem, Darmstadt, Germany
Glycin (C2H5NO2)	Carl Roth, Karlsruhe, Germany
Human serum complement	Tecomedical Group, Bünde, Germany
Lisposomes (F12, F5)	BioNTech RNA Pharmaceuticals, Mainz Germany
Isoflurane	Baxter, Deerfield, IL
Isopropyl alcohol	Merck, Darmstadt, Germany
Murine Interferon-g (IFN-g)	Peprotech, London, UK
Magnesium chloride (MgOAc2)	Sigma-Aldrich, Saint Louis, MO
MPLA-SM VacciGrade™	Invivogen, Toulouse, France

N,N,N`,N`-Tetramethylethylendiamin (TEMED)	AppliChem, Darmstadt, Deutschland
ODN 2216 VacciGrade™	Invivogen, Toulouse, France
ODN 1826 VacciGrade™	Invivogen, Toulouse, France
Pierce ECL Western Blotting Substrate	Thermo Scientific, Schwerte, Germany
Penicilline-Streptomycin (10.000 U/ml)	Thermo Fisher Scientific, Schwerte, Germany
PBS solution	Thermo Fisher Scientific, Schwerte, Germany
Potassium bicarbonate (KHC3)	Sigma-Aldrich, Saint Louis, MO
Pyrophosphatase, Inorganic	Sigma-Aldrich, Saint Louis, MO
Pam3CysK4	Invivogen, Toulouse, France
Poly(I:C)	Invivogen, Toulouse, France
PageBlue Protein Staining Solution	Thermo Scientific, Schwerte, Germany
Pam3CSK4 VacciGrade™	Invivogen, Toulouse, France
rNTP	Thermo Fisher Scientific, Schwerte, Germany
RiboLock Rnase Inhibitor	Thermo Fisher Scientific, Schwerte, Germany
R848	Invivogen, Toulouse, France
ssRNA Ladder	BioLabs, Frankfurt am Main, Germany
Sodium azide (NaN3)	Sigma-Aldrich, Saint Louis, MO
Sodium chloride, 5M	Thermo Fisher Scientific, Schwerte, Germany
sodium lauryl sulfate (SDS)	AppliChem, Darmstadt, Deutschland
SuperSignal West Femto Chemiluminescent Substrat	Thermo Scientific, Schwerte, Germany
Streptavidin-alkaline phosphatase(AP)	Sigma-Aldrich, Saint Louis, MO
SpeI	BioLabs, Frankfurt am Main, Germany
Streptavidin-HRP Conjugate	Sigma-Aldrich, Saint Louis, MO
Spermidin	Carl Roth, Karlsruhe, Germany
Trypan blue	Sigma-Aldrich, Saint Louis, MO
Triton-X 100	AppliChem, Darmstadt, Germany
Trypton	Becton Dickinson, Heidelberg, Germany
T7 RNA POL >100U/UL 25000U	Thermo Fisher Scientific, Schwerte, Germany
T4-DNA-Ligase	Fermentas, St. Leon-Rot, Deutschland
Tris Base (C4H11NO3)	AppliChem, Darmstadt, Germany
TURBO™ DNase (2 U/µL)	Thermo Fisher Scientific, Schwerte, Germany
Tween20	Carl Roth, Karlsruhe, Germany
Urea (CH4N2O)	Carl Roth, Karlsruhe, Germany
XhoI	BioLabs, Frankfurt am Main, Germany
Water, nuclease-free	Carl Roth, Karlsruhe, Germany
Pyrophosphatase, Inorganic	Sigma-Aldrich, Saint Louis, MO
Pam3CysK4	Invivogen, Toulouse, France
Poly(I:C)	Invivogen, Toulouse, France
PageBlue Protein Staining Solution	Thermo Scientific, Schwerte, Germany
Pam3CSK4 VacciGrade™	Invivogen, Toulouse, France
rNTP	Thermo Fisher Scientific, Schwerte, Germany
RiboLock Rnase Inhibitor	Thermo Fisher Scientific, Schwerte, Germany
R848	Invivogen, Toulouse, France
ssRNA Ladder	BioLabs, Frankfurt am Main, Germany
Sodium azide (NaN3)	Sigma-Aldrich, Saint Louis, MO
Sodium chloride, 5M	Thermo Fisher Scientific, Schwerte, Germany
sodium lauryl sulfate (SDS)	AppliChem, Darmstadt, Deutschland
SuperSignal West Femto Chemiluminescent Substrat	Thermo Scientific, Schwerte, Germany
Streptavidin-alkaline phosphatase(AP)	Sigma-Aldrich, Saint Louis, MO
SpeI	BioLabs, Frankfurt am Main, Germany
Streptavidin-HRP Conjugate	Sigma-Aldrich, Saint Louis, MO
Spermidin	Carl Roth, Karlsruhe, Germany
Trypan blue	Sigma-Aldrich, Saint Louis, MO
Triton-X 100	AppliChem, Darmstadt, Germany
Trypton	Becton Dickinson, Heidelberg, Germany
T7 RNA POL >100U/UL 25000U	Thermo Fisher Scientific, Schwerte, Germany
T4-DNA-Ligase	Fermentas, St. Leon-Rot, Deutschland
Tris Base (C4H11NO3)	AppliChem, Darmstadt, Germany
TURBO™ DNase (2 U/µL)	Thermo Fisher Scientific, Schwerte, Germany

Tween20	Carl Roth, Karlsruhe, Germany
Urea (CH4N2O)	Carl Roth, Karlsruhe, Germany
XhoI	BioLabs, Frankfurt am Main, Germany
Water, nuclease-free	Carl Roth, Karlsruhe, Germany

2.1.9 Oligonucleotide

Name	Type	Sequence	Company
NP71-Seq1_Fo	DNA oligo (Oligo hybridisation)	5´-CTAGTCCCAGGATGTGCTCTCTGATGCAAGGTTCAACTCTCCCTAGGAGC-3´	MWG Operon, Ebersberg, Germany
NP71-Seq1_Re	DNA oligo (Oligo hybridisation)	3´-AGGGTCCTACACGAAGACTACGTTCCAAGTTGAGAGGGATCCTCGAGCT-5´	MWG Operon, Ebersberg, Germany
NP71-Seq2_Fo	DNA oligo (Oligo hybridisation)	5´-CTAGTGTCTGGAGCCGCAGGTGCTGCAGTCAAAGGAGTTGGAACAATGGC-3´	MWG Operon, Ebersberg, Germany
NP71-Seq2_Re	DNA oligo (Oligo hybridisation)	3´-AAGACCTCGGCGTCCACGACGTCAGTTTCCTCAACCTTGTTACCGAGCT-5´	MWG Operon, Ebersberg, Germany
NP71-Seq3_Fo	DNA oligo (Oligo hybridisation)	5´-CTAGTTGATGGAATTGGTCAGAATGATCAAACGTGGGATCAATGATCGGC-3´	MWG Operon, Ebersberg, Germany
NP71-Seq3_Re	DNA oligo (Oligo hybridisation)	3´-AACTACCTTAACCAGTCTTACTAGTTTGCACCCTAGTTACTAGCCGAGCT-5´	MWG Operon, Ebersberg, Germany
NP71-Seq4_Fo	DNA oligo (Oligo hybridisation)	5´-CTAGTAACTTCTGGAGGGGTGAGAATGGACGAAAAACAAGAATTGCTTC-3´	MWG Operon, Ebersberg, Germany
NP71-Seq4_Re	DNA oligo (Oligo hybridisation)	3´-ATTGAAGACCTCCCCACTCTTACCTGCTTTTTGTTCTTAACGAAGAGCT-5´	MWG Operon, Ebersberg, Germany
NP71-Seq44_Fo	DNA oligo (Oligo hybridisation)	5´-CTAGTAACTTCTGGAGGGGTGATTGCTTC-3´	MWG Operon, Ebersberg, Germany
NP71-Seq44_Re	DNA oligo (Oligo hybridisation)	3´-ATTGAAGACCTCCCCACTAACGAAGAGCT-5´	MWG Operon, Ebersberg, Germany
NP71-Seq45_Fo	DNA oligo (Oligo hybridisation)	5´-CTAGTAACTTCTGGAGGGGTGAGAATAAGAATTGCTTC-3´	MWG Operon, Ebersberg, Germany
NP71-Seq45_Re	DNA oligo (Oligo hybridisation)	3´-ATTGAAGACCTCCCCACTCTTATTCTTAACGAAGAGCT-5´	MWG Operon, Ebersberg, Germany
Inno71-5A_Fo	DNA oligo (Oligo hybridisation)	5´-CTAGT AACTTCTGGAGGGGTGAGAATC- 3´	MWG Operon, Ebersberg, Germany
Inno71-5A_Re	DNA oligo (Oligo hybridisation)	3´-ATTGAAGACCTCCCCACTCTTAGAGCT- 5´	MWG Operon, Ebersberg, Germany
NP228/12/45_Pro	DNA PCR primer	5´-GCGCACTAGTAGCAAAAGCAGGGTAGATAATCA -3´	MWG Operon, Ebersberg, Germany
NP21/71_Pro	DNA PCR primer	5´-GCGCACTAGTCCCAGGATGTGCTCTCTGATGCA -3´	MWG Operon, Ebersberg, Germany
NP33_Pro	DNA PCR primer	5´-GCGCACTAGTGCCGCATTTGAAGATCTAAGAGT -3´	MWG Operon, Ebersberg, Germany
NP53_Pro	DNA PCR primer	5´-GCGCACTAGTGAACTCAAACTCAGTGATTATGA -3´	MWG Operon, Ebersberg, Germany
NP61_Pro	DNA PCR primer	5´-GCGCACTAGTAAAGTGGATGAGAGAACTCATCC -3´	MWG Operon, Ebersberg, Germany
NP82_Pro	DNA PCR primer	5´-GCGCACTAGTATGAAAGAATGTGCAACATTCTC -3´	MWG Operon, Ebersberg, Germany
NP92_Pro	DNA PCR primer	5´-GCGCACTAGTTGCCTGTGTGTATGGACCTGCCG -3´	MWG Operon, Ebersberg, Germany
NP228/33_Re	DNA PCR primer	3´- TCTTTTTATGGGAACAAAGATGAGAGCTCTCG -5´	MWG Operon, Ebersberg, Germany
NP12/61_Re	DNA PCR primer	3´- GAGAACAAGCGTGGCCTTACCTAGAGCTCTCG -5´	MWG Operon, Ebersberg, Germany
NP21/92_Re	DNA PCR primer	3´- ACCACACCTACCGTACGGTAAGAGAGCTCTCG -5´	MWG Operon, Ebersberg, Germany
NP45_Re	DNA PCR primer	3´- ACCTGCTAAGATGTAGGTTTACAGAGCTCTCG -5´	MWG Operon, Ebersberg, Germany
NP53_Re	DNA PCR primer	3´- GGATATATGTCCTCTCATTTGCCGAGCTCTCG -5´	MWG Operon, Ebersberg, Germany
NP71_Re	DNA PCR primer	3´- ACCTGCTTTTTGTTCTTAACGAAGAGCTCTCG -5´	MWG Operon, Ebersberg, Germany
NP82_Re	DNA PCR primer	3´- GAGCTCTCGCAACGAGTGTTCAGGACGGACGG -5´	MWG Operon, Ebersberg, Germany
ODN 2216	TLR9 DNA ligand	5'-GsGsGGGACGATCGTCGsGsGsGsGsG- 3'	Invivogen, Toulouse, France
ODN 2395	TLR9 DNA ligand	5'-TsCsGsTsCsGsTsTsTsTCGGCGCGCGCCG-3'	Invivogen, Toulouse, France
ODN 1826	TLR9 DNA ligand	5'-TsCsCsAsTsGsAsCsGsTsTsCsCsTsGsAsCsGsTsT-3'	Invivogen, Toulouse, France
ssRNA40PTO	TLR7/8 RNA ligand	5'-GsCsCsCsGsUsCsUsGsUsUGsUsGsUsGsAsCsUsC-3'	Biomers, Ulm, Germany
ssRNA41PTO	TLR7/8 RNA ligand (Neg. control)	5'-GsCsCsCsGsAsCsAsGsAsAsGsAsGsAsCsAsC-3'	Biomers, Ulm, Germany

2.1.10 Peptides

All peptides were synthesized by JPT Peptide Technologies, Berlin, Germany. Peptides were delivered as lyophilized powder and stored at -20 °C until usage.

Peptides	Company
#79	JPT Peptide Technologies, Berlin, Germany
#TU18.2	JPT Peptide Technologies, Berlin, Germany
#88	JPT Peptide Technologies, Berlin, Germany

2.1.11 Hardware

Programm	Company
Adobe Photoshop CS6	Adobe Systems Incorporated, San Jose, CA
Adobe Illustrator CS6	Adobe Systems Incorporated, San Jose, CA
Excel 2010	Microsoft, Redmond, WA
FlowJo X	TreeStar, Ashland, OR
Graphpad Prism 6	GraphPad Software, San Diego, CA
SYFPEITHI database	Ramensee et al. http://www.syfpeithi.de

2.2 Methods

2.2.1 Chimeric Hepatitis B virus core antigen (HBcAg) derived virus-like particles (VLPs)

HBcAg#CLDN6-VLP constructs were generated as previously described [36] and presented in Figure 2.1. The position of the inserted epitope and glycine linker within the HBcAg backbone differend between the HBcAg backbones i.e. used backbone A (Replacement of HBcAg amino acid sequence from position 74 to 81 by CLDN6 epitope) or H (Replacement of HBcAg amino acid sequence from 79 to 80 by CLDN6 epitope).

Figure 2.1: Schematic representation of recombinant HBcAg-#CLDN6 constructs.

All HBcAg constructs were expressed in the E. coli strain BL21 (DE3) [128]. A starting culture in 10 mL LB medium supplemented with 100 µg/mL Carbenicillin was used to inoculate 2 L TB auto-induction-medium (AIM) that also supplemented with 100 µg/ml Carbenicillin. The expression was stopped 7 hours after inoculation and the cells were harvested via centrifugation. The VPL-containing cells were resolubilized in lysis buffer and the VLPs were released by mechanical disruption of the cells using a Avestin homogeniser. Cell debris and insoluble proteins were removed by centrifugation at 27,000 x g at 4°C for 30 min. For the further purification of chimeric HBcAg VLPs, a modified protocol of Wizemann et al. using mild denaturating conditions was applied [129]. All purification steps are summarized in Figure 2.2. The purity of All purification steps was anaylzed using 12% NuPAGE-SDS-PAGE (ThermoFisher) under reducing conditions (Figure 2.2. b and c).

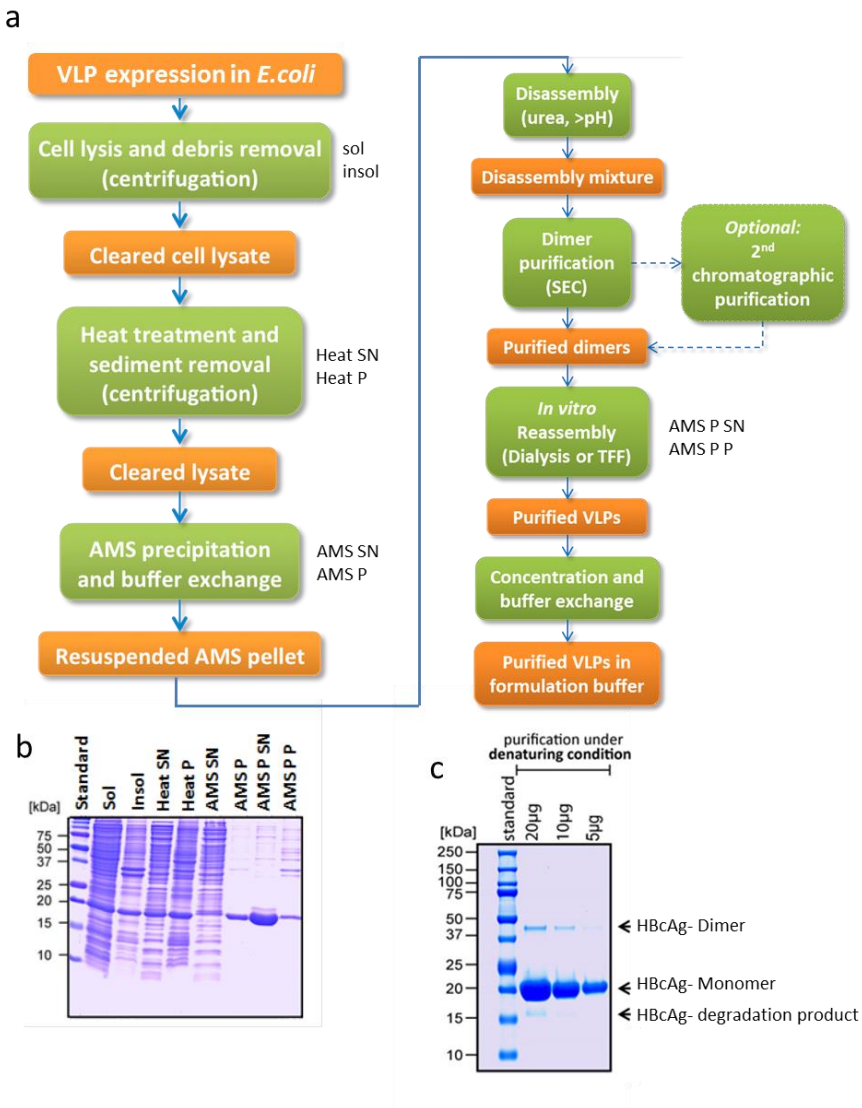

Figure 2.2: Purification of chimeric HBcAg VLPs. a) Workflow of all purification steps required for HBcAg-VLP production. b and c) 12% NuPAGE-SDS-PAGE (ThermoFisher) under reducing conditions, followed by colloidal blue staining. b) In-process-controls of primary recovery including solubility and precipitation steps (Heat and AMS) c) Purity control of HBcAg-#CLDN6-VLPs bevore immunization P = Pellet; SN = Supernatant; AMS = ammonium sulfate precipitation; Sol = Soluble; Insol = Insoluble. SEC = Size Exclusion Chromatography; TFF = Tangential Flow Filtration; Standard: Precision Plus protein standard dual color (Biorad).

2.2.2 Analyses of VLP conformation by Dot blot

A Dot blot presents a simplification of a Western blot and is used to detect biomolecules. For biotinylated HBcAg-CLDN6 VLP detection, nitrocellulose membranes with a pore size of 0.2µm were used. After equilibration in PBS and the subsequent drying of the membrane, the purified samples were continually dotted in 2µL fractions directly onto the nitrocellulose membranes (1µg) until complete adsorbtion. The membranes were treated with blocking buffer (5% (w/v) skimmed milk powder in PBS (w/v)) for 1h at RT and moderate shaking, followed by 1h of incubation with the relevant primary antibody (mAb3120, recognizing correctly assembled VLPs (1:10 000 in 5% (v/v) FBS/DPBS) or streptavidin HRP controlling the biotinylation efficiency (1:4000 in 5% (v/v) FBS/DPBS). After that, the membranes were

washed three times with 0,1% (v/v) Tween20 in PBS (three times with approximately 20ml Wash buffer for 10min). Membranes treated with streptavidin HRP were directly developed by the application of Lumi-Light Western blotting substrate (Pierce) for chemiluminescence detection at a wavelenght of 425nm. Membranes treated with mAB3120 were incubated with a secondary g-α-m-HRP antibody (1:20 000 in 5% (v/v) FBS/DPBS) for 30 min at RT and moderate shaking. Afterwards the membranes were washed again (three times with approximately 20ml Wash buffer for 10min) three times with 0,1% (v/v) Tween20 in PBS and subsequently developed by the application of Lumi-Light Western blotting substrate (Pierce) for chemiluminescence detection at a wavelenght of 425nm.

2.2.3 Native agarose gel electrophoresis

The native agarose gel electrophoresis (NAGE) was applied to analyze the integrity of the purified HBcAg-CLDN6 VLPs. Thereby, gels containing 1% (w/v) of agarose (AppliChem, Darmstadt) in 1x TAE buffer were loaded with 10µg purified CLDN6 VLPs per well. The electrophoresis was performed in 1xTAE buffer for 1-3 h by 50 V. Subsequently, the gels were stained for 30 min by RT under shaking (140 rpm) with PageBlue (Thermo Scientific, Schwerte) and destained ON using water.

2.2.4 Asymmetric Flow Field-Flow Fractionation with Multi-Angle Light scattering

For further analysis of the particles integrity and aggregation states of HBcAg-CLN6 constructs, Asymmetric Flow Field-Flow Fractionation (AF4) coupled with Multi-Angle Light scattering (MALS) was applied. Whereas the AF4 is responsible for size-based separation, the MALS detector (miniDawn TREOS) deliver molar mass and the radius of gyration data of the separated nanoparticles. Bevor loading (10 µl) the samples were sterile filtrated. Data analysis was performed using ASTRA® 6.1-Software.

2.2.5 IsRNA constructs, *in vitro* transcription and purification

Plasmid templates for the in vitro transcription (IVT) of isRNAs were based on the pST1-A120 vector described by Kuhn, A. et al. [130]. The selected double-stranded (ds) Influenza NP DNA fragments (see section 2.1.9) were generated by oligonucleotide hybridization (Section 2.2.6) or amplified by standard polymerase chain reaction (PCR) as described previously using the listed primers (see section 2.1.9) [131, 132]. By PCR assay, the pST1-A120 DNA template bearing the whole NP sequence was applied. Subsequently, the generated ds DNA fragments were cloned between SpeI and XhoI restriction sites of pST1-A120 using standard molecular biology methods, which were cited and described in detail by Holtkamp et al. [133]. The resulting plasmids were linearized with XhoI restriction enzyme (Fermentas, ThermoFisher) and purified by magnetic bead separation using Dynabeads MyOne Carboxylic Acid (Invitrogen). The IVT reaction was performed as described in published protocols [134]. The small-scale purification of in vitro transcribed RNAs was performed with

silica-based membranes using the RNeasy Mini Kit (QIAGEN) according to the manufacturer's instructions. For the large scale purification of IVT RNAs, an FPLC-based method using a weak anion exchange column (HiTrap DEAE Sepharose FF, GE Healthcare) was applied [135]. Purified isRNA was eluted in RNase-free H2O and the RNA concentration was measured by UV260nm spectroscopy on a Nanodrop 1000 (Thermo Scientific, Wilmington, DE, USA). To estimate the isRNA purity and integrity, denaturing or native polyacrylamide gel electrophoresis and Bioanalyzer 2100 (Agilent Technologies, Santa Clara, CA, USA) assays were applied.

2.2.6 Oligonucleotide hybridization

Double-stranded (ds) oligonucleotides with sticky ends for cloning into linearized, dephosphorylated and quality controlled pST1-A120 vectors were generated by hybridization of single-stranded oligonucleotides in a thermocycler at the following conditions:

Hybridization mixture:

16µl	ddH2O
2µl	10x PCR Puffer
1µl	sense Oligo (100µM)
1µl	antisense Oligo (100µM)

Hybridization conditions:

Time	**Temperatur**
15 min	95°C
30 min	80°C
30 min	70°C
30 min	64°C
30 min	60°C
30 min	56°C
30 min	52°C
30 min	48°C
Infinite	45°C

Subsequently, the ds oligonucleotides were directly cloned in a pST1-A120 vector or stored at -20°C.

2.2.7 Liposomes and formulations

Depending on whether they were to be used for *in vitro* or *in vivo* experiments, purified Influenza NP derived isRNAs were formulated with cationic lipids differing in their lipid/helper-lipid composition and surface charge. To ensure an optimal cellular uptake in *in vitro* experiments, isRNAs were formulated with the liposomal composition F5 (50% mol

DOTMA, 50% mol CHOL), whereas the composition F12 (66.6 %mol DOTMA, 33.4% mol DOPE) was used for *in vivo* experiments. F12 formulations permitted a high serum stability of isRNAs and spleen targeting of isRNA-lipoplexes after i.v. administration.

2.2.8 Preparation of immunostimulatory small RNA-lipoplexes (isRNA-LPX)

The isRNA formulation in liposomes F5 or F12 were applied in a laminar air flow cabinet (HERAsafe, Hanau, Germany) under RNAse free and sterile conditions. Lipoplex formation was performed by diluting the isRNA candidate with RNAse free water and 1.5 M NaCl solution followed by adding the needed amount of the Liposomes to achieve the desired charge ratio at a final NaCl concentration of 150 mM. Whereas isRNA-LPX adjuvant for *in vivo* testing was prepared to result in a charge ratio of 1,3:2 (lipid to RNA ratio) using F12 liposomes, the lipoplex formation with a charge ratio of 1:2 was performed with liposomes F5 for the *in vitro* testing. isRNA LPX adjuvant and F5 formulated isRNAs were ready to use after an incubation time of 10 min at RT. RNA-LPX size and zeta potential were measured by photon correlation spectroscopy (PCS; 380 ZLS submicron particle/zeta potential analyzer, PSS Nicomp). Before the retro-orbitale or subcutaneous injection in mice, the isRNA-LPX adjuvant was mixed in a ratio of 1:1 with HBcAg-CLDN6 VLPs and briefly vortexed.

2.2.9 Control adjuvants and synthetic RNA oligonucleotides

The TLR3 agonist Poly (I:C), the TLR7/8 ligand CL097, (a derivative of the imidazoquinoline compound R848) the human TLR8 agonist ssRNA40 complexed with cationic lipid (LyoVec), the human/murine TLR9 agonist type C CpG ODN2395 and the human TLR9 agonist type D CpG ODN2216 were purchased from Invivogen and were used as control adjuvants in various experiments. Bafilomycin A1 (Invivogen) was used as an endosomal acidification inhibitor to block TLR activation. Complete and incomplete Freund's adjuvant (CFA/IFA) were used for s.c. control immunizations according to the manufacturer's instructions (Sigma-Aldrich). The chemically synthesized isRNA NP71-Seq4 (Chem. Synth.) and Poly (A) RNA used as controls were purchased from Biomers.

2.2.10 Synthetic peptides

For several requirements, such as peptide ELISA (See section 2.2.12.2) and IFN-γ ELIspot (See section 2.2.12.7), synthetic peptides with or without a G4SG4 linker were ordered by JPT Peptide Technologies, Berlin, Germany. All peptides were dissolved in DMSO resulting in a concentration of 1 µg/µl. Subsequently, they were stored in 50 µL Aliquots at -20 °C until further use. The applied peptides are listed in section 2.1.10.

2.2.11 Cell Biological Methods

2.2.11.1 Thawing of frozen cells

Cryovials containing frozen cells were removed from liquid nitrogen storage and immediately placed into a 37° C pre-warmed water bath. By gently swirling, cells were quickly thawed and transferred to the laminar airflow hood. Before opening, the vials were externally disinfected with 70% Ethanol. The cell suspension was then pipetted into 10 mL of prewarmed complete growth medium (Section 2.1.1.). After centrifugation (300 x g, 5 min), the medium supernatant was aspirated and the pellet was resuspended in the appropriate cell medium and subsequently seeded in a T75 culture flask (Greiner, Frickenhausen, Germany). Afterward, the cells were incubated for at least one day in an incubator at 37°C and 5% or 7.5 % CO_2 depending on cell-type before further sub-cultivation.

2.2.11.2 Cell culture media

Primary human and mouse cells were cultured in RPMI1640 supplemented with 10% (v/v) heat-inactivated FBS, 1% (v/v) non-essential amino acids (NEAA), 1% (v/v) sodium pyruvate and 0,5% (v/v) Penicillin/Streptomycin solution. Chinese Hamster Ovary (CHO) K1 cells stably transfected with human CLDN6 or human CLDN9 were obtained from TRON gGmbH (Mainz, Germany) and cultured in DMEM supplemented with 10% (v/v) heat-inactivated FBS, 1 mg/mL G418 and 0.5% (v/v) Penicillin/Streptomycin solution. Wildtype human embryonic kidney (HEK) 293 cells or HEK293 cells stably co-expressing human TLR3, TLR7 or TLR8 and an NF-κB-inducible luciferase reporter gene were obtained from (Invivogen) and cultured in DMEM supplemented with 10% (v/v) heat-inactivated FBS, 1% (v/v) NEAA, 1% (v/v) sodium pyruvate and 0.5% (v/v) Penicillin/Streptomycin solution. Depending on the HEK293 transfectant used, the medium was additionally supplemented with Blasticidin (10 µg/ml), Zeocin (100 µg/ml) or Geneticin (250 µg/ml), all from Invivogen. FBS was purchased from Biochrom and all other cell culture reagents from Gibco.

2.2.11.3 Cultivation of cell lines

All used cell lines and tumor cells were thawed as described in section 2.2.11.1 and cultured in their corresponding growth medium (See section 2.2.11.2). For further sub-cultivation, the cells were detached by aspirating the culture medium, adding an appropriate amount of Accutase solution (Sigma-Aldrich, Schnelldorf, Germany) and incubated at 37°C for 5 min. After dissolving, 10 mL of cell culture medium was added and the cells were resuspended by gently pipetting up and down. Afterwards, cells were counted as described in section 2.2.11.4 and seeded into a new culture flask with 175 cm^2 growth surface area (Corning, Sigma-Aldrich, Schnelldorf, Germany).

2.2.11.4 Cell Counting

Cell numbers and their viability were measured using an automated Vi-CELL XR cell viability analyzer (Beckman Coulter, Krefeld, Germany) or a Neubauer hemocytometer (Brand,

Wertheim, Germany). When cell counting using a Neubauer chamber, a standard procedure was performed as previously described by Strober et al. [136]. The Vi-Cell cell counting method combines the standard trypan blue staining method for determination of cell viability and cell counting using the advanced digital image technology. The Vi-cell instrument requires 500 µL of sample volume, which is mixed in a ratio of 1:1 with trypan blue. Based on cell type specific parameters (Table 2.1) the Vi-Cell can define cell concentration, viability and other parameters.

Table 2.1: Cell type specific parameters of the Vi-cell XR cell viability analyzer.

Parameters	CHO-K1-WT	CHO-K1-CDN6	CHO-K1-CDN9	Spleen, BM	BMDCs	hu PBMCs	CT26_WT	CT26_CLDN6	HEK-WT	HEK-TLR
Minimum diameter (µm)	8	5	5	3	3	5	9	10	11	10
Maximum diameter (µm)	24	50	50	25	25	16	26	26	24	40
Number of images	50	20	20	25	25	15	50	50	50	20
Aspirate cycles	1	1	1	1	1	1	1	1	1	1
Trypan blue mixing cycles	3	2	2	3	2	2	3	3	3	2
Cell brightness (%)	85	85	85	90	90	85	81	80	79	90
Cell sharpness (%)	100	100	100	90	95	100	65	70	70	100
Viable cell spot brightness	85	65	65	85	65	55	87	95	5	90
Viable cell spot area (%)	5	5	5	8	5	5	10	10	7	6
Minimum circularity	0	0	0	0	0	0	0	0	0,9	0
Decluster degree	Medium	Medium	Medium	Medium	Medium	Medium	Low	Low	Medium	Medium

2.2.11.5 Freezing of cells

Concentration and viability of cells were determined using Vi-Cell XR cell viability analyzer (Beckman Coulter, Krefeld, Germany) (See section 2.2.11.4). Subsequently, 2-5 x 10^6 cells were centrifuged (300 x g, 5 min) and the SN aspirated. Afterwards, the cells were resuspended in 500 µL of FBS (Not heat inactivated) and transferred into 4° C pre-cooled 2 mL cryogenic storage vials (Greiner Bio-One, Frickenhausen, Germany). 500 µL of freezing medium (See section 2.1.1.) was added to the resuspended cells and the vials were inverted 2-3 times. The vials were transferred into a 4° C precooled freezing container (Mr. Frosty, Thermo Scientific, Braunschweig, Germany). The freezing container (Mr. Frosty) was stored overnight at -80° C. The next day thecryogenic storage vials had to be transferred into the vapor phase of liquid nitrogen for long-term storage.

2.2.11.6 Isolation of human PBMCs and pDCs

Human PBMCs were freshly isolated from blood of donors by Ficoll density gradient centrifugation as described in Lin, Z. et al.[137]. Plasmacytoid dendritic cells (pDCs) were isolated from human PBMCs using MACS-separation technology and the CD304 MicroBead Kit (Miltenyi Biotec).

2.2.11.7 Isolation of mouse bone marrow cells, splenocytes, pDCs and cDCs

Mouse bone marrow cells (BMCs) were harvested from murine femurs and tibias using standard protocols. Erythrocytes were lysed by incubation for 5 min with 5 mL cold Red Blood Cell (RBC) lysis buffer (Sigma-Aldrich), followed by the addition of 20 mL of 1x PBS (Gibco) to stop the lysis reaction. BMCs were pelleted by centrifugation and resuspended in

cell culture medium. Mouse splenocytes were prepared as described in Kreiter, S. et al. PDCs were isolated from splenocytes by MACS-separation (See section 2.2.12.3) using the mouse pDC isolation kit II (Miltenyi Biotec). Conventional DCs (cDCs; CD11c high, B220 low) were generated from mouse BMCs by cultivation for 6 days in the presence of 20 ng/mL GM-CSF and 20 ng/mL IL4 (both from Peprotech).

2.2.12 Immunological Assays

2.2.12.1 Complement-dependent cytotoxicity (CDC) assay

To analyze antibody-mediated cytocidal effector functions, complement-dependent cytotoxicity (CDC) assays were performed. CHO-K1 cells stably expressing human CLDN6 were incubated at a concentration of $1x10^4$ cells/well in a 96-well plate (Corning Costar, Sigma-Aldrich) for 17.5 h at 37°C and 7.5 % CO_2. Subsequently, the cells were incubated for 80 min in a total volume of 50 µL/well with 5 µL polyclonal mouse antiserum diluted in 32 µL culture medium and 13 µL human serum complement (Quidel Corporation) as a complement source. Mouse sera were derived from immunizations experiments with differently adjuvanted HBcAg-#A79 VLPs. A CLDN6 specific monoclonal antibody (Ganymed Pharmaceuticals AG, Mainz) in a concentration of 600 or 150 ng/mL was used as a positive control. Heat-inactivated human serum complement served as negative control and for confirmation of a complement dependent antibody-mediated cytolytic effect. Untreated cells and cells lysed by Triton X-100 (Applichem) were used as benchmarks for 0% and 100% cell lysis respectively. Cell viability was analyzed with the XTT-assay based Cell Proliferation Kit II (Roche Diagnostics) according to the manufacturer's instructions. Absorption at 480 nm was measured with Infinite M200 Pro reader (Tecan). The antibody-mediated cytolytic activity was calculated using the following equation:

% cell lysis = 100 - ((Signal antiserum – (Signal 100% lysis/Signal 0%lysis)) x 100)

2.2.12.2 Mouse immunoglobulin isotyping ELISA

Streptavidin-coupled 96-well plates (Nunc, ThermoFisher) were coated for 1 h with 100 ng/well of biotinylated #A79-peptide (JPT Peptide Technologies) followed by blocking of uncoated surfaces for 1 h with 300 µL/well 1x PBS, 2% (v/v) FBS and washing with 1x PBS, 0,05% Tween20 (Sigma-Aldrich) using a HydroSpeed plate washer (Tecan). Polyclonal mouse antisera were 10-fold serially diluted with 1x Casein blocking buffer (Sigma-Aldrich) and 100 µL of diluted sera were added per well and incubated for 1 h with slight agitation on a shaking platform (Infors). Bound antibodies were detected after additional washing steps by incubation for 1 h with 1:5000 diluted, HRP-conjugated, goat anti-mouse IgG isotype-specific secondary antibodies (ThermoFisher) followed by final wash steps and the addition of TMB-substrate (Sigma-Aldrich) according to the manufacturer's instructions. Absorption at 450 nm was measured with an Infinite M200 Pro reader (Tecan). All steps were performed at room temperature and antiserum dilutions were measured in triplicates.

2.2.12.3 Magnetic-Activated Cell Sorting

Immune cell enrichment was performed using Magnetic-Activated Cell Sorting (MACS) technologies. Specific monoclonal antibodies with small magnetic beads specifically bound to surface proteins and accordingly the cells can be selectively magnetically separated. MACS was performed according to the manufacturer's instructions. The appropriate cells were stained with beads conjugated antibodies in MACS buffer for 15-20 min at 2-8 °C. Subsequently, the cells were washed one time with approximately 5-10 mL of MACS buffer per 10^8 cells and afterward, the cells were resuspended up to 10^8 cells in 500 µL of buffer and added to a MACS column LS placed in the magnetic field and pretreated with 2 mL MACS Buffer. Subsequently, the cell suspension was applied onto the column, followed by three wash steps with 3 mL of MACS buffer. The column was removed from the separator magnet and the labeled cells were eluted by addition of 5 mL of MACS buffer by pushing a plunger into the column.

2.2.12.4 Flow cytometry

Induction of specific antibodies against the native CLDN6 protein after immunization with adjuvanted or non-adjuvanted HBcAg-#A79 VLPs was analyzed by flow cytometry. 2x10^5 CHO-K1 CLDN6 or CLDN9 cells per well were incubated for 1 h at 4°C with polyclonal mouse antiserum diluted 1:100 in FACS-buffer (1x PBS, 5% (v/v) FBS, 5 mM EDTA). After three wash steps, the cells were stained for 30 min at 4°C with an AlexaFluor 647-conjugated goat anti-mouse IgG (H+L) secondary antibody (ThermoFisher, Schwerte, Germany) diluted 1:600 in FACS-buffer. Unbound antibodies were removed by additional wash steps and the viability was determined using 7-AAD (Sigma-Aldrich, Steinheim, Germany). Fluorescence signals of living cells were detected by a FACS Canto II system (BD Biosciences).

2.2.12.5 Immunofluorescence Staining

Immunofluorescence (IF) staining was performed as previously described [36]. In brief, the coverslips were coated with poly-L-lysine for 1 hour at room temperature to improve the cell adhesion, washed with 10 mL dH2O and coated with $2{,}0x10^4$ - $5{,}0{\cdot}10^4$ CHO-K1 cells stably transfected with human or murine CLDN6 or CLDN9 protein for 24 hours. After washing the cells were stained under native conditions with the mouse antiserum and control monoclonal antibodies (See Section 2.1.6). Subsequently, the cells were washed, fixated in 100 % methanol (-20°C) for 5 min at 4°C. Afterwards, the fixed cells were washed (PBS) and incubated with secondary antibodies (g-α-r/-m –Cy/-DyLight) for 30 min at RT in the dark. Slides were washed, mounted in fluorescence mounting medium, and images were performed with Zeiss Imager-M2 Axio fluorescence microscopes (Carl Zeiss AG, Oberkochen, Germany).

2.2.12.6 Cytokine detection

IFN-α and other selected cytokines were detected in the supernatants from human or mouse cells or in mouse blood serum using commercially available ELISA kits (PBL Assay Science) or the Bio-Plex system using Bio-Plex Pro Kit III and cytokine-specific Bio-Plex coupled magnetic beads (BioRad) following the manufacturer's instructions.

2.2.12.7 IFN-y ELISpot analysis

$5x10^5$ freshly isolated mouse splenocytes were incubated in a 96-well plate (Merck Millipore) coated with anti-IFN-y monoclonal antibody (10 µg/mL AN18, Mabtech) in the presence of 5µg/mL #A79 or an irrelevant peptide (JPT Peptide Technologies) for 18 h at 37°C. Plates were sequentially incubated with biotin-conjugated secondary anti-IFN-y monoclonal antibody (R4-6A2, Mabtech) and ExtrAvidin-Alkaline Phosphatase (Sigma-Aldrich) before cytokine secretion was detected by adding BCIP/NBT substrate (Sigma-Aldrich). For each group technical triplicates were performed. Plates were scanned and analyzed using an ImmunoSpot S5 Versa ELISpot analyzer, ImmunoCapture software 6.3 and ImmunoSpot software 5.0.3 (all Cellular Technology Ltd.).

2.2.12.8 *In vitro* stimulation of cells with isRNAs

Cell stimulation with isRNAs or controls was performed in triplicates in 96-well plates (Corning) with a total volume of 200 µL. Unless otherwise noted 5x10^5 cells per well were used and stimulated for 12-16 h at 37°C and 5% CO2 with F5-formulated isRNAs in a concentration of 0.167 µg/well or control reagents using concentrations as indicated in the examples.

2.2.12.9 *In vivo* stimulation and immunization experiments

For *in vivo* stimulation experiments, Balb/c mice were injected i.v. in their retrobulbar venous plexus with different amounts of F12-formulated isRNAs. Depending on the experimental setup, blood samples for serum preparation were collected at different time points after injection as indicated in the examples. Blood serum was prepared after clotting by centrifugation using standard protocols and was stored until further use at -20°C. Immunization experiments were performed by i.v. injection of 20 µg F12-formulated isRNAs mixed with 50 µg purified HBcAg-#A79 VLPs (total volume 100 µL) into the retrobulbar venous plexus. Unless otherwise indicated, three injections were applied with two weeks intervals and the final blood samples were taken 10 days after the last immunization. Preparation of blood serum was performed as described previously.

2.2.13 Animals

2.2.13.1 Housing and mouse strains

Female Balb/cJRj and C57BL/6 mice were obtained from Janvier Laboratories (France). BDCA2-DTR transgenic mice bred on a C57BL/6 background express the simian diphtheria toxin receptor (DTR) specifically in plasmacytoid dendritic cells (pDCs) and were purchased from the Jackson Laboratory (USA). Mice were 6 to 10 weeks of age at the onset of experiments. All animals were maintained under pathogen-free conditions.

2.2.13.2 Anesthesia

Animals were anesthetized using a composite of 2.5% isoflurane and oxygen. Mice were taken in an anesthesia chamber (Perkin Elmer, Waltham, MA, USA) and kept until movement stopped. Subsequently, mice were taken out of the chamber. The followed experimental procedure was performed within 10-30 s before the mice woke up.

2.2.13.3 Blood extraction and serum preparation

Mice were anesthetized and blood was retrieved via the retro-orbital vein using a microhaematocrit capillary tube (BRAND, Wertheim, Germany). To detect the antibody response, the serum was needed. For serum preparation blood was directly transferred into a Micro tube 1.1 mL Z-Gel (Sarstedt, Numbrecht, Germany). After centrifugation (15,000 x g, 5 min) the cells could be removed and the obtained serum was stored at -20°C until further use.

2.2.13.4 Tumor Models

To analyze the antitumoral efficacy of the cancer vaccine candidates, tumor cells (Table 2.2) were inoculated s.c. to the right flank of mice (s.c. model). Tumor growth was measured by caliper every 2-3 days using the formula $(A \times B^2)/2$ (A is the largest and B the smallest diameter of the tumor). For induction of lung tumors (i.v. Model), tumor cells were injected intravenously into the tail vain of mice. For this, mice were kept for 1-5 min under red light and transferred into a restrainer. The health condition of mice was frequently monitored and documented. Animals were sacrificed as soon as signs of distress, breathing problems (For i.v. and s.c.) or a tumor volume above 1500 mm^3 (only s.c. model) occurred. For i.v. model, the tumor nodules were counted after ink staining and formalin fixation (see section 2.2.13.5)

Table 2.2: The used tumor cell lines which stably transfected with mmCLDN6

Tumor Cell line	Genetic background	Tissue origin	Cell number/ injection	Injection volume	Injection route
CT26_mmCLDN6	Blab/c	Colon carcinoma	1x106 cells/mice	100 µl	s.c and i.v.
E0771_mmCLDN6	C57BL/6	Colon carcinoma	2x105 cells/mice	100 µl	s.c.

2.2.13.5 Staining and Counting of Lung Tumor Nodules

Staining and counting of lung tumor nodules were performed as described by Kreiter et al. [138]. Briefly, mice were sacrificed 14-17 days after tumor inoculation. The trachea was pinched off with forceps above the injection site to direct the pressure into the lung. After injection of the tracheal ink (See section 2.1.1), the lung was excised, washed with PBS, transferred to approximately 5 mL of Fekete's solution (See section 2.1.1) and incubated overnight at 2-8 °C. The tumor nodules were quantified by the size and counted so that a nodule twice as large as a the smallest nodule in the experiment would count for two tumor nodules and so forth. The maximum number of counted nodules was 500 (everything above 500 was indistinguishable).

2.2.14 *In silico* analysis

2.2.14.1 MHC binding prediction

MHC binding prediction was performed using SYFPEITHI. It is a database of MHC ligands and peptide motifs [139] comprising more than 7000 peptide sequences known to bind class I and class II MHC molecules.

2.2.14.2 Statistical analysis

All results are expressed as mean +/- standard error of the mean (SEM). Statistical calculations were performed using GraphPad Prism software version 6. T-test was used to compare two groups. For more than two groups one-way ANOVA was used. The difference between the groups were considered to be statistically significant when $P<0.05$.

3 Results

3.1 HBcAg-VLPs as model antigens for the evaluation of isRNA-LPX adjuvants.

In this thesis, liposomally formulated immunostimulatory RNAs (isRNAs) also designated as isRNA lipoplexes (isRNA-LPX), should be developed and evaluated as potential adjuvants used in combination with protein-based vaccines for active cancer immunotherapy. Hence, the proper evaluation and selection of isRNA-LPX candidates required a well characterized antigen and an antigen-carrier platform, which has to be recognized and taken up by APCs.
The antigen-carrier platform used in this thesis was based on chimeric HBcAg-VLPs that had been developed and optimized by BioNTech Protein Therapeutics GmbH in recent years. VLPs represent biological nanoparticles consisting of one or more viral envelope or structural proteins but no viral genome. Therefore, VLPs are non-infectious and already entered the clinics as prophylactic vaccines against viruses from which they originated. The high intrinsic immunogenicity of HBcAg-VLPs can be transferred to heterologous epitopes (e.g. derived from cancer antigens) inserted at specific sites of the HBcAg molecule. These chimeric HBcAg-VLPs retain the immunological properties of wildtype (WT) HBcAg-VLPs and are able to induce long-lasting, high titer antibody responses against the inserted epitopes. Reasons for the observed high immunogenicity are mainly based on biochemical and especially biophysical properties, like the VLP size in the nanometer range (diameter <50 nm) and the highly repetitive, dense display and optimal spacing of the inserted heterologous antigen epitopes [34]. Accordingly, chimeric HBcAg-VLPs were used as model antigens to evaluate isRNA-LPX adjuvants with the aim to increase the immunogenicity of this vaccine format.

3.1.1 Chimeric HBcAg-VLPs are mainly bound by naïve B cells.

Several publications reported that the first APCs interacting with HBcAg-WT VLPs are mainly naïve B cells [34, 140]. However, at later time points DCs and macrophages are also able to take up immune complexed HBcAg-WT VLPs. When designing a new adjuvant for chimeric HBcAg-VLPs, in which prominent HBcAg-WT epitopes responsible for naïve B cell binding are replaced by foreign epitopes, the primary APCs should be known in advance, in order to design an adjuvant with high specificity and stimulatory activity with regard to this cell type.
Therefore, in a first set of experiments, chimeric HBcAg-VLPs were generated as described previously [36] and were biotinylated with increasing amounts of Sulfo-NHS-Biotin followed by removal of non-bound, free Biotin using dialysis. To analyze the biotinylation efficiency and correct morphology of biotinylated chimeric HBcAg-VLPs simultaneously, dot blot analysis was performed and the results are presented in Figure 3.1.

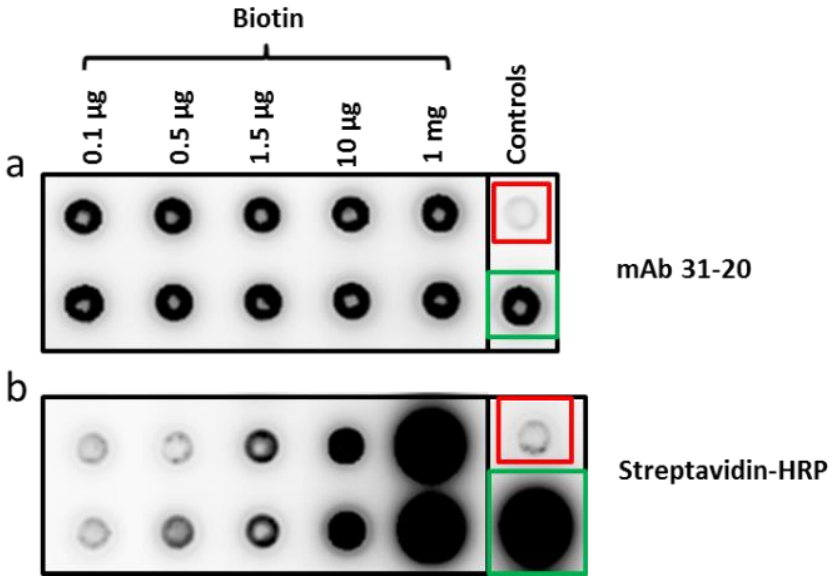

Figure 3.1: Dot blot analysis of biotinylated chimeric HBcAg-VLPs. 1µg of biotinylated, chimeric HBcAg-VLPs were dotted on a nitrocellulose membrane and analyzed for biotinylation efficiency and correct VLP morphology. **a)** Conformation stability of biotinylated, chimeric HBcAg-VLPs was controlled by mAb31-20 specifically recognizing correctly assembled VLPs. Coating of buffer (red box) served as negative control and considered as background. Coating of non-biotinylated chimeric HBcAg-VLPs was used as a positive control (green box). mAb 31-20 binding was detected with an HRP-conjugated goat anti-mouse IgG as a secondary antibody diluted 1:20 000 followed by substrate incubation. **b)** Biotinylation efficiency was analyzed using 1:4000 diluted streptavidin conjugated HRP, followed by substrate incubation . Buffer coating (red box) served as negative control. A biotinylated protein was used as a positive control (green box). Signal detection for a) and b) was conducted by an ImageQuant LAS system.

Starting from 1.5µg biotin, a dose-dependent biotinylation of chimeric HBcAg-VLPs could be demonstrated using streptavidin conjugated HRP (Figure 3.1 b). No biotinylation was detected if 0.1µg or 0.5µg biotin were applied for biotinylation. The analysis of the effect of the biotinylation process on the correct VLP morphology (Figure 3.1 a) revealed no significant change when using the HBcAg-VLP conformation specific mAb 31-20 for VLP detection. Regardless of the amount of biotin used, the chimeric HBcAg-VLPs remained their native conformation.

In a next step, the correct morphology of biotinylated, chimeric HBcAg-VLPs was aditionally analyzed by an antibody-free detection method. Therefore, we applied AF4-MALS to analyze the integrity and the aggregation status of biotinylated, chimeric HBcAg-VLPs. The AF4-MALS method separated nanoparticles of different sizes by asymmetrical flow field-flow fractionation (AF4) followed by Multi-Angle Light Scattering (MALS) analysis. By using MALS, the light scattering intensity of the separated nanoparticles was measured at different discrete angles. The molar mass and the radius of gyration (rg, corresponding to the root mean square radius) served as main readout parameters. The obtained results of the AF4-MALS analysis of biotinylated, chimeric HBcAg-VLPs are shown in Figure 3.2.

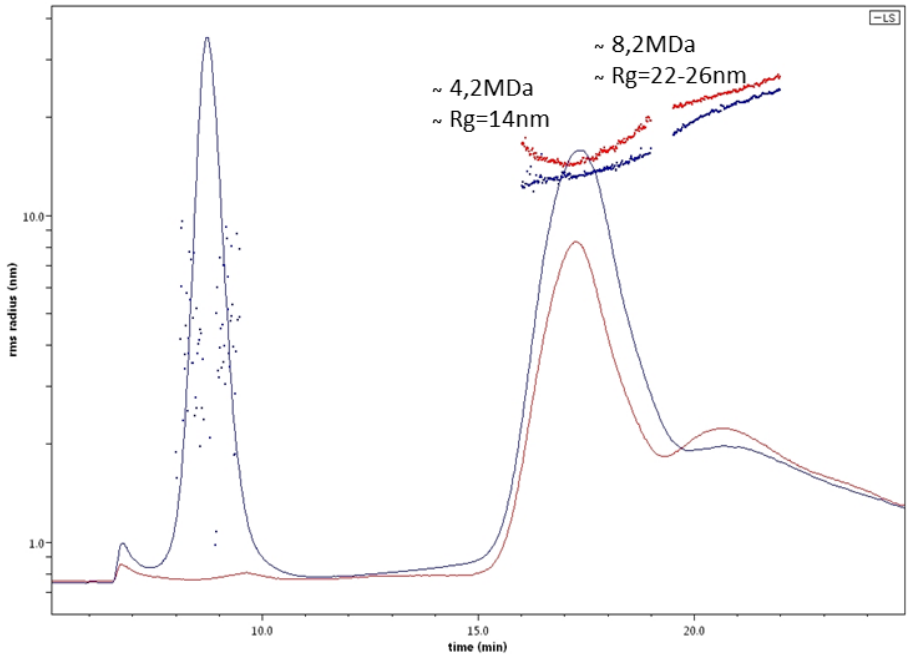

Figure 3.2: AF4-MALS analysis of biotinylated, chimeric HBcAg-VLPs. Illustrated are the fractograms of biotinylated, chimeric HBcAg-VLPs (1mg HBcAg-VLPs mixed with 10µg Biotin) separated and characterized by AF4-MALS. The detection was performed by using the light scattering detector. The blue line corresponds to biotinylated, chimeric HBcAg-VLPs without applying spin column purification for eliminating the biotin excess. The red line corresponds to biotinylated, chimeric HBcAg-VLPs with biotin excess elimination by spin column purification. MDa: megadalton; Rg: radius of gyration; nm: nanometer.

The fractograms of biotinylated, chimeric HBcAg-VLPs with or without applying elimination of free biotin excess revealed the presence of more than one subpopulation. The first peak (blue line, no elimination of free biotin) corresponded to biotin as the smallest particle in the sample. Its elimination by spin column purification can be detected by MALS analysis (red line, missing first peak). The additional peak in both samples with a resolution time of approx. 17.5 min represented HBcAg-VLPs monomers with a molecular weight of ~4,2 MDa. The shoulder of this peak (resolution time approx. 21 min) represented HBcAg-VLP dimers (~8,2 MDa). The formation of undesired chimeric HBcAg-VLP aggregates could be not detected.

The dot blot and AF4-MALS data revealed that biotinylation of chimeric HBcAg-VLPs was successfully achieved without affecting the native conformation of correctly assembled VLPs and not leading to VLP aggregates. Therefore the quality controlled, biontinylated, chimeric HBcAg-VLPs could be used for subsequent *in vitro* cellular binding assays.

In vitro analysis of cellular VLP-binding experiments was performed by incubating purified whole human PBMCs with increasing amounts of biotinylated, chimeric HBcAg-VLPs purified from free biotin. In addition to the analysis of chimeric HBcAg-VLP binding to naïve B cells and DCs (monocytes), as described in the literature, NK cell and T cell binding was analyzed too. VLP-binding to specific PBMC subpopulations was identified by flow cytometry using fluorescent dye labeled mAbs against cell type specific surface markers. VLP-binding was calculated as % of all cells of a given subpopulation bound to biotinylated, chimeric HBcAg-VLPs as shown in Figure 3.3.

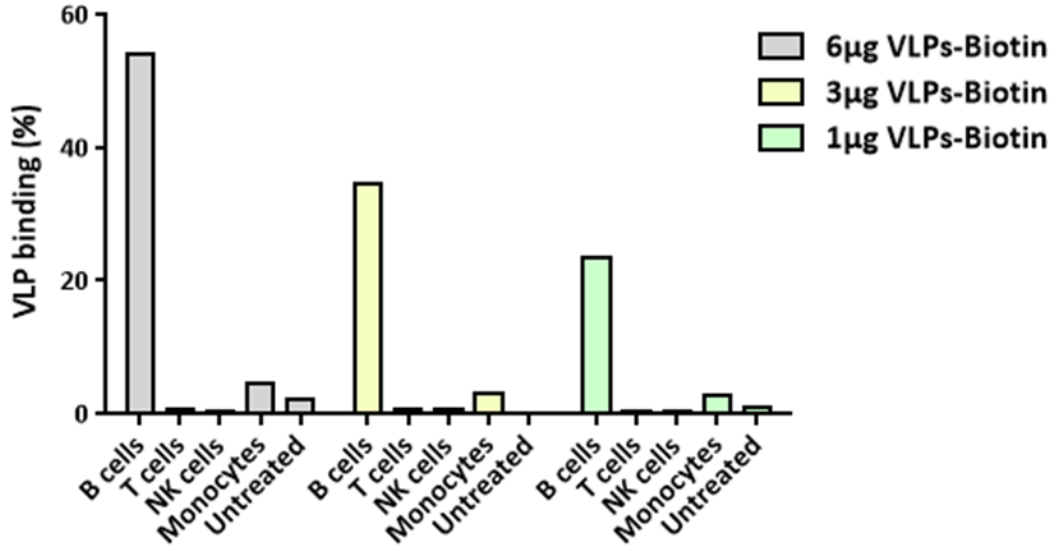

Figure 3.3: Flow cytometric analysis of biotinylated, chimeric HBcAg-VLPs binding to immune cells. $1x10^6$ whole human PBMCs were incubated with 1µg, 3µg or 6µg biotinylated chimeric HBcAg-VLPs for 1h on ice. Afterwards, the cells were washed extensively with PBS and incubated with streptavidin-APC (BD); CD19-PE (BD); CD11c-FITC (Miltenyi), CD16-PerCP-Cy 5.5 (BD) and CD3-PE-Cy7 (BD) for 30 min on ice and protected from light. Aqua live dead reagent was used to gate only for viable cells. Untreated cells (negative control) corresponded to cells only stained with cell type specific reagents, but not incubated with biotinylated, chimeric HBcAg-VLPs.

The *in vitro* cellular binding assay clearly demonstrated that naïve B cells are the main cell type to which biotinylated, chimeric HBcAg-VLPs are bound. A dose-dependent binding of biotinylated VLPs on B cells was detectable, indicating that naïve B cells could also bind to the used chimeric HBcAg-VLP model antigen, despite a partial deletion of the amino acid residues 76-85 located in the MIR of HBcAg that was described to be necessary for naïve B cell binding of VLPs [141]. Only a small portion (<5 %) of all monocytes (including DCs) were able to bind the chimeric HBcAg-VLPs whereas NK and T cells showed no ability to bind the used biotinylated, chimeric HBcAg-VLPs.

3.1.2 Selection of CLDN6-epitope displaying chimeric HBcAg-VLPs.

The tight junction protein CLDN6 is an embryonically expressed antigen, which is largely absent in healthy adult tissue. However, CLDN6 is highly expressed in a wide range of cancers, such as ovarian cancer and non-small-cell lung cancer [142-144]. Therefore, CLDN6 was described as an ideal tumor-associated antigen (TAA) and was used in an accompanying study of BioNTech Protein Therapeutics GmbH to identify immunogenic epitopes displayed on the surface of chimeric HBcAg-VLPs.

Various CLDN6 epitopes were selected and genetically inserted in the HBcAg MIR. To increase the variability of the used non-modular HBcAg display platform, a set of different HBcAg backbones were tested. Each backbone was characterized by a specific epitope insertion site, thereby replacing different amino acids located in the HBcAg MIR. The main goal of this accompanying study was to design chimeric HBcAg-VLPs carrying a CLDN6 epitope, which can induce a target-specific immune response against the whole CLDN6 protein in its native conformation on the surface of living cells. The cloning, production and

screening process of potential chimeric CLDN6 HBcAg-VLP lead structures fulfilling the above mentioned main goal was based on biochemical (e.g. solubility of the chimeric VLPs after expression in *E.coli*) and immunological parameters. However, these processes were not part of this thesis and will be described elsewhere.

In order to develop a RNA-based adjuvant to enhance the immunogenicity of chimeric HBcAg-VLPs (and other protein-based vaccines), representing the main objective of this thesis, two chimeric CLDN6-epitope displaying HBcAg-VLPs were initially selected based on the results of the above mentioned immunological screening studies. In mouse immunization experiments, both chimeric HBcAg-CLDN6 VLPs elicited a weak but detectable antibody-response against the CLDN6 protein that could be slightly enhanced by standard R&D adjuvants like CFA/IFA. Therefore, both chimeric HBcAg-CLDN6 VLPs were suited for the development of isRNA-adjuvants further improving the immunogenicity of these vaccines and comparing the results to standard adjuvants.
The selected CLDN6 epitopes and there main characteristics (sequence, position in CLDN6 and epitope prediction) are presented in Figure 3.4.

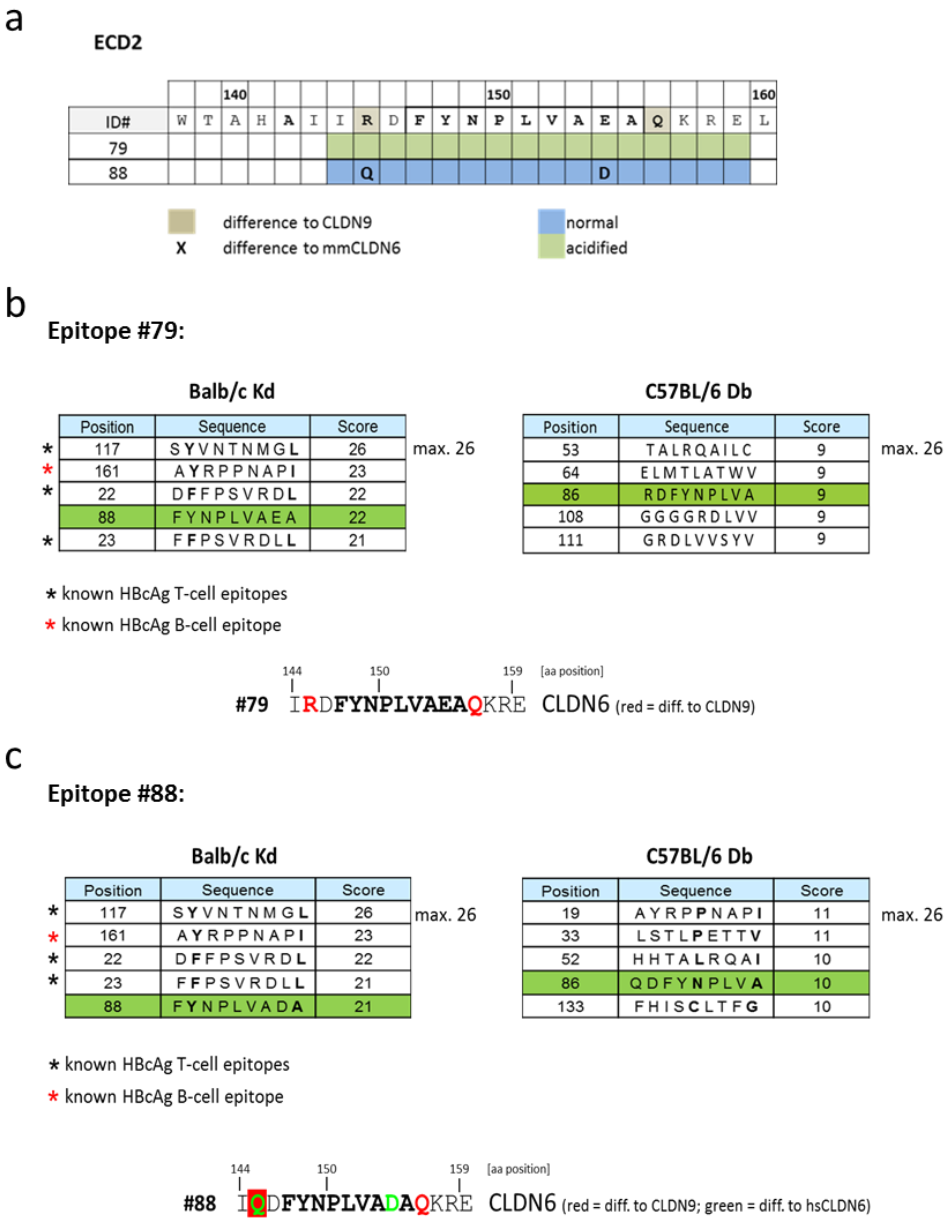

Figure 3.4: The selected CLDN6 epitopes #79 vs. #88. a) Amino acid (aa) sequence comparison between epitope #79 and #88. While #88 (blue) was not modified, #79 (green) was flanked by adding glutamic acid linkers on the epitope N and C terminus when inserted into HBcAg. The epitope position according to the human CLDN6 extracellular domain 2 (ECD2) is indicated. Amino acids with light brown underlay color represent aa that differ in human CLDN6 from the closely related human CLDN9 protein. Bold aa in the #88 epitope sequence indicate aa specific for murine CLDN6. **b)** and **c)** Prediction scores for Kd (Balb/c mice) or Db (C57BL6 mice) restricted T cell epitopes within epitope #79 and #88. T cell epitopes located in #79 or #88 are marked by green cells. Black * indicate HBcAg T cell epitopes known from the literature. Red * indicate known HBcAg B cell epitopes. The maximal (max.) score achieved in the *in silico* prediction is presented on the right side of the table. For prediction using SYFPEITHI software [145] the whole sequence of the respective HBcAg construct (HBcAg-#A79 or HBcAg-#H88) was used. The sequence under the tables illustrates the selected #79 or #88 sequence, the position of the predicted T cell epitope within #79 or #88 and aa differences to CLDN9 or human CLDN6 (#88 only).

The epitope #79 (IRDFYNPLVAEAQKRE) was derived from the extracellular domain 2 (ECD2) of the human CLDN6 protein. #79 differed from the corresponding sequence part of the closely related human CLDN9 protein (I**Q**DFYNPLVADA**L**KRE) and the murine CLDN6 orthologue epitope #88 (I**Q**DFYNPLVA**D**AQKRE) in only two amino acid positions (Figure 3.4. a). CLDN9, as the most related CLDN family member to CLDN6, was applied as a control for

testing the cross-reactivity of the induced antibody responses in most subsequently performed immunological studies.

Two different HBcAg backbones were used as carriers to generate chimeric HBcAg-CLDN6 #79 or #88 VLPs. Peptide #79 was inserted in the MIR and replaced aa 74-81 (Backbone A; resulting in HBcAg-#A79 VLPs), whereas peptide #88 was replacing aa 79-80 (Backbone H; resulting in HBcAg-#H88 VLPs) of the HBcAg-WT protein. In addition, epitope #79 and #88 were flanked on both sides with glycine-rich linkers (G_4SG_4) for increased flexibility before insertion into the HBcAg backbone [36].

Insertion of heterologous epitopes into the MIR of HBcAg might result in insoluble and/or misfolded HBcAg monomers or VLPs. Billaud *et al.* discovered that the addition of glutamic or aspartic acid residues on both sides of the epitope could significantly improve the solubility and correct assembly of chimeric HBcAg-VLPs [146]. Thus, epitope #79 but not #88 was additionally flanked on the C and N terminus with two glutamic acid linkers (G_4SG_4-EE-#79-EE-G_4SG_4) to increase proper folding and assembly (Figure 3.4. a).

Unexpectedly, the epitopes FYNPLVA**E**A from sequence #79 and FYNPLVA**D**A from sequence #H88 were predicted as potential T cell epitopes restricted to MHC class I H2-Kd molecules (Balb/c mice). The predicted scores for #79 or #88 Kd epitopes (score = 22 or 21) were comparable to those of known T cell epitopes from the HBcAg backbone molecule (scores 21-26) described in the literature. In contrast, prediction scores of potential T cell epitopes within #79 or #88 restricted to MHC class I H2-Db molecules (C57BL6J mice) were much lower (9 or 10), whereas known Db restricted T cell epitopes from the HBcAg carrier reached scores up to 26. However, for both CLDN6 epitopes it should be noted for further immunological studies that they might represent a combined B and T cell epitope in Balb/c mice.

3.1.3 Production and quality control of chimeric HBcAg-CLDN6 VLPs.

For subsequent immunization studies evaluating the immunostimulatory potency of isRNA-based adjuvants, both chimeric HBcAg-CLDN6 VLP constructs (HBcAg-#A79 and HBcAg-#H88 VLPs) were produced as previously described [36] (See section 2.2.1). Afterwards, diverse quality control (QC) methods for identity, purity and correct VLP assembly were performed. A QC example for HBcAg-#A79 VLPs purified under R&D conditions is shown in Figure 3.5.

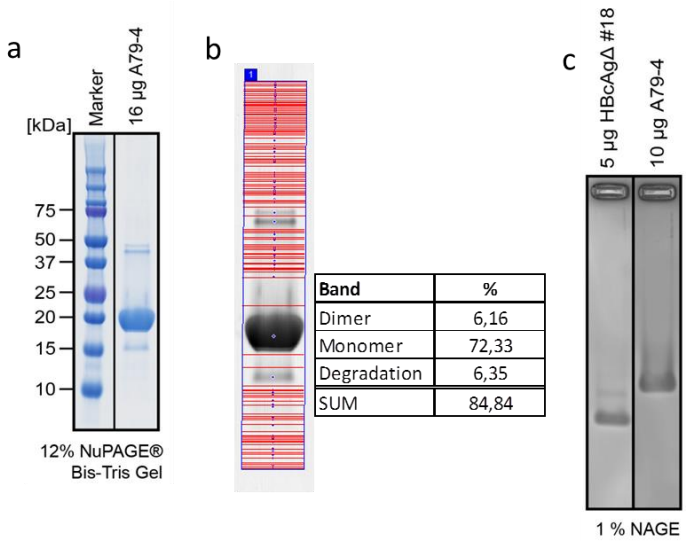

Figure 3.5: Quality control of chimeric HBcAg-#A79 VLPs. a) 12% NuPAGE-SDS-PAGE under reducing and denaturing conditions, followed by colloidal blue staining. 16µg HBcAg-#A79 VLPs in Tris buffer were loaded onto the gel. Marker: PageRuler marker. **b)** Densitometric analysis of colloidal blue-stained NuPAGE-SDS-PAGE from HBcAg-#A79 VLPs, which was performed using the software ImageQuant TL 8.1. **c)** PageBlue staining of an 1% native agarose gel loaded with 10µg purified HBcAg-#A79-VLPs (A79-4 = batch 4) and 5µg of HBcAgΔ-VLPs (HBcAgΔ #18 = batch 18) as reference standard.

NuPAGE-SDS-PAGE analysis revealed one main band with an apparent molecular weight (MW) of ~20 kDa that was in good agreement with the predicted MW of the chimeric HBcAg-monomer. Furthermore, three additional bands (at ~15kDa, 40kDa and 45kDa) with much lower signal intensity could be observed (Figure 3.5. a). By Western Blot analysis using other chimeric HBcAg-VLPs and mAbs specific for the N- or C-terminal end of HBcAg monomers, we could previously demonstrate that the band at ~15kDa represents an N-terminal degradation product of HBcAg, whereas both bands at 40/45 kDa are reflecting HBcAg-dimers, for which it is well known that they can be detected even under reducing and denaturating conditions (data not shown). Therefore, the additional fainter bands did not represent host cell protein (HCP) contaminations but product related components (PRC).

Densitometric analysis of colloidal blue-stained NuPAGE-SDS-PAGE of HBcAg-#A79 VLPs allowed measuring the degree of purity with high sensitivity and precision (Figure 3.5. b). For the calculation of the purity, the band intensity of the monomer and those of PRCs were added. The shown batch of HBcAg-#A79 VLPs had a purity of nearly 85% that was sufficient for further immunization studies. Material with a purity <80% was discarded and not used for immunization experiments.

Native agarose gel electrophoresis (NAGE) followed by PageBlue staining revealed a distinct band for chimeric HBcAg-#A79 VLPs comparable to the band of HBcAgΔ-VLPs as reference standard, confirming the correct assembly of the chimeric HBcAg-#A79 molecules into VLPs (Figure 3.5. c). The migration difference of HBcAg-#A79 VLPs and HBcAgΔ-VLPs was expected and is mainly based on their different charge, as NAGE visualizes intact chimeric VLPs displaying the CLDN6 epitope 180 or 240 times in their surface. Thus, subtle charge differences of HBcAg-#A79 monomers are multiplied in HBcAg-#A79 VLPs and causing the observed migration difference in comparison to HBcAgΔ-VLPs.

In summary, a set of correctly assembled, CLDN6-epitope displaying HBcAg-VLPs could be generated and produced with high purity. Both chimeric HBcAg-CLDN6 VLPs were used subsequently in immunization studies with the objective to identify highly immunostimulatory isRNA adjuvants, improving the humoral and/or cellular immunogenicity of these chimeric VLP vaccines.

3.1.4 Selection of commercially available adjuvants to improve the immunogenicity of HBcAg-#A79 VLPs.

After successful purification of HBcAg-#A79 and HBcAg-#H88 VLPs, an initial mouse immunization study was performed in order to evaluate the efficacy of a broader spectrum of commercially available adjuvants representing different adjuvant classes when co-administered with HBcAg-#A79 VLPs. Based on the fact that many pattern recognition receptors (PRR) agonists have been developed as adjuvants for recombinant protein vaccines, we were able to figure out the most promising classes and test them in combination with HBcAg-#A79 VLPs. Table 3.1 illustrates the selected adjuvants.

Table 3.1: List of adjuvants used in combination with HBcAg-#A79 VLPs. s.c.: subcutaneous (green); i.m.: intramuscular (orange); CFA: Complete Freund's Adjuvant; IFA: Incomplete Freund's Adjuvant*;* R848*:* Resiquimod; Pam3CSK4: synthetic triacylated lipopeptide that mimics the acylated N-terminus of bacterial lipopeptides; AddaVax: MF-59 like squalene-based oil-in-water nano-emulsion.

Groups	Adjuvants	Route of administration	Dose/mice	Targeted PRRs
1	-	s.c.	-	-
2	-	i.m.	-	-
3	CFA/IFA	s.c.	50% volume	TLR2/4; NLRP3…
4	R848	s.c.	20µg	TLR7 and 8
5	Monophosphoryl Lipid A	i.m.	10 µg	TLR4
6	Pam3CSK4 VacciGrade™	i.m.	20 µg	TLR2
7	AddaVax	s.c.	50% volume	TLR2/4 and 9
8	Aluminium Hydroxide	s.c.	50% volume	NLRP3…

The humoral immune responses upon repetitive s.c. or i.m. immunizations with HBcAg-#A79 VLPs in combination with the adjuvants listed above were analyzed subsequently by two different methods.

3.1.5 Analysis of induced humoral immune responses upon co-administration of commercially available adjuvants with HBcAg-#A79 VLPs.

The selected adjuvants were co-administered in combination with HBcAg-#A79 VLPs into 6-10 week old female Balb/c mice using the intended immunization route as listed in Table 3.1. Mice were immunized three times according to the immunization schedule presented in Figure 3.6. a. Antibody-titers against the linear CLDN6 #79 peptide as well as recognition of the native CLDN6 protein were analyzed by ELISA and flow cytometric analysis (FACS), respectively.

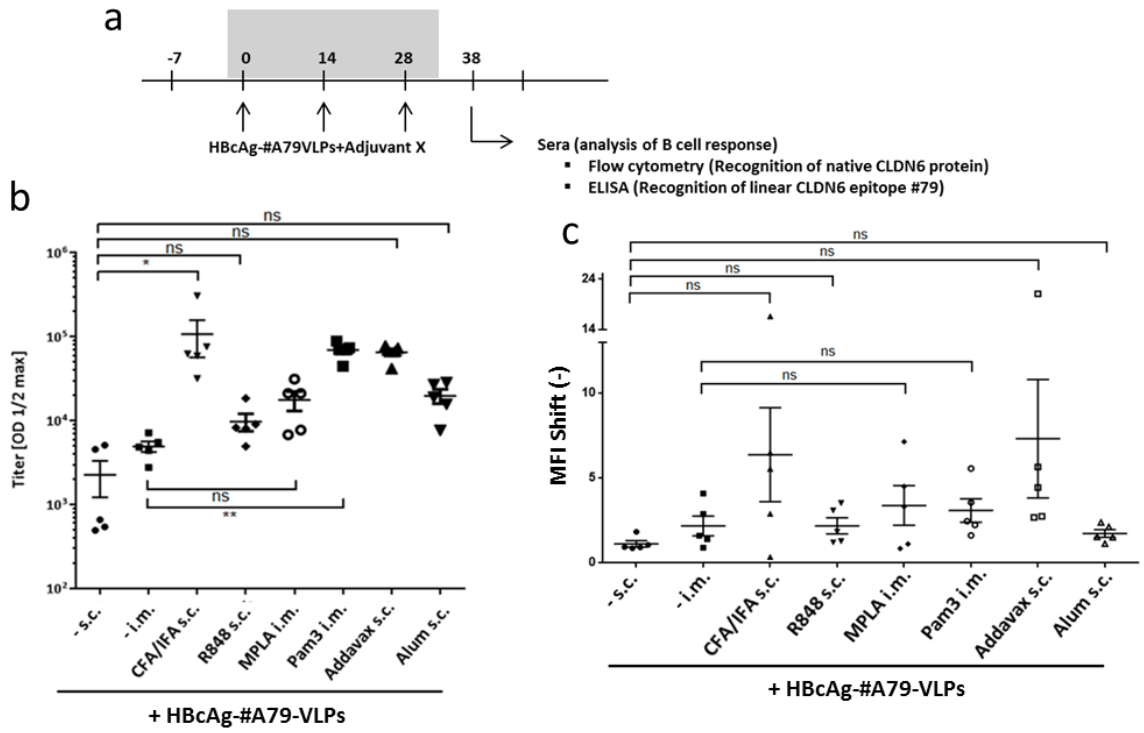

Figure 3.6: ELISA and FACS analysis of the humoral immune response after immunization of HBcAg-#A79 VLPs in combination with different commercially available adjuvants. Balb/c mice (n=5 per group) were immunized three times s.c. or i.m at two-week intervals with HBcAg-#A79 VLPs alone, or in combination with several classes of adjuvants. **a)** Applied immunization schedule. **b)** IgG antibody titer analysis by epitope #79 peptide ELISA. Illustrated are the calculated half-maximal antibody titers. **c)** FACS analysis of sera using CHO-K1 cells stably expressing hsCLDN6 protein on their surface. The specific antibody binding was detected with AlexaFluor647 conjugated goat anti-mouse secondary antibodies. Illustrated is the x-fold MFI shift of final vs. corresponding pre-bleeds. For statistical analysis the software GraphPad Prism 7 performing a one way ANOVA test was used. Each adjuvant group was compared to s.c. or i.m. immunized mice (depending on the application route of the adjuvant) without the addition of adjuvants. The difference between the groups were considered to be statistically significant at $P<0.05$. ns = Not significant; MPLA: Monophosphoryl Lipid A; Pam3: Pam3CSK4.

The calculated half-maximal antibody titers as analyzed by CLDN6 #79 peptide ELISA (Figure 3.6. b) revealed that the immunization (s.c. or i.m.) with non-adjuvanted HBcAg-#A79 VLPs resulted in low IgG antibody titers. No significant increase of IgG antibody titers were observed by s.c. immunization with HBcAg-#A79 VLPs adjuvanted with R848, MPLA or Alum. A statistical significant, moderate to strong increase of the half-maximal antibody titer was only observed by immunizations of HBcAg-#A79 VLPs in combination with CFA/IFA or Pam3. However, antibody titers against the linear CLDN6 #79 epitope might be misleading and don't necessarily reflect antibody reactivity against the CLDN6 protein in its native conformation. Therefore, in addition to the ELISA assays, the sera were analyzed by FACS using living CHO-K1 cells stably expressing hsCLDN6 on their surface (Figure 3.6. c). The FACS results revealed a weakly increased induction of specific anti-CLDN6 IgG antibodies by all tested adjuvant groups when combined with HBcAg-#A79 VLPs, with the exception of CFA/IFA and AddaVax adjuvants showing a slightly stronger effect. However, none of the increased MFI-shift was statistically significant when compared to mice immunized without the addition of adjuvants. Furthermore, CFA/IFA and AddaVax co-administration resulted in a strong inter-individual variability that might be caused by the depot effect of the stable emulsions built during the formulation procedure of adjuvant and antigen which was first

demonstrated by Herbert *et al.* [147]. In addition, both types of adjuvants (CFA/IFA and AddaVax) are only intended for research purposes using animal models as they are too toxic for human use [148].
Thus, the results clearly demonstrated that there was a need for a novel, highly immunostimulatory adjuvant used in combination with chimeric HBcAg-VLP-based vaccines but also for other protein-based vaccines. The adjuvant to be developed had to be able to induce a strong immune response without undesired, harmful side effects and preferably without a strong inter-individual variability within the test group.

3.2 Evaluation of isRNA-LPX as an adjuvant for chimeric HBcAg-VLPs.

Having shown that the antibody response against the native CLDN6 protein was not statistical significantly improved by combining HBcAg-#A79 VLPs with the adjuvants listed in Table 3.1, the question remained, how to design and develop an adjuvant that strongly enhances the immunogenicity of chimeric HBcAg-VLPs while still inducing a target specific immune response. Furthermore, the administration route had to be considered, as chimeric HBcAg-VLP vaccines and adjuvant should reach the same lymphatic organ in order to exert maximal and combined efficacy.
Based on the fact that B cells were also the primary binding cells for chimeric HBcAg-VLPs (see Figure 3.3), we decided to develop a RNA-based adjuvant specifically targeting TLR7 that is strongly upregulated in B cells by stimulation of B cell receptors (BCR; e.g. by binding to HBcAg-VLPs) and by type I interferons [149]. Furthermore, TLR7 is constitutively expressed in plasmacytoid dendritic cells (pDCs), the main cellular producers of type I interferon [106]. Thus, the combined action of BCR and type I interferon stimulation might result in high levels of TLR7 in B cells whose stimulation by TLR7 agonists (RNA-based adjuvant) in combination with an appropriate antigen (chimeric HBcAg-VLPs) will lead to a strong activation of B cells (including proliferation, somatic hypermutation, Ig class switching and differentiation in plasma or memory cells).

It has been previously published that whole Influenza A (InfA) genomic RNA is capable to induce high levels of interferon-alpha (IFN-α) in pDCs by means of TLR7 stimulation [106]. In order to identify small, InfA-derived highly effective RNA fragments with defined TLR specificity, we initially selected InfA nucleoprotein (NP), InfA hemagglutinin (HA) and InfA nonstructural protein (NS) RNA as parental sequences and analyzed their immunostimulatory capacity in initial *in vitro* orientation experiments. Based on the results, one of the InfA full length RNAs should be selected to establish a sequential fragmentation strategy for the subsequent identification of defined, short immunostimulatory, single-stranded RNA molecules (isRNAs) mainly responsible for the TLR7-dependent, IFN-α inducing activity.

To enable the selection of a single InfA full length RNA segment for further fragmentation, two different *in vitro* readout systems were established and applied. The first system was

based on the *in vitro* induction of whole human PBMCs followed by measurement of the lead cytokines IFN-α and tumor necrose factor-alpha (TNF-α) levels in the cell culture supernatant. The preferred cytokine induction profile should by high IFN-α and low TNF-α. It is important to note that the human PBMC assay was very much donor dependent. Therefore, at least three donors or (if necessary) up to five donors were analyzed. The interpretations and the corresponding conclusions were done in consideration of the donor-dependent cytokine profiles.The second system used *in vitro* stimulation of HEK293 cells stably co-expressing human TLR3, TLR7 or TLR8 and an NF-κB-inducible luciferase reporter gene (HEK293-TLRx system). This system allowed the analysis of the TLR specificty of the selected InfA RNA full length sequences. A high TLR7 specificty was preferred.

The following full length RNA sequences derived from InfA were analyzed:

- RNA No. I Influenza A virus (A/Bangkok/235/89 (H3N2)), hemagglutinin gene, partial CDS (HA1 region); GenBank: D49962.1 = **HA-Full**
- RNA No. II Influenza A virus (A/Puerto Rico/8/34 (H1N1)), nucleoprotein gene, complete CDS; GenBank: M38279.1 = **NP-Full**
- RNA No. III Influenza A virus (A/duck/ Hong Kong/205/1977 (H5N3)), segment 8 (NS 1 and NS2 genes), complete CDS; GenBank: CY005593.1 = **NS-Full**

Figure 3.7 shows the IFN-α and TNF-α levels in the cell supernatant after *in vitro* stimulation of whole human PBMCs with InfA HA, NP or NS full length RNAs. All RNAs were liposomally formulated with liposomes F5 for increased *in vitro* transfection efficacy. More than three PBMC donors were tested but only one result is shown as an example.

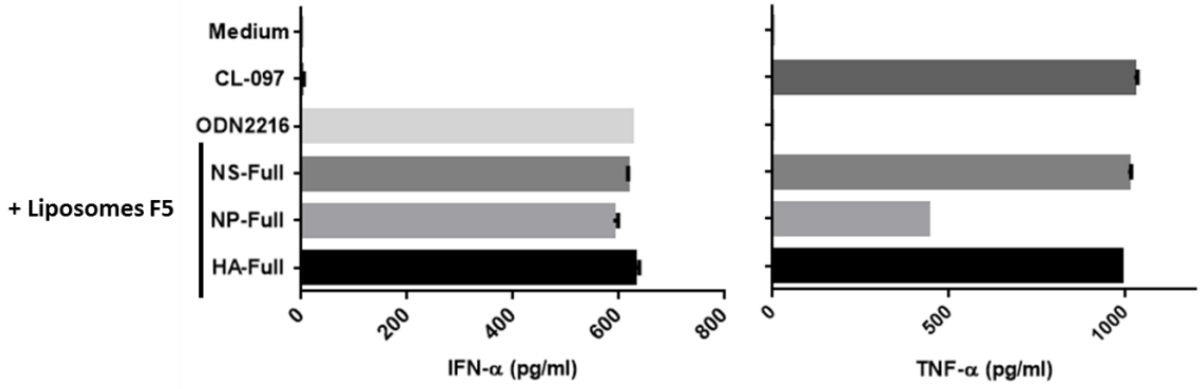

Figure 3.7: *In vitro* stimulation of whole human PBMCs by formulated InfA RNA candidates NP, NS and HA. 1x10^6 freshly isolated human PBMCs per well were stimulated with F5-formulated full lenth (x-Full) NP, NS and HA RNA (0,167 µg/well). As positive control for IFN-α induction, the cells were stimulated with unformulated CL-097 (0,2 µg/well) an imidazoquinoline derivative and TLR7/8 agonist. As positive control for TNF- induction, the cells were stimulated with unformulated CpG ODN2216 (5 µg/ml) an agonsit for TLR9. Unstimulated cells (Medium) served as negative control. The secretion of IFN-α and TNF-α were measured by commercially available ELISA kits (eBioscience). Experiments were performed in biological triplicates.

All three InfA-derived full length RNA sequences induced comparable high levels of IFN-α in the same range as CL-097 as positive control. However, InfA NP full length induced only a moderate or even weak (in some donors) TNF-α response, whereas InfA NS-Full and HA-Full

led in all tested donors to a very high TNF-α secretion that was in the same range as the positive control CpG ODN2216.

Subsequently, the full length InfA-derived RNAs were tested for their human TLR specificity/cross-reactivity in HEK293-TLR3, -TLR7 -TLR8 and -TLR0 (no TLR expression) cells, co-expressing a NF-κB-inducible luciferase reporter gene (see Figure 3.8). All RNAs were liposomally formulated with liposomes F5 for increased *in vitro* transfection efficacy.

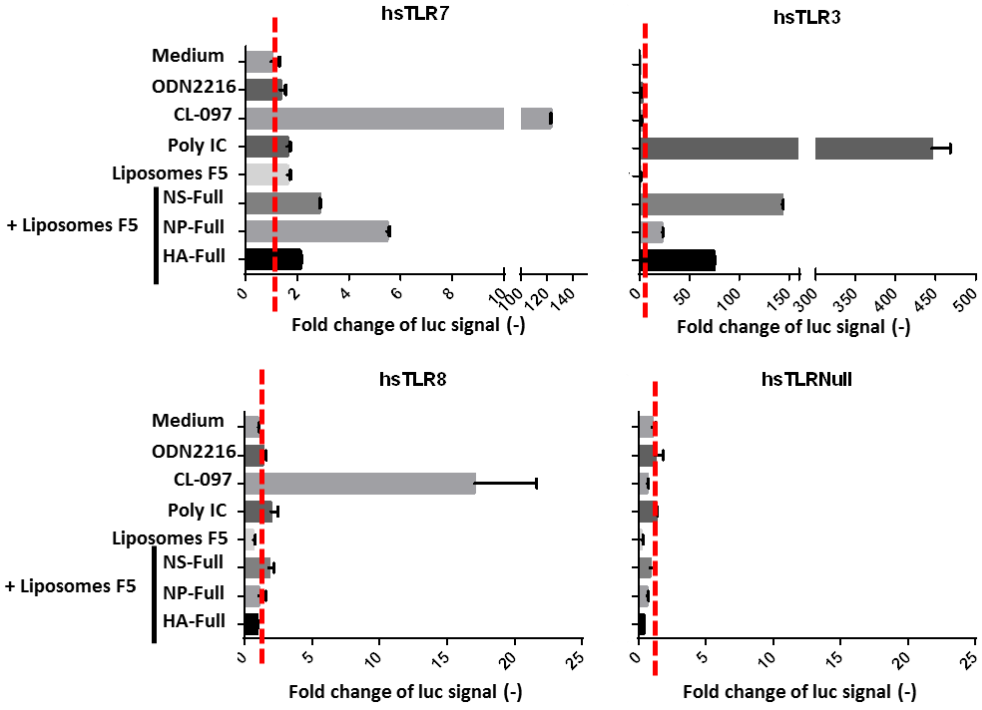

Figure 3.8: *In vitro* stimulation of HEK293-TLR cells with formulated InfA full length RNA candidates NP, NS, and HA. HEK293 cells stably co-expressing human TLR3, TLR7 or TLR8 in addition to an NF-κB-inducible luciferase reporter gene and HEK293 cells stably expressing only NF-κB-inducible luciferase reporter gene (hsTLRNull) were incubated with F5-formulated InfA RNA candidates (NS-, NP-, HA-Full) (0,167 µg/well). Positive controls were unformulated Poly (I:C) for TLR3 and unformulated CL-097 for TLR7 and TLR8. Unformulated ODN2216, empty Liposomes F5 and medium served as negative controls. TLR activation is expressed as x-fold change of the luciferase reporter gene signal. The dashed red line indicates the background luciferase signal, based on luciferase signals received for untreated (Medium) cells.

Formulated InfA NP full length RNA activated the NF-κB-inducible luciferase reporter gene in HEK293 cells expressing human TLR7 to a higher extent than InfA NS or InfA HA sequences. In contrast, formulated NS- and HA-Full induced the luciferase reporter gene strongly in human TLR3 co-expressing HEK293 cells, whereas the induction luciferase expression mediated by InfA NP full length RNA was only moderate. No significant luciferase signals were obtained after stimulation of human TLR8 expressing HEK293 cells with the InfA RNA candidates. CL-097 (TLR7/8 agonist) stimulation of this cell line led to a strong increase in luciferase signal, proofing the functionality of the reporter gene system in HEK293-TLR8 cells.

Both *in vitro* systems clearly favored InfA NP full length RNA as the best candidate for further fragementation studies to identify small isRNA fragments. In comparison to InfA HA or NS, InfA NP stimulation was preferentially leading to more pronounced IFN-α secretion when

compared to TNF-α and exhibited the highest TLR7 specificty. Therefore, InfA NP full length RNA was selected for further fragmentation experiments.
Increasingly smaller fragments of InfA NP full length RNAs had to be produced with high purity using a robust and repeatable production and purification process that will be described in the next section, before describing the results of the InfA NP fragementation cycles.

3.2.1 Production of isRNAs by *in vitro* transcription (IVT) and resulting sequences.

All isRNA sequences were synthesized by a previously described *in vitro* transcription (IVT) system [130] using bacteriophage T7 polymerase for IVT RNA production. Only a few, shorter isRNAs were additionally produced by chemical synthesis for comparison studies. Figure 3.9 is showing a schematic overview of the IVT isRNA synthesis process and the resulting isRNA sequences exemplified for the isRNA NP71-Seq4.

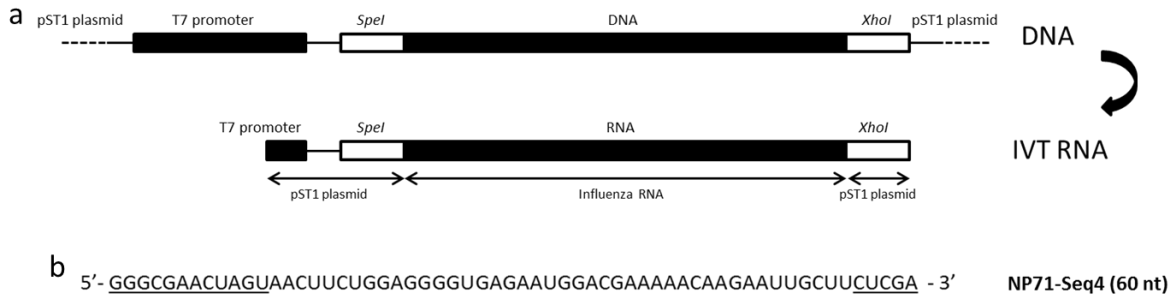

Figure 3.9: Synthesis of isRNAs by *in vitro* transcription, composition and sequence of isRNAs. a) DNA sequences encoding selected InfA NP fragments were cloned downstream of a bacteriophage T7 RNA polymerase promoter into plasmid pST1 using *Spe*I and *Xho*I restriction sites; **b)** IVT RNA synthesized by T7 RNA polymerase consisted of the isRNA of interest flanked on both sides by short sequences (underlined) derived from pST1 plasmid template.

IVT isRNA sequences will be flanked on both sides by short sequence stretches derived from the pST1 plasmid template, as exemplified for isRNA NP71-Seq4 sequence in Figure 3.9. b. In addition, several publications have shown that T7 polymerase can produce a heterogeneous 3' end or 5' extensions due to run-off transcripts [150, 151]. Therefore, the real 3' and 5' end might slightly differ from the theoretical IVT isRNA sequence shown in Figure 3.9 b. Thus, the composition and end structures of IVT isRNAs had to be analyzed more closely, after producing and purifying sufficient amounts of isRNA using the methods described afterwards.

3.2.2 Purification of IVT isRNAs.

After *in vitro* transcription, IVT isRNA samples were purified by a silica-based membrane for small-scale purification or by a FPLC-depending method for large-scale purification. The FPLC purification was based on a protocol already published by Easton *et al*. [152] and uses weak anion-exchange chromatography columns for the separation of unincorporated nucleotides,

small abortive products and full length IVT isRNAs. An example of a typical FPLC elution profile and the subsequent peak analysis is shown in Figure 3.10.

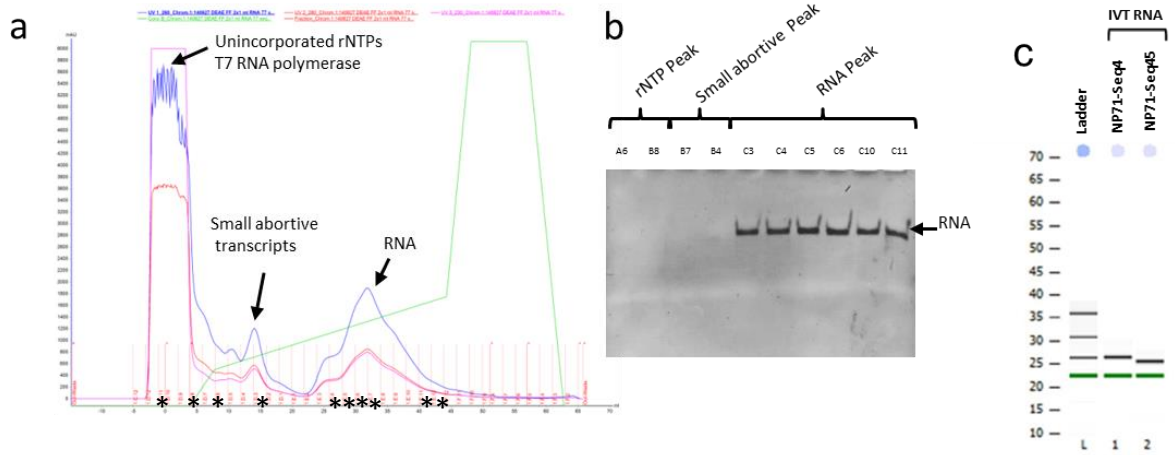

Figure 3.10: FPLC-based purification of IVT isRNA NP71-Seq4 using weak anion-exchange chromatography. a) FPLC elution profile after addition of 5 mL IVT isRNA NP71-Seq4 using DEAE-sepharose chromatography. Blue/red/pink line: OD measurement at 260/280/230 nm. Green line: percentage of salt buffer B used for elution. Fractions analyzed in b) are indicated by a *. **b)** Denaturing PAA gel analysis of selected elution fractions. RNA was visualized by gel staining with 0.1% GelRed. **c)** Chip capillary electrophoresis analysis of NP71-Seq4 and NP71-Seq45 using the Bioanalyzer 2100 system. The green bars indicate an internal loading marker.

The FPLC elution profile was characterized by three distinguishable main peaks. Based on *in house* knowledge of BioNTech Protein Therapeutics and published literature [151, 153], the first large peak represented the T7 polymerase and unincorporated rNTPs that did not bind to the DEAE matrix at 0% salt concentration. The complete removal of T7 polymerase and unincorporated rNTP contaminations was achieved by a short salt gradient up to approximately 10% buffer B (buffer A with 2M sodium chloride). At approximately 30% buffer B, small abortive RNA fragments eluted and could be completely eliminated from full length isRNAs. The third peak corresponded to the target IVT isRNAs. The elution of digested template DNA in the IVT reaction was not detectable in the elution profile, possibly due to its very low concentration.

To demonstrate that the third peak corresponded to the target IVT isRNA product, a denaturing PAA gel electrophoresis of selected elution fractions was applied (Figure 3.10. b). As expected, full length IVT isRNA could be detected only in the third peak and was successfully separated from all other IVT components including unincorporated rNTPs, T7 RNA polymerase, small abortive transcripts and plasmid DNA. To demonstrate the purity, the purified IVT isRNA product was also analyzed by chip capillary electrophoresis using the Bioanalyzer 2100 system (Figure 3.10. c). As an example, purified isRNAs NP71-Seq4 and NP71-Seq45 are presented and were detected as a single, distinct band, indicating their high purity.

3.2.3 Quality control of purified IVT isRNAs.

After purification with silica-based membranes or weak anion exchange columns, IVT RNAs were quality controlled using a variety of analytical methods that are exemplified for NP71-Seq4 in comparison to chemically synthesized NP71-Seq4 as benchmark in Figure 3.11.

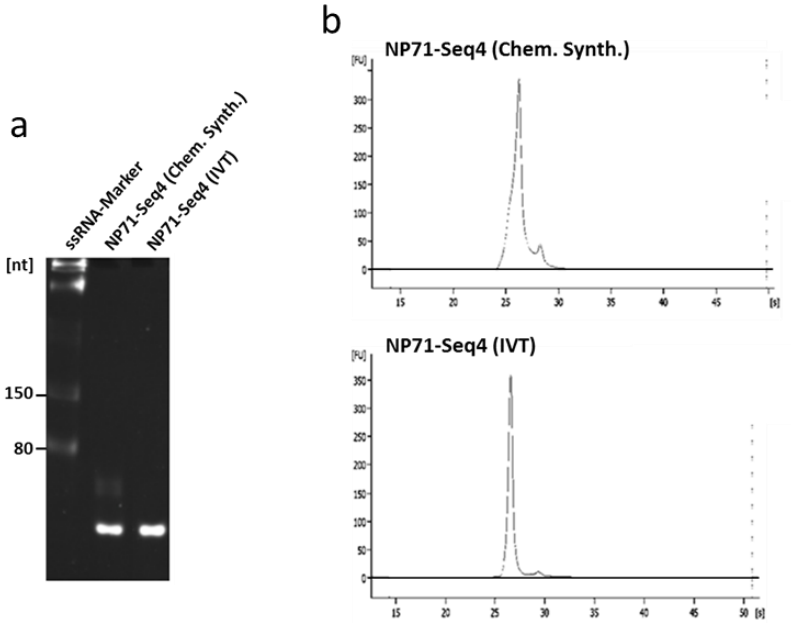

Figure 3.11: Quality control after purification of NP71-Seq4 by the FPLC-based method. As a reference to IVT RNA, chemically synthesized NP71-Seq4 is presented as well. **a)** Native PAA gel analysis of NP71-Seq4. ssRNA-Marker = Low Range ssRNA ladder in a formaldehyde containing loading buffer. **b)** Chip capillary electrophoresis analysis of IVT NP71-Seq4 and chemically synthesized NP71-Seq4 (Chem. Synth.) using the Bioanalyzer 2100 system. Shown are thr fractograms for better visualization of peak shoulders.

The native PAA gel (Figure 3.11. a) and capillary electrophoresis results (Figure 3.11. b) revealed that NP71-Seq4 (IVT) was characterized by a distinct single band of the expected size and a homogenous product without any sign of RNA integrity loss. In contrast, chemically synthesized NP71-Seq4 isRNA displayed a peak-shoulder when applying chip capillary electrophoresis, indicating a more heterogeneous RNA product.
After showing high purity and homogeneity of purified IVT isRNA products, the next experiments should reveal the real composition and end sequences of IVT isRNAs.

3.2.4 Electrospray ionization mass spectrometry (ESI-MS) analysis of IVT isRNA NP71-Seq45

As already mentioned in section 3.2.1, the resulting IVT RNA sequences were flanked on both sides by short stretches derived from the pST1 plasmid template. In addition, several studies reported that during IVT reactions, the T7 polymerase can produce a heterogeneous 3’ end or 5’ extension of run-off transcripts [153, 154]. Therefore, the content and end structures of purified IVT isRNA were analyzed in more detail by electrospray ionization mass spectrometry (ESI-MS, performed by Biospring). Results were exemplified for the IVT RNA sequence NP71-Seq45 in Figure 3.12.

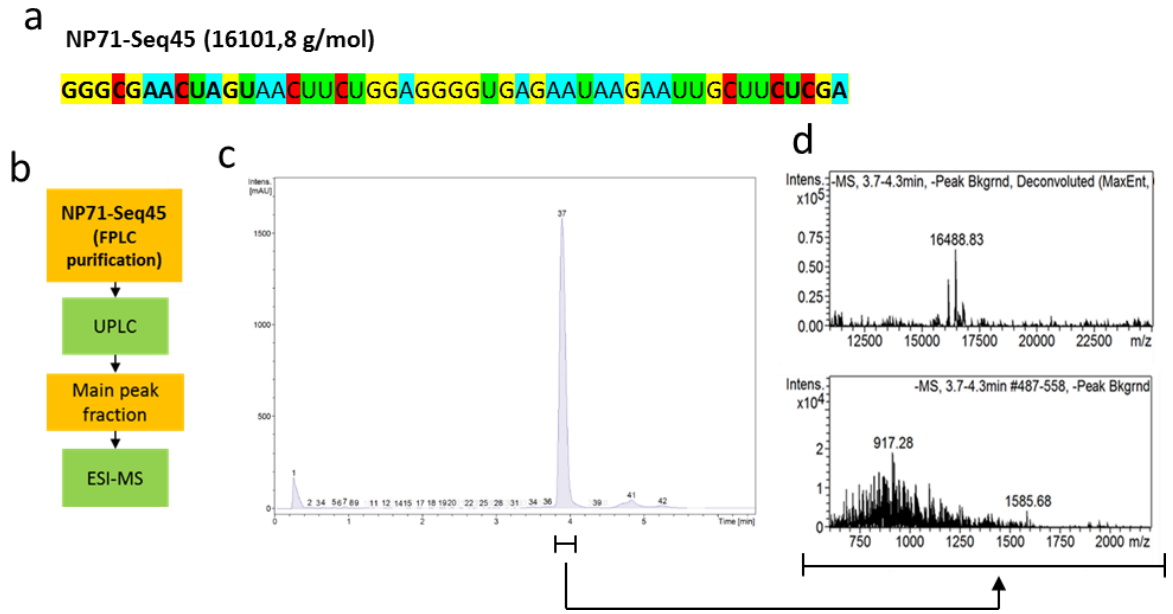

Figure 3.12: Ultra Performance Liquid Chromatography (UPLC) and ESI-MS analysis of purified NP71-Seq45 IVT isRNA sequence. a) Predicted sequence and corresponding calculated molecular weight of NP71-Seq45 isRNA. For better visualization the nucleotides are colored in yellow (G), red (C), green (U) or blue (A). Bold nucleotides at the 5' and 3' end indicate nucleotides derived from the pST1 template. **b)** Experimental plan for the UPLC ESI-MS analysis. **c)** UPLC elution profile. The main elution peak is indicated by a bar under the fractogram. **d)** ESI-MS analysis of the main UPLC peak of purified IVT isRNA NP71-Seq4. The lower panel shows the original and the upper panel the deconvoluted spectrum of the analyzed sample. Numbers in the spectra reflect molecular weights of main peaks in Dalton. m/z: molecular mass number/charge number of the ion.

Only minor, neglectable contaminants were detectable after UPLC of the FPLC purified IVT isRNA material (Figure 3.12. c). ESI-MS analysis of the main UPLC peak fraction revealed that the molecular weight (MW) of IVT isRNA NP71-Seq45 was approximately 16489 dalton (Da) (Figure 3.12. d; deconvoluted spectrum) and thus 388 Da higher then the predicted MW. Therefore, it was highly likely that NP71-Seq45 isRNA contains a single additional nucleotide at the 5' or 3' end (personal communication Biospring) that would be also in accordance with the molecular weight of ribonucleotide monophosphates ranging from 323 to 363 Da.

In general a robust and reproducible IVT RNA production process could be established, including the small or large scale purification of isRNAs to high purity and RNA integrity. However, the T7 polymerase depending IVT synthesis was leading to the addition of DNA template derived nucleotides and single extra nucleotides that have been taken into account when performing secondary structure predictions especially for small isRNA molecules. Nevertheless, the established IVT RNA production process made it possible to carry out further experiments for the identification of InfA NP-derived isRNA lead candidates by iterative fragmentation cycles, which depended on continuous production of various isRNAs with consistent quality.

3.3 Identification of high immunostimulatory isRNA fragments derived from the InfA NP encoding gene by iterative fragmentation and *in vitro* screening cycles.

The established robust and reproducible IVT RNA synthesis and purification process enabled the realization of an iterative fragmentation and *in vitro* screening strategy to identify small, highly immunostimulatory RNAs (is RNAs) with high specificity for TLR7 and preferential IFN type I induction. Figure 3.13 represents a schematic drawing of the whole implemented fragmentation strategy for InfA NP and gives an overview of the location of the isRNA sequences within InfA NP and for smaller isRNA molecules also their predicted secondary structure.

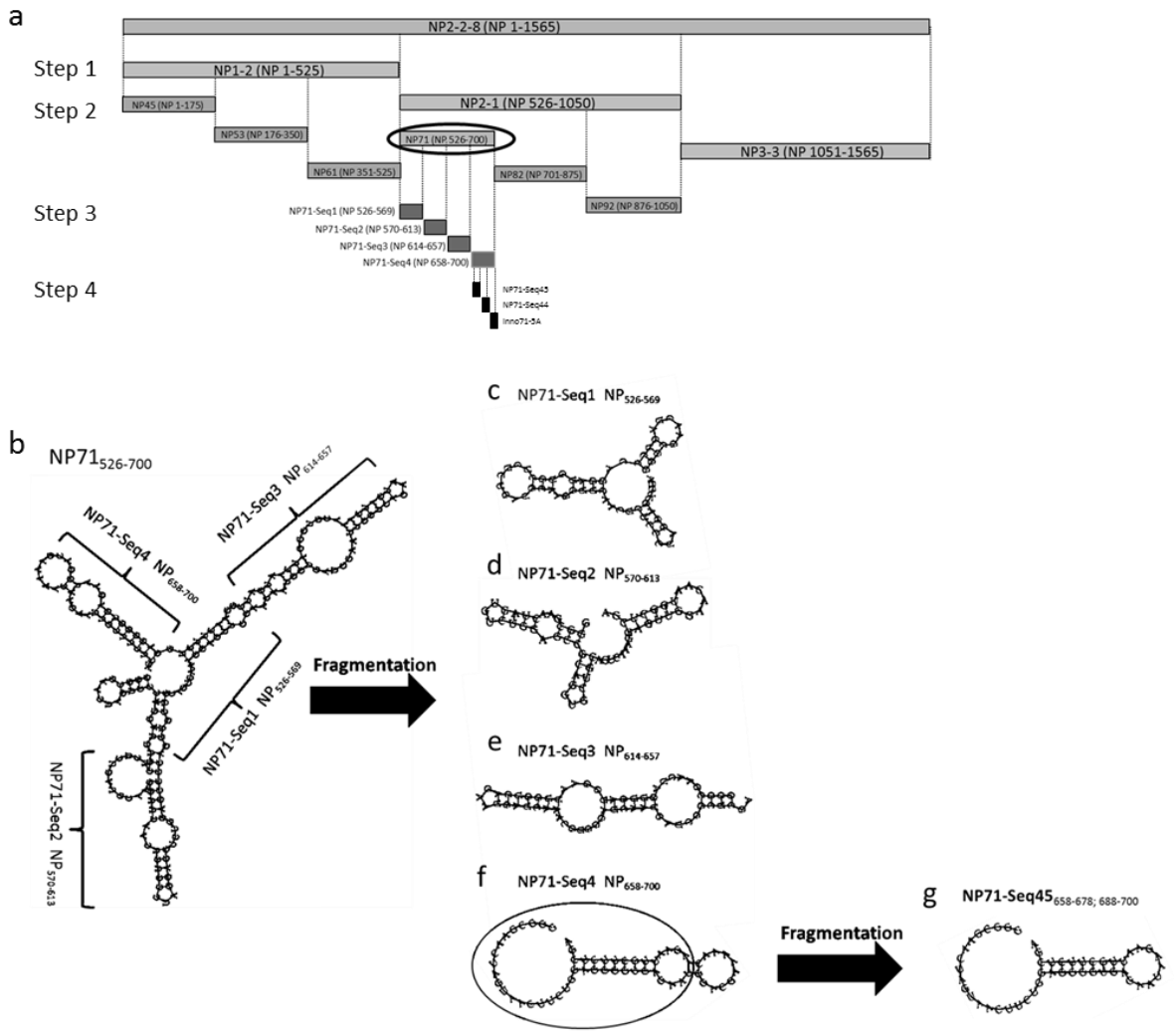

Figure 3.13: Sequential fragmentation of InfA NP encoding RNA enabled the identification and selection of small isRNAs with defined TLR specificity and cytokine induction profile. a) The parental NP encoding RNA NP2-2-8 was fragmented in four sequential steps. The localization of NP sequence fragments tested in this thesis is schematically shown. $NP71_{526-700}$ is marked by a circle and was further fragmented as shown in c-f. **b)** The size of $NP71_{526-700}$ enabled a more robust secondary structure prediction that was taken into account for further fragmentations. **c-f)** RNA fragments derived from $NP71_{526-700}$ and their predicted secondary structure. NP71-Seq4 is marked by a circle and was further fragmented. **g)** Structure and nucleotide content of the isRNA lead candidate NP71-Seq45.

Four sequential fragmentation steps have been performed in total. The first two steps were simply based on the subdivision of the ancestor RNA fragment into three thirds of approximately equal length. The size of the fragments derived from step two enabled more robust secondary structure predictions that were taken into account for further fragmentation steps that finally resulted in the identification and selection of small isRNA lead candidates.

All NP-derived RNA fragments were analyzed *in vitro* using the human PBMC stimulation assay for determining the induced cytokine profile and the HEK293-TLRx system for analyzing the TLR specificity (see Section 3.2). Both assays were the basis for decision-making to select NP-derived RNA fragments for subsequent fragmentations.
For fragmentation step one and two, only the results of the PBMC stimulation assays will be shown.

Step 1:
The InfA NP full length RNA sequence (NP2-2-8) was selected because of its highest preference for TLR7 and a more pronounced IFN type I induction in comparison to TNF-α. In the first fragmentation step, the InfA NP full length RNA sequence was subdivided into three sequences with approximately equal lengths of around 525 nucleotides (see Figure 3.14).

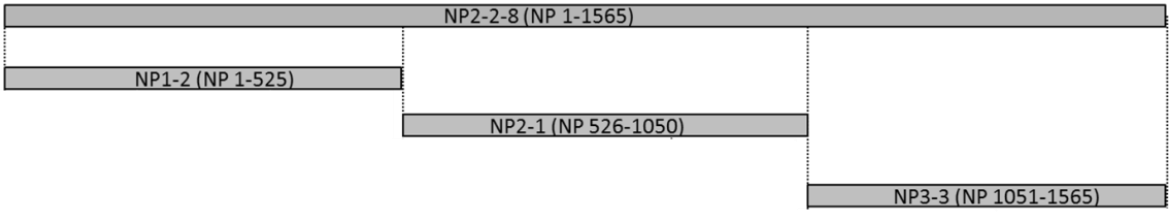

Figure 3.14: The first step of the applied fragmentation strategy. The parental InfA NP full length sequence was subdivided into the three fragments NP1-2, NP2-1 and NP3-3. NP= nucleoprotein-encoding isRNA molecule.

All sequences were produced by *in vitro* transcription, purified in small scale and quality controlled. After confirmation of equal purity the InfA NP fragments NP1-2, NP2-1 and NP3-3 were tested in comparison to the parental InfA NP full length RNA using the whole human PBMC cytokine secretion assay (see Figure 3.15). All IVT RNAs were formulated with liposomes F5 for optimized transfection efficacy.

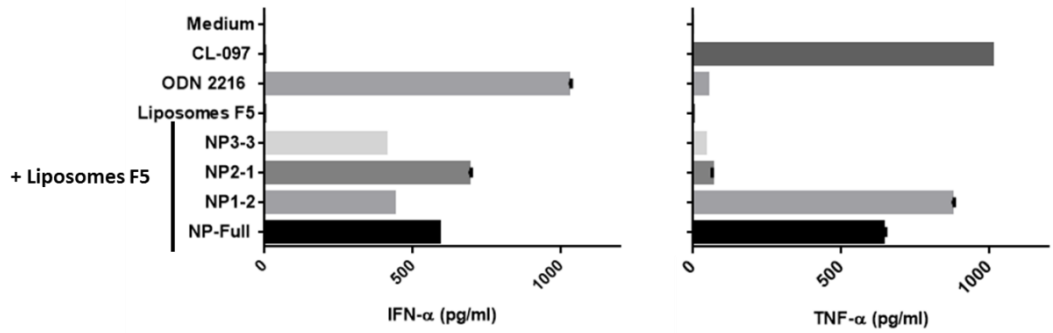

Figure 3.15: *In vitro* stimulation of whole human PBMCs by formulated IVT isRNA candidates from the first fragmentation step. 1x10^6 freshly isolated human PBMCs per well were stimulated with F5-formulated InfA NP full length RNA (NP-Full) or fragments NP1-2, NP2-1 and NP-3-3 (0,167 µg/well). As controls, the cells were stimulated with unformulated CL-097 (0,2 µg/well), unformulated CpG-ODN216 (5 µg/ml), empty Liposomes F5 or were kept unstimulated (Medium). The secretion of IFN-α and TNF-α in the cell culture supernatant was measured by commercially available ELISA kits (eBioscience). The samples were measured in biological triplicates.

The *in vitro* stimulation of human PBMCs clearly indicated that stimulation with RNA fragment NP2-1 resulted in IFN-α levels that were higher than for the other tested RNA fragments and even higher then for the parental InfA NP full length RNA. In addition, NP2-1 (but also NP3-3) stimulation induced only very weak TNF-α levels whereas the strong TNF-α induction capacity of InfA NP full length RNA seemed to be located by large extent within the fragment NP1-2. These results could be confirmed for more than three donors. Based on the highest IFN-α and only very low TNF-α induction levels, NP2-1 was chosen as the best candidate for the next fragmentation step.

Step 2:

The selected RNA sequence NP2-1 was further subdivided in three fragments of nearly equal lengths (see Figure 3.16). Out of interest, sequence NP1-2 was also fragmented into three sequences of equal lengths (see Figure 3.13. a) in order to track down the fragment responsible for the very high TNF-α secretion. Interestingly, the *in vitro* activities of formulated NP45, NP53, NP61 in PBMCs did not differ from each other (data not shown). Thus, they were not further analyzed.

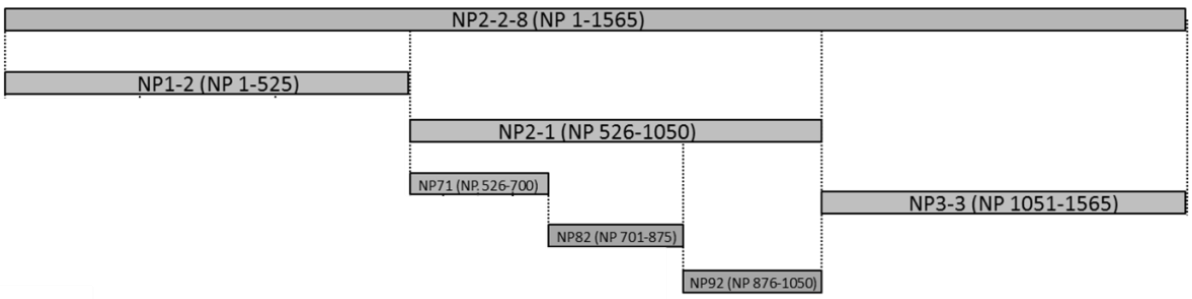

Figure 3.16: The second step of the applied iterative fragmentation strategy. The selected NP2-1 fragment was subdivided into the three fragments NP71, NP82 and NP92 of approx. equal length. NP= nucleoprotein-encoding isRNA molecule.

Similarily to fragmentation step 1, the selected isRNA fragments NP71, NP82 and NP92 were synthesized by *in vitro* transcription, purified, quality controlled and used in comparison to their ancestor sequence NP2-1 in the whole human PBMC cytokine secretion assay to

determine the levels of the lead cytokines IFN-α and TNF-α for further fragment selection (Figure 3.17). All IVT RNAs were formulated with liposomes F5 for optimized transfection efficacy.

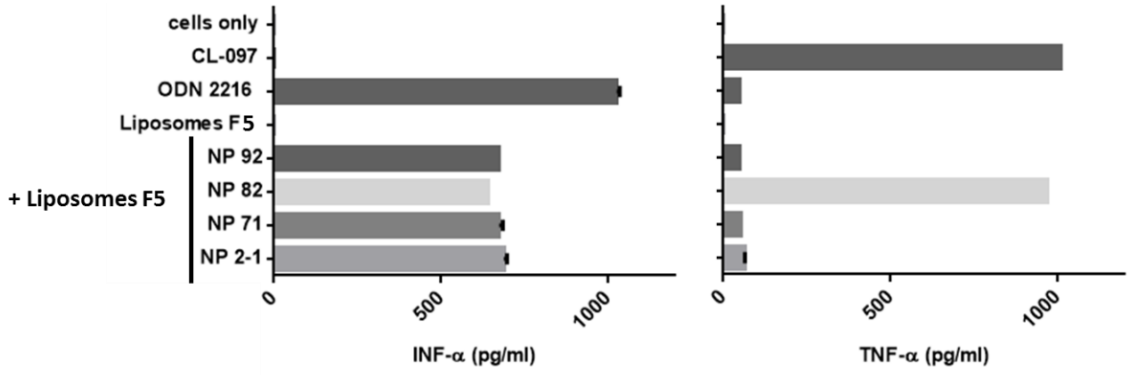

Figure 3.17: *In vitro* stimulation of whole human PBMCs by formulated IVT isRNA candidates from the second fragmentation step. 1x10^6 freshly isolated human PBMCs per well were stimulated with F5-formulated NP2-1, NP71, NP82 and NP92 isRNAs (0,167 µg/well). As controls, the cells were stimulated with unformulated CL-097 (0,2 µg/well), unformulated CpG-ODN216 (5 µg/ml) and empty Liposomes F5 or left untreated (cells only). The secretion of IFN-α and TNF-α in the cell culture supernatant was measured by commercially available ELISA kits (eBioscience). Experiments were performed in biological triplicates.

NP71, NP92 and their ancestor isRNA NP2-1 induced very similar cytokine levels upon human PBMC stimulation that were charaterized by high level of IFN-α and low levels of TNF-α. Interestingly, isRNA NP82 led to a high IFN-α and TNF-α secretion although stimulation with the ancestor sequence NP2-1 induced only low levels of TNF-α. The analysis of cytokine secretion was performed with PBMCs from five different donors and revealed that NP92 was inducing moderate levels of TNF-α secretion and varying levels of IFN-α in some donors whereas the cytokine induction profile for NP71 was consistent for all donors (data not shown). Therefore, isRNA NP71 was selected for the next fragmentation step.

Step 3:

In addition to the generated data of the *in vitro* cytokine secretion assays, the secondary structure prediction using the RNAfold server [155] also played an important role in our discovery and screening platform. However, *in silico* secondary structure predictions were much more reliable (leading to higher predictions scores) for smaller RNA fragments. Thus, secondary structure predictions were only implemented from fragmentation step three onwards.

Secondary structure prediction of the selected isRNA NP71 was performed and is shown in Figure 3.13. b. It turned out that the predicted structure of isRNA NP71 consisted of three arms and a central core element. Consequently we decided to subdivide NP71 in fragmentation step 3 in four small RNA sequences reflecting the predicted secondary structure of NP71. The fragments were designated as NP71-Seq1 (core element), NP71-Seq2, NP71-Seq3 and NP71-Seq4 (see Figure 3.13 and Figure 3.18). The secondary structures of these fragments were predicted again and approximately mirrored their predicted structure in NP71 (see Figure 3.13 c-f).

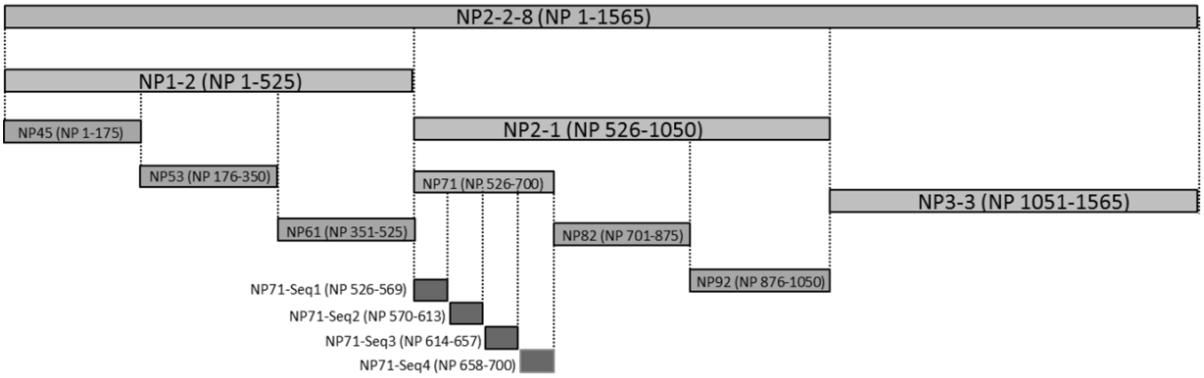

Figure 3.18: The third step of the applied iterative fragmentation strategy. The selected NP71 fragment was subdivided into the four fragments NP71-Seq1, NP71-Seq2, NP71-Seq3, NP71-Seq4 according to the secondary structure prediction of NP71. NP = nucleoprotein-encoding isRNA molecule.

The *in vitro* immunostimulatory capacity of the selected isRNA fragments was initially determined by using the human PBMCs cytokine secretion assay. In contrast to the PBMC assay performed at fragmentation step 1 and 2, the isRNA test candidates were used in two different concentrations (0.167 and 0.041 µg/well) reflecting either the equivalent amount in grams or the equivalent molarity to the larger parental NP71 RNA fragment. In this fragmentation step, the critical point was to find PBMC donor(s) in which the parental sequence NP71 could induce at least moderate TNF-α responses. Otherwise the selection of isRNA fragments with an even more pronounced capability to induce high levels of IFN-α and low or no levels of TNF-α could not be conducted. In two of the five tested donors, NP71 induced high levels of IFN-α and moderate levels of TNF-α. The results for all isRNAs from fragmentation step 3 in comparison to the ancestor fragment NP71 is illustrated for one of these two donors in Figure 3.19. All IVT isRNAs from fragmentation step 3 were formulated with liposomes F5 for optimized transfection efficacy. isRNA NP71 was used formulated with liposomes F5 but also unformulated.

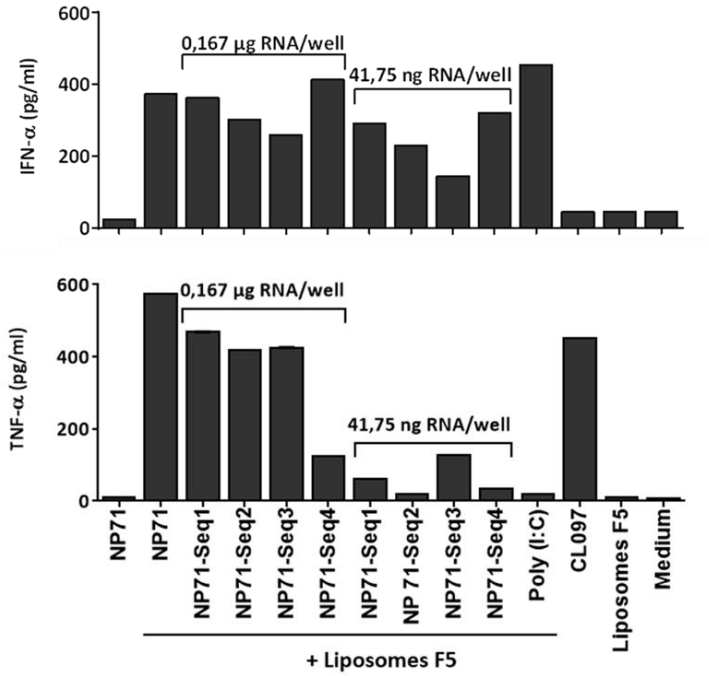

Figure 3.19: *In vitro* stimulation of whole human PBMCs by formulated IVT isRNA candidates from the third fragmentation step. 1x10^6 freshly isolated human PBMCs per well were stimulated with F5-formulated NP71, NP71-Seq1, NP71-Seq2, NP71-Seq3 and NP71-Seq4 (0,167µg/well or 41,75 ng RNA/well). As controls, the cells were stimulated with unformulated NP71 (0,167 µg/well), unformulated CL097 (0,2 µg/well), F5-formulated poly(I:C) (0,167µg/well) or with empty Liposomes F5. Untreated cells (Medium) served as negative control. The secretion of IFN-α and TNF-α was measured by commercially available ELISA kits (eBioscience). The samples were measured in biological triplicates.

The results confirmed that the immunostimulatory activity of the tested isRNAs was strictly depending on the appropriate liposomal formulation, as exemplified for NP71 (0.167 µg/well) with and without formulation. The parental NP71 isRNA fragment induced high levels of IFN-α and moderate levels of TNF-α. In contrast to cytokine release into the cell supernatant after stimulation with formulated NP71, the ELISA assay revealed that stimulation of human PBMCs with isRNA NP71-Seq4 resulted in the favored cytokine induction profile with high IFN-α and very low TNF-α amounts. All other test candidates caused a more balanced induction of both cytokines that became prominent especially when using higher RNA concentrations (0.167 µg/well).

In order to analyze how specific and to which extent the nucleotide-sensing endosomal TLR7 is activated, the formulated isRNA candidates from the third fragmentation step and their ancestral isRNA fragment NP71 were incubated with HEK293 cells stably co-expressing human TLR7, TLR8 or without TLRs (TLR0). The induction of the luciferase reporter gene was compared to untreated (medium only) cells and is shown in Figure 3.20.

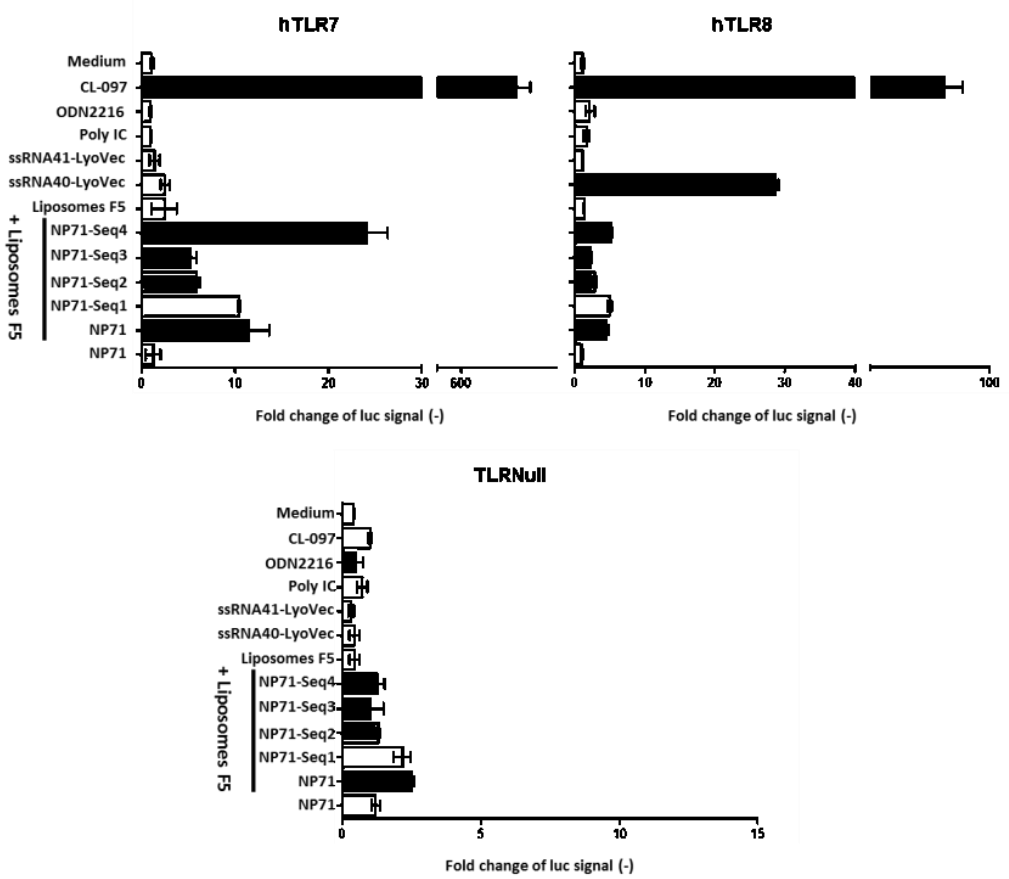

Figure 3.20: *In vitro* stimulation of HEK293-TLR cells with formulated IVT isRNA candidates from the third fragmentation step. HEK293 cells stably co-expressing human TLR7 or TLR8 in addition to an NF-κB-inducible luciferase reporter gene and HEK293 cells stably expressing only NF-κB-inducible luciferase reporter gene (TLRNull) were incubated with F5-formulated IVT isRNA candidates (0.167µg/well). Positive controls were F5-formulated Poly (I:C) for TLR3, unformulated CL-097 for TLR7 and TLR8,. unformulated CpG-ODN2216 for TLR9 and ssRNA40-LyoVec for TLR8. Empty F5-liposomes, unformulated NP71, ssRNA41-LyoVec and medium served as negative controls.

The results indicated that isRNA NP71-Seq4 induced the luciferase reporter gene in human TLR7 co-expressing HEK293 cells much more strongly than the parental isRNA NP71 and the other isRNA sequences from fragmentation step 3. A very weak activation of the luciferase reporter gene was detectable in human TLR8 co-expressing cells but also in HEK293 cells only expressing the NF-κB-inducible luciferase reporter gene (TLRNull) for all tested isRNA sequences and thus might represented unspecific background activation. Based on the induced cytokine profile and its higher TLR7 specificity, isRNA NP71-Seq4 was selected for further fragmentation.

Step 4:

The fourth fragmentation step represented the last step of the applied sequential fragmentation strategy and included a thorough analysis of the predicted secondary structure of isRNA NP71-Seq4 and the diligent selection of further isRNA fragments (see Figure 3.21).

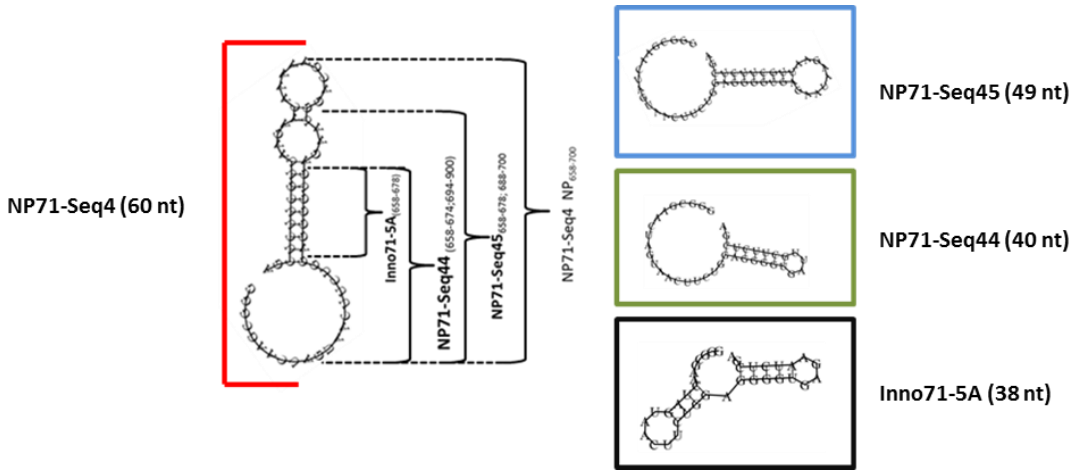

Figure 3.21: The fourth and last step of the applied iterative fragmentation strategy. The selected NP71-Seq4 fragment was subdivided into the three fragments NP71-Seq45, NP71-Seq44 and Inno71-5A according to the secondary structure prediction of NP71-Seq4. The length and position of the isRNA fragments within NP71-Seq4 are indicated. NP = nucleoprotein-derived isRNA molecule; nt = nucleotides.

The secondary structure analysis of isRNA NP71-Seq4 illustrated that the molecule was characterized by two closed loop structures (one terminal and one internally located), a stable RNA-duplex and an open loop structure. The last fragmentation step was mainly based on the rational to conserve the stem-loop structure in the descendant isRNA fragments. Thus, isRNA NP71-Seq45 showed a high structural similarity to NP71-Seq4 except the lack of the terminal closed loop structure. isRNA NP71-Seq44 also displayed a similar structure like RNA sequence NP71-Seq4, but lacked both closed loop structure. Inno71-5A was the smallest isRNA fragment and consisted only of the stable RNA-duplex of isRNA NP71-Seq4. However, as already described in section 3.2.1 and 3.2.4, all isRNAs were flanked on both sides by short nucleotide stretches derived from the pST1 plasmid template and potentially an additional nucleotide at the 5' or 3' end. Hence, the obtained secondary structures were likely to be slightly different to the expected structures. This could be clearly seen by sequence Inno71-5A. Instead to finish in a stable RNA duplex only, the additional nucleotides added during *in vitro* transcription resulted in a secondary structure prediction with two small RNA duplices, two closed loop structures and one open loop structure. Therefore, Inno71-5A represented the most unstable isRNA sequence of fragmentation step 4.

In accordance to the *in vitro* analysis of the fragmentation steps before, the selected isRNA fragments from step 4 were initially analyzed using the human PBMC IFN-α secretion assay (Figure 3.22).

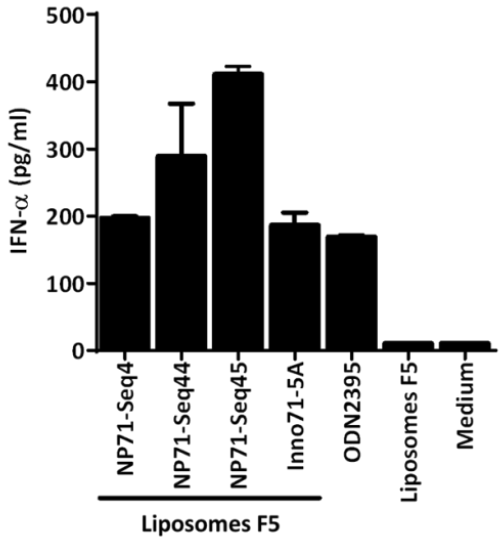

Figure 3.22: *In vitro* stimulation of whole human PBMCs by formulated IVT isRNA candidates from the fourth fragmentation step. 1x10^6 freshly isolated human PBMCs per well were stimulated with F5-formulated NP71-seq4, NP71-seq44, NP71-Seq45, and Inno71-5A (0,167µg/well). As controls, the cells were stimulated with unformulated Cpg-ODN2395 (1 µg/well), and empty Liposomes F5. The secretion of IFN-α was measured using commercially available ELISA kits. Experiments were performed in biological triplicates.

All tested isRNA sequences derived from fragmentation step 4 induced equally high or even higer levels of IFN-α in PBMCs than their parental isRNA NP71-Seq4. The strongest effect was obeserved for NP71-Seq45 isRNA that stimulated human PBMCs two secrete twice the amount of IFN-α levels than their parental NP71-Seq4.

Next we analyzed which isRNA sequence led to the strongest induction of luciferase reporter gene expression in human TLR7 co-expressing HEK293 cells (Figure 3.23).

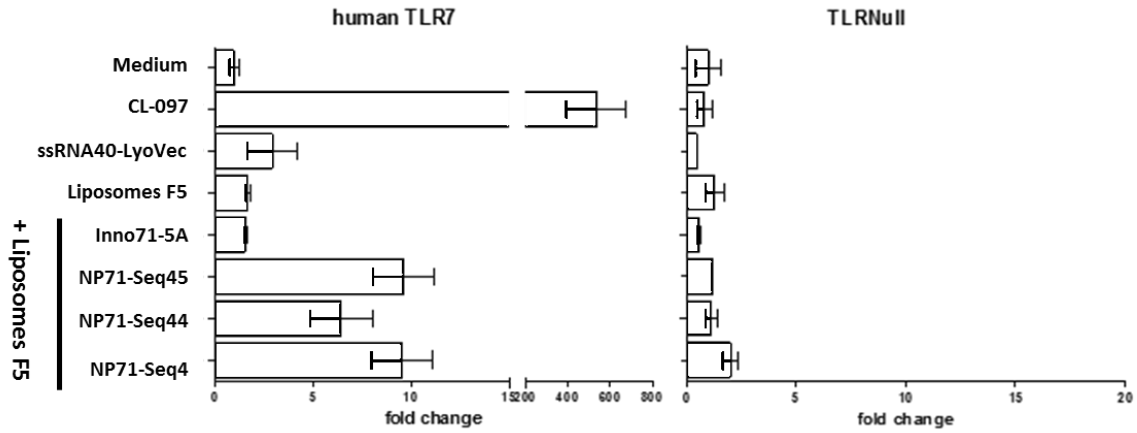

Figure 3.23: *In vitro* stimulation of HEK293-TLR7 cells with formulated IVT isRNA candidates from last fragmentation step. HEK293 cells stably co-expressing human TLR7 in addition to an NF-κB-inducible luciferase reporter gene and HEK293 cells only expressing the NF-κB-inducible luciferase reporter gene were incubated with F5-formulated IVT RNA candidates (0,167µg/well). Positive controls were unformulated CL-097 for human TLR7 and ssRNA40-LyoVec for murine TLR8/TLR7. Empty F5-liposomes and untreated cells (Medium) served as negative controls.

The results of the HEK293-TLRx assay clearly showed that isRNAs NP71-Seq45 and the parental isRNA NP71-Seq4 activated the lucifearse reporter gene in human TLR7 co-expressing HEK293 cells to a comparable extent. In comparison, isRNA NP71-Seq44 showed

a slightly reduced luciferase induction. Interestingly, stimulation with Inno71-5A did not lead to a luciferase expression higher than stimulation with empty liposomes F5 and thus, Inno71-5A might not be a agonist for human TLR7.

In addition to both *in vitro* standard assays, we included a further *in vitro* assays to analyze the selected isRNA sequences of the fourth fragmentation step in more detail.
It has been reported that pDCs are the main cellular producers of IFN-α upon stimulation with viral ssRNA or small molecules such as Resiquimod R848. However, TLR7 stimulation in pDCs resulting in IFN-α induction is dependent on specific sequence motifs of ssRNAs [110, 156, 157]. Therefore, we wanted to investigate whether the selected isRNAs from the fourth fragmentation step are able to target pDCs and show a similar or varying capacity to activate IFN-α production. Human pDCs were isolated and enriched from PBMCs using MACS technology and then incubated together with liposomes F5-formulated isRNA candidates. Whole human PBMCs (at a lower cell number) and PBMCs depelted from pDCs (eluate product by positive selection during the MACS isolation procedure) served as controls (Figure 3.24).

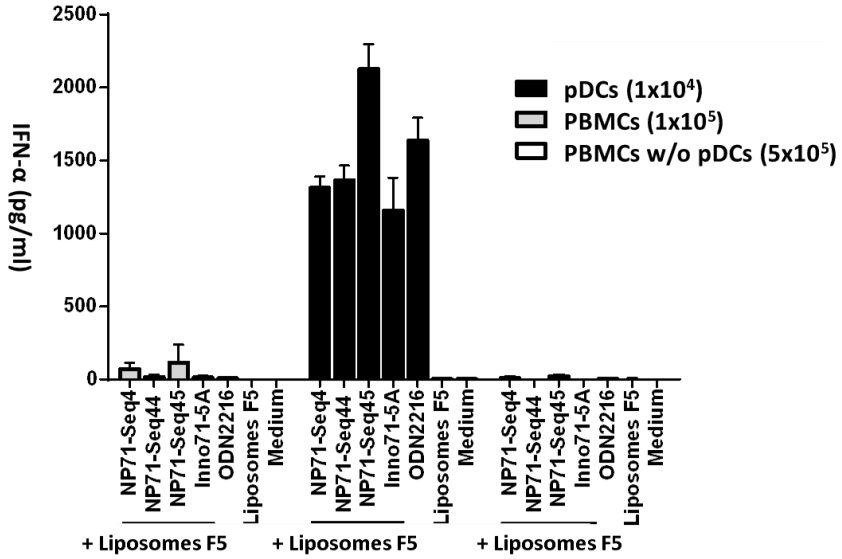

Figure 3.24: *In vitro* stimulation of whole human PBMCs ($1x10^5$ cells/well); enriched pDCs ($1x10^4$ cells/well) and PBMCs depleted from pDCs ($5x10^5$ cells/well) with liposome F5-formulated isRNA NP71-Seq4; NP71-Seq44, NP71-Seq45 and Inno71-5A. Empty F5-liposomes and cells treated with medium only (Medium) served as negative controls. Unformulated CpG-ODN2216 (5 µg/ml) served as positive control for IFN-α induction. Experiments were performed in biological triplicates.

The IFN-α ELISA results demonstrated that pDCs can be targeted by liposomally formulated isRNAs and produce large amounts of the target cytokine IFN-α. PBMCs depleted of pDCs showed a strongly decreased IFN-α induction when compared to whole PBMCs, indicating that pDCs acted as the main IFN-α producers and strongly responded to the selected isRNAs. As already observed in the human PBMC cytokine release assay, NP71-Seq45 induced the highest amount of IFN-α in pDCs whereas isRNA NP71-Seq45 and Inno71-5A induced similar levels as the ancestor isRNA NP71-Seq4.

Based on the presented *in vitro* studies, NP71-Seq45 was selected as the most promising isRNA adjuvant lead candidate and was subsequently characterized in more detail together with the parental isRNA NP71-Seq4 in further *in vitro* studies.

3.4 *In vitro* characterization of the isRNA adjuvant lead structure NP71-Seq45

As an additional *in vitro* experiment for the characterization of the isRNA adjuvant lead structure NP71-Seq45, an indirect confirmation test for TLR7 signalling was performed. In this experiment we analyzed if the IFN-α induction upon stimulation with F5-formulated isRNA NP71-Seq45 was dependent on nucleic acid sensing endosomal TLRs. Therefore, we used Bafilomycin A1 as an endosomal acidification inhibitor and thus, indirectly as an endosomal TLR stimulation inhibitor. Freshly isolated whole human PBMCs were pretreated with Bafilomycin A1 and subsequently incubated with F5-formulated NP71-Seq45 isRNA. Afterwards, the IFN-α secretion in the cell culture supernatant was measured by an ELISA assay (Figure 3.25).

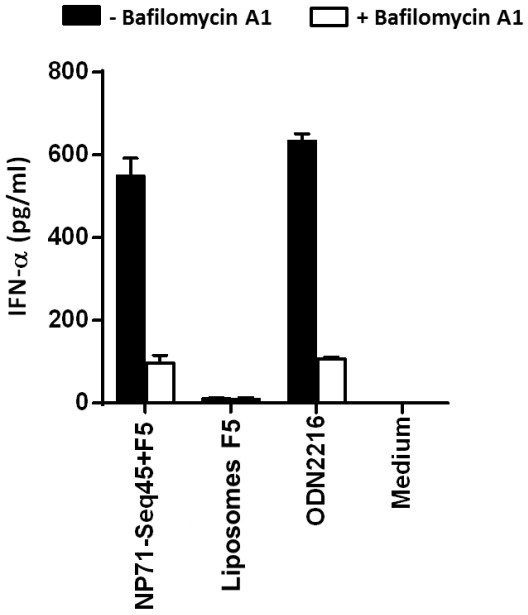

Figure 3.25: isRNA NP71-Seq45 mediated induction of IFN-α in human PBMCs is depending on endosomally located TLRs. Freshly isolated whole human PBMCs were pretreated for 1 h with 250 nM Bafilomycin A1. The Bafilomycin A1 pre-treated PBMCs and untreated PBMCs were incubated subsequently for 14 h with F5-formulated NP71-Seq45 (0,167 µg/well), empty Liposomes F5, unformulated Cpg-ODN226 as positive and medium as negative control. Experiments were performed in biological triplicates.

As expected, Bafilomycin A1 pre-treatment strongly decreased the induction of IFN-α by CpG-ODN2216. A similarly strong reduction of IFN-α secretion could be observed by pre-treatment of PBMCs incubated with Bafilomycin A1 followed by F5-formulated isRNA NP71-Seq45 stimulation, indicating that isRNAs were recognized by an endosomally located TLR. To be noted, the cell viability was not affected by the used Bafilomycin A1 concnetration in combination with the added amounts of NP71-Seq45 or CpG-ODN2216 (data not shown).

In the next experiment, we analyzed the cytokine profile induced in human PBMCs by F5-formulated isRNA NP71-Seq45 and its parental fragment NP71-Seq4 in more detail using a multiplexed bead immunoassay (Figure 3.26). With this assay we were able to analyze the secceretion of IFN-α, IL10, IL6, TNF-α and IFN-γ into the cell culture supernatant.

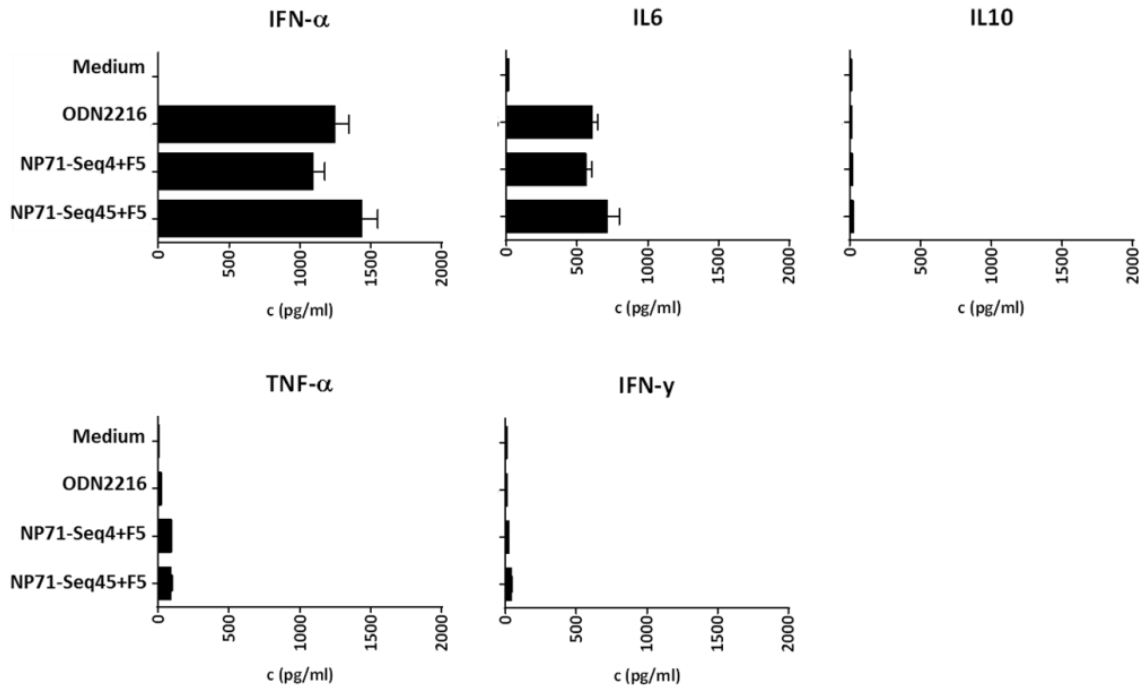

Figure 3.26: F5-formulated isRNAs induce high levels of IFN-α but only marginal levels of IFN-γ, TNF-α, and IL10 in human PBMCs. 1x10^6 freshly isolated human PBMCs per well were stimulated with F5-formulated isRNA NP71-seq4 or NP71-seq45. As controls, the cells were stimulated with unformulated CpG-ODN2216 (1 µg/well) or left untreated (Medium). The cytokine secretion in the cell culture supernatant was analyzed by a multiplexed bead immunoassay (Biorad).

In accordance with previous results, the F5-formulated isRNA NP71-Seq45 induced higher levels of IFN-α than its parental sequence NP71-Seq4. Both isRNAs acted only as weak inducers for the strongly pro-inflammatory cytokines IFN-γ and TNF-α or the anti-inflammatory cytokine IL10. However, stimulation with isRNA NP71-Seq45 or NP71-Seq4 resulted in the secretion of the moderate pro-inflammatory cytokine IL6 in which the levels were comparable to those induced by CpG-ODN2216 incubation.

A further *in vitro* experiment was conducted in order to analyze the *in vitro* functionality of F5-formulated isRNA NP71-Seq45 with respect to the upregulation of the early cell activation marker CD69. Therefore, human PBMCs were incubated with isRNA NP71-Seq45 and subsequently the expression status of CD69 on the surface of several immune cell populations (B cells, NK cells, mDCs, pDCs and monocytes) was analyzed by flow cytometry (FACS). The results are exemplified for PBMCs derived from one donor in Figure 3.27.

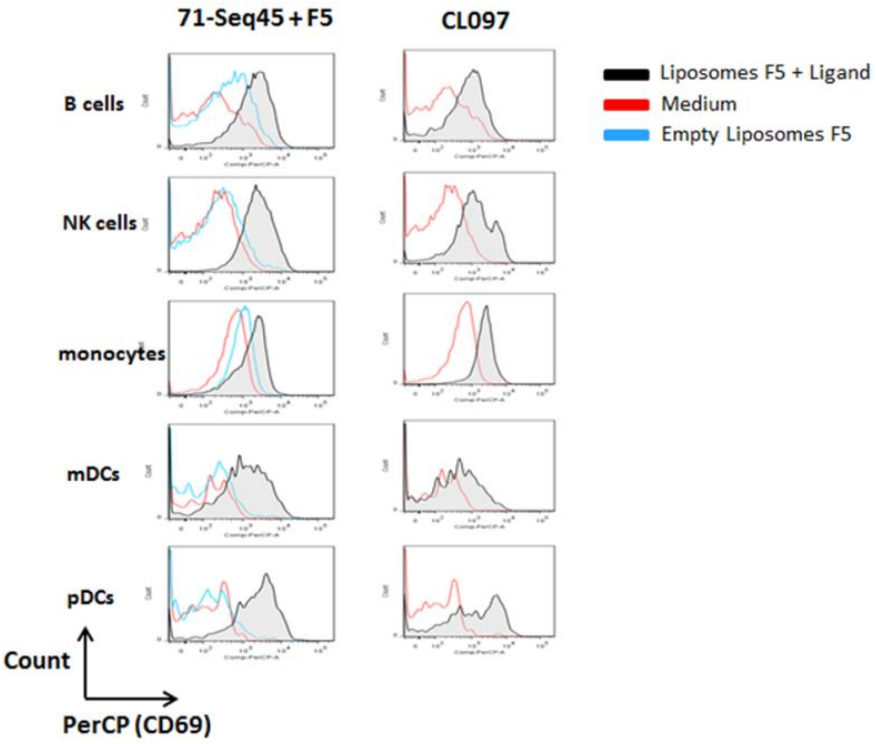

Figure 3.27: Upregulation of the early activation marker CD69 on several human immune cell populations upon stimulation with F5-formulated isRNA NP71-Seq45. 1x10^6 freshly isolated human PBMCs per well were stimulated with F5-formulated NP71-seq45 (Liposomes F5 + Ligand). As controls, the cells were stimulated with unformulated CL-097, empty F5 Liposomes or left untreated (Medium). The cells were collected and stained with anti-CD16-FITC (NK cells), anti-BDCA2-APC (pDCs), anti-BDCA3-PE (mDCs), anti-CD19-BV421 (B cells) and anti-CD14-APC Cy7 (monocytes) in combination with anti-CD69-PerCp. Stained cells were analyzed by FACS Canto II and the histogram illustrated only living cells. The presented results were from one donor. Similar data were obtained by two other PBMC donors.

The stimulation of human PBMCs by F5-formulated isRNA NP71-Seq45 led to upregulation of the early activation marker CD69 on the surface of all analyzed immune cells. In particular, the upregulation of CD69 on pDCs (BDCA2) was clearly demonstrated by formulated isRNA NP71-Seq45 and also by the TLR7/8 ligand CL-097. Furthermore, formulated isRNA NP71-Seq45 and CL-097 did induce a slightly weaker upregulation of CD69 on the surface of mDCs (BDCA3). On B cells, NK cells and monocytes the CD69 marker was strongly upregulated by isRNA NP71-Seq45 and by the positive control CL-097. The empty liposomes did not induce the upregulation of CD69, except on B cells in which the CD69 was marginally upregulated.

To finalize the *in vitro* stimulation analysis, the functionality of F5-formulated isRNA NP71-Seq45 and the parental sequence NP71-Seq4 were tested in mouse splenocytes and bone marrow cells. The control of the immunostimulatory activity in mouse cells was critically important, because all following *in vivo* studies (including immunization studies and tumor models) should be conducted in mice as an animal model. The cytokine expression profile (IFN-α vs. TNF-α) upon stimulation of mouse splenocytes and bone marrow derived cells (only IFN-α) are presented in Figure 3.28.

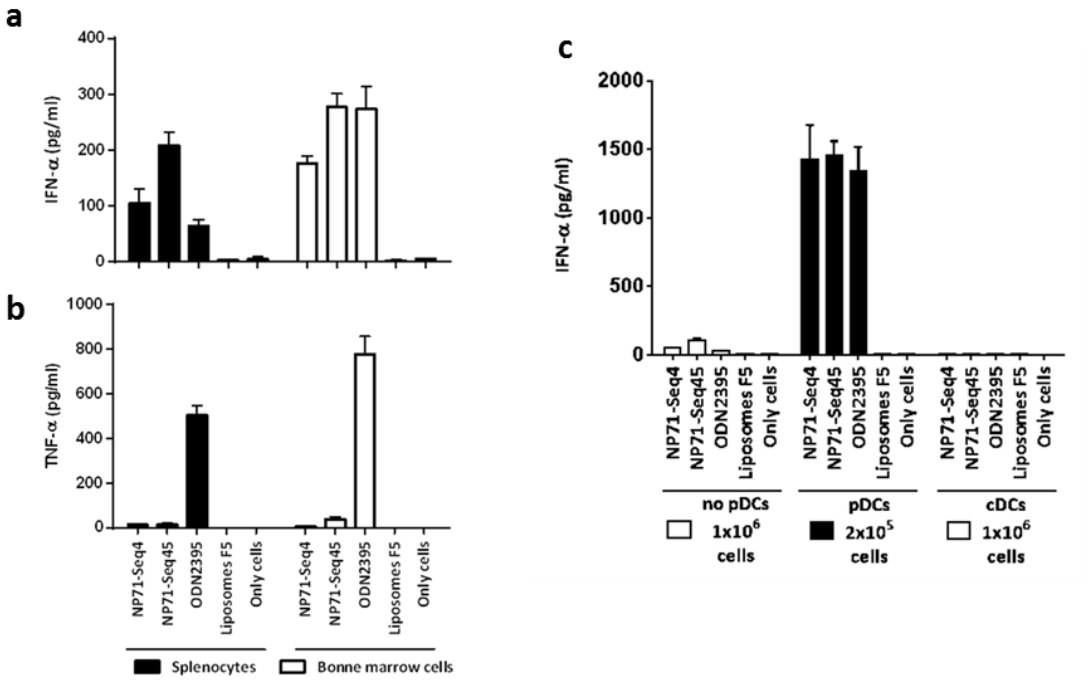

Figure 3.28: *In vitro* stimulation of mouse cells with F5-formulated NP71-Seq4 and NP71-Seq45. a-b) Balb/c derived splenocytes and bone marrow cells were generated and incubated with F5-formulated isRNA NP71-Seq4 and NP71-Seq45 (0,167 µg/well). As positive control unformulated CpG-ODN2395 (0,5 µg/well) was used. Empty liposomes and untreated cells (Only cells) served as negative controls. **c)** Mouse bone marrow cells were enriched for pDCs or cDCs by using MACS technology. The flow through of the pDC enrichment was used to analyze bone marrow cells with reduced pDC content (no pDCs). Stimulation of cells was performed as described for a and b. All assays were performed in biological triplicates.

The previously generated *in vitro* data using human PBMCs could be confirmed in mouse cells. The F5-formulated isRNA NP71-Seq45 induced IFN-α secretion more strongly than the parental isRNA NP71-Seq4 in splenocytes but also in bone marrow-derived cells. Whereas the formulated isRNAs induced a strong IFN-α response and only marginal TNF-α levels in splenocytes (Figure 3.28 a and b), the unformulated TLR9 agonist class C CpG ODN2395 led to a strong induction of both, IFN-α and TNF-α. Furthermore, the tested isRNAs were able to induce a strong IFN-α expression an secretion in pDCs but not in cDCs. Thus, the secretion of IFN-α was strictly dependent on pDCs, as already observed using human cells.

Taken together, the performed iterative fragmentation strategy, secondary structure predictions and *in vitro* screenings of the Influenza A nucleoprotein encoding gene allowed us to define small isRNAs, which induced high levels of IFN-α in human and also in mouse cells. The isRNA sequences of the last fragmentation step displayed a high specificity for TLR7 and a very promising cytokine induction profile. Focussing on both lead cytokines, the isRNA sequences could induce a very strong IFN-α response combined with only a very weak TNF-α induction in all tested donors. Therefore, isRNAs of the last fragmentation step, with a special focus on the most promising lead candidate NP71-Seq45, were transferred to subsequently performed *in vivo* studies.

3.5 isRNA-LPX exerts its adjuvant activity in an IFN-α dependent manner.

In contrast to the liposomal formulation F5 used in *in vitro* experiments, the liposomal formulation F12 was used for all *in vivo* studies. F12 was originally developed by the BioNTech AG and was adapted for an optimal delivery of RNA molecules (including isRNAs) into the spleen after i.v. administration [118]. Therefore, chimeric HBcAg-VLPs as model antigen were also administered i.v. to ensure the delivery of both, the adjuvant and the immunogen, to the same lymphatic organ and to maximize the immune response.

3.5.1 Induction of specific B cell response by F12-formulated isRNAs in combination with HBcAg-#A79 VLPs

In the previous experiments it could be demonstrated that the isRNAs of the last fragmentation step (NP71-Seq 44, NP71-Seq45 and Inno71-5A) were all able to induce very strong IFN-α levels in bulk human PBMCs and in mouse cells (splenocytes and bone marrow-derived cells). However, it could be also observed that these isRNA fragments had a slightly different IFN-α induction capacity when compared to each other.
In order to investigate whether these small differences in *in vitro* assays became also visible in *in vivo* studies, and also to confirm the selection of NP71-Seq45 as the most promising lead structure, we performed an initial mouse immunization experiment. Selected isRNAs were formulated with liposomes F12 and co-admistered i.v. with chimeric HBcAg-#A79 VLPs. The induced antibody-titer against the inserted epitope #79 was analyzed by a peptide ELISA assay and the specific humoral immune response against the native CLDN6 target protein by flow cytometry (FACS). In addition to the isRNAs of the last fragmentation step, the ancestor isRNA fragments NP71-Seq4 and NP2-1 were analyzed as well (see Figure 3.29).

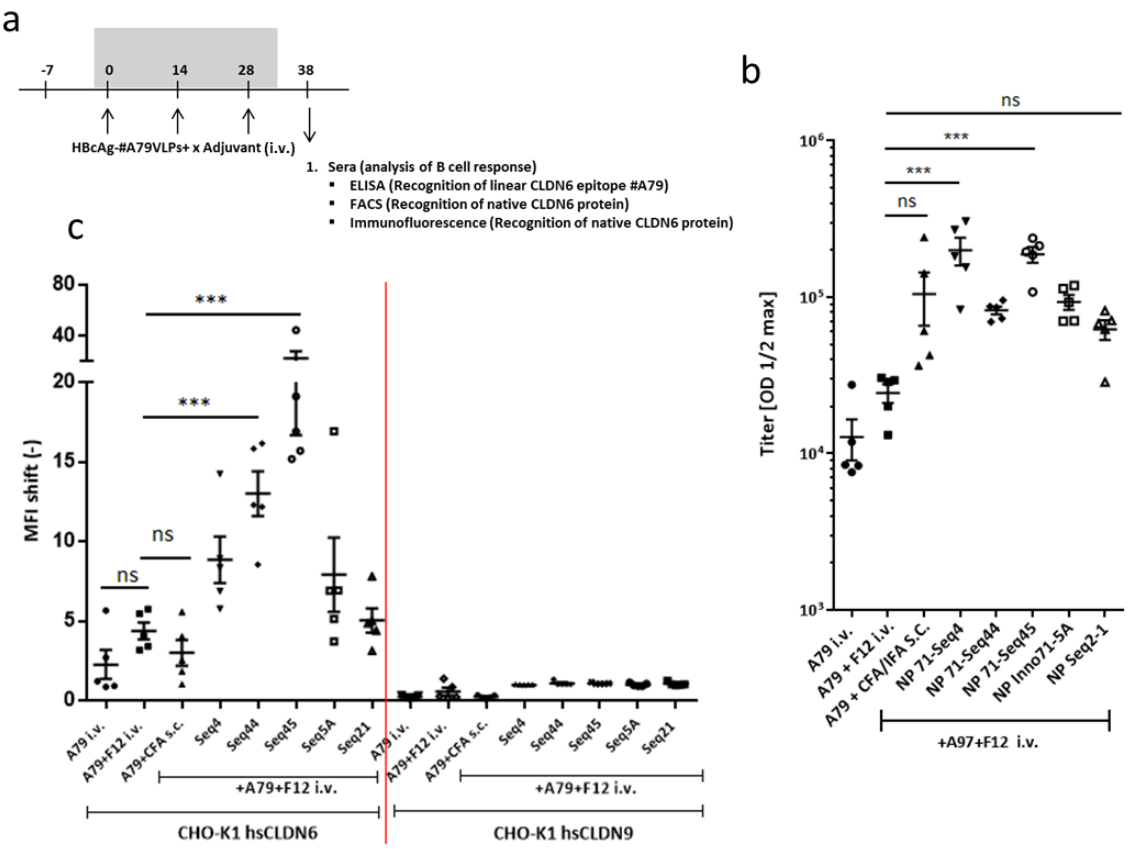

Figure 3.29: F12-formulated isRNAs in combination with HBcAg-#A79 VLPs induce an antigen-specific antibody response *in vivo*. a) Immunization schedule. Balb/c mice were immunized i.v. three times at two-week intervals (day 0, 14 and 28) with HBcAg-#A79 VLPs combined with F12-formulated isRNA NP71-Seq4 (Seq4), NP71-Seq44 (Seq44), NP71-Seq45 (Seq45), NP Inno71-5A (Seg5A) or NP Seq2-1 (Seq21). Mice immunized with empty F12 liposomes in combination with HBcAg-#A79 VLPs (A79+F12), non-adjuvanted HBcAg-#A79 VLPs (A79), or adjuvanted with CFA/IFA (immunized s.c.; A79+CFA/IFA) served as controls. Ten days after the third immunization, blood samples were taken for analysis of the antigen-specific humoral immune response. **b)** IgG antibody titer analysis by epitope #79 peptide ELISA. Illustrated are the calculated half-maximal antibody titers. **c)** FACS analysis using CHO-K1 hsCLDN6 (left side of the red line) and CHO-K1 hsCLDN9 expressing cells (right side of the red line). The specific antibody binding was detected with AlexaFluor647 conjugated goat anti-mouse secondary antibodies. Illustrated is the x-fold MFI shift of final vs. corresponding pre-bleeds. For statistical analysis the software GraphPad Prism 7 performing a one way ANOVA test comparing each group to the A79+F12 group was used. The difference between the groups were considered to be statistically significant at $P<0.05$. ns = not significant, ***$p < 0.001$ vs. HBcAg-#A79 VLP+F12 i.v. group. One way ANOVA test for b) and c). Shown are the mean values +/- SEM.

As shown in Figure 3.29. b, i.v. immunization of non-adjuvanted HBcAg-#A79-VLPs induced only a very weak half-maximal antibody titer. The addition of empty liposomes F12 or the adjuvant CFA/IFA (immunized s.c.) to the vaccine could slightly increase the antibody titer against the #79 epitope. However, only the co-administration of F12-formulated isRNAs, especially NP71-Seq4 and NP71-Seq45, strongly and statistical significantly increased the antibody titers against the linear #79 CLDN6 epitope. Interestingly, the ancestral and much longer isRNA sequence NP2-1 induced only a marginal adjuvant effect that was not significant when compared to HBcAg-#A79 VLPs in combination with empty F12 liposomes.
However, the main goal of the used chimeric VLP vaccine/isRNA combination was the induction of antibodies, which were able to specifically bind the CLDN6 target antigen in its native conformation on the surface of living cells. Therefore, the FACS data (Figure 3.29 c) was more relevant to judge the isRNA-mediated immunostimulatory effects and illustrated that HBcAg-#A79 VLPs immunized without the addition of adjuvants induced a weak antigen-

specific immune response, with only one animal showing a positive reaction with a MFI shift greater than 2.5 fold (2.5 fold were considered as positive antigen-specific antibody responses). The antigen-specific immune response was slightly, but statistically not significant increased by the adjuvantation with CFA/IFA or empty F12-liposomes. As already demonstrated in Figure 3.29, the CFA/IFA group induced a specific immune response characterized by a strong interindividual variability. The i.v. co-administration of HBcAg-#A79-VLPs and F12-formulated isRNAs strongly increased the CLDN6 antigen-specific antibody response, without increasing any unspecific binding of antibodies to the closely related CLDN9 protein.

As already presented in Figure 3.22 isRNAs of the final fragmentation step induced high but slightly varying levels of IFN-α in human and also in mouse cells. Surprisingly, this difference was reflected quite consistent and even more pronounced also in the induced CLDN6 specific B cell response. The highest IFN-α secretion and by far the strongest specific B cell response was achieved by isRNA NP71-Seq45 followed by NP71-Seq44. Co-administration of isRNA Inno71-5A, although achieving relatively high IFN-α levels in *in vitro* experiments, did not result in significantly enhanced antibody response against the native CLDN6 protein. Interestingly, isRNA NP71-Seq4, strongly increasing the half-maximal antibody titer against the linear #79 epitope, failed to promote antibody response against the native CLDN6 protein.

Taken together, the results of this *in vivo* immunization study clearly supported the selection of isRNA NP71-Seq45 as the most promising adjuvant lead candidate and proofed that the applied fragmentation strategy was successful in terms of identifying small InfA-derived RNA molecules with superior immunostimulatory capacity than their ancestors. The latter conclusion was clearly justified when comparing the results of NP Seq 2-1 with NP71-Seq45.

The individual sera that induced the strongest CLDN6 antigen specific immune responses were analyzed additionally on unfixed CLDN6 expressing cells by immunofluoresence microscopy (IF) to confirm the FACS results (see Figure 3.29). CLDN9 expressing cells served again as a specificity control of the induced antibodies.

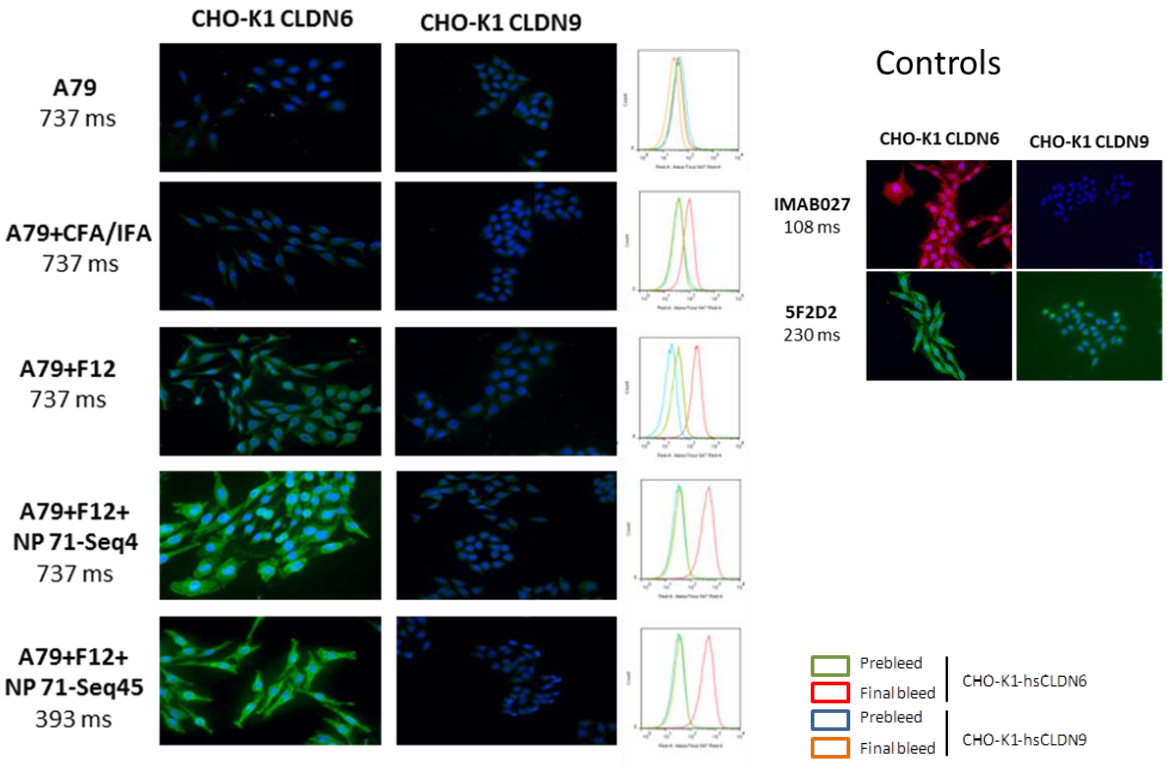

Figure 3.30: IF analysis for the reactivity of selected sera against the native CLDN6 protein. Stably transfected CHO-K1 CLDN6 or CLDN9 expressing cell lines were stained under native conditions with selected sera of immunized mice (serum dilution: 1:100). Analyzed sera included sera derived from immunizations with HBcAg-#A79 VLPs in combination with CFA/IFA (A79+CFA/IFA), empty F12-liposomes (A79+F12), F12-formulated isRNA NP71-Seq4 (A79+F12+NP71-Seq4), F12-formulated NP71-Seq45 (A79+F12+NP71-Seq45) or non-adjuvanted VLPs (A79). Bound antibodies were detected with the secondary antibody G-α-r-AlexaDyLight488. IF images are shown with the corresponding FACS histograms. Controls were the CLDN6 specific mAb IMAB027 (1µg/ml, stained with a Cy3 labeled secondary antibody) and the CDLN6/9 cross-reactive hybridoma supernatant 5F2D2 (dilution 1:4). The applied exposure times for image taking are indicated. Hoechst 33342 was used for nuclear staining and IF images were taken with a Zeiss Imager-M2 Axio fluorescence microscope.

The IF analysis confirmed the previous FACS results. Serum from mice immunized with HBcAg-#A79 VLPs alone or adjuvanted with CFA/IFA showed only a very weak or undetectable reactivity against the native CLDN6 target antigen. The co-administration of empty liposomes F12 with HBcAg-#A79 VLPs could slightly improve the antigen-specific antibody responses. However, only the combination of HBcAg-#A79 VLPs and F12-formulated isRNAs elicited a strong antibody reactivity against the native CLDN6 protein and the strongest immune responses was obtained by co-administration of isRNA NP71-Seq45. To be noted, the IF exposure time for the serum obtained after immunzation with isRNA NP71Seq45 adjuvanted HBcAg-#A79 VLPs had to be cut in half in comparison to the other exposure times in order to avoid an over-exposure of the image.

In summary, especially the isRNA adjuvant NP71-Seq45 could significantly increase the immunogenicity of CLDN6 targeting chimeric HBcAg-#A79 VLPs, justifying its selection as lead structure. Therefore, further *in vivo* eperiments focussed on isRNA NP71-Seq45 and tried to elucidate its *in vivo* mode of action in more detail.

3.5.2 Antigen-specific antibody responses induced by F12-formulated isRNA in combination with HBcAg-#A79 VLPs are depending on TLR7 signaling in pDCs and pDC derived IFN-α.

The previously generated *in vitro* data revealed that the pDCs were the main target cells of F5-formulated isRNAs and accordingly the main producer of the cytokine IFN-α (Figure 3.24 and Figure 3.28. c). Subsequently, we could demonstrate that the identified formulated isRNAs exerted their immunostimulatory effect mainly by endosomal TLR activation (Figure 3.29). In this section, we tried to confirm the *in vitro* obeservations, especially the profound role of pDCs as the main IFN-α producers upon isRNA-LPX stimulation also *in vivo*.

In a first experiment, we used BDAC2-DTR transgenic mice that have a simian diphtheria toxin receptor (DTR) under the transcriptional control a human C-type lectin domain family 4, member C (CLEC4C or BDCA2) promoter. Treatment of these mice with diphtheria toxin (DT), resulted in the *in vivo* depletion of pDCs. DT-treated BDAC2-DTR mice and untreated C57BL/6 wildtype mice were immunized i.v. with HBcAg-#A79 VLPs combined with F12-formulated NP71-Seq45 isRNA using the standard immunization schedule. Induction of IFN-α was analyzed 4h after the first immunization by ELISA. Antibody responses against human CLDN6 or CLDN9 (as specificity control) were analyzed ten days after the last immunization by FACS. The results are shown in Figure 3.31

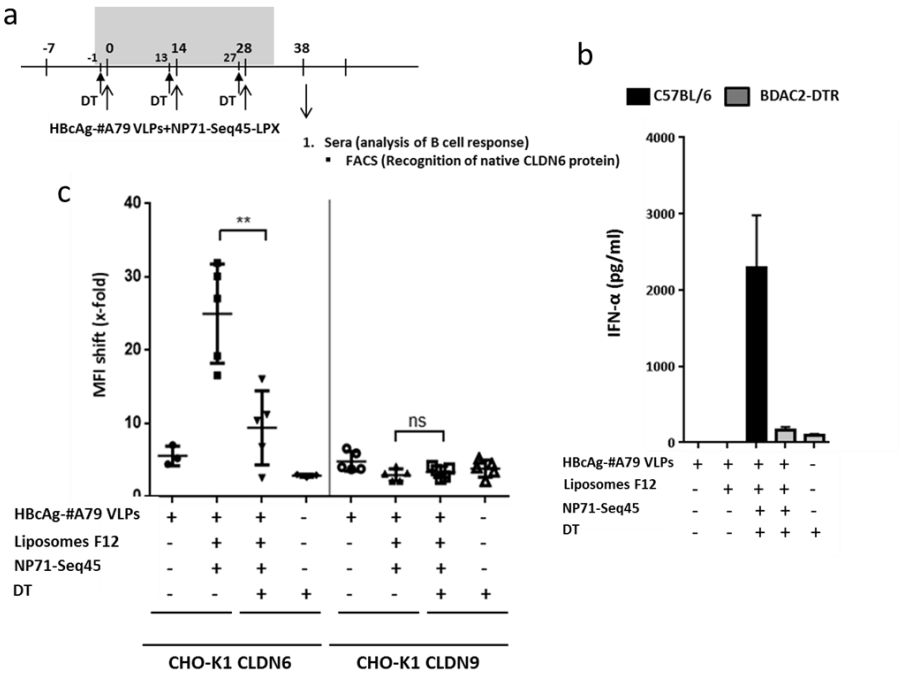

Figure 3.31: CLDN6-specific B cell responses induced by isRNA-LPX NP71-Seq45 in combination with HBcAg-#A79 VLPs are mainly dependent on pDCs. a) Treatment schedule. DT-treated BDAC2-DTR (4.5ng DT/g mouse) and untreated C57BL/6 mice were immunized i.v. three times at an interval of 14 days with HBcAg-#A79 VLPs combined with F12-formulated NP71-Seq45 isRNA. Controls were C57BL/6 wildtype mice immunized with HBcAg-#A79 VLPs alone or in combination with empty F12-liposomes and BDAC2-DTR mice treated with DT alone but not receiving the antigen plus isRNA adjuvant. **b)** ELISA-based IFN-α analysis in mouse sera which were taken 4h after the third immunization. A commercially available ELISA kit was used for analysis. **c)** FACS analysis of sera taken at d38 using CHO-K1 hsCLDN6 or CHO-K1 hsCLDN9 expressing cells. The specific antibody binding was detected with AlexaFluor647 conjugated goat anti-mouse secondary antibodies. Illustrated is the x-fold MFI shift of final vs. corresponding pre-bleeds. For statistical analysis the software GraphPad Prism 7 performing a one way ANOVA test was used. The difference between the groups were considered to be statistically significant at $P<0.05$. ns = not significant, **$p<0.01$. Student's t test for c). Shown are the mean values +/- SEM.

The IFN-α ELISA (Figure 3.31. b) revealed that the IFN-α level was strongly induced in C57BL/6 mice 4h after the immunization with F12-formulated isRNA NP71-Seq45 in combination with HBcAg-#A79 VLPs. In contrast, only minor amounts of IFN-α were secreted in BDAC2-DTR mice treated with DT and receiving the same antigen/adjuvant combination. We also showed that the immunization with HBcAg-#A79 VLPs alone or in combination with empty F12-liposomes were not able to trigger any IFN-α secretion *in vivo.* As observed before, the obtained data for IFN-α secretion was clearly reflected in the induction of target specific antibodies (Figure 3.31 c). Analysis of CLDN6 specific antibodies by FACS revealed that the DT-mediated depletion of pDCs in BDAC2-DTR mice caused a highly significant reduction in the CLDN6 antigen-specific antibody response upon immunization with F12-formulated NP71-Seq45 isRNA in combination with HBcAg-#A79 VLPs, when compared to antibodies induced by this antigen/adjuvant co-administration in C57BL/6 wildtype mice.

The obtained *in vivo* data using BDAC2-DTR transgenic mice confirmed previous *in vitro* results showing that pDCs could be stimulated by isRNA-LPX and are the main cellular producers of IFN-α. Furthermore, the systemic release of IFN-α by pDCs was determined as a crucial factor for the induction of target-specific, enhanced antibody responses.

3.5.3 The immunostimulatory activity of isRNA NP71-Seq45 is largely dependent on its specific RNA sequence.

It has been previously reported that the GU content in small ssRNAs strongly affects their specificity for TLR7 [53, 106]. In order to analyze the contribution made by the primary RNA sequence and the predicted secondary RNA structure to the immunostimulatory activity of isRNA NP71-Seq45, the RNA sequence NP71-Seq52 was designed *in silico* and synthesized by *in vitro* transcription. NP71-Seq52 mimicked the predicted secondary structure of isRNA NP71-Seq45, but was characterized by the lack of GU motifs and accordingly the reduction of total uridine content in the RNA stem structure (see Table 3.2: Direct comparison between isRNA sequence NP71-Seq45 and the designed RNA sequence NP71-Seq52.).

Table 3.2: Direct comparison between isRNA sequence NP71-Seq45 and the designed RNA sequence NP71-Seq52. IVT = *in vitro* transcription; ds = double-stranded; U content = uridine content. For the RNA secondary structure the RNAfold web server was used.

RNA name and way of production	Base content	Origin	ds lenght	U content (Loop/Stem)	Predicted secondary structure
NP71-Seq45 (IVT)	50	viral	11	5/6	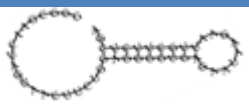
NP71-Seq52 (IVT)	46	*in silico* design	10	1/1	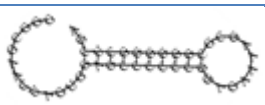

As already mentioned in section 3.2.1, all produced IVT RNAs were flanked on both sides by short stretches derived from the pST1 plasmid template. These stretches contained two uridines and therefore the NP71-Seq52 RNA contained two uridines in the open-loop structure as well.

For the evaluation of the immunostimulatory capacity of NP71-Seq52-LPX in comparison to isRNA NP71-Seq45-LPX and the parental, F12-liposomes formulated isRNA NP71-Seq4, Balb/c mice were immunized with HBcAg-#A79 VLPs and formulated RNAs according to the standard immunization regime. Four hours after the first immunization, sera were taken for analysis of the IFN-α release *in vivo*. Ten days after the last immunization, sera were taken for FACS analysis of the induced antibody response against the native CLDN6 target protein (see Figure 3.33).

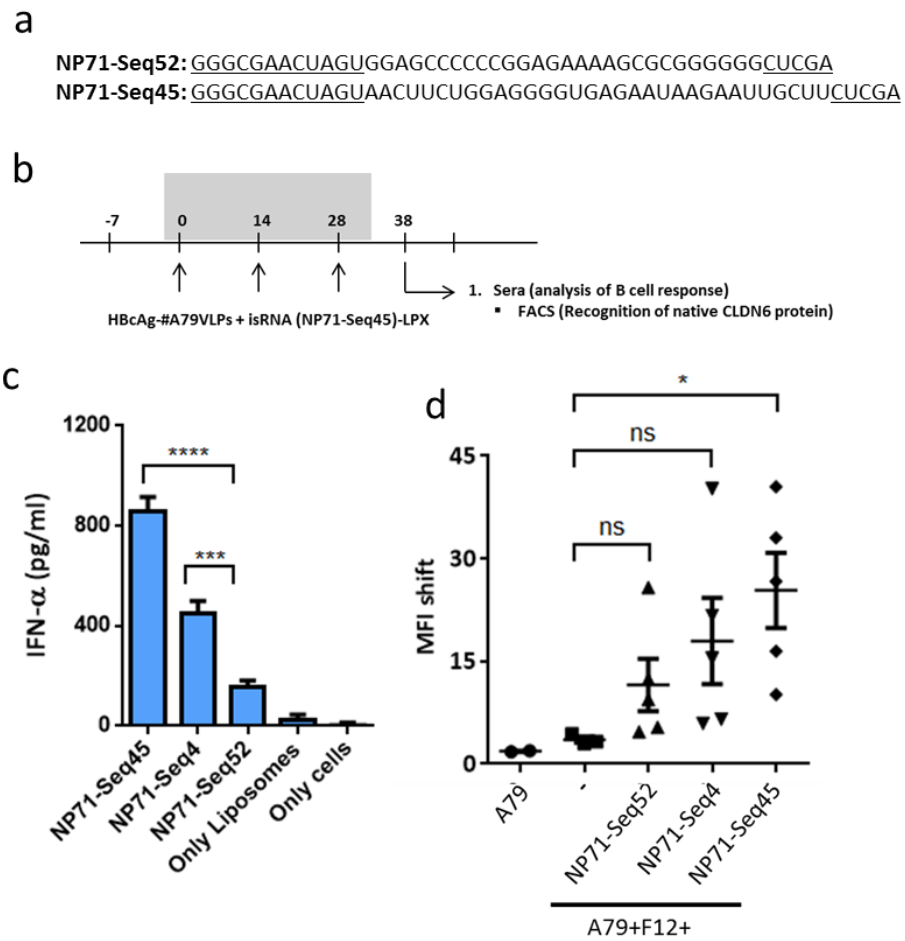

Figure 3.32: IFN-α secretion and CLDN6 target specific antibody responses after co-administration of HBcAg-#A79 VLPs and NP71-Seq52. a) RNA sequence of NP71-Seq52 and NP71-Seq45. Nucleotides derived from the pST1-template are undelined. **b)** Applied immunization regime. Balb/c mice (n=10 per group) were immunized with HBcAg-#A79-VLPs alone (A79), adjuvanted with empty liposomes F12 (-) or adjuvanted with F12-formulated NP71-Seq4; NP71-Seq45 or NP71-Seq52. **c)** IFN-α levels in medium supernatant after in vitro stimulation of human PBMCs with the test items ON by 37°C . A commercially available ELISA kit was used for the determination of IFN-α levels. **d)** FACS analysis of induced target specific antibody responses using CHO-K1 cells stably expressing hsCLDN6. The specific antibody binding was detected with AlexaFluor647 conjugated goat anti-mouse secondary antibodies. Illustrated is the x-fold MFI shift of final vs. corresponding pre-bleeds. For statistical analysis the software GraphPad Prism 7 performing a one way ANOVA test was used. The difference between the groups were considered to be statistically significant at P<0.05. ns = not significant, P*<0.05, ***p < 0.001, ****p < 0.0001 vs. NP71-Seq52 for c) and A79+F12 i.v. group for d). One way ANOVA test for c) and d). Shown are the mean values +/- SEM.

The obtained IFN-α ELISA data indicated a significantly decrease of systemic IFN-α release in mice that had been immunized i.v. with F12-formulated NP71-Seq52 and the chimeric CLDN6 VLPs (Figure 3.29. c). However, IFN-α levels in NP71-Seq52-LPX treated mice were still slightly higher than in mice treated with empty F12-liposomes. Interestingly, and as previously demonstrated *in vitro* (Figure 3.22), we could confirm in this experiment that formulated isRNA NP71-Seq45 stimulated the IFN-α secretion more strongly than formulated NP71-Seq4. We could also show that empty liposomes did not result in the induction of IFN-α. Furthermore and in accordance with previous results, the difference in the induced amounts of IFN-α in the tested groups were reflected to a similar extent in the target specific antibody response (Figure 3.29. d). NP71-Seq52-LPX in combination with HBcAg-#A79 VLPs induced a weakly elevated antibody response against the CLDN6 protein that was statistically not significant to the immune reponse using empty F12-liposomes. Although RNA sequence NP71-Seq52 still contained a few uridine residues and probably trace amounts of dsRNA contaminations, due to the small scale purification with mini columns, that might led to a stimulation of TLR3, the target specific antibody response and the IFN-α induction *in vivo* were significantly weaker than those induced by NP71-Seq45-LPX.
These results raised the conclusion that the primary sequence of NP71-Seq45 containing GU motifs in the stem and loop structure were mainly responsible for the TLR7 dependent IFN-α induction in pDCs and subsequently increased antibody responses against the CLDN6 target molecule. However, the involvement of secondary structures or other factors (e.g. RNA length and accessability to TLR7) in the immunostimulatory activity could not completely excluded. This was demonstrated by using F12-formulated isRNA NP71-Seq4 that had a higher GU motif content than NP71-Seq45 but resulted in a weaker IFN-α and accordingly also weaker antibody induction.

3.5.4 Repetitive i.v. administration of F12-formulated isRNAs led to a systemic TLR response tolerance.

As described in the literature, the repeated systemic application of TLR-ligands can induce a state of so called immune TLR response tolerance [158, 159]. This well-known effect could negatively affect the adjuvant efficacy and consequently the whole immune response when combining TLR agonists as adjuvants with protein-based vaccines. Therefore, it was necessary to find out if the identified, TLR7 specific isRNAs formulated in liposome F12 could also induce TLR response tolerance after repetitive i.v. injection, and in which time intervals isRNAs can be administered without leading to a TLR response tolerance.
To address these questions, mice were immunized i.v. with isRNA NP71-Seq4-LPX using two different immunization schedules. The immunization was performed without the addition of HBcAg-#A79 VLPs and ELISA analysis of IFN-α serum levels 4 hours after each injection served as readout assay (Figure 3.29. a).

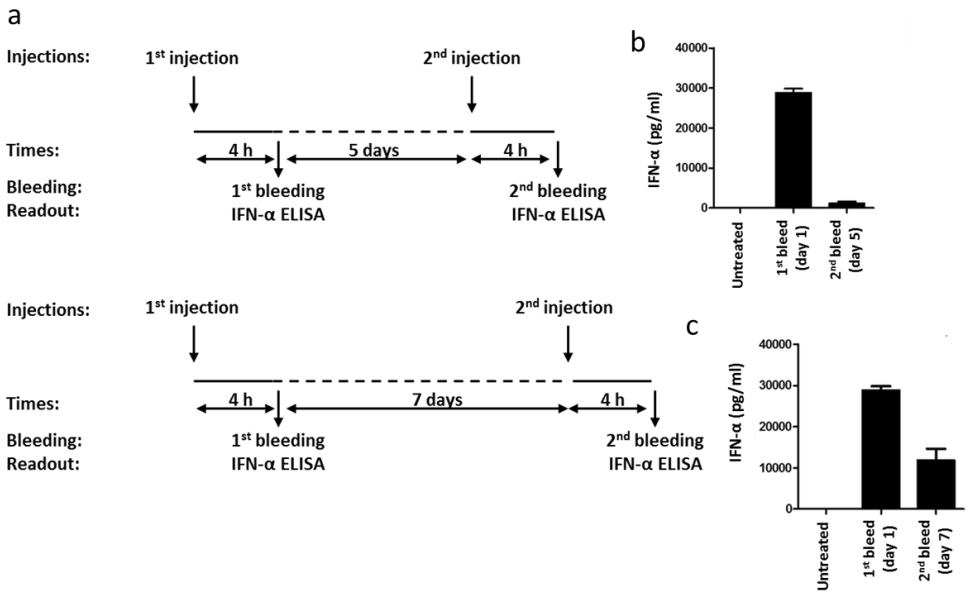

Figure 3.33: Repetitive i.v. administration of F12-formulated isRNA led to a systemic TLR response tolerance. a) Applied immunization schedules. F12-formulated NP71-Seq4 isRNA was injected i.v. twice into Balb/c mice at an interval of 5 (1st group, upper panel) or 7 days (2nd group, lower panel). **b)** and **c)** Serum levels of IFN-α detected by ELISA. Blood samples were taken 4h after each injection and serum levels of IFN-α were determined by a commercially available ELISA assay.

The results clearly revealed that the administration of F12-formulated NP71-Seq4 isRNA at a time interval of 5 days resulted in a pronounced TLR response tolerance effect with a strongly diminished IFN-α secretion after the second injection. However, a partial TLR response recovery could be already achieved by an injection interval of 7 days. Hence, to ensure a maximal isRNA-LPX adjuvant effect when combined with HBcAg-CLDN6 VLPs, i.v. co-administration had to be applied with a minimal time interval of 10-14 days.

3.6 *In vivo* analysis of the induced CLDN6-target specific immunity.

Previous experiments could show that the strongest adjuvant activity and target specific antibody response were reached by i.v. administered HBcAg-#A79 VLPs in combination with F12-formulated isRNA sequence NP71-Seq45. These *in vivo* results justified the *in vitro* based selection of isRNA NP71-Seq45-LPX as most promising lead structure. Thus, most of the subsequent experiments were performed only with isRNA NP71-Seq45 and its ancestor isRNA NP71-Seq4 as a reference.

3.6.1 Antigen-specific B cell responses upon immunization with HBcAg-#A79 VLPs in combination with isRNA-NP71-Seq45-LPX are adjuvant dose dependent.

Dose-response curves or concentration-effect relations upon applying isRNA adjuvants or adjuvants in general are considered as important parameters for safety evaluations by identifying the minimal concentration needed to maximize the adjuvantive effect. For the establishment of dose-response curves, Balb/c mice were i.v. immunized with increasing doses of F12-formulated NP71-Seq45 isRNA and mouse serum samples were taken after 1, 3,

5, 8 and 24 h post injection to analyze the time and dose dependent systemic release of IFN-α *in vivo* as measured by ELISA. The results are shown in Figure 3.34.

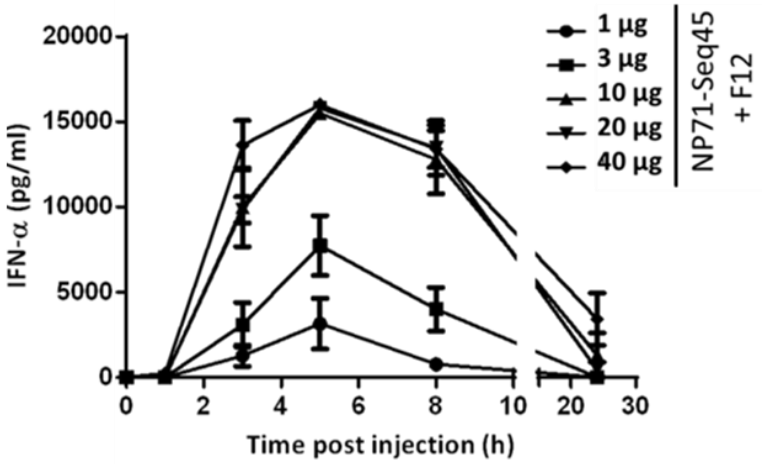

Figure 3.34: Time and dose-dependent IFN-α response upon isRNA-LPX immunization. Balb/c mice (n=5 per group) were i.v. immunized with increasing doses (1, 3, 10, 20 and 40 µg) of F12-formulated NP71-Seq45 isRNA. Blood samples were taken after 1, 3, 5, 8 and 24 h post injection and serum levels of IFN-α were determined by a commercially available IFN-α ELISA assay. The assay was performed in biological triplicates. Shown are the mean values +/- standard error of the mean (SEM).

Irrespective of the administered NP71-Seq45 isRNA dose, the maximal IFN-α induction *in vivo* was already achieved 5 h after immunization and declined back to normal levels soon thereafter. The i.v. administration of 10 µg NP71-Seq45 isRNA was already sufficient for a maximal stimulatory effect and could not be increased or prolonged by higher doses. Even after injection of 40 µg isRNA, no adverse systemic side effects were detectable by visual inspection of the mice, indicating the good tolerability of isRNAs after systemic application.

In order to correlate the observed dose-dependent *in vivo* IFN-α induction with the antigen-specific antibody response, Balb/c mice were immunized i.v. three times in two week intervals with a fixed dose (50 µg per injection) of HBcAg-#A79 VLPs adjuvanted with increasing doses of F12-formulated NP71-Seq45 isRNA. Ten days after the final immunization, serum samples were taken and analyzed by FACS for antibodies specifically recognizing the native CLDN6 protein (Figure 3.35).

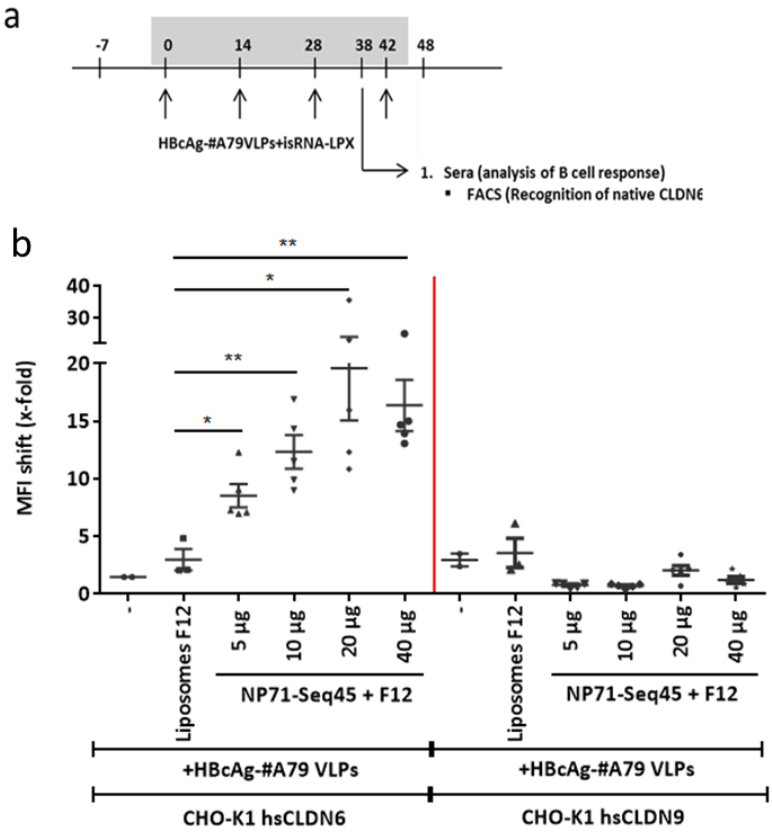

Figure 3.35: isRNA dose dependency of the specific antibody response against native CLDN6 protein. a) Applied immunization schedule. Five Balb/c mice per group were i.v. injected three times in two week intervals with 50 µg HBcAg-#A79 VLPs per immunization in combination with different doses (5, 10, 20 and 40 µg per immunization) of F12-formulated NP71-Seq45. Ten days after the last immunization, serum samples (final serum) were taken and analyzed by FACS. **b)** FACS analysis of the antigen-specific humoral immune responses upon immunization with NP71-Seq45 adjuvanted HBcAg-#A79-VLPs. Antigen specificity was analyzed by using CHO-K1 cells stably expressing hsCLDN6 (left side of the red line) or hsCLDN9 (right side of the red line). Non-adjuvanted HBcAg-#A79 VLPs and VLPs co-administered with empty F12 liposomes served as controls. Illustrated is the MFI shift of final vs. corresponding pre-bleeds. For statistical analysis the software Graph Pad Prism 7 performing a t-test comparing each isRNA group to the HBcAg-#A79 VLPs + empty F12 liposomes group. The difference between the groups were considered to be statistically significant at $p<0.05$. *P<0.05, **p < 0.01 vs. A79+F12 i.v. group for b). t- test was performed. Shown are the mean values +/- SEM is shown.

The FACS data revealed that already 5 µg isRNA was sufficient to significantly induce and enhance CLDN6 specific antibody responses when compared to responses induced by HBcAg-#A79 VLPs in combination with empty F12 liposomes. In addition, an isRNA dose-dependent antigen-specific antibody response up to a concentration of 20 µg/injection isRNA, with no further increase when applying 40 µg/injection, was detectable. This dose dependency resembled the dose-dependent induction of IFN-α secretion, which again points towards a crucial role of IFN-α in the adjuvant activity of F12-formulated isRNAs.

Taken together, the results of section 3.5.4 and 3.6.1 enabled the identification of an optimal time period (10-14 days) between the immunization intervals and an optimal isRNA dosage (20 µg/injection) to enhance the humoral immune response against native CLDN6.

As noted before (see Figure 3.4), the selected CLDN6 epitope #79 was predicited as a potential T cell epitope as well. Therefore, the following experiments were performed in order to analyze the isRNA dose dependency for the induction of antigen-specific T cell

responses upon immunization with HBcAg-#A79-VLPs in combination with isRNA-NP71-Seq45-LPX and to compare the T cell induction efficacy of different adjuvants.

3.6.2 isRNA-LPX co-administration with HBcAg-#A79 VLPs induces a strong T cell response against the inserted CLDN6 epitope.

To analyze the induction of CLDN6 epitope #79 specific T cell responses and the role of IFN-α in T cell induction, the immunized mice of the experiment shown in Figure 3.35 were boosted a fourth time with 50 µg HBcAg-#A79-VLPs adjuvanted with increasing doses (5, 10, 20 and 40 µg/injection) of F12-formulated isRNA NP71-Seq45. Five days later, the mice were sacrificed and splenocytes were generated. Subsequently, an *ex-vivo* IFN-γ ELISpot assay was applied (see Figure 3.29).

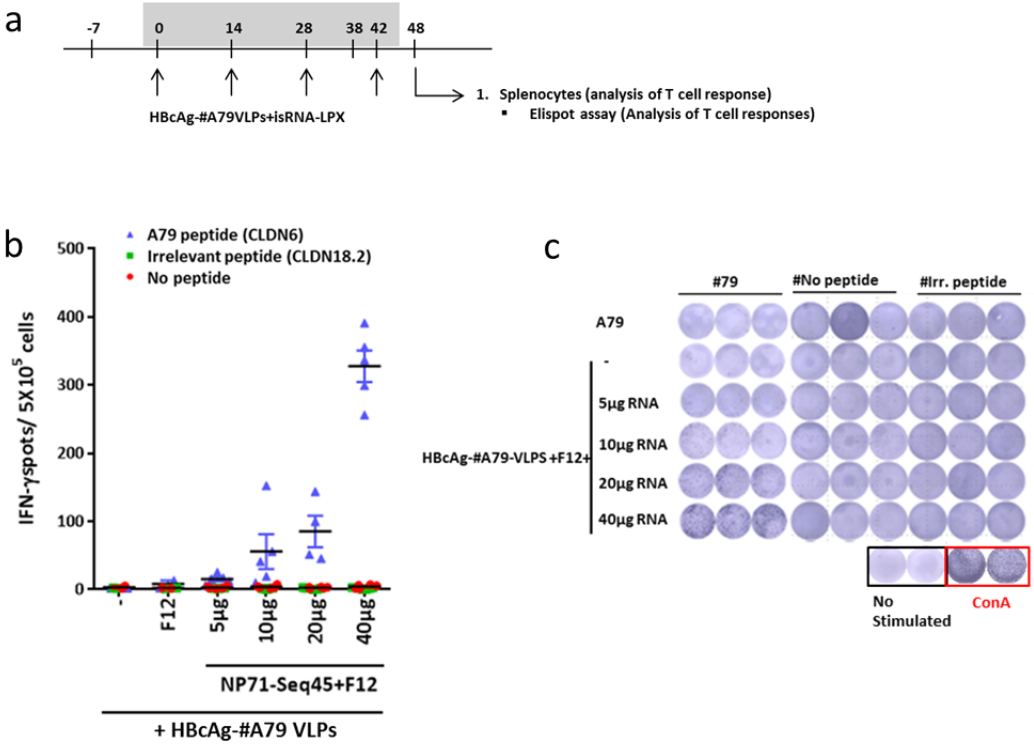

Figure 3.36: isRNA NP71-Seq45-LPX dose-dependent induction of CLDN6 epitope #79 specific T cells. a) Immunization schedule. Balb/c mice (n=5 per group) were immunized four times with HBcAg-#A79 VLPs adjuvanted with increasing doses of F12-formulated NP71-Seq45 isRNA (5, 10, 20, 40 µg isRNA). Non-adjuvanted HBcAg-#A79 VLPs and VLPs co-administered with empty F12 liposomes served as controls. Five days after the fourth immunization, the mice were sacrificed and splenocytes were generated for an IFN-γ ELISpot assay. **b)** Count of IFN-γ spots/5x10^5 splenocytes from indicated mice after restimulation with CLDN6-#79 peptide (A79 peptide), an irrelevant peptide derived from CLDN18.2 or without the addition of a peptide (No stimulated). Shown are the mean values +/- SEM. **c)** Original IFN-γ ELISpot plate used for spot counting. Concavalin A (ConA) stimulation served as positive and non-stimulated splenocytes as negative control. The assay was performed in biological triplicates.

Immunization with non-adjuvanted HBcAg-#A79 VLPs did not result in any detectable T cell response against the CLDN6 #79 peptide. In contrast, a strong enhancement of #79-peptide specific T cell responses was already detectable by IFN-γ ELISpot when applying at least 10 µg/injection isRNA-LPX. The #79-specific T cell response was further enhanced by increasing the isRNA adjuvant dosage up to 40 µg/injection of F12-formulated NP71-Seq45. Unspecific

T cell reactivity against an irrelevant peptide derived from the TAA CLDN18.2 was completely absent, even when applying the highest NP71-Seq45 dose of 40 µg/injection.

These results suggested the following conclusions: a) the selected CLDN6-#79 epitope is indeed a combined B and T cell epitope; b) HBcAg-#A79 VLPs are able to induce a combined B and T cell response that is strictly depending on the co-administration of F12-formulated isRNAs and c) the antigen-specific B and T cell response show a different isRNA dose dependency. The maximal antibody response can be induced already with 20 µg isRNA-NP71-Seq45-LPX, whereas the T cell response can be further enhanced by applying 40 µg isRNA-LPX per injection.

The question remained whether the observed #79-epitope specific T cell induction was related to the discovered new isRNA adjuvants or whether other adjuvant classes, such as CFA/IFA, are also capable to induce a #79-epitope specific T cell response when co-administered with HBcAg-#A79 VLPs.
To answer this question, Balb/c mice were injected four times with 50 µg/injection HBcAg-#A79 VLPs in combination with CFA/IFA (s.c.), empty F12-liposomes (i.v.), F12-formulated Poly (A) oligoribonucleotides (ORN; i.v.), F12-formulated NP71-Seq45 or its parental isRNA NP71-Seq4 (both i.v.). Six days after the last immunization, mice were sacrified and splenocytes isolated for an IFN-γ ELISpot assay. Poly (A) ORN is well-known for not being able to induce cytokine release in DCs [123] and served in this experimental setting as an additional control to analyze the effect of RNA loaded liposomes F12 in the spleen (Figure 3.37).

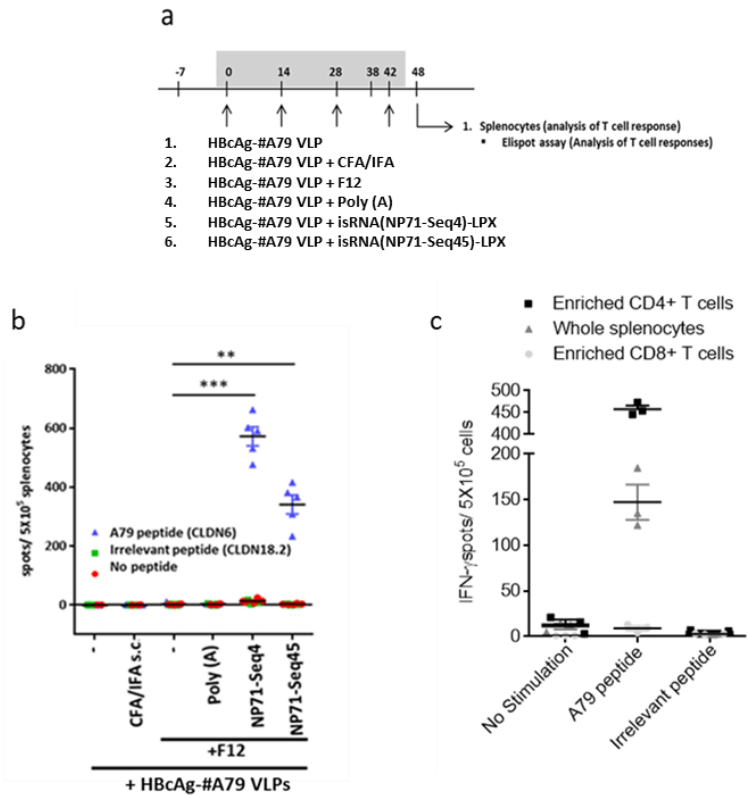

Figure 3.37: IFN-γ-ELISpot analysis of CLDN6 epitope #79-specific CD4+ T cells elicited upon immunization with F12-formulated isRNAs or adjuvant controls in combination with HBcAg-#A79-VLPs. a) Applied immunization regime. Balb/c mice (n=5 per group) were immunized four times in two week intervals with HBcAg-#A79-VLPs alone or adjuvanted with CFA/IFA; Poly (A) ORN, empty F12 liposomes or F12-formulated isRNA sequence NP71-Seq4 and NP71-Seq45, respectively. Six days after the last immunization, mice were sacrified to generate splenocytes for an IFN-γ ELISpot. **b)** Count of IFN-γ spots/5x10^5 splenocytes from indicated mice after restimulation with CLDN6-#79 peptide, an irrelevant peptide derived from CLDN18.2 or without the addition of a peptide (No peptide). c) The combination isRNA-LPX/HBcAg-#A79 VLPs lead to induction of target specific CD4+ T cells. The generated whole splenocytes (2x10^{5}cells/100µl/well); the enriched CD4+/CD+8 (2x10^{5}cells/50µl medium/well) in combination with whole BMDCs (2x10^{5}cells/50µl medium/well) or CD4/CD8 depleted splenocytes (2x10^{5}cells/100µl medium/well) of immunized mice generating using MACS technologie were restimulated with medium, irrelevant or #79 CLDN6 peptide. Illustrated are the spots number counted from the generated IFN-γ-ELISpot Plate. Shown are the mean values +/- SEM. For statistical analysis the software Graph Pad Prism 7 performing an one way ANOVA test comparing each group to the HBcAg-#A79 VLPs + empty F12-liposomes group was used. The difference between the groups were considered to be statistically significant at p<0.05. **P<0.01, ***p < 0.001 vs. A79+F12 i.v. group. One way ANOVA test was performed. Shown are the mean values +/- SEM is shown.

The IFN-γ ELISpot analysis indicated that immunizations using HBcAg-#A79 VLPs adjuvanted with Poly (A) ORN or CFA/IFA, as well as the addition of empty F12-liposomes, resulted in a complete lack of any detectable T cell response. In contrast, co-administration of both isRNAs induced a highly significant #79 peptide-specific T cell response. Interestingly, the parental isRNA NP71-Seq4 led to a higher number of IFN-γ spots when compared to its fragment isRNA NP71-Seq45.

Thus, the identified isRNAs administered i.v. in a liposomal formulation can act as an adjuvant to boost the generation of humoral and cellular antigen-specific immune responses *in vivo,* when combined with HBcAg-#A79 VLPs. Furthermore, we could show that the CLDN6 epitope #79 indeed represented a combined B and T cell epitope. In addition, we sought to uncover the phenotype of the induced T cell responses. As we already mentioned (Figure 3.4), the epitopes FYNPLVAEA from sequence #79 was predicted as potential T cell epitopes restricted to MHC class I H2-Kd molecules (Balb/c mice). To address this issue we re-stimulated whole splenocytes or the enriched CD4+/CD+8 cells co-cultured with BMDCs of immunized balb/c mice from group 6 with medium, irrelevant or #79 CLDN6 peptide (Figure

3.37.a). Unexpectedly, the results revealed that the epitope #79 specific T cell responses were mediated by $CD4^+$ helper T cells (Figure 3.37.c). Thus, the CD8+ T cells depleted splenocytes and the enriched CD4+ were able to recognize the epitopes FYNPLVAEA on surface of APCs by elevating the IFN-y responses measuring by ELISpot assay (Figure 3.37.c).

3.6.3 Antigen-specific antibodies elicited by immunization with F12-formulated isRNAs and HBcAg-#A79 VLPs kill target positive cells by CDC.

The successful and effective use of vaccine adjuvants is dependent on their potency to induce target specific immune responses. In case of the induction of a humoral immune response, the elicited antibodies must be able to bind the target protein with high specificity in its native conformation on the surface of living cells. However, for therapeutic cancer vaccines it is equally important that the induced antibodies are capable to mediate cytocidal effector functions like complement dependent cytotoxicity (CDC) or antibody dependent cellular cytotoxicity (ADCC) leading to cell killing of target positive cells. ADCC and CDC are the main cytolytic effector function mediated by the Fc part of the antibody and was shown to play a crucial role in mAb-based immuntherapies against cancer [36]. In order to analyze CDC-dependent cytotoxic effector functions of selected antisera elicited by immunizations using HBcAg-#A79 VLPs in combination with isRNA-LPXs or other adjuvants, a CDC-assay with unpurified sera derived from the immunization experiment shown in Figure 3.35 was applied.

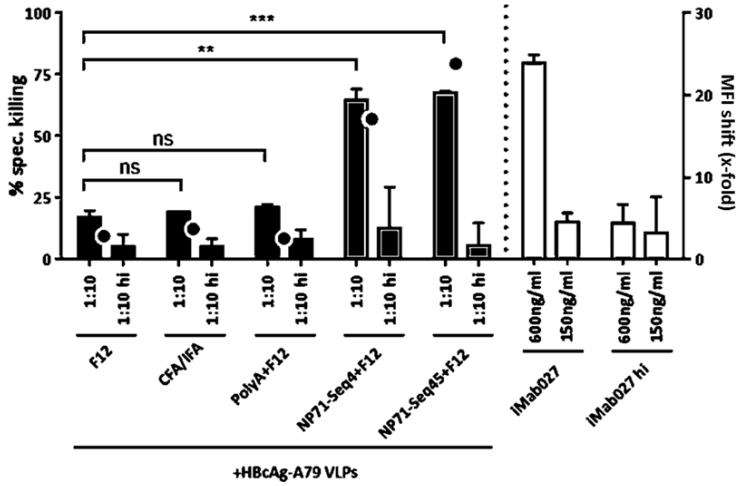

Figure 3.38: The CLDN6 specific antibodies induced by isRNA-LPX in combination with HBcAg-#A79-VLPs killed target positive cells by CDC. CHO-K1 cells stably expressing hsCLDN6 were incubated with selected 1:10 diluted polyclonal mouse antisera and human serum complement as a complement source. Mouse sera were selected on the basis of FACS results (Figure 3.35. a). Sera with the strongest CLDN6-specific B cell response in their respective group were used for the CDC assay (black bars). Their corresponding x-fold MFI-shifts (Y-axis at the right-side) were illustrated as black circles. A purified CLDN6-specific mAb (iMab027; Ganymed Pharmaceuticals AG, Mainz) with defined concentration and known CDC-capacity was used as a positive control (white bars). Heat-inactivated (hi) human serum complement served as negative control and for confirmation of a complement dependent antibody-mediated cytolytic effect. Untreated cells and cells lysed by Triton X-100 were used as benchmarks for 0% and 100% cell lysis, respectively. Cell viability was analyzed with the XTT-assay based Cell proliferation Kit II according to the manufacturer's instructions. The antibody-mediated cytolytic activity was calculated by the following equation: % cell lysis = 100% - ((Signal antiserum - Signal 100% lysis/Signal untreated cells) x 100) and is illustrated on the left-side Y-axis. For statistical analysis the software Graph Pad Prism 7 and an one way ANOVA test comparing each group to the HBcAg-#A79 VLPs + empty F12 liposomes (F12) group was used. The difference between the groups were considered to be statistically significant at $p<0.05$. ns = not significant, **P<0.01, ***p < 0.001 vs. A79+F12 i.v. group. One way ANOVA test was performed. Shown are the mean values +/- SEM is shown.

The CDC-assay revealed that sera from mice immunized with HBcAg-#A79 VLPs and F12-formulated isRNAs exert efficient cytocidal effector functions. The cytolytic activity was strictly depending on active complement, as heat-inactivated complement (1:10 hi) strongly diminished cell killing. Sera derived from immunizations with HBcAg-#A79 VLPs in combination with empty F12-liposomes, CFA/IFA or adjuvanted with F12-formulated Poly (A) ORN were not able to exert a comparable cytolytic effector function. In addition, the CDC-mediated cell killing of the induced antibodies was largely correlating with their calculated MFI-shift (Figure 3.38).

Thus, the induced antibodies upon i.v. immunization with HBcAg-#A79 VLPs in combination with isRNA-LPX were not only able to bind the CLDN6 target protein with high specificity in its native conformation but also exerted target-specific, potent cytocidal effector functions, which is a prerequisite for antibody-mediated anti-tumoral effects of active cancer vaccines.

3.6.4 Immunization of F12-formulated isRNA NP71-Seq45 in combination with HBcAg-#A79 VLPs resulted in a balanced antigen-specific IgG2a/IgG1 response.

For a better understanding of the adjuvant properties of the identified isRNAs in combination with the model antigen HBcAg-#A79 VLP, the determination of the immunoglobulin (Ig) isotype switch can provide insights whether the vaccine composition influences the balance between the Th1 or Th2 profile of the immune response. Although the overall Th1/Th2 concept might be rather vague, Th1 responses can be characterized by an enhanced cellular immunity, whereas Th2 responses are dominated by enhanced humoral immune response [160]. However, in many cases the optimal scenario would seem to be a well balanced Th1 and Th2 response, suited to different kinds of immune challenge [120].
In the mouse system, the presence of elevated IgG2a isotype levels is indicative of a Th1 mediated immune response, whereas high levels of IgG1 antibodies are a hallmark of a Th2 mediated immune response.
For the analysis of Ig isotype levels, sera from mice immunized as described in Figure 3.29 were used for titrations. IgG1 or IgG2a antibodies specifically recognizing the linear CLDN6 #79-peptide were analyzed by a peptide ELISA using secondary antibodies specific for the respective Ig isotypes (see Figure 3.39).

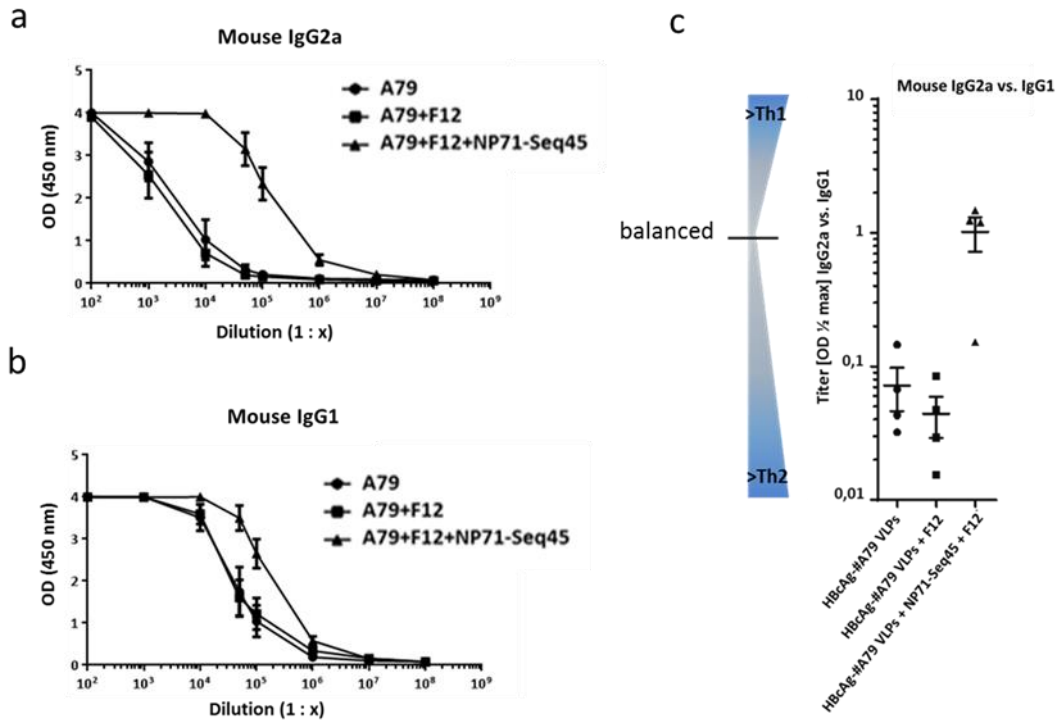

Figure 3.39: Co-administration of isRNA-LPX and HBcAg-#A79 VLPs resulted in a balanced antigen-specific IgG2a/IgG1 (Th1/Th2) response. Sera from mice immunized as described in Figure 3.36.a were used in a #79 peptide ELISA assay. The Ig isotype of antibodies recognizing the linear #79-epitope was detected by using mouse Ig2A or IgG1 specific, HRP-conjugated secondary antibodies. a and b) Global fit of the OD_{450} data obtained by titrating mouse sera. **a)** Titration curve of #79-epitope specific IgG1 isotypes. **b)** Titration curve of #79-epitope specific IgG2a antibodies. **c)** Ratio of the calculated half-maximal IgG2a and IgG1 antibody titers. Values <1: predominant Th2 response; values = 1: balanced response; values >1: predominant Th1 response. Antiserum dilutions were measured in triplicates. Shown are mean values +/- SEM.

The immunization with non-adjuvanted HBcAg-#A79 VLPs or VLPs combined with empty F12-liposomes resulted in high CLDN6 #79 epitope-specific IgG1 and very low IgG2a antibody titers, indicating a predominantly Th2 driven immune response. In contrast, antibodies raised by immunizations with HBcAg-#A79 VLPs adjuvanted with F12-formulated NP71-Seq45 elicited moderately higher IgG1 and strongly enhanced #79-peptide specific IgG2a antibody titers, resulting in a balanced Th1/Th2 immune response.
The generated data clearly indicated that isRNA-LPX co-administration led to the induction of a strong Th1 response in addition to a moderate enhancement of a Th2 response, very likely in an IFN-α dependent manner.

The results described in section 3.6.1 to 3.6.4 can be summarized as followed: a) isRNA-LPX as an adjuvant could enhance the immunogenicity of the VLP-based vaccine; b) The induced immune responses combined a strong and antigen-specific B and T cell response; c) The induced antigen-specific antibodies were able to trigger a CDC-dependent effector function; and d) isRNA-LPX co-administration resulted in balanced IgG2a/IgG1 or Th1/Th2 immune response.

3.6.5 Antibodies elicited by isRNA-LPX combined with HBcAg-#A79 VLP immunizations are cross-reactive against murine CLDN6.

In section 3.5 and 3.6, we could show that antibodies induced by vaccination with isRNA-LPX in combination with chimeric HBcAg-VLPs displaying the human CLDN6-derived epitope #79 on their surface could recognize the native human CLDN6 (hsCLDN6) protein presented on CHO-K1 cells. However, for the establishment of syngenic mouse tumor models with murine CLDN6 (mmCLDN6) expressing cell lines (described in 3.7.1), it was important to analyze if the antibodies induced by HBcAg-#A79 VLPs immunization recognized native mmCLDN6 as well. A positive result would enable HBcAg-#A79 VLPs to be used in mouse tumor models. Furthermore, we wanted to analyze if the immunization with isRNA-adjuvanted HBcAg-#H88 VLPs, displaying the murine CLDN6 #88-epitope corresponding to the hsCLDN6 specific epitope #79 (see Figure 3.4), resulted in immune responses against mmCLDN6 comparable to those elicited by HBcAg-#A79 VLP immunizations against hsCLDN6. Comparable results and efficacies would enable the switch to a completely mouse-specific vaccination system (mmCLDN6 epitope and mmCLDN6 expressing target cells). However, it should be noted that in contrast to epitope #79, mmCLDN6 epitope #88 was displayed in the context of a different HBcAg-backbone (backbone H) and was not acidified by the addition of acidic linkers on both sides of the epitope (see also Figure 3.4).

Balb/c mice were immunized i.v. with HBcAg-#A79 VLPs or HBcAg-#H88 VLPs alone or in combination with an isRNA-LPX adjuvant using the standard immunization schedule. Ten days after the third immunization, blood samples were taken and a FACS-based assay using the murine tumor cell line CT26 stably expressing mmCLDN6 on their surface was performed. We frequently observed very low MFI-shifts when comparing immune serum (after three vaccinations) with pre-serum derived from animals immunized with wildtype HBcAg-VLPs. Therefore, the cut-off for a successful CLDN6 antigen-specific antibody response was set to a MFI-shift of 2.5-fold (immune serum vs. pre-serum) (Figure 3.40). Subsequently, to analyse the effector function of the induced CLDN6 specific antibody responses a CDC assay using CHO-K1 stably expressing mmCLDN6 on their surface was also performed.

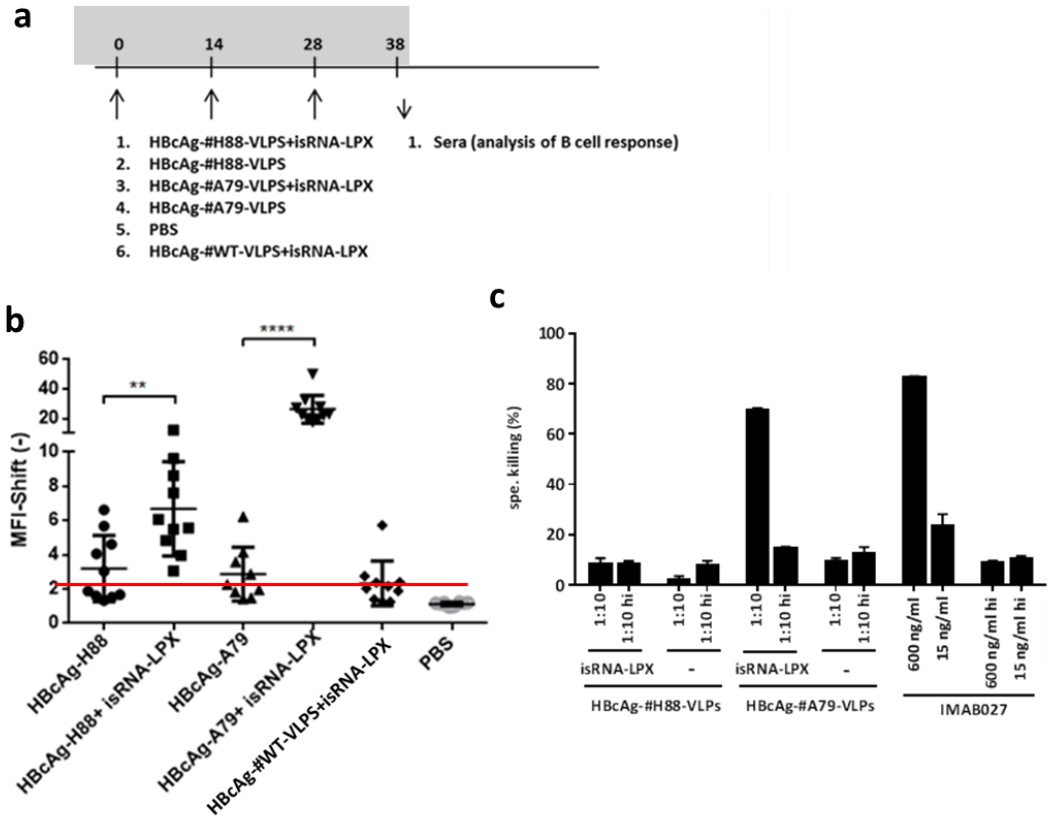

Figure 3.40: Analysis of humoral immunity elicited by immunization with isRNA-adjuvanted HBcAg-#A79 or -#H88 VLPs. **a)** Immunization schedule. Balb/c mice (n=10 per group) were immunized i.v. three times at two-week intervals with HBcAg-#A79 VLPs or HBcAg-#H88 VLPs alone or in combination with F12-formulated isRNA NP71-Seq45 (isRNA-LPX). Untreated mice (PBS), mice immunized with non-adjuvanted HBcAg-CLDN6 VLPs and a group immunized with isRNA-LPX adjuvanted HBcAg-#WT-VLPs served as controls. Ten days after the third immunization, blood samples were taken for analysis of the antigen-specific humoral immune response. **b)** FACS analysis using CT26 cells stably transfected with mmCLDN6 protein. Detection of bound antibodies was expressed as MFI-shift (Final serum vs. Pre-serum). The red line indicates the cut-off for a successful antibody response set to a MFI-shift of 2.5 fold. c) CDC analysis using CHO-K1 stably transfected with mmCLDN6 protein. The antibody-mediated cytolytic activity was calculated by the following equation: % cell lysis = 100% - ((Signal antiserum - Signal 100% lysis/Signal untreated cells) x 100) and is illustrated on the left-side Y-axis. The difference between the groups were considered to be statistically significant at $p<0.05$. $^{**}p < 0.01$, $^{****}p < 0.0001$ vs. no adjuvanted groups d). Student's t test was applied. Shown are the mean values +/- SEM is shown.

Immunization with non-adjuvanted HBcAg-#H88 or HBcAg-#A79 VLPs resulted in a weak, partial immune response. Only a few animals in these groups contained mmCLDN6 specific antibodies whose x-fold MFI-shift were above the 2.5-fold cut-off (red line). The mean MFI-Shift in these groups did not significantly differ from unspecific antibodies elicited by immunization with HBcAg-#WT VLPs. Adjuvantation of CLDN6-epitope displaying HBcAg-VLPs with isRNA-LPX resulted in highly increased MFI-shifts. Interestingly, the immunization with HBcAg-#A79 VLPs in combination with isRNA elicited antibodies recognizing the mmCLDN6 protein in its native conformation, although #79 represented a hsCLDN6 specific epitope that differed at two aa positions from its mouse homolog #88 (see also Figure 3.4). Unexpectedly, the calculated antibody MFI-shifts after immunization with HBcAg-#H88 VLPs (mouse specific CLDN6 epitope) were significantly lower than those from antibodies induced upon isRNA adjuvanted HBcAg-#A79 VLP vaccination.

Both results, the cross-reactivity of HBcAg-#A79 VLP elicited antibodies against mmCLDN6 and a weaker antibody response against mmCLDN6 when using HBcAg-#H88 VLPs, could be confirmed by FACS-analysis with two other tumorigenic mmCLDN6 stably transfected cell lines with C57BL/6 genetic background (MC38 and E0771) (data not shown).

In addition to the FACS-analysis, a CDC assay was also performed. The results revealed that sera from mice immunized with HBcAg-#A79 VLPs and isRNA-LPX exert efficient cytocidal effector functions despite the fact that the used CHO-K1 cells stably expressed mmCLDN6. The cytolytic activity was strictly depending on active complement as heat inactivated complement (1:10 hi) strongly diminished cell killing. In contrast, sera derived from immunizations with isRNA adjuvanted HBcAg-#H88 VLPs were not able to exert a comparable effector function. The cytocidal effector function of the induced antibodies was largely correlating with their calculated MFI-shift (Figure 3.40. c).

3.6.6 T cell responses induced by isRNA-LPX combined with HBcAg-#A79 VLP immunizations are cross-reactive against the murine CLDN6 epitope #88.

Cross-reactivity of HBcAg-#A79 VLP induced antibodies against mmCLDN6 might be explained by the relatively long sequence of the inserted #79 epitope leading to a conformational structure on the VLP surface that could closely mimic the native mmCLDN6 and hsCLDN6 ECD2 structure. Therefore, antibodies reacting against the native CLDN6 proteins might recognize a conformational epitope that is not affected by the two amino acid difference between the #79 and #88 epitope.
Out of interest, we also analyzed the ability of the induced CLDN6 specific T cells to recognize the corresponding mouse or human CLDN6 peptide presented in the context of MHC molecules on the surface of murine APCs. Selected Balb/c mice (n=5 per group) from the previous experiment were immunized for a fourth time with isRNA NP71-Seq45-LPX adjuvanted HBcAg-#A79 VLPs or HBcAg-#H88 VLPs. Six days after the fourth immunization, animals were sacrificed and splenocytes generated to analyze the induction of peptide specific T cell response by an ELISpot assay (Figure 3.41). Thereby, we aimed to analyze whether the T cells that were induced by immunization with isRNA-LPX adjuvanted HBcAg-#A79-VLPs or HBcAg-#H88-VLPs could re-stimulated by APCs, which were already loaded with the human #79 or murine #88 CLDN6 peptide.

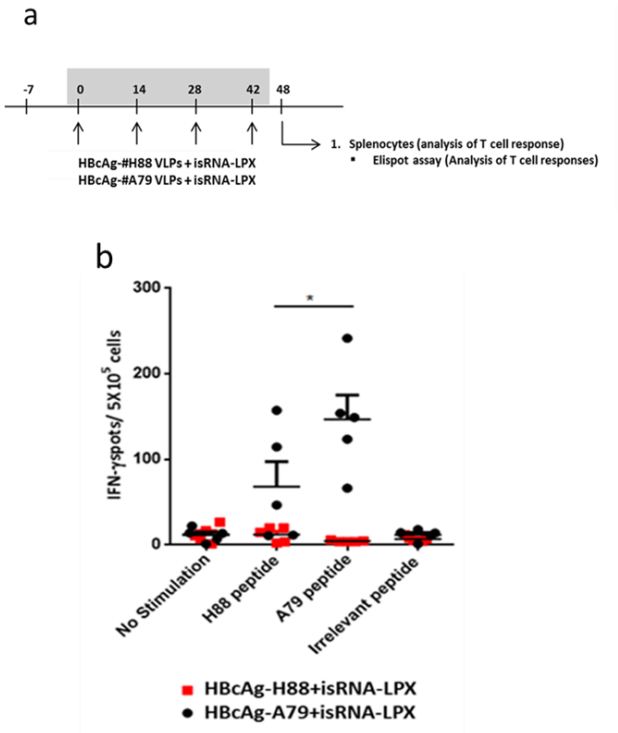

Figure 3.41: CLDN6-specific T cells induced by vaccination with isRNA-NP71-Seq45-LPX adjuvanted HBcAg-#A79 VLPs recognize the corresponding mouse CLDN6 epitope #88. a) Immunization schedule. Balb/c mice (n=5 per group) were i.v. injected four times on days 0, 14, 28 and 42 with isRNA-NP71-Seq45-LPX adjuvanted HBcAg-#A79 or HBcAg-#H88 VLPs. Mice were sacrificed six days after the last immunization (day 48) and splenocytes were generated. **b)** ELISpot analysis showing the number of IFN-γ spots/5x10^5 splenocytes from immunized mice after restimulation with peptides #79 (A79) or #88 (H88). Unstimulated splenocytes and splenocytes stimulated with an irrelevant peptide served as controls. The difference between the groups were considered to be statistically significant at $p<0.05$. *$p < 0.05$. Student's t test was applied. Shown are the mean values +/- SEM is shown.

The ELISpot analysis confirmed that isRNA-NP71-Seq45-LPX adjuvanted HBcAg-#A79 VLPs were able to induce specific T cells strongly recognizing the corresponding human #79 CLDN6 peptide (as already shown in Figure 3.36 and 3.37). Unexpectedly, T cells in three out of five mice immunized with isRNA-LPX and HBcAg-#A79 VLPs also recognized, but to a weaker extent, the murine #88 CLDN6 peptide although the predicted Kd restricted epitope of #88 differed at one amino acid position from the predicted human CLDN6 #79 Kd restricted epitope. Furthermore, immunization with isRNA-LPX adjuvanted HBcAg-#H88 VLPs did not result in any detectable T cell response, neither against the mmCLDN6 #88, nor the hsCLDN6 #79 peptide. This result was also not expected, because epitope #88 contained a predicted T cell epitope restricted to MHC class I Kd as well and whose prediction score was not different from the score of the #79 T cell epitope (see Figure 3.4).

The weaker antibody response after immunization with HBcAg-#H88 VLPs in comparison to HBcAg-#A79 VLPs, the observed cross-reactivity of HBcAg-#A79 VLP induced T cells against the murine CLDN6 #88 peptide and the complete lack of reactivity of T cells induced by adjuvanted HBcAg-#H88 VLP immunization remained unclear and should be analyzed in more detail in the following experiments.

3.6.7 Immunization with isRNA-LPX adjuvanted HBcAg-#A101 VLPs induced a better humoral immune response than HBcAg-#H88 VLP vaccination.

The observed significant differences in the humoral and cellular immune response after immunization with isRNA-LPX adjuvanted HBcAg-#A79 or HBcAg-#H88 VLPs were unexpected but not completely surprising. One obvious reason for the differences in the induced antibody response might rely on the different HBcAg-backbones used for the VLP constructs (backbone A for #A79 and backbone H for #H88) and the lack of glutamic acid linkers flanking the #88 epitope. Both components could affect the orientation and conformation of the presented CLDN6 #88 epitope resulting in weaker antibody responses against the CLDN6 protein in its native conformation.
Therefore, we decided to design and produce a new chimeric HBcAg-VLP construct for the presentation of the murine CLDN6 epitope corresponding to the human CLDN6 #79 epitope. The construct HBcAg-#A101 was identical to HBcAg-#A79 with respect to the same HBcAg backbone A and acidification of the inserted epitope, but contained the murine homologue of the human CLDN6 epitope #79. Accordingly, HBcAg-#A101 differed from HBcAg-#H88 only by the used backbone and the glutamic acid linkers flanking the murine epitope. A comparison between epitope #79, #88 and #101 as well as the used chimeric HBcAg constructs is shown in Figure 3.42.

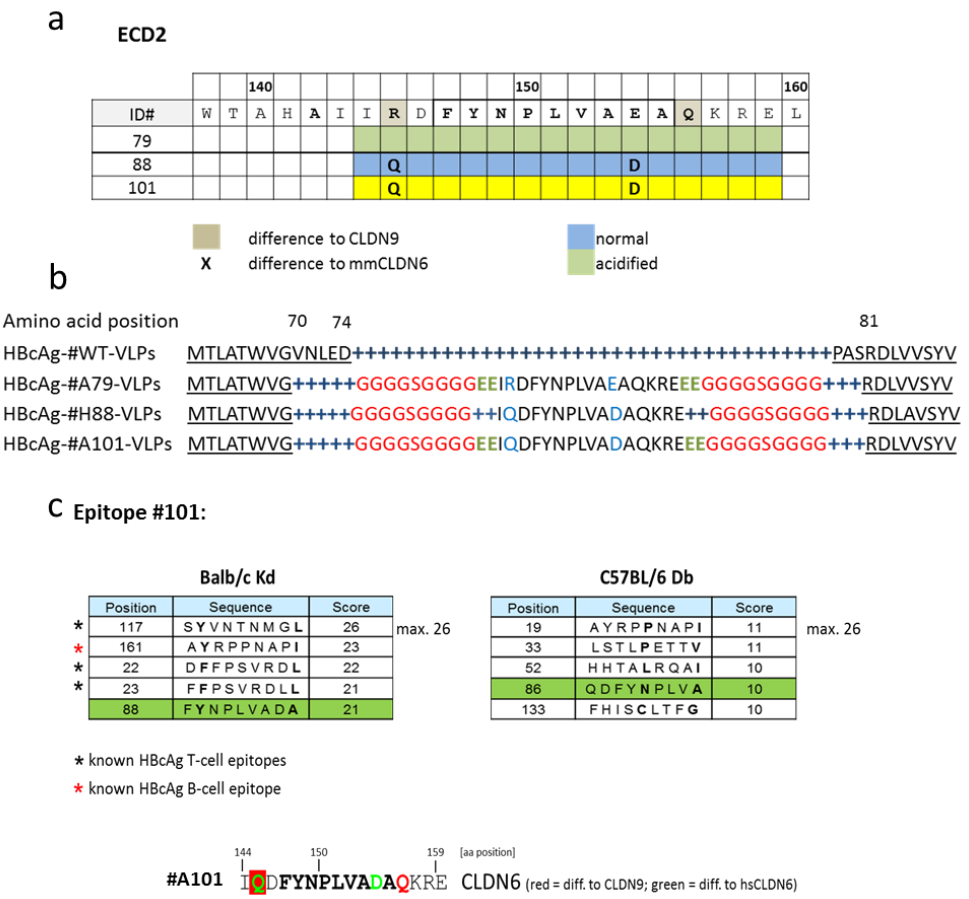

Figure 3.42: Sequence characterization of epitope #101 and HBcAg-#A101 constructs. a) Amino acid sequence comparison between epitope #79, #88 and #A101. While #88 (blue) was not modified, #79 (green) and #101 (yellow) were flanked by adding glutamic acid linker on the N and C terminus of the epitope. The epitope position according to the human CLDN6 extracellular domain 2 (ECD2) is indicated. Amino acids with light brown underlay color represent aa differing in human CLDN6 from the closely related human CLDN9 protein. Bold aa in the #88 and #101 epitope sequence indicate aa specific for murine CLDN6. **b)** Comparison of the aa sequence corresponding to residues 62-89 in HBcAg-#WT and chimeric HBcAg-#CLDN6 VLPs. The underlined aa residues in the chimeric constructs are derived from HBcAg-WT. Red aa indicate the G_4SG_4 linker. Green aa represent the glutamic acid (EE) linker. Blue aa indicate the differences between hsCLDN6 and mmCLDN6. Residues located in the HBcAg MIR and deleted in the chimeric constructs are marked by a +. **c)** Prediction score for Kd (Balb/c mice) or Db (C57BL6 mice) restricted T cell epitopes within epitope #101 (marked by green cells). Black * indicate HBcAg T cell epitopes known from the literature. Red * indicate known HBcAg B cell epitopes. The maximal (max.) score achieved in the *in silico* prediction is presented on the right side of the table. For prediction using SYFPEITHI software [145] the whole sequence of the HBcAg-#A101 construct was used. The sequence under the tables illustrates the #101 sequence (identical to #88), the position of the predicted T cell epitope within #101 and aa differences to CLDN9 or human CLDN6.

Differences and similarities of the constructs HBcAg-#A79, -#H88 and -#A101 can be nicely seen in Figure 3.42 b. As expected, it was *in silico* predicted that also #101 contained a potential T cell epitope restricted to MHC class I H2-Kd molecules (Balb/c mice) with a high prediction score in the similar range as known Kd epitopes derived from the HBcAg backbone. In contrast, prediction scores for potential #101 Db-restricted epitopes (C57BL/6) were rather low. The highest #101 derived epitope had a score of 10, whereas other epitopes derived from the HBcAg-backbone had scores up to 26. Therefore, it was highly unlikely that #A101 contained a potential, Db-restricted epitope.

In a first immunization experiment we wanted to investigate the *in vivo* functionality of HBcAg-#A101 VLPs after co-administration with isRNA NP71-Seq45-LPX. In order to directly address the effect of the HBcAg backbone on the nature of the induced target specific

immunity, HBcAg-#A101 VLPs were compared with HBcAg-#H88 VLPs. Furthermore, we compared the extent of the induced CLDN6-specific humoral immune response in Balbc/c and C57BL/6 mice. The results of the FACS analysis using CHO-K1 cells stably expressing murine CLDN6 (mmCLDN6) or CHO-K1 wildtype cells are shown in Figure 3.43.

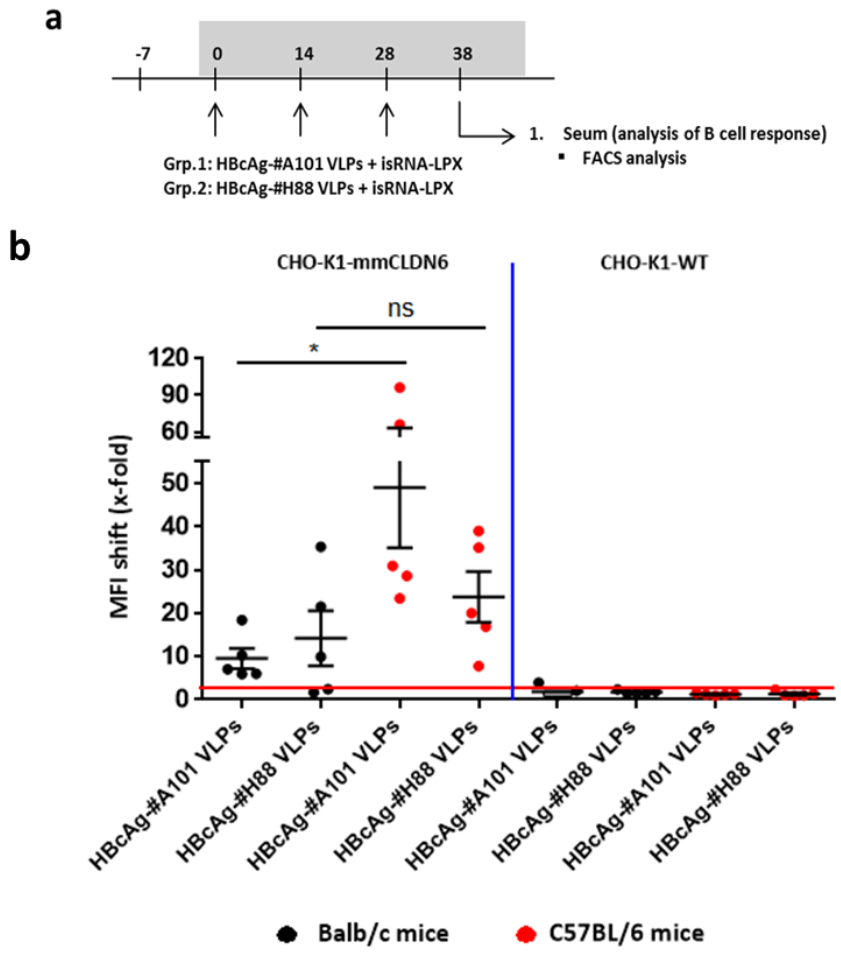

Figure 3.43: CLDN6 specific antibody response upon immunization with isRNA NP71-Seq45-LPX adjuvanted HBcAg-#A101 VLPs or HBcAg-#H88 VLPs. a) Immunization schedule. Balb/c (n=5 per group) and C57BL/6 (n=5 per group) mice were immunized i.v. thirce times at two-week intervals with HBcAg-#A101 VLPs or HBcAg-#H88 VLPs in combination with the isRNA-LPX adjuvant. Six days after the fourth immunization, blood samples were taken for FACS analysis of the antigen-specific humoral immune response. **b)** FACS analysis using CHO-K1-cells stably transfected with mmCLDN6 (left side of the blue line) or CHO-K1 wildtype (WT) cells (right side of the blue line). Detection of bound antibodies was expressed as x-fold MFI-shift (Final serum vs. Pre-serum). The red line indicates the cut-off for a successful antibody response set to a MFI-shift of 2.5 fold. Shown are the mean values +/- SEM. The difference between the groups were considered to be statistically significant at $p<0.05$. ns = not significant; *$P<0.05$.

Interestingly, we observed that the calculated MFI-shifts after immunization of C57BL/6 mice with isRNA-LPX adjuvanted HBcAg-#A101 and HBcAg-#H88-VLPs were generally stronger than those after immunization of Balb/c mice with the same vaccine formulations. In addition, the CLDN6-specific B cell response in C57BL/6 induced after immunization with HBcAg-#A101 VLPs was stronger than those induced upon vaccination with isRNA-LPX adjuvanted HBcAg-#H88 VLPs. However, this difference was unequivocally visible only in C57BL/6 mice.

Having seen a beneficial effect of isRNA-LPX adjuvanted HBcAg-#A101 VLPs on the induction of CLDN6-specific antibody responses (especially in C57BL/6 mice), we subsequently analyzed the CLDN6 #101-epitope specific T cell responses.

3.6.8 Immunization with isRNA-LPX adjuvanted HBcAg-#A101 VLPs induced #101 epitope specific T cell response in Balb/c and particularly in C57BL/6 mice.

As shown previously, the murine CLDN6 epitope #88 and #101 were not predicted to contain a MHC class I Db-restricted (C57BL/6 mice) T cell epitope. In contrast, the prediction scores for a Kd-restricted (Balb/c mice) T cell epitope were in the same range as for already known HBcAg-derived and Kd-restricted epitopes. However, in the following experiment we analyzed the CLDN6 epitope specific T cell responses induced by combined isRNA-LPX and HBcAg-#H88 or -#A101 VLP immunization in both, Balb/c and C57BL/6 mice. Furthermore, we included APCs loaded with HBcAg-#WT VLPs as a further control in the ELISpot assay, because HBcAg-specific T cell responses should be induced in both mice strains.
Balb/c and C57BL/6 mice from the previous experiment (Figure 3.43) were sacrificed six days after the fourth immunization and splenocytes were generated in order to perfrom an *ex vivo* IFN-γ ELISpot assay. Results are shown in Figure 3.44.

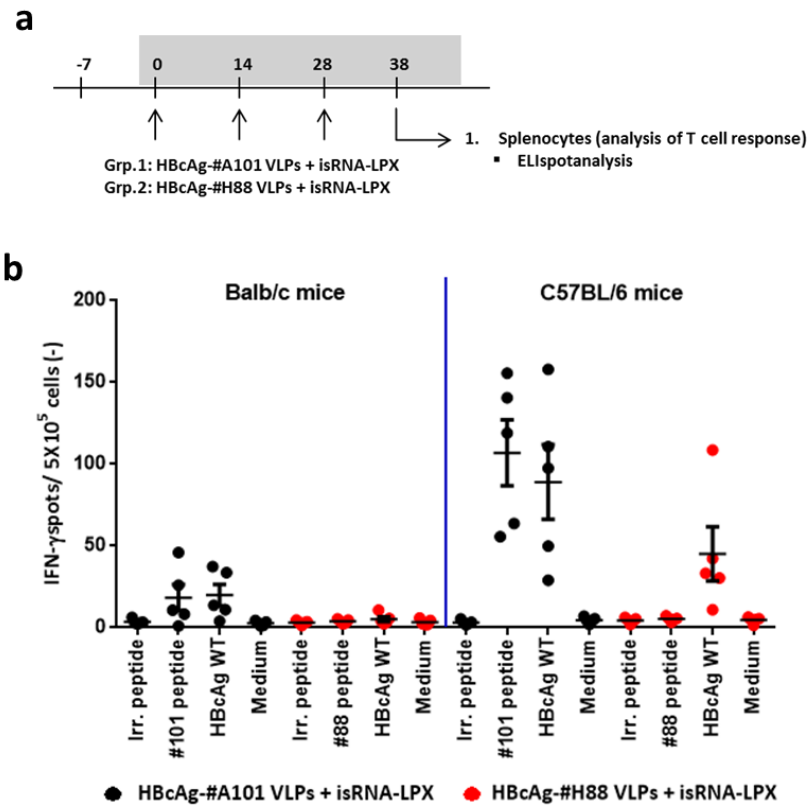

Figure 3.44: CLDN6 epitope specific T cells induced by vaccination with isRNA-LPX adjuvanted HBcAg-#A101 VLPs or HBcAg-#H88 VLPs recognize their corresponding mouse epitopes #101 or #H88 to different extents. a) Immunization schedule. Balb/c mice (n=5 per group) and C57BL/6 (n=5 per group) were i.v. injected four times on day 0, 14, 28 and 42 with isRNA-LPX adjuvanted HBcAg-#A101 or HBcAg-#H88 VLPs. Mice were sacrificed six days after the last immunization (day 48) and splenocytes were generated. **b)** ELISpot analysis. Illustrated are the number of IFN-γ spots/5x10^5 splenocytes from immunized mice after re-stimulation with CLDN6 peptides #101 or #88. Splenocytes stimulated with an irrelevant peptide (Irr. peptide), HBcAg-WT VLPs or left untreated (Medium) served as controls. Shown are the mean values +/- SEM.

The obtained ELISpot data was rather interesting. The data clearly revealed that isRNA NP71-Seq45-LPX adjuvanted #HBcAg-#101 VLPs were able to induce T cells specifically recognizing the mouse #101 CLDN6 peptide in C57BL/6 and in Balb/c mice. However, the induced T cell response was much higher in C57BL/6 mice than in Balb/c mice. The same phenomenon was observed when analyzing HBcAg backbone-derived T cell responses (APC loading with HBcAg-#WT VLPs). In contrast, adjuvanted HBcAg-#H88 VLP immunization failed to induce a #88 epitope specific T cell response in both mouse strains. Remarkably, T cell responses against HBcAg-backbone derived epitopes could be only observed in C57BL/6 mice immunized with isRNA-LPX adjuvanted HBcAg-#H88 VLPs. No such response was detectable after immunization of Balb/c mice and the response detected in C57BL/6 mice was profoundly weaker when compared to C57BL/6 mice immunized with HBcAg-#A101 VLPs.

The comparison of the induced humoral and cellular immune responses upon vaccination of Balb/c and C57BL/6 mice with isRNA-LPX adjuvanted HBcAg-#H88 or -#A101 VLPs led to the following conclusions: a) The HBcAg-backbone selected for epitope presentation and/or epitope acidification had an impact on the strength of the induced target specific B and T cell response, with HBcAg-#A101 VLPs showing a superior effect over HBcAg-#H88 VLPs. b) isRNA-LPX adjuvanted HBcAg-#A101 VLP immunization was able to induce a CLDN6 epitope specific T cell response in Balb/c mice. However, compared to T cell responses elicited by HBcAg-#A79 VLPs, the response was rather weak. c) isRNA-LPX adjuvanted HBcAg-#A101 VLP immunization of C57BL/6 mice resulted in a strong epitope-specific T cell response. This result contradicted the *in silico* predictions using the SYFPEITHI database. Therefore, it indicated that the observed T cell response was not a $CD8^+$ T cell response directed against a MHC class I restricted epitope, but instead a $CD4^+$ T cell response against a larger MHC class II restricted epitope al already demonstrated by HBcAg-#A79 (Figure 3.37). d) Immunization with isRNA-LPX adjuvanted HBcAg-#H88 VLPs resulted only in a weak T cell response against the HBcAg-backbone in C57BL/6 mice but not in Balb/c mice. The elicited immune responses in C57BL/6 mice were generally much higher than in Balb/c mice. Therefore, tumor models should be established preferentially in C57BL/6 mice (if possible) to ensure a maximal immune response effect.

In the next set of experiments, we wanted to analyze the observed immune response differences upon immunization with HBcAg-#H88 or -#A101 VLPs and between C57BL/6 and Balb/c mice in more detail.

3.6.9 Differential binding of chimeric and wildtype HBcAg-VLPs to naïve B cells derived from C57BL/6 or Balb/c mice.

Milich *et al*. and others have previously reported that wildtype HBcAg-VLPs specifically bind to B cell receptors (BCRs) on the surface of naïve B cells [34, 141]. In addition, Lazdina *et al*. demonstrated that the *in vivo* binding of HBcAg-VLPs by naïve B cells and subsequently the immune response against the VLPs can be negatively affected by deletion of defined aa

residues within the MIR of wildtype HBcAg-VLPs [141]. Thus, deletion of aa content 76-85 of HBcAg-WT destroyed naïve B cell binding, while deletion of aa sequence 79-85 did not show any influence [141].

Our approach of insertion of foreign CLDN6 epitopes into the HBcAg MIR did replace defined aa residues at the tip of HBcAg molecules and thus, may affect chimeric HBcAg-VLP binding by naïve B cells and subsequent immune responses. Furthermore, the deleted aa residues differed between the used HBcAg-backbones A and H (3.42. b). Therefore, these diverse properties of our tested HBcAg-#CLDN6 constructs might directly influence the VLP binding to naïve B cell and accordingly the might explain the observed differences in the antigen-specific humoral immune response after HBcAg-#H88 or -#A101-VLP immunization.

To address this hypothesis, we performed *ex vivo* experiments measuring the direct binding of different HBcAg-VLP constructs to naïve B cells. Splenocytes isolated from non-immunized Balb/c or C75BL/6 mice were incubated with different chimeric but also wildtype HBcAg-VLPs and binding to B cells was detected by using B cell (CD19) and titrated VLP-specific (polyclonal rabbit anstiserum) antibodies. Results of the anti-HBcAg VLP antibody titration in relation of the overall percentage of B cells binding to the HBcAg-VLP constructs are shown in Figure 3.45.

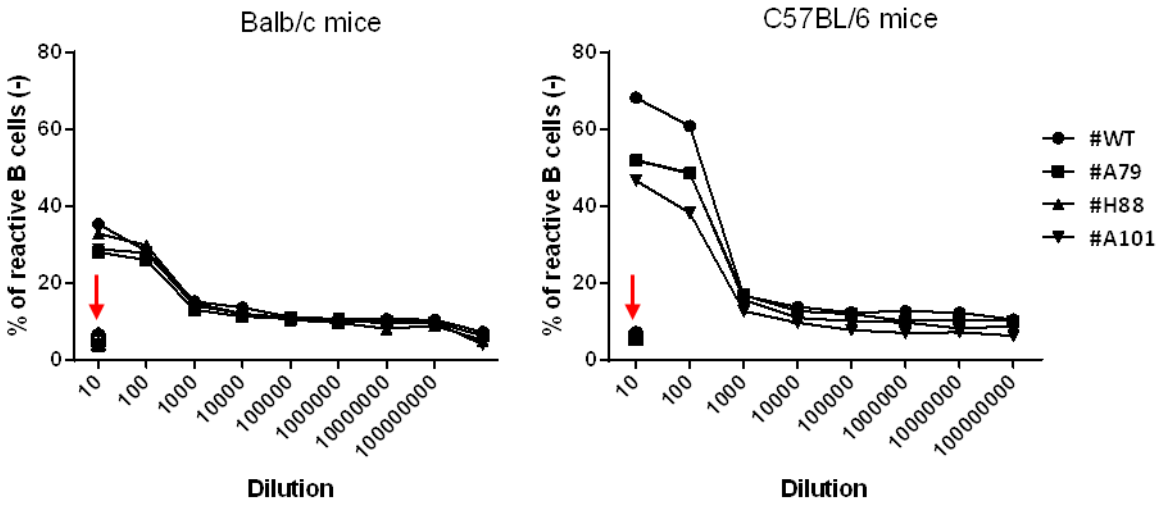

Figure 3.45: Binding of chimeric and wildtype HBcAg-VLPs to naïve B cells: A total of $1x10^6$ generated splenocytes from non immunized Balb/c or C75BL/6 mice were incubated on ice with Fc-receptor blocking reagent, followed by incubation on ice with equal amounts of. HBcAg-#A79 (#A79), HBcAg-#H88 (#H88) and HBcAg-#A101 VLPs (#A101). Incubation with wildtype HBcAg-VLPs (#WT) served as positive binding control. Rabbit anti-HBcAg polyclonal antibody was 8-fold serially diluted and used for detection of bound HBcAg-VLPs. Afterwards, the B cells and bound anti-HBcAg antibodies were specifically stained with PE-anti CD19 and AlexaFluor® 647 conjugated goat anti-rabbit IgG (H+L), respectively. Non-specific binding of detection antibodies (background) was controlled by omitting the addition of rabbit anti-HBcAg polyclonal antibodies (red arrows). The percentage of living naïve B cells binding to HBcAg-VLPs is shown on the y-axis.

As shown in the titration curves, the binding of naïve B cells to all tested HBcAg-VLP constructs was dose-dependent. Interestingly, naïve B cells from C57BL/6 mice were able to bind all tested HBcAg-VLP constructs more efficient than those from Balb/c mice. This finding could explain our previous observation that the induction of target specific antibodies in C57BL/6 mice after immunization with HBcAg-#CLDN6 VLPs was significantly stronger than in Balb/c mice (see Figure 3.43). Furthermore, C57BL/6 derived naïve B cells

bound HBcAg-wildtype VLPs more efficiently than the tested chimeric HBcAg-#CLDN6 VLPs. However, it should be emphasized that the used rabbit anti-HBcAg polyclonal antibodies were generated by immunization with wildtype HBcAg-VLPs, which could explain the better B cell binding of HBcAg-#WT VLPs simply by a better antibody detection rate.

The obtained data clearly demonstrated the ability of the chimeric HBcAg-VLPs to be bound by naïve B cells despite the fact that the HBcAg MIR was strongly modified including aa replacements by the inserted CLDN6 epitopes. Furthermore, differential humoral responses in C57BL/6 vs. Balb/c mice upon chimeric HBcAg-VLP immunization might be explained by the observed discrepancy in the binding of HBcAg-VLPs to B cell derived from C57BL/6 or Balb/c mice.

The immunological *in vivo* evaluation revealed that the i.v. co-administration of HBcAg-#A79 VLPs and isRNA NP71Seq45-LPX resulted in the strongest and simultaneous induction of mmCLDN6-specific B and T cell responses when compared to the other isRNA adjuvanted HBcAg-VLP constructs (see Table 3.3).

Table 3.3: Features and immunological evaluation of used chimeric HBcAg-VLP constructs. hs = *Homo sapiens*; mm = *Mus musculus*; A and H = HBcAg backbones; Acidification indicates glutamic acid linkers flanking the inserted epitope (**+** available; **-** not available); T cell epitope prediction of MHC class I restricted epitopes was performed using SYFPEITHI database [145]; - no signal; +/- very weak; + detectable; ++ strong; +++ very strong; n.a.not available.

Epitope	Origin	HBcAg backbone	Acidifi-cation	$CD8^+$ epitope prediction		T cell induction (*in vivo*)		B cell binding		Ab induction (*in vivo*)	
				C57BL/6	Balb/c	C57BL/6	Balb/c	C57BL/6	Balb/c	C57BL/6	Balb/c
#79	hs	A	+	-	+	n.a.	++	++	+/-	+++	++
#88	mm	H	-	-	+	-	-	++	+/-	+	+
#101	hs	A	+	-	+	++	+/-	++	+/-	++	+

Hence, to evaluate the prophylactic and therapeutic anti-tumoral *in vivo* efficacy of the identified isRNA lead candidate NP71-Seq45, HBcAg-#A79 VLPs should be co-adminsitered. Vaccination of isRNA-LPX adjuvanted HBcAg-#H88 VLPs served as a comparison in prophylactic tumor models. Unfortunately, HBcAg-#A101 VLPs could not be used in the subsequent tumor models, because of their non-availability when starting the tumor models.
Due to the differential immunological response behaviour of Balb/c and C57BL/6 mice, syngeneic mouse tumor models had to be established for both genetic backgrounds. The initial development of the mouse tumor models will be described in the next section.

3.7 Anti-tumoral efficacy of isRNA-LPX in combination with chimeric HBcAg-VLP based vaccines.

One of the main objectives of this thesis was to develop a small RNA-based, TLR7 specific adjuvant with strong and defined immunostimulatory activity that is capable to improve the

anti-tumoral efficacy of HBcAg-VLP based cancer vaccines. In the previous sections we could show that the co-administration of isRNA-LPX with HBcAg-#A79 VLPs induced a strong and CLDN6 target-specific humoral and cellular immune response. In the subsequent sections we wanted to analyze if the observed effects can be transferred to mouse tumor models and if the co-administration of isRNA-LPX indeed resulted in an enhanced anti-tumoral efficacy. In addition, we also analyzed the anti-tumoral activities induced by immunization with isRNA adjuvanted HBcAg-#H88 VLPs that showed a weaker induction of a CLDN6-specific humoral immune response and no CLDN6-epitope specific T cell induction.

3.7.1 Establishment of mmCLDN6 expressing syngeneic mouse tumor models.

Suitable syngenic mouse solid tumor models for the *in vivo* evaluation of anti-tumoral effects upon immunization with isRNA NP71-Seq45-LPX adjuvanted HBcAg-#A79 VLPs had to fulfill the following prerequisites: a) a fully active innate and adaptive immune system suitable for active immunization strategies; b) not too aggressive tumor growth kinetics to ensure sufficient time for three immunizations with two-week intervals (therapeutic tumor vaccination); c) high engraftment rates at lowest possible cell number to minimize the number of mice needed; d) stable mmCLDN6 expression after tumor cell inoculation for at least 60 days; and e) possibility to perform s.c. and i.v. tumor models.

For the establishment of mmCLDN6 expressing, syngeneic s.c. mouse tumor models, CT26 cells were used for Balb/c and MC38 or E0771 cells for C57BL/6 mice. All cell lines were stably transfected with mmCLDN6. In a first experiment, the *in vivo* growth kinetics of the tumorigenic CLDN6-expressing cell lines were analyzed by using three different cell numbers for s.c. inoculation. The objective of the titration experiment was to find out a suitable, minimal cell number that would be able to build solid tumors with an engraftment rate of 70-100%, as well as having a slow growth kinetic (see Figure 3.46).

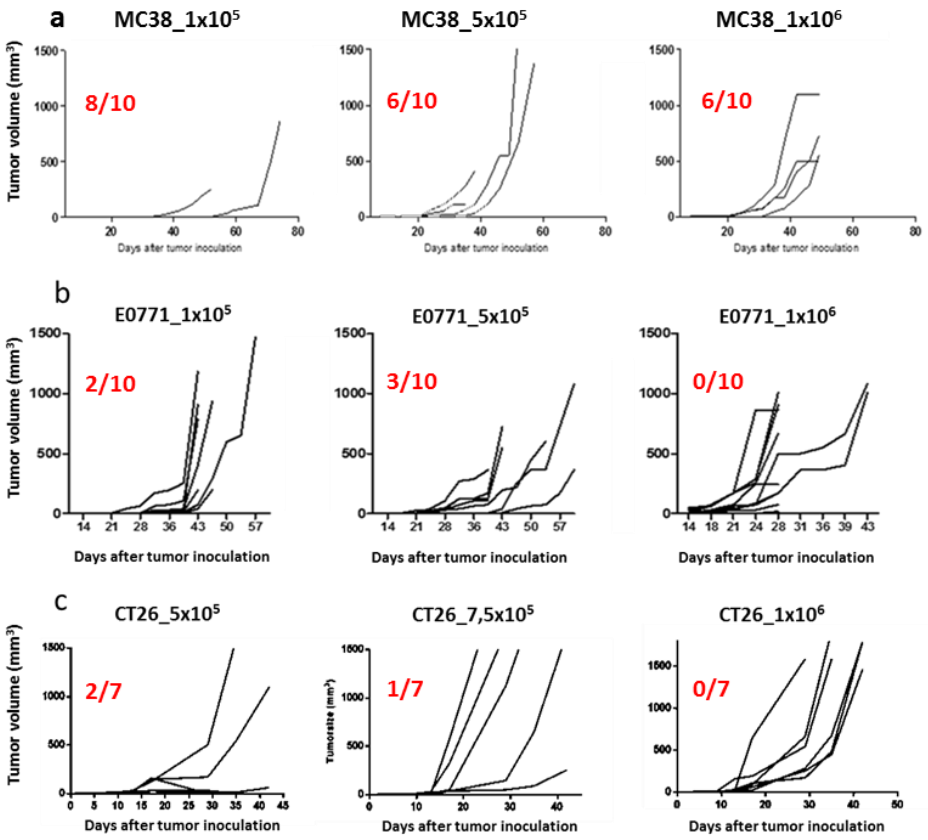

Figure 3.46: *In vivo* growth kinetics and engraftment rates of different numbers of mmCLDN6-expressing MC38, E0771, and CT26 tumor cells after s.c. inoculation. The tumor cells were inoculated s.c. by injection of the indicated cell numbers into the right flank of Balb/c or C57BL/6 mice (n=7 or 10). The tumor growth was measured over a period of 40 days. **a)** Tumor growth of mmCLDN6-expressing MC38 cells in C57BL/6 mice. **b)** Tumor growth of mmCLDN6-expressing E0771 cells in C57BL/6 mice. **c)** Tumor growth of mmCLDN6-expressing CT26 cells in Balb/c mice. The number of mice with no measurable tumor growth (no engraftment) are shown as red numbers in comparison to the numer of mice per group.

mmCLDN6-expressing MC38 tumor cells (Figure 3.46. a) showed a very low engraftment rate (<40% tumor bearing mice) for all tested cell numbers. Furthermore, MC38 tumors turned necrotic and burst from day 30 onwards. Therefore, MC38 tumor cells were discarded from the further establishement of syngeneic tumor models. In contrast, inoculation of mmCLDN6-expressing E0771 tumor cells resulted in an engraftment rate of 80-90% for all tested cell numbers and the formed tumors showed an accelerated growth behavior from day 39 onwards (Figure 3.46. b). This effect was becoming evident especially when inoculating $1x10^5$ or $5x10^5$ cells/mouse. For mmCLDN6-expressing CT26 tumor cells, the inoculation of $1x10^5$ cells/mouse led to no detectable engraftment (data not shown) and inoculation of $5x10^5$ or $7{,}5x10^5$ cells/mouse were only slightly improving tumor cell engraftment. However, the inoculation of $1x10^6$ cells/mouse resulted in an engraftment rate of 90% (Figure 3.46. c right). Similar to E0771 tumor cells, a accelerated tumor growth became visible from day 30 onwards. In general, the growth kinetics showed a high interindividual variation, irrespective of the tumor cell line used.

Based on the results for the engraftment rate and tumor growth kinetics, mmCLDN6-expressing E0771 cells ($5x10^7$ cells/mouse) and CT26 cells ($1x10^6$ cells/mouse) were selected for the further establishment of syngeneic, s.c. mouse tumor models.

In the next step, the stability of mmCLDN6 expression on tumor cells after inoculation was assessed. Here, it was important that the inoculated tumor cells enabled an experimental timeframe of at least 35-45 days to achieve maximal immune responses after three immunizations in two-weeks intervals. Therefore, established s.c. CT26 or E0771 tumors were removed 31 days post-inoculation and mmCLDN6 expression was analyzed in cell suspensions by flow cytometry using the CLDN6 specific mAb IMAB027 (see Figure 3.47).

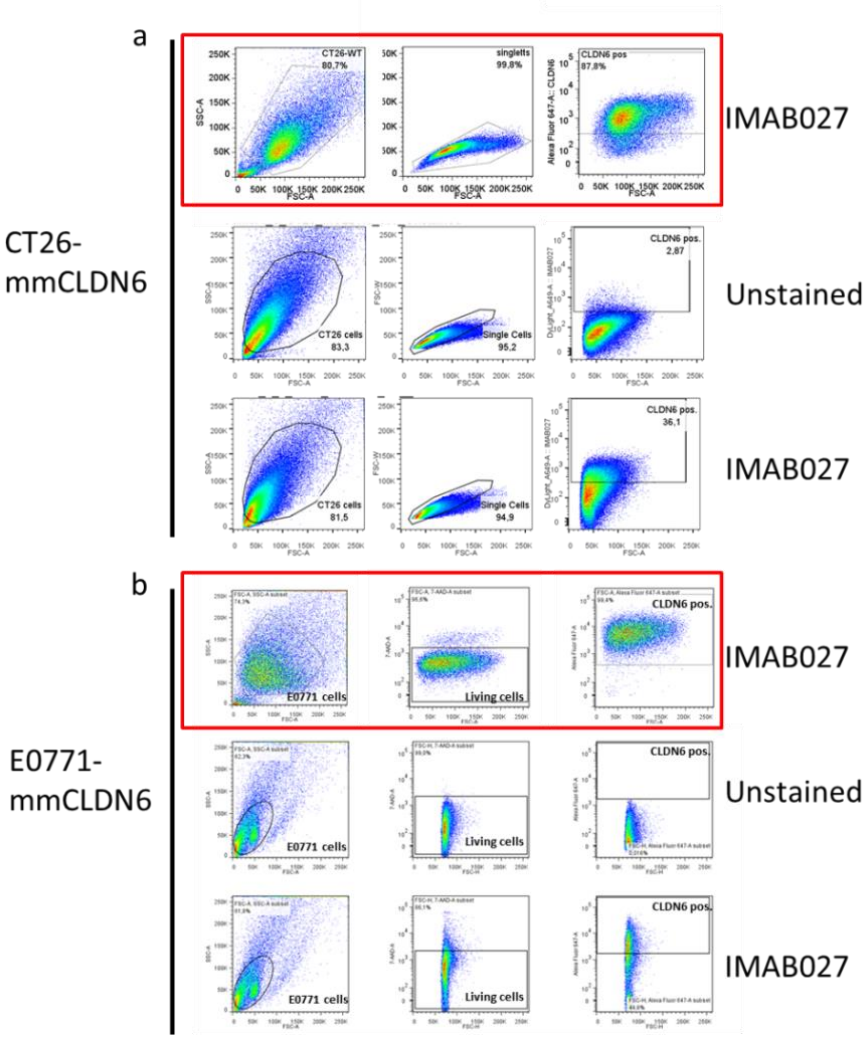

Figure 3.47: FACS analysis of mmCLDN6-expressing CT26 and E0771 tumor cells at day 31 post-inoculation. Tumor cells were inoculated s.c. into the right flank and mice were sacrificed at day 31 post inoculation. Established tumors were removed and single cell suspensions were generated. Subsequently, a FACS assay were performed using the CLDN6 specific IMAB027 mAb. **a)** FACS analysis at day 31 after inoculation of $1x10^6$ mmCLDN6-expressing CT26 tumor cells in Balb/c mice. Unstained cells and IMAB027 stained (red box) cell cultures prior to inoculation served as controls. **b)** FACS analysis at day 31 after inoculation of $5x10^5$ mmCLDN6-expressing E0771 cells in C57BL/6 mice. Unstained cells and IMAB027 stained (red box) cell cultures prior to inoculation served as controls.

The performed FACS analysis revealed that mmCLDN6 expression in established CT26 tumors was clearly decreased (from 88% positive cells prior inoculation to 36% at day 31 after inoculation) but still evident at day 31 post-inoculation. E0771 cells derived from established s.c. tumors showed a similar picture, with approximately half of all living E0771 cells being positive for mmCLDN6 expression 31 days post inoculation when compared to E0771 tumor cell prior-inoculation (50% vs. 100%).

This clear loss of mmCLDN6 expression upon inoculation of the tumor cell was not optimal, because it beared the risk that mmCLDN6-negative cells, which can not be attacked by the induced CLDN6-specific immune responses, might outgrow at a later stage of the envisioned therapeutic tumor models.

In summary, two tumor cell lines, one adressing Balb/c mice and another for usage in the C57BL/6 genetic background, with a high engraftment rate and not too-fast tumor growth could be successfully identified and established for s.c. syngeneic tumor models. However, both cell lines showed at significant reduction of mmCLDN expression upon tumor cell inoculation. Furthermore, a lung mouse tumor model using CT26-mmCLDN6 tumor cells could be successfully established too (data not shown).

3.7.2 Prophylactic vaccination only of isRNA NP71-Seq45-LPX adjuvanted HBcAg-#A79 VLPs leads to complete immune protection in a Balb/c syngeneic s.c. tumor model.

After establishing syngeneic tumor models in C57BL/6 and Balb/c mice, we analyzed the anti-tumoral efficacy and potency of the induced immune responses against the CLDN6-target protein initially by prophylactic vaccination with isRNA NP71-Seq45-LPX adjuvanted HBcAg-#A79 VLPs and HBcAg-#H88 VLPs. In the first prophylactic model we used Balb/c mice s.c. inoculated with mmCLDN6-expressing CT26 tumor cells. Balb/c mice were immunized three times (day 1, 14 and 28) with different vaccine compositions and ten days after the third immunization blood samples were taken for analysis of the antigen-specific humoral immune response. One day later the mice received s.c. $1x10^6$ CT26 cells/mouse and were monitored afterwards for another 42 days (see Figure 3.48).

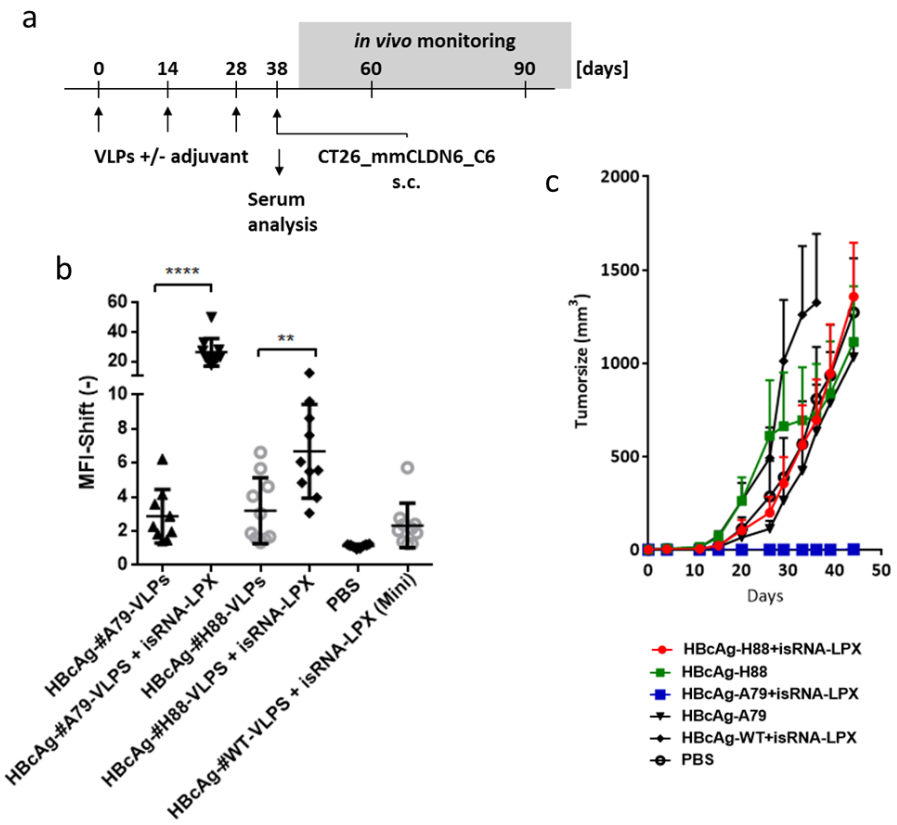

Figure 3.48: Prophylactic vaccination with isRNA NP71-Seq45-LPX adjuvanted HBcAg-#A79-VLPs induced a complete and efficient tumor growth control of mmCLDN6-expressing tumor cells in a syngeneic, s.c. tumor model. a) Treatment schedule. Balb/c mice (n=10 per group) were immunized i.v. three times with HBcAg-#A79 VLPs or HBcAg-#H88 VLPs alone or in combination with isRNA-LPX. As control groups, mice were immunized with HBcAg-#WT-VLPs adjuvanted with isRNA-LPX or PBS. Ten days after the last immunization blood samples were taken for analysis of the CLDN6 antigen-specific humoral immune response and one day later $1x10^6$ CT26-mmCLDN6 cells were inoculated s.c. to the right flank of each Balb/c mice and then monitored for another 42 days. **b)** FACS analysis of induced specific B cell responses in the sera taking at day 38 using CT26-mmCLDN6 tumor cells. Detection of bound antibodies was expressed as x-fold MFI-shift (Final serum vs. Pre-serum). **c)** *In vivo* tumor growth curves. Tumor sizes are illustrated as mean tumor size +/- SEM until day 42 after tumor cell inoculation. The difference between the groups were considered to be statistically significant at $p<0.05$. ***$p < 0.001$, ****$p < 0.001$ vs. no adjuvanted HBcAg-#A79-VLPs group. Student's t test was applied. Shown are the mean values +/- SEM.

Confirming previous results, the co-administration of HBcAg-#A79 or -#H88 VLPs and isRNA NP71-Seq45-LPX induced significant but rather different levels of antibodies recognizing the native CLDN6 target protein. Non-adjuvanted HBcAg-#A79 VLPs induced only a barely detectable humoral immune response. The tumor growth analysis revealed that the prophylactic immunization with isRNA-LPX adjuvanted HBcAg-#A79 VLPs resulted in a complete tumor control in all animals, whereas the immunization with isRNA-LPX adjuvanted HBcAg-#H88 VLPs led to no protection of mice against tumor growth. To be noted, two mice of the untreated group (PBS group) also remained tumor free due to lack of tumor cell engraftment. Nevertheless, the highly significant anti-tumoral activity after co-administration of HBcAg-#A79 VLPs and isRNA NP71-Seq45-LPX could be clearly demonstrated. Mice immunized with isRNA-LPX adjuvanted HBcAg-#WT VLPs were not able to control tumor growth and their tumor growth curves were similar to mice immunized with non-adjuvanted HBcAg-#A79 VLPs, HBcAg-#H88 VLPs or the PBS control group. The

result of isRNA-LPX adjuvanted HBcAg-#WT VLPs indicated that in a prophylactic setting, the administration of isRNA NP71-Seq45-LPX with a non-CLDN6 specific immunogen did not exert any anti-tumoral effect.
Subsequently, we additionally analyzed the induction of #79-epitope-specific T cells by IFN-γ ELISpot using tumor-free mice from the group immunized with HBcAg-#A79 VLPs or HBcAg-#H88 VLPs plus isRNA NP71-Seq45-LPX. The mice were immunized a fourth time and five days later splenocytes were generated for the ELISpot assay. The obtained data confirmed our previous findings of a strong T cell response only by the group which were immunized with isRNA-LPX adjuvanted HBcAg-#A79 VLPs with the ability of the induced T cells to recognize the murine epitope #88 of the mmCLDN6 protein (data not shown).

In order to confirm the obtained results of the prophylactic s.c. tumor model, we subsequently tested the anti-tumoral protection in a second prophylactic i.v. tumor model.

3.7.3 Prophylactic vaccination of only isRNA NP71-Seq45-LPX adjuvanted HBcAg-#A79 VLPs leads to complete immune protection in a Balb/c syngeneic i.v. tumor model.

The observed anti-tumoral efficacy of the induced CLDN6 target-specific immunity by prophylactic immunization with HBcAg-#A79 VLPs and isRNA NP71-Seq45-LPX should be confirmed in another syngeneic, prophylactic tumor model. In this second model, we used again mmCLDN6-expressing CT26 tumor cells and Balb/c mice, but in contrast to the first model, the tumor cells were inoculated i.v. leading to lung tumor nodules. Ten days after applying the standard immunization protocol as described in the first prophylactic tumor model, $5x10^5$ mmCLDN6-expressing CT26 tumor cells were inoculated i.v. and mice were monitored in average for another 17 days. At the end of the life span, lungs were dissected and stained with ink for manually, macroscopic counting of tumor nodules (see Figure 3.49).

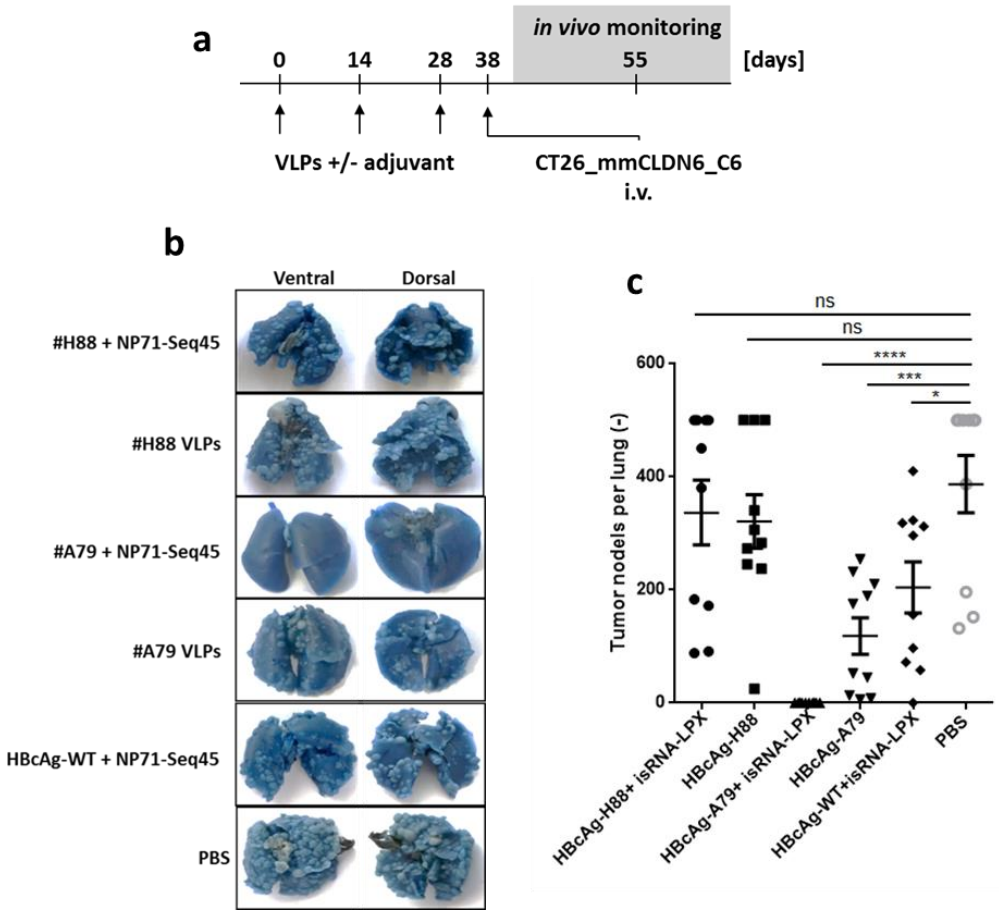

Figure 3.49: Prophylactic vaccination with isRNA NP71-Seq45-LPX adjuvanted HBcAg-#A79 VLPs mediated a complete and efficient tumor growth control of mmCLDN6 expressing cells in a syngeneic i.v. tumor model. a) Treatment schedule. Balb/c mice (n=10 per group) were immunized i.v. three times with HBcAg-#A79-VLPs or HBcAg-#H88-VLPs alone or in combination with isRNA NP71-Seq45-LPX. As control groups, mice were immunized with HBcAg-#WT-VLPs adjuvanted with isRNA-LPX or PBS. Ten days after the last immunization $5x10^5$ CT26-mmCLDN6 cells were inoculated i.v. into the tail vein. The mice were monitored regularly for approximately another 17 days before lung dissection. **b)** Number of tumor nodules per lung (mean +/- SEM). **c)** Exemplary ink-stained lungs from differently vaccinated mice. The difference between the groups were considered to be statistically significant at $p<0.05$. *$p < 0.05$; ***$p < 0.001$, ****$p < 0.0001$ vs. no adjuvanted HBcAg-#A79-VLPs group. One way ANOVA test was applied. Shown are the mean values +/- SEM.

In contrast to the prophylactic s.c. model, a slight anti-tumoral effect could be achieved in the i.v. model upon immunization with non-adjuvanted HBcAg-#A79 VLPs or (with an even weaker effect) when using isRNA adjuvanted HBcAg-#WT-VLPs. However, the macroscopic analysis of the lungs derived from mice vaccinated with HBcAg-#A79 VLPs and isRNA-LPX revealed again a complete inhibition of tumor gowth and formation of tumor nodules in the lung. This demonstrated the strong anti-tumoral activity of the induced CLDN6-target specific immunity within this group (Figure 3.49.b and c). Confirming the results of the prophylactic s.c. tumor model, no protection against tumor growth after vaccination with HBcAg-#H88 VLPs and isRNA NP71-Seq45-LPX could be detected.

3.7.4 CLDN6-specific antibodies induced by immunization with isRNA-adjuvanted HBcAg-#H88 VLPs are able to control tumor growth in C57BL/6 mice.

The previous experiments showed that the induced CLDN6-specific humoral immune response in Balb/c mice after immunization with HBcAg-#H88 VLPs plus isRNA NP71-Seq45-LPX was not able to control tumor growth in a prophylactic setting (Figure 3.48 and Figure 3.49). This observation could be explained either by the complete lack on an epitope #88 specific T cell response as shown before (see Figure 3.44), or by the diminished antibody response and CDC effector mechanisms against CLDN6 expressing cells upon Balb/c immunization with isRNA-adjuvanted HBcAg-#H88 VLPs in comparison to the vaccination with HBcAg-#A79 VLPs (see Figure 3.40).

Previously we observed that the induced CLDN6-specific antibody response after immunization of C57BL/6 mice with HBcAg-#H88 VLPs was better than in Balb/c mice (see Figure 3.43), whereas an epitope #88 specific T cell response was still absent. This difference in the immune response behavior against isRNA-LPX adjuvanted HBcAg-#H88 VLPs in Balb/c and C57BL/6 mice enabled us to analyze the contribution of the CLDN6-specific antibody response and the CLDN6-epitope specific T cell response to the prophylactic anti-tumoral effect in more detail. Therefore, C57BL/6 mice were immunized with isRNA-adjuvanted HBcAg-#H88 VLPs using the standard immunization schedule, followed by the s.c. inoculation of syngeneic, mmCLDN6-expressing E0771 tumor cells. As comparative controls, C57BL/6 mice were immunized pre-inoculation with isRNA-LPX adjuvanted HBcAg-#A79 VLPs or left untreated (see Figure 3.50).

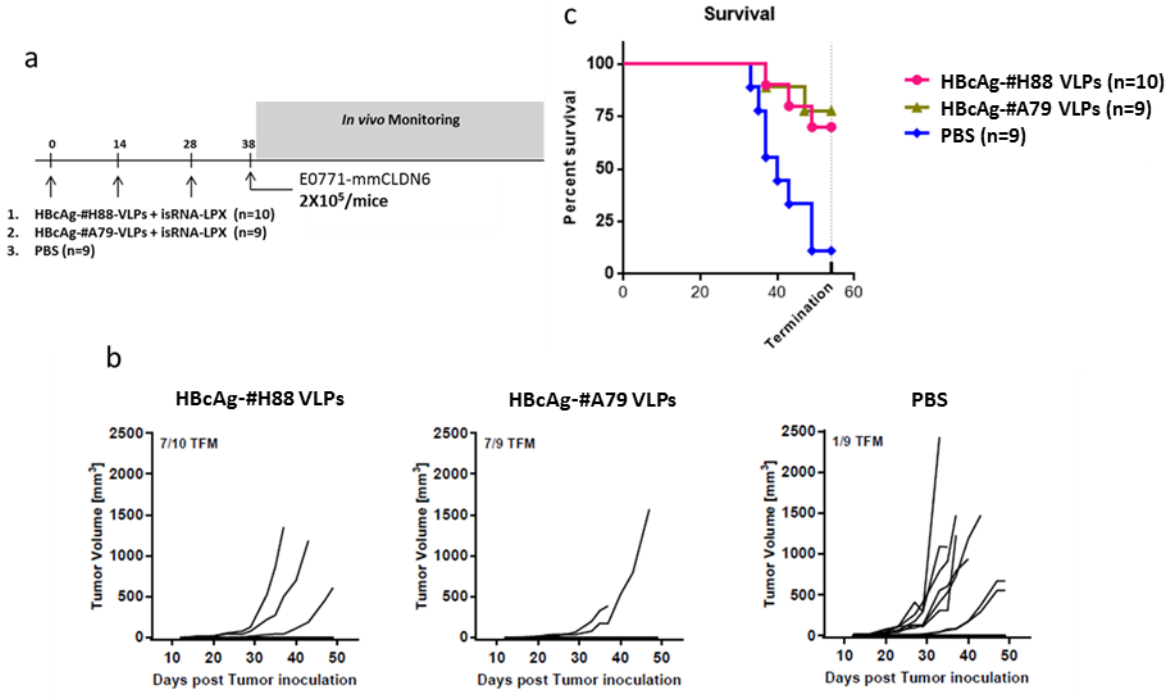

Figure 3.50: Prophylactic vaccination with isRNA-LPX adjuvanted HBcAg-#H88 or -#A79-VLPs protected C57BL/6 mice from tumor growth. a) Treatment schedule. C57BL/6 mice (n=9 or 10 per group) were immunized three times i.v. with isRNA-adjuvanted HBcAg-#H88 or -#A79-VLPs. PBS treated mice served as a negative control. Ten days after the last immunization $2x10^5$ E0771-mmCLDN6 tumor cells were inoculated s.c. into the right flank. **b)** Illustration of the individual tumor growth curves until the end of the experiment at day 54 after tumor cell inoculation.TFM: tumor free mice. **c)** Kaplan-Meier plot showing the survival of the mice up to 54 days after tumor cell inoculation.

In contrast to Balb/c prophylactic tumor models, the results of the prophylactic C57BL/6 tumor model clearly showed that the resulting CLDN6-specific antibody responses after immunization with isRNA-LPX adjuvanted HBcAg-#H88 VLPs was sufficient to exert a significant protective, antitumoral effect. Only in three out of ten mice tumor growth was detectable and led to the death of the animals (Figure 3.50. b and c). A slightly more potent prophylactic anti-tumor efficacy was obtained if the mice were immunized with HBcAg-#A79 VLPs and isRNA-LPX. In this case, only in two out of nine mice the tumors grew and led to the death of the animals (Figure 3.50.b and c). In the PBS control group, one mouse left tumor free, due to the non-engraftment of the E0771 tumor cells.

In conclusion, CLDN6-specific antibodies induced by immunization with isRNA-LPX adjuvanted HBcAg-#H88 VLPs could control the growth of CLDN6 expressing tumor cells in C57BL/6 but not in Balb/c mice. The reason for this difference remained unclear, but might rely on the somewhat increased antibody levels in C57BL/6 mice, on a different susceptibility of the used tumor cells to antibody-mediated cytocidal effector mechanisms or a general difference in the immune response between Balb/c and C57BL/6 mice (e.g. stronger isRNA-LPX mediated activation of innate immune cells).

3.7.5 Therapeutic vaccination of isRNA NP71-Seq45-LPX adjuvanted HBcAg-#A79 VLPs leads to significant anti-tumoral efficacy in a Balb/c syngeneic s.c. tumor model.

Given the fact that the prophylactic efficacy of CLDN6-specific B and/or T cells triggered significant tumor control in immunocompetent mice, their therapeutic application had also to be analyzed. The established standard immunization schedule, characterized by three vaccinations with two week intervals, ensured the highest induction of CLDN6-specific B cell approximately from day 38 (data not shown). The *in vivo* analysis of T cell kinetics still needs to be analyzed. The question remained whether the therapeutic immunization with isRNA-LPX adjuvanted HBcAg-#A79 VLPs using the standard immunization schedule could induce an immune response that is able to control tumor growth. In order to address this issue, $1x10^6$ CT26-mmCLDN6 tumor cells were inoculated s.c. to the right flank of Balb/c mice. One day after tumor cell inoculation, the mice were vaccinated with isRNA-LPX adjuvanted HBcAg-#A79 VLPs or controls according to the standard immunization schedule and tumor growth was monitored for approximately another 65 days (see Figure 3.51.).

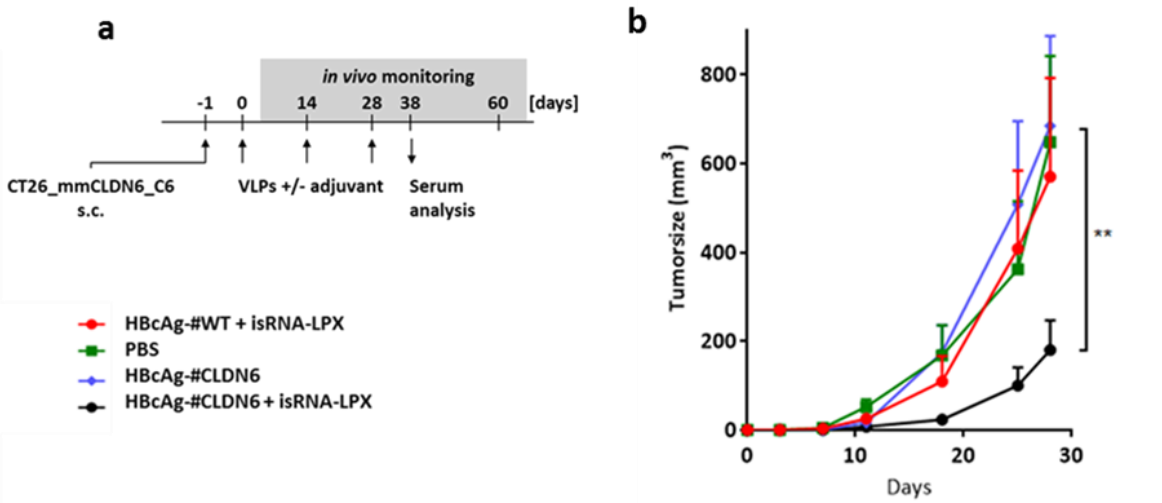

Figure 3.51: Therapeutic vaccination with isRNA-LPX adjuvanted HBcAg-#A79 VLPs induced an efficient growth control of CLDN6-expressing tumor cells. a) Applied immunization and tumor cell inoculation schedule. $1x10^6$ CT26-mmCLDN6 tumor cells were inoculated s.c. into the right flank of Balb/c mice. One day after tumor cell inoculation the mice were immunized three times (at day 0, 14 and 28) with non-adjuvanted HBcAg-#A79 VLPs or adjuvanted with isRNA-LPX. Mice immunized with HBcAg-#WT + isRNA-LPX or with PBS only served as controls. The mice were monitored for approximately 65 days after tumor cell inoculation. **b)** Tumor growth curves. The difference between the groups were considered to be statistically significant at $p<0.05$. **$p<0.001$ vs. the non-adjuvanted group. Student's t test was applied. Shown are the mean values +/- SEM.

Three immunizations with HBcAg-#A79 VLPs and isRNA-LPX given every 14 days resulted in beneficial therapeutic anti-tumoral effects (Figure 3.51. black line). HBcAg-#A79 VLPs alone could not control the tumor growth. This indicates the important role of the isRNA-LPX adjuvant by improving the immunity and the antigenicity of HBcAg-#A79 VLPs (Figure 3.51 blue line). Beside the adjuvant, HBcAg-#A79 VLPs is essential as a part of our standard vaccine for triggering the specific immune response. This might be highlighted by the lack of beneficial therapeutic anti-tumoral effects post-immunization with isRNA-LPX adjuvanted HBcAg-#WT VLPs (Figure 3.51 red line). Tumor growth was accelerated with the addition of PBS as a negative control (Figure 3.51 green line). It needs to be noted that in the control groups, in particular the PBS groups, the tumors grew fast and 50% of the mice had to be sacrificed since the tumor size met the endpoints (1500 mm^3) within 28 days.

To validate the obtained data, we repeated similar experiment testing the anti-tumoral activity of the induced anti-CLDN6 immunity by vaccination with RNA adjuvanted HBcAg#A79 VLPs. In this setting we tested also mice group which were immunized with RNA adjuvanted HBcAg-#H88 VLPs. Als control group the mice were received only PBS (Figure 3.52. a).

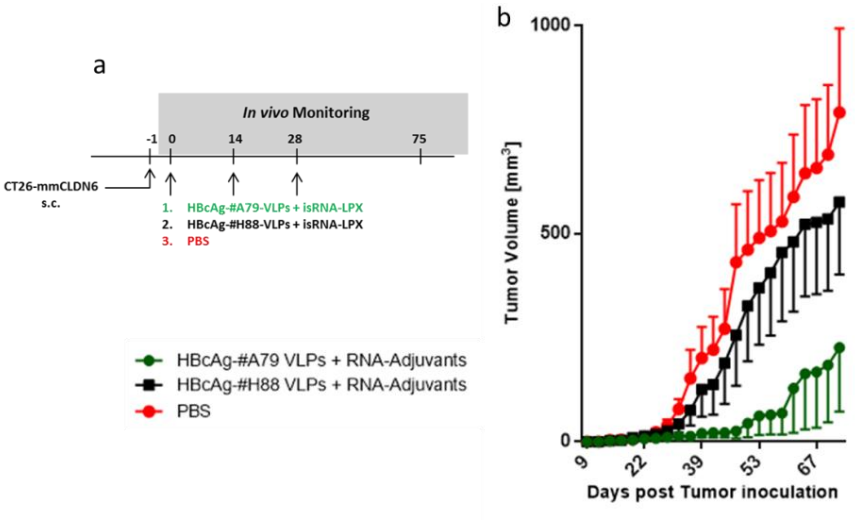

Figure 3.52: Beneficial therapeutic efficacy could be confirmed only after vaccination with isRNA adjuvanted HBcAg-#A79 VLPs. 1x106 CT26-mmCLDN6 tumor cells were inoculated s.c. to the right flank of Balb/c mice. 1 day after tumor cell inoculation the mice were immunized three times (d0, d14, d28) with isRNA adjuvanted HBcAg-#A79 VLPs or HBcAg-#H88 VLPs. As controls, the mice were immunized with PBS. The mice were monitored for approximately 75 days. a) Immunization schedule; b) Tumor growth. Shown are the mean values +/- SEM.

The generated data illustrated clearly the beneficial therapeutic anti-tumoral effects in the mice which were challenged s.c. with $1x10^6$ CT26-mmCLDN6 tumor cells and received one day later three immunizations with RNA adjuvanted HBcAg-#A79 VLPs in an interval of 14 days. Unfortunately, no therapeutic antitumoral efficacy was detected in mice which were immunized with RNA adjuvanted HBcAg-#H88 VLPs confirming the obtained data generating after prophylactic vaccination with the same vaccine (Figure 3.48 and Figure 3.49). The tumor growth of this group behaved almost similar to the PBS group.

In summary, the co-administration of isRNA-LPX adjuvant and HBcAg-#A79 VLPs efficiently improved the antigenicity of the VLP vaccine by triggering target-specific B and CD4+ T cells simultaneously. The induced immune responses reduced tumor growth in Balb/c mice and showed an antitumoral responses. Furthermore, the no therapeutic efficacy of the induced CLDN6 specific immunity after immunization with RNA adjuvant and HBcAg-#H88-VLPs indicated the important role of the CLDN6 specific B and CD4+ helper T cells for inducing the effection function in therapeutic setting. However, this conclusion has to be confirmed by further experiments.

4 Discussion

Target specific induction of adaptive immune responses against tumor-associated antigens (TAAs) is an already established strategy to fight cancer diseases [12, 36, 161]. Furthermore, chimeric TAA-presenting *Virus-like particle* (VLP)-based vaccines have been shown to be an attractive modality for inducing target specific immune responses after active immunization [123, 162, 163]. However, the successful therapeutically active application of such type of vaccines often depends on co-applied adjuvants, specifically enhancing the vaccine induced adaptive immune responses [164].

In this thesis we presented the identification and pre-clinical development of the first systemically administrable, small RNA-based adjuvant (called isRNA-LPX) that could significantly improve the immunogenicity and induced anti-tumoral activities of vaccines based on chimeric (foreign epitope presenting) *Hepatitis B virus core antigen* (HBcAg)-derived VLPs. The identified isRNA-LPX adjuvant lead structure consisted of a small immunostimulatory (is) RNA-sequence (NP71-Seq45) and the recently described cationic liposomal formulation F12 that already entered clinical trials [118]. The isRNA-LPX adjuvant acted mainly via *Toll-like receptor* 7 (TLR7) stimulation in plasmacytoid dendritic cells (pDCs) resulting in a strong interferon-α (IFN-α) and weak tumor necrosis factor-α (TNF-α) induction *in vitro* and *in vivo* (Section 3.3 step 4; and 3.6.1). The intravenous (i.v.) co-administration of HBcAg-Claudin6 (CLDN6) epitope-presenting VLPs and isRNA-LPX allowed the simultaneous targeting of the adjuvant and the vaccine to the same lymphatic organ in order to maximize adaptive immune responses. Compared to non-adjuvanted or CFA/IFA adjuvanted immunizations (gold standard), the addition of isRNA-LPX to chimeric HBcAg-VLPs dramatically enhanced the humoral immune response against the target protein in its native conformation (Figure 3.29) and induced antibodies exerting potent antibody-mediated cytotoxic effector functions (Figure 3.28) in an IFN-α/TLR7 dependent manner (Section 3.5.2). Furthermore, only the addition of isRNA-LPX to the VLP-based vaccine resulted in the induction of a tumor-antigen epitope specific cellular immune response (Figure 3.36). The ability of the induced target specific immunity to trigger anti-tumoral activities was successfully analyzed in several syngeneic tumor models using tumor cell lines stably expressing the murine CLDN6 protein. The obtained results proofed the strong anti-tumoral efficacy of isRNA-LPX adjuvanted chimeric HBcAg-VLPs (Section 3.7).

4.1 Identification and initial characterization of isRNA-LPX adjuvants

4.1.1 The applied fragmentation strategy led to the successful identification of isRNA candidates with specific immunostimulatory profiles

Despite considerable efforts, so far only few anti-cancer vaccine adjuvants have been approved for use in clinical practice by the European or US American regulatory agencies (EMEA or FDA) for preventing virus-induced cancers [94, 165]. In fact, the most commonly

used adjuvant in human vaccines is Aluminium hydroxide (Alum, like in Alhydrogel) which was characterized to enhance Th2-type humoral responses [166]. However, until now, no therapeutic efficacy could be reached using such types of adjuvants in combination with protein-based vaccinations [47].

As an alternative, different kinds of TLR agonist as adjuvants for cancer vaccines have demonstrated a good prophylactic but also therapeutic potential of this adjuvant class in preclinical studies [162, 167, 168]. However, it is still under debate which type of TLR(s) should be targeted and accordingly which type of agonistic molecules should be used in order to obtain the most promising adjuvant activities in combination with protein-based vaccines, in our case VLP-based immunogens.
In this regard, Martins *et al*. could show a significant increase of antigen-specific, poly-functional $CD4^+$ and $CD8^+$ T cell responses and antibody responses in C57BL/6 mice and Hartley guinea pigs that were immunized with a dsRNA mimicking, poly(I:C) LC adjuvanted VLP-based vaccine [169]. Furthermore, Heidenreich *et al*. demonstrated the superior efficacy of ssRNA-based adjuvants (named RNAdjuvant) vs. dsRNA poly(I:C) in combination with a peptide derived from HPV-16 E7 protein to enhance antigen-specific $CD8^+$ T cells and anti-tumoral efficacy using a TC-1 tumor model [120]. Thus, targeting ssRNA TLR sensors including TLR7 or TLR8 may be a reasonable strategy to establish a new adjuvant class that is capable to improve the quality and quantity of host adaptive immune responses when used in vaccine formulations against infectious diseases or cancer and was pursued as the main objective in this thesis.
In addition, targeting antigen-presenting cells (APCs) such as dendritic cells (DCs) and B cells is a key factor for the induction of an adaptive anti-tumoral immune responses [166]. Both cell types are known to express nucleic acid sensors including TLR7 constitutively or after activation for the recognition of viral infections that result in a strong induction and secretion of the cytokine IFN-α [39]. Furthermore, B cells are known to act as the primary APCs and DCs as secondary APCs for HBcAg-VLPs [170, 171], the selected model vaccine format used in this thesis. Therefore, the main focus of this thesis was to develop a TLR7 agonist specifically targeting B cells or DCs and inducing high levels of the lead cytokine IFN-α finally resulting in the induction of strong and target antigen-specific humoral and cellular adaptive immune responses.

Currently, several strategies have been developed and applied for the identification of TLR agonist [161]. Frequently, these strategies aim to identify small molecule-based and can be classified as discovery platforms based on rational design or on high-throughput screening of compound libraries [161] [121]. Thus, VentiRx Pharmaceuticals has reported a series of benzodiazepine TLR8 agonists identified from high-throughput screenings [167]. Interestingly, most of these screenings were executed using only human cells and many of the identified TLR8 agonists exerted a significantly reduced innate immunostimulatory activity in mouse cells [161].

In this thesis, we established and applied a strategy based on rational design and (potential) high-throughput screening. Our strategy used iterative RNA-sequence fragmentation cycles combined with *in vitro* tests (human and mouse cells) using viral-derived RNA-sequences with already published immunostimulatory profiles as starting points. First steps of the fragmentation strategy were not-biased on the existence of potentially immunostimulatory active sequences motifs, but later steps included secondary structure predictions for a more defined way in the selection of small RNA fragments for further test rounds. The high efficiency of the applied strategy was proven by the identification of small RNAs with an extraordinary capacity to activate the innate immune system in a TLR7-specific manner (Figure 3.13). Furthermore, the applied strategy was not restricted to TLR7 and could be expanded for the identification of agonists with other TLR-specificities (data not shown). In addition, further optimizations can be envisioned to accelerate the established process in order to establish a high-throughput-like process, such as the establishment of automated processes during *in vitro* tests or first fragmentation cycles and the optimization of secondary structure analysis.

Improvement of tissue and/or cell type targeting, safety and tolerability are also important tasks when discovering and establishing new types of adjuvants. Hence, covalent conjugation or formulation-assisted delivery present new options to improve those parameters [161]. Ilyinskii *et al*. demonstrated that co-delivery of TLR7/8 or TLR9 agonists and an antigen in synthetic vaccine particles induced a strong increase of humoral and cellular immune responses [172]. In accordance to these results, Heidenreich *et al*. showed that RNAdjuvant needs to be complexed with a polymeric carrier to achieve maximum efficiency [120]. In this thesis, we aimed to formulate the identified lead structure isRNA NP71-Seq45 with cationic liposomes to achieve specific lymphoid tissue targeting after systemic administration.

4.1.2 The role of administration route for selecting cationic liposomes F12

Application of cationic adjuvants for delivering antigens using intramuscular (i.m.) or subcutaneous (s.c.) administration routes frequently resulted in the stimulation of only weak antigen-specific immune responses [173]. One reason for this obervation might be based on the relatively low abundance of immune cells at the injection sites. However, a prerequisite of a cancer vaccine-mediated potent induction of antigen-specific B and T cell immunity is the targeting of high numbers of APCs capable to uptake, process and cross-present the antigen-epitopes to T cells [123, 174]. In fact, the spleen as the central lymphoid tissues comprises all major types of APCs, including macrophages, DCs, B cells and monocytes [175]. Therefore, the main reason for the usage of the well-characterized cationic liposomes F12 for formulation of the identified isRNAs, as applied in this thesis, was the ability of F12 to transport isRNAs specifically to the spleen after i.v. injection [118]. To date, relatively few vaccine adjuvants based on TLR agonists have been injected i.v. [176-179]. Most of them have been administrated alone and in free form without any kind of formulation. Actually,

they were tolerated well and might induce a specific immunity, but the clinical outcomes were unsatisfactory.

To improve the efficacy of TLR-based adjuvants we decide to used isRNA-LPX as an adjuvant in combination with HBcAg-#CLDN6 VLP based antigens. The quality control data by AF4-MALS revealed that the engineered isRNA-LPX nanoparticles were stable, monodisperse, present a particle size between 200-400nm and were fully resistant to degradation by mouse serum at 37°C (data not shown). Furthermore, the dose-dependency experiments when administrating isRNA-LPX i.v. showed the same dose response profile as published by Kranz *et al*. [180]. Here, mRNA coding for hemagglutinin protein (HA) from Influenza A virus was complexed with cationic liposomes F12 (mRNA-LPX) and applied i.v.. Both, the isRNA-LPX and mRNA(HA)-LPX immunizations induced high level of IFN-α already 5-6 h after i.v. administration (Figure 3.34 and [118]. Interestingly, Wilson *et al*. reported, that the maximum percentage of cells in spleen and liver positive for adjuvant uptake was reached between 4 and 8 h after the i.v. administration of lipid nanoparticle encapsulated CpG-ODNs [181]. Furthermore, Lan *et al*. also found that the level of IFN-α peaked approximately 8 h after administration of stabilized immunemodulatory RNA compounds [182]. The maximal IFN-α secretion at 4-6 h after i.v. administration can be explained by an accumulation effect.

Furthermore, adverse effects after injection of even 40 µg isRNA-LPX were not visible, indicating the good tolerability of isRNAs after systemic application (Figure 3.34). However, formal clinical chemistry and toxicology data have been not yet generated. But, the published clinical data from Kranz *et al*. showed that the i.v. administration of the applied cationic liposomes F12 as a carrier of four encoding mRNAs (NY-ESO-1, MAGE-A3, tyrosinase, and TPTE) were well-tolerated with only transient flu-like symptoms [180]. These observations were in agreement with previous observations demonstrating the low toxicity and good tolerability of lipid nanoparticle formulated with nucleic acid agonists including TLR7 and TLR9 ligands [181, 183].

4.1.3 Local application of isRNA-LPX adjuvant

Based on the finding that the systemic co-administration of the isRNA-LPX adjuvant and chimeric HBcAg-VLPs was safe and could induce a very strong CLDN6-specific humoral immune response in mice, it was anticipated that the local co-administration of this combination would also mediate an antigen-specific immunity with similar capacities. In line with this anticipation, Mohsen *et al*. reported that local co-delivering (s.c.) of TLR9 or TLR7 agonist-based adjuvants and a chimeric VLP-based vaccine without any physical linkage successfully target the same APCs in lymph nodes resulting in strong cytotoxic T lymphocyte (CTL) responses in mice [184]. Indeed, the TLR ligand and the antigen were packaged in separate VLPs and mixed prior the administration [184]. A similar result was obtained by Heidenreich *et al.* [120]. Using intradermal (i.d.) injection as a local administration route, they demonstrated the strong enhancement of antigen-specific multifunctional $CD8^+$ T cell responses and also antibody responses after co-dilevering of RNAdjuvant and a peptide derived from the HPV-16 E7 protein [120]. Therefore, we also investigated if the local co-

administration of isRNA-LPX and HBcAg-#A79-VLPs induced a superior CLDN6-specific humoral immune response if compared to benchmark water-in-oil based adjuvants (CFA/IFA and Montanide ISA 51) (Figure 5.1). The immune-enhancing effect of CFA/IFA and ISA 51 is considered to be dependent on depot formation at the site of the injection, which is characterized by the slow release of the injected antigen [185, 186]. In turn, isRNA-LPX adjuvant induced only a transient secretion of cytokines (3.34.b) and chemokines (3.26) without any sign of depot effect. As already known from the literature, the induced cytokine and chemokines can result in immune cell trafficking to the injection site, which leads to additional cytokine secretion and accordingly formation of a local immune-competent environment [186]. The enhancement of MHC and co-stimulatory molecule expression guides the maturation of APCs and the increase of the antigen-processing and -presentation. The loaded and mature APCs migrate into the lymph nodes to encounter and induce B and T cell responses. It needs to be emphasized that the applied slightly negative charged isRNA-LPX was developed and optimized for i.v. administration [118] and may not be optimal for local administration. Thus, further experiments are required to optimize the local co-administration of isRNAs. The challenge will be to discover and to find a suitable carrier formulation that can be used to deliver the isRNAs efficiently to the TLR-expressing cells.
Nguyen *et al*. reported that s.c. injection of liposomally formulated RNA-based adjuvants strongly induced IFN-α secretion *in vivo* and enhanced humoral and cellular immune responses when combined with protein-based vaccines [122]. In particular, positive charged DOTAP complexed RNAs (15:1 L/R) led to the highest levels of cytokine induction [122]. Thus, it can be envisioned that positively charged, engineered isRNA-LPX may be better suited for local administration. Therefore, liposome-isRNA complexes should be tested in different lipid to RNA ratios in further experiments.

In fact, the i.v. co-administration of cationic liposomes F12 and chimeric HBcAg-#CLDN6 VLPs triggered a superior induction of target-specific immune responses compared to its local administration using s.c. as an injection site (data not shown). Therefore, i.v. administration was taken for the further establishment and design our chimeric HBcAg-based cancer vaccine.

4.2 Mode of action of isRNA-LPX adjuvant

4.2.1 isRNA-LPX adjuvant mediated its strong immunostimulatory activities mainly via TLR7.

We and others have shown that the successful use of recombinant proteins for active vaccination is not only linked to the antigen, but also to the type of adjuvant used. In order to fulfill our expectations of developing an adjuvant that is suitable for i.v. immunization, and thus inducing a very strong target-specific immune response that is capable of controlling tumor growth in mice, F12 liposomes were used [118]. Our data indicated that isRNA-LPX induced IFN-α in pDCs expressing TLR7 (Figure 3.24, 3.25, 3.31, 3.32 and 3.33). In

fact, the primary immune cells that produce IFN-α in response to ssRNA are pDCs, although mDCs and monocytes can also trigger an IFN-α cytokine response, but at much lower level when compared to pDCs [122, 187]. The chemokine IP10 (CXCL10) as a type I cytokine is also released by pDCs in response to ssRNA signaling through the TLR7 receptor [106, 110, 122]. In turn, the immune cells that would be expected to secrete the proinflammatory cytokine IL6 are mainly mDCs, monocytes, macrophages or monocyte-derived DCs [122, 188, 189]. However, pDCs could also secrete IL6 after stimulation with ssRNA [106, 110]. In particular, the used liposomes for formulation mediate the efficient uptake of RNA by DC populations and macrophages in various lymphoid tissues [118]. Thus, the strong IL6 release as observed in this thesis appeared to be dependent on the isRNA delivery, preferably to pDCs or macrophages. However, this hypothesis needs further exploration.
Restimulation experiments clearly revealed that isRNA-LPX increased the secretion of Th1 cytokines (Figure 3.36). No IL10 induction could be detected (Figure 3.26). This finding was further supported by the analysis of isRNA-LPX induced immunoglobulin (Ig) subclasses *in vivo* (Figure 3.38) (Section 3.5.4 and 4.3.2). For further confirmation that the isRNA-LPX exerted their immunostimulatory activities mainly via the TLR7 receptor, the *in vitro* transcribed NP71-Seq52 (Table 3.3), that was characterized by the lack of GU-motifs in the stem structure was extensively analyzed *in vitro* and *in vivo* (Figure 3.32). Based on the results and the published literature, the absence of GU-motifs in the RNA sequence diminished the IFN-α induction *in vivo* (Figure 3.32.c). In line with this notion, Heil *et al*. revealed that G and U-rich ssRNA oligonucleotide derived from HIV-1 virus induced IFN-α and inflammatory cytokine expression in DCs and macrophages [110]. Zhang *et al*. determined the tertiary structure of TLR7 in its activated form induced by guanosine and ssRNA containing U and revealed the ligand specificity and activation mechanism of TLR7 (Figure 1.6). Thus, the combination guanosine and polyuridine ssRNA affected the dimerization state of TLR7 and resulted in induction of defined cytokines [190, 191]. More interestingly, the induction of CLDN6-specific antibodies was also negatively affected by adjuvantation of HBcAg-#A79-VLPs with F12-formulated NP71-Seq52 (Figure 3.32.d).

We concluded that our isRNA-LPX stimulated mainly TLR7 after endosomal uptake by pDCs and this led to a upregulation of activation markers on the surface of several immune cells and the induction of a target cytokines such as IFN-α and IP10. A final proof of this conclusion could be done using TLR7-deficient mouse strains like C57BL/6 TLR7-/- which were not available during this PhD thesis.

4.2.2 The recognition of isRNA-LPX adjuvant by cytosolic pattern recognition receptors

Besides the endosomal TLR activation and the induction of type I interferon, the activation of cytosolic pattern recognition receptors (PRRs), such as protein kinase R (PKR), was a matter of investigations. The mechanisms of foreign antigen uptake in DCs comprise three main endocytic pathways termed phagocytosis, macropinocytosis, and receptor-mediated endocytosis [192]. Moreover, macropinocytosis was identified to be the major uptake

mechanism of RNA-LPX [118]. In turn, we investigated whether the isRNA-LPX was not only restricted for the endosomal targeting by macropinocytosis, but if it can end up also in the cytosol of the target cells and by default other cytosolic-PRRs or enzymes may be activated. Among these are the retinoic acid inducible gene I (RIG-I), the melanoma differentiation antigen 5 (MDA5) and PKR as PRRs. It is well-known that RIG-I, MDA5 and PKR specifically recognize viral RNA ligands [193]. MDA-5 recognizes and detects long double-stranded RNA [154, 194] and therefore can be excluded as specific receptors for the selected small isRNAs. It has been reported that RIG-I receptor binds blunt-ended dsRNAs bearing a triphosphate on the 5' end [195, 196]. Additionally, the minimal length of RNA required to activate RIG-I receptor seems to be 10 or 19 bp [154, 194]. While the non-blunt ended RNA sequence NP71-Seq45 as part of isRNA-LPX and also the other selected small isRNAs (Figure 3.21) present a non-stable duplex region with the internal loop structure (Figure 3.21), those isRNA sequences can be very probably not recognized and bound by an RIG-I receptor. Nevertheless, *in vivo* studies using e.g. C57BL/6 MAVS-/- (also known as Cardif-/-) mice to investigate whether the RIG-I receptor is involved in the adjuvant activity of isRNA-LPX has not yet been performed. Furthermore, the PKR stimulation by isRNA-LPX was investigated and the data revealed that isRNA-LPX stimulated slightly the PKR receptor (data not shown).

4.2.3 IFN-α secretion affects the induction of antigen-specific antibodies and T cells

As it was repeatedly reported and now confirmed by this study, IFN-α is the lead and dominant cytokine that exert DC activation and maturation [197, 198]. Thus, the absence of IFN-α in mice treated with αIFNARI blocking antibody resulted in no maturation of pDCs and cDcs after immunization with isRNA-LPX (data not shown). Interestingly, by diminishing the IFN-α secretion due to depletion of pDCs in BDAC2-DTR mice, the number of induced CLDN6 specific antibodies was significantly decreased (Figure 3.31.c and Figure 3.31.b). In this context, type I IFNs including IFN-α were found to systemically activate $CD4^+$, $CD8^+$ T cells, NK and B cells [199, 200]. Confirming our observation, Hervas *et al*. have shown that type I interferon, including IFN-α, potently enhance primary antibody responses against soluble antigens and increased the production of all IgG subtypes with long-live and memory features [200, 201]. Furthermore, the isRNA-LPX stimulation *in vivo* led to a time- and dose-dependent induction of IFN-α (Figure 3.34.b) correlating with the *in vivo* induction of antigen-specific B response after co-administration with HBcAg-#A79-VLPs (Section 3.6.1). Strikingly, the antigen-specific antibody responses correlated largely with the induced IFN-α secretion *in vitro* (Figure 3.22, 3.29 and 3.30). The F12-formulated isRNA NP71-Seq45 induced the highest IFN-α secretion and, as expected, the strongest antigen-specific antibody responses if it was combined with HBcAg-#A79-VLPs (Figure 3.24, 3.28, 3.29 and 3.30).

As mentioned above and repeatedly reported in the literature, IFN-α enhances stimulatory acitivites on the level of the adaptive immunity and has been shown to stimulate B and T cell responses [202]. Interestingly, no correlation between induced IFN-γ secreting T cells and IFN-α secretion may be detected. Indeed, the parental isRNA NP71-Seq4 led to a higher

number of IFN-γ spots when compared to its fragment isRNA NP71-Seq45 (Figure 3.28 and 3.37). In this context, Crouse *et al*. reported that IFN-α seems to be involved in Th1 cell differentiation by increasing IL2 secretion of T cells in mice, which results in increasing of STAT5 signaling inhibiting the differentiation of T follicular helper cells (Tfh cells) [203]. Furthermore, previous work has demonstrated the role of inflammatory cytokines including IL6 in promoting Tfh cell phenotype through upregulation of STAT3 [204]. STAT3 is known to counteract indirectly the type I IFN-driven Th1 cell differentiation and promote T follicular helper (TFH) cell differentiation by reducing CD25 expression and directly competing with STAT5 for binding to the Bcl6 locus [203-205]. We noted here that isRNA(NP71-Seq45)-LPX (=isRNA-LPX) exerted stronger IL6 cytokine secretion in immune cells than isRNA(NP71-Seq4)-LPX (Figure 3.26) which can explain the reduction of IFN-γ spots originated of Th1 immune responses.

Based on the presented results, IFN-α seems to be the crucial factor that provokes the induction of the antibody responses. In addition, it needs to be emphasized that even the i.v. injection von 40 µg isRNA formulated F12 liposomes (Figure 3.34) did not lead to visible adverse effects, indicating the good tolerability of formulated isRNAs after systemic application.

4.3 HBcAg-CLDN6 VLPs as model antigen for evaluating isRNA-LPX adjuvants

4.3.1 Characterization of the applied HBcAg-CLDN6 VLPs

More than 88 studies based on VLP vaccines are currently undergoing clinical evaluation and some of those are designed for prophylactic cancer treatment [18, 206]. Several VLP vaccines that are based on non-chimeric, wildtype VLPs, such as Cervarix (GlaxoSmithKline) and Gardasil (Merck), have been already approved for use as prophylactic vaccines against human cervical cancer [207]. Unfortunately, no therapeutic anti-tumoral efficacy has been achieved in clinical trials using these vaccines [208]. However, VLP-based vaccine platforms can be also used to deliver heterologous antigens, including tumor-associated antigens (TAAs) and accordingly may be applied as a promising vaccine format not only to prevent but also to treat cancer.
Indeed, Cytos AG initiated in 2006 the first chimeric VLP-based cancer vaccine testing the safety and immunogenicity of a Melan-A VLP vaccine in advanced stage melanoma patients (NCT00306553). A specific antigen-specific CTL response could be induced in patients which were treated with Melan-A VLP co-administered with CpG-ODNs as a TLR9 targeting adjuvant [206]. Thus, a potent stimulation of the innate immune system followed by a potent, VLP-vaccine mediated upregulation of antigen-specific B and T cell responses might be a promising way to control tumor growth [174].

HBcAg-VLPs as an antigen carrier for shared or individualized TAAs might be a good vaccine format to achieve a beneficial therapeutic activity if it will be combined with adjuvants

bearing strong immunostimulatory activities. HBcAg-VLPs without the positively charged arginine-rich C-terminal domain (nucleotide-binding domain, NBD) were successfully used as carriers for the presentation of self-molecules and antigenic epitopes, which are derived from defined TAA molecules and could simultaneously induce a strong antigen-specific B and/or T cell response [36, 46, 59, 209].

In this study, the TAA CLDN6 was used as a shared tumor target antigen and correctly assembled, chimeric HBcAg-VLPs carrying foreign CLDN6 epitopes could be generated (Figure 3.2 and 3.5). Furthermore, when selecting CLDN6 epitopes for genetic insertion into the HBcAg major immunodominant region (MIR) important criteria had to be considered [36]. Thus, the cross-reactivity of the induced antibody response to CLDN9, which is closely related to the CLDN6 protein but expressed in several healthy tissues had to be prevented [209]. Here we could show that the careful selection of CLDN6 epitopes, as exemplified for HBcAg-#A79 VLPs, resulted after immunization in a humoral immune response with high specificity for the native CLDN6 protein expressed on the surface of living cells (Figure 3.4, and 3.29). No cross-reactivity against CLDN9 was detected by using CLDN9 transfectants, despite the fact that the CLDN6 #79 epitope differs only in two positions from the corresponding sequence of the CLDN9 protein (Figure 3.4 and 3.29). Similar observations had been made by Klamp *et al*. who showed that antibodies induced upon immunization with chimeric CLDN18.2-epitope presenting HBcAg-VLPs bind with high precision the native target protein CLDN18.2 on the surface of living cells but not to the corresponding epitope of the CLDN18.1 splice variant that differs by only one amino acid [36]. More important was that these antibodies lysed only and with high selectivity CLDN18.2-positive cells in CDC dependent manner [36].

The biophysical and biochemical features of the inserted epitopes play a crucial role when generating self-assembling chimeric HBcAg-VLPs. It is well known that not all chimeric proteins are able to build nanoparticles. In this context, Karpenko *et al*. reported that insertion of amino acids with high hydrophobicity, large volume, and high β-strand index prevented self-assembling of chimeric nanoparticles [210]. Indeed, these parameters seemed to be considered by selcting epitopes for the C-termini insertion [210]. Thus, the oligonucleotide encoding the CLDN6 epitope #79 ($CLDN6_{142\text{-}159}$: I**R**DFYNPLVA**E**AQKRE) and #88 ($CLDN6_{142\text{-}159}$: I**Q**DFYNPLVA**D**AQKRE) could be successfully inserted into the MIR of truncated HBcAg-VLPs and correct self-assembly of chimeric HBcAg-VLPs could be demonstrated by NuPAGE-SDS-PAGE and PageBlue stained native agarose gel electrophoresis (Figure 3.5). A direct detection of the engineered CLDN6 epitope in the context of HBcAg-VLPs could not be performed as no CLDN6 epitope-specific monoclonal antibody (mAb) was available. However, the correct assembly of HBcAg-#A79 VLPs was demonstrated using the conformation-specific mAB 3120 (Figure 3.1) and the detection of the inserted CLDN6 was indirectly verified by demonstrating the ability of such nanoparticles to induce antibody responses in mice, which recognize, besides the HBcAg backbone, also the linear #79 epitope by peptide ELISA (Figure 3.6.b and 3.29.b).

Furthermore, AF4-MALS analysis of the engineered chimeric HBcAg nanoparticles displayed an average molecular weight (MW) of approximately 4,2 MDa (Figure 3.2). This corresponds

to the theoretically determined MW of HBcAg nanoparticles ranging between 3,7 and 4,9 MDa depending on the T=3 or T=4 symmetry of the NBD-truncated HBcAg-VLPs which was also reported by Pumpens *et al*. (Figure 3.4.b) [58]. In addition, the radius of HBcAg-VLPs was also determined by AF4-MALS analysis and the obtained data demonstrated a radius of approximately 15 nm corresponding to the predicted radius (Figure 3.2). In this context, McGonigle and others reported that HBcAg particles are dimorphic and they form two icosahedrally symmetric particles T3 with 30 nm and T4 with 34 nm diameter [57, 211, 212].

In conclusion, modified chimeric HBcAg-VLPs displaying defined epitopes of CLDN6 on their surface could be generated. The designed chimeric HBcAg-VLPs generated stable capsids, which could be specifically bound by B cells (Figure 3.3) and induced strong antigen-specific immune responses against the HBcAg-backbone and also the inserted CLDN6 epitope.

4.3.2 Characterization of CLDN6-specific immune responses induced upon immunization with isRNA-LPX and HBcAg-CLDN6 VLPs

Klamp *et al.* reported that the immunization of mice or rabbits with chimeric HBcAg-CLDN18.2 VLPs led to induction of antibodies that were able to bind specifically to the target protein CLDN18.2 in its native conformation on the surface of living cells. Subsequently, the CLDN18.2 specific antibodies were shown to be capable of killing target positive cells by CDC and ADCC [36]. Interestingly, 3D-reconstructions of the used chimeric HBcAg-VLPs illustrated that the linker-flanked epitope of CLDN-Link VLPs has a higher flexibility than CLDN-VLPs [36]. This factor seemed to have a profound influence on the B cell response. Hence, the induced target-specific antibody responses by CLDN-Link-VLPs were able to bind the linear CLDN18.2 epitope (ELISA data) but also the native CLDN18.2 protein (FACS data) stronger than those induced by CLDN-VLPs [36].
Therefore, the constructs HBcAg-#A79 and HBcAg-#H88 VLPs were designed with linker-flanked CLDN6 epitopes #79 and #88, respectively. Furthermore, the insertion of the selected CLDN6 epitope in the MIR region of HBcAg-VLPs did not diminish the antibody response against the HBcAg backbone (data not shown). This finding confirmed those of Klamp *et al.,* who found that all VLPs with or without inserted epitopes induced antibodies against the HBcAg backbone with similar endpoint titers [36]. In our approach, the obtained data indicated that the main B cell responses, which are induced by chimeric HBcAg-VLPs, are restricted to the inserted epitope and not to the HBcAg backbone (data not shown).
The insert position seems to have an essential influence on the display and the immunogenicity of foreign epitopes presented on the surface of HBcAg-VLPs [213, 214]. Whereas C-terminally inserted epitopes are the least well exposed and the least immunogenic, N-terminally inserted foreign epitopes are better exposed and thus more immunogenic. The insertion into the MIR domain of HBcAg-monomer offers the best variant for the epitope accessibility and accordingly the highest immunogenicity [215, 216].
Storni *et al.* could successfully demonstrate that the insertion of the MHC class I-restricted peptide p33 derived from LCMV into the C-terminus of HBcAg-VLPs enhances a specific CTL

response *in vivo*. In the study by Storni *et al*. CpG-ODNs as TLR9 agonists were used as an adjuvant [216]. In accordance to these results, we also demonstrated by *in situ* staining using MHC class I tetramers that the C-terminal insertion of known T cell epitopes such as p33 or gp70 could induce a strong and specific T cell response when combined with isRNA-LPX (data not shown, part of the master thesis of Kai Pumpa, BioNTech Protein Therapeutics).

In 2016, Chu *et al*. showed that the insertion of the model CTL epitope HPV16 E7 into the MIR of HBcAg-monomer induces a E7-specific CTL response, which led to tumor growth control in a TC-I-grafted mouse tumor model [46]. In this thesis, we sought to investigate whether HBcAg-VLPs carrying a CLDN6-specific epitope, which was predicted represent a reasonable Kd-restricted peptide (Figure 3.4), would also enhance potent antigen-specific immunity. An antigen-specific B and T cell response against CLDN6 could be generated *in vivo* by i.v. immunization of isRNA-LPX adjuvanted HBcAg-#A79 VLPs, while only a target-specific B cell response against CLDN6 was induced after immunization with isRNA-LPX adjuvanted HBcAg-#H88 VLPs (Figure 3.39 and 3.40). Confirming to the observation made by chu *et al*. and our results, Malik *et al*. could show that generated chimeric HBcAg-VLPs expressing preS1 residues at the tip of the spike region (insertion site at position 79-80 of HBcAg) are able to induce both HBcAg-specific T cells and antibodies against preS1 [163].

Actually, the induced immune responses by immunization with HBcAg-VLPs that carried the CLDN6 epitope #79 was profoundly different to those induced by chimeric HBcAg-VLPs that displayed the CLDN6 epitope #88 on their surface. However, the immunization of mice with isRNA-LPX adjuvanted HBcAg-#A101-VLPs carrying the endogenous epitope #101 resulted also in an induction of CLDN6 specific B and also T cells (Figure 3.43 and 3.44). As described in section 3.6.7, the construct HBcAg-#A101 was similar to HBcAg-#A79 with respect to the same HBcAg backbone A and the additional acidification of the inserted epitope, but contained the murine homologue of the human CLDN6 epitope #79. Accordingly, HBcAg-#A101 differed from HBcAg-#H88 only by the used backbone and the glutamic acid linkers flanking the murine epitope (Figure 3.42). In fact, glutamic acid linkers were added especially to increase the solubility of the HBcAg-#A79 VLPs and HBcAg-#A101 VLPs as described also by Billaud *et al*. But glutamic acid linkers can additionally, in combination with Glycin-rich linkers, increase the optimal surface presentation of the inserted epitope to the immune cells, which lead to an increase of the induced immune responses [217]. These observations were in line with the finding made by Klamp *et al*. demonstrating by 3D-reconstructions the high flexibility of CLDN-Link-VLPs compared to CLDN-VLPs despite the both could form nanoparticles [36]. Interestingly, antibodies induved by CLDN-Link-VLPs were more capable than those induced by CLDN-VLPs to recognize and bind the target protein [36]. Subsequently, the position of the inserted epitope #88 versus #79 and #A101 within the MIR domain of the HBcAg backbone was different. This can result in a different epitope conformation and accordingly changes the following presentation to different parts of the induced immune system. As previously mentioned and published by Schödel *et al*. and others the insert position within the MIR domain seems to have an essential influence on the display and the immunogenicity of the foreign epitopes carried by the HBcAg-VLPs [215, 218-220]. The examination of #88 in backbone A or #79 and #101 in backbone H or rather the

addition of the glutamic acid linker on the C and N terminus of the #88 peptide has not yet performed. But some factors seem to play a crucial role in the nature of the induced immune responses and accordingly have to be analyzed profoundly.
The question remained if pre-existing HBcAg-backbone specific antibodies, potentially due to a previous HBV infection, would negatively influence our cancer vaccine approach. In particular, it was reported that such antibodies can trigger antibody-dependent phagocytosis and enhance antigen clearance, which resulted in a reduction of antigen uptake by APCs and accordingly diminished the immune responses [46]. This is not in agreement with another finding that confirmed the ability of pre-existing antibodies to enhance the immune response by increasing the antigen uptake of APCs [46]. Generally, this point was addressed by our group and other groups and the obtained data confirmed that pre-existing anti-HBcAg antibodies didn't negatively influence the antigen-specific immune responses [46, 221].

4.3.3 CLDN6 specific immunity elicited by isRNA-LPX and HBcAg-#A79 VLP immunizations are cross-reactive against murine CLDN6.

Interestingly, we found that the i.v. immunization with isRNA-LPX adjuvanted HBcAg-#A79 VLPs effectively stimulated murine CLDN6 specific humoral immune responses, which was evidenced by the ability of the induced antibody to bind the native murine CLDN6 on the surface of tumor cells (Figure 3.39). In addition, isRNA-LPX adjuvanted HBcAg-#A79 VLP vaccination successfully enhanced murine CLDN6 specific cellular immune responses, which was highlighted by elevated IFN-γ responses and accordingly by increased numbers of IFN-γ expressing T lymphocytes in the splenocytes stimulated with the #88 or #79 peptide (Figure 3.40). However, the immunization with isRNA-LPX adjuvanted HBcAg-#H88 VLPS could not induce IFN-γ expressing T lymphocytes, to be able to trigger specific immune responses if they encounter the MHC-I presented #88 or #79 epitopes (Figure 3.40).
Thus, the exogenous HBcAg-#A79 can most likely break immune tolerance more easily than the endogenous HBcAg-#H88 VLPs when they are co-administered with the isRNA-LPX adjuvant in mice. Strikingly, despite the Kd-restricted T cell epitope $\#79_{147\text{-}155}$ differing to $\#88_{147\text{-}155}$ by just a single amino acid (Figure 5.1), HBcAg-#A79 VLP vaccination was capable to elevate IFN-γ expressing T cells in splenocytes, when restimulated with the $\#88_{147\text{-}155}$ peptide. In support of this notion, Slansky *et al.* reported that amino acid substitutions in a natural MHC I-restricted tumor antigen enhance the stability of the MHC-peptide-TCR complex followed with a stronger induction of the specific T cells [222]. Hence, the one amino acid difference in the predicted #79 epitope compared to the endogenous #88 can be the reason for the increased stability of the MHC-peptide-TCR complex, which resulted in a strong antigen-specific T cell response. Therefore, the altered selected epitope (rescue procedure) which has to be inserted in the MIR of HBcAg for an optimal presentation to the immune cells could be an alternative for inducing a strong and desired T cell responses and accordingly B cell responses. Brentville *et al*. reported that the treatment with the altered

peptide, in particular, citrullinated peptide, can enhance T cell responses that were able to overcome cancer immunosuppression more strongly than the wildtype variant [223].
However, the capability of HBcAg-#A101 in combination with isRNA-LPX to induce also simultaneously B and T cell responses revealed the importance of antigen design approach (Figure 3.42.b) and illustrated clearly that all used HBcAg-CLDN6 constructs were similarly capable to break tolerance explaining by the strong induction of humoral B cell responses after immunization with isRNA-LPX adjuvanted HBcAg-#H88 VLPs. In order to better understand the ability of the induced T cells resulted after immunization with isRNA-LPX adjuvanted HBcAg-#A79 VLPs to recognize the mouse #88 epitope, we performed a FACS staining assay defining the T cell subtype as already described [224]. Interestingly, we found that our vaccine induces CLDN6 specific $CD4^+$ T cells which can explain the obtained cross-reactivity (data not shown). Thus, Kreiter *et al*. reported that $CD4^+$ T cell recognition of mutations (or rather amino acid substitution) may be less stringent length and sequence requirement for peptides binding to MHC class II molecules as compared to MHC class I epitopes [138].

4.3.4 Immunization of isRNA-LPX in combination with HBcAg-#A79 VLPs resulted in a balanced antigen-specific IgG2a/IgG1 response

Successful vaccination strategies against cancer might depend on the induction of antigen-specific antibodies that are able to bind their target protein in its native conformation and subsequently mediate target positive cell killing via immune effector mechanisms (Figure 4.1). Indeed, human IgG1 and IgG3 are able to upregulate the classical complement pathway and to bind to Fcγ receptors more efficient than IgG2 [225, 226] (Figure 4.1). Immunization with non-adjuvanted HBcAg-#A79 VLPs or VLPs combined with empty F12-liposomes resulted in high IgG1 and very low IgG2a antibody titers, leading to a predominantly Th2 immune response. On the other hand, antibodies elicited upon immunizations with HBcAg-#A79 VLPs adjuvanted with isRNA-LPX had moderately higher IgG1 and strongly induced #79-peptide-specific IgG2a antibody titers, resulting in a balanced Th1/Th2 immune response (Figure 3.38). These observations were in accordance with results published by Heidenreich *et al*. when analyzing OVA-specific IgG1 and IgG2c antibodies induction in mice after immunization with RNAdjuvant and OVA compared to OVA alone [119].
Furthermore, isRNA-LPX adjuvant drove the Th1 immune response by elevating the induction of IgG2a and the induced antigen-specific B cell response efficiently exerted cytocidal effector functions (Figure 3.37). The triggered antibody effector function was strictly depending on active complement (Figure 3.37). In fact, mouse IgG isotypes have different affinity to FcγRs and capacity to active complement [227, 228]. Mouse IgG2a and 2b are known as complement-fixing IgGs [228].
Interestingly, the antigen-specific antibodies elicited by immunizations using CFA/IFA adjuvant in combination with HBcAg-#A79 VLPs were not able to exert efficient cytocidal effector functions (Figure 3.37). Actually, CFA consisting of heat-killed *Mycobacterium tuberculosis* is usually important to prime Th1 immune responses after prime immunization,

while the IFA adjuvant, which presents only the water-in-oil emulsion without any bacterial content, is applied as an adjuvant for the following immunizations and responsible for the induction of Th2 immune responses [229, 230]. Thus, the applied standard immunization scheme using CFA/IFA as adjuvants should induce a balanced Th1/Th2 type immunity [231]. The decisive factors seem to be not only the type of the induced immune response, but more importantly the quality (binding the native target protein) and the quantity (level of the induced target specific antibodies) of the enhanced B cell immune responses. Therefore, the cytocidal effector function of the induced antibodies largely correlated with their calculated MFI-shift (Figure 3.37).

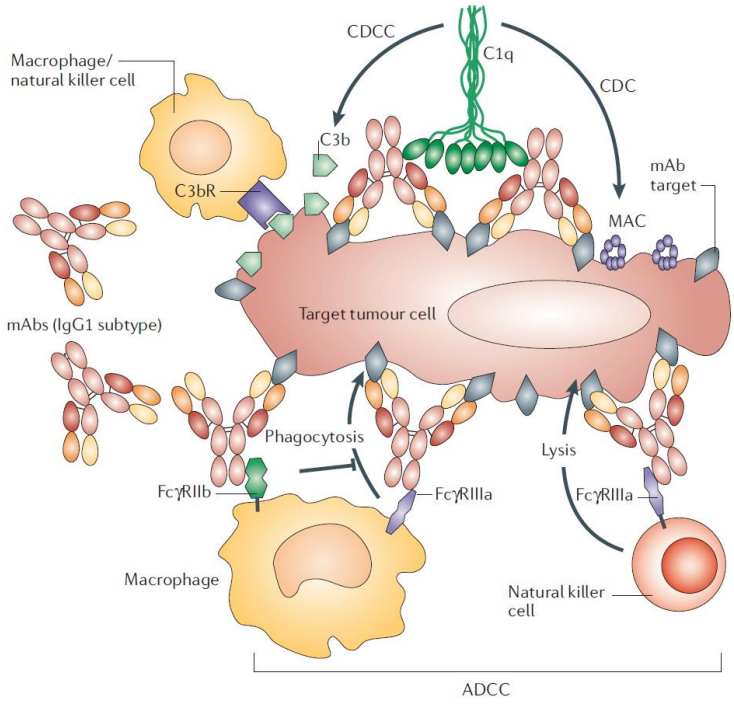

Figure 4.1: Effector functions of the antibody subclasses IgG1 and IgG3. The induced target specific antibodies bind the specific target on a tumor cell. Afterward, complement C1q interacts more efficiently with the CH2 constant domain of IgG1 and IgG3 antibodies. This interaction results in the upregulation of a proteolytic cascade of the complement classical pathway and followed with the formation of a membrane-attack complex for the killing of antigen-positive tumor cells. This biological killing mechanism is called complement dependent cytotoxicity (CDC). During the first complement signaling pathway, a second complement called C3b is generated and binds to macrophage and natural killer (NK) cells, which accordingly allows those cells to perform their biological activities including phagocytosis and cytolysis. This killing effect called complement-dependent cell-mediated cytotoxicity (CDCC). Such antibodies could induce another killing effect that termed antibody-dependent cellular cytotoxicity (ADCC). Thereby, other immune cells with effector features such as NK cells or macrophages can bind the CH3 constant domain of the antibody through Fcγ receptors. Thus, mAb-coated tumor cells can be phagocytosed or lysed. Adapted from ''Comparing antibody and small-molecule therapies for cancer'' by Imai *et al.* Nat Rev Cancer, 2006; 6(9):714-27.

Besides CDC, ADCC and CDCC are considered as the main relevant antibody effector mechanisms [226, 232] (see Figure 1.4). ADCC and CDCC assays are so far not established using CLDN6 endogenously expressing or stable transfected cell lines. Based on the presented CDC data, the isRNA-LPX adjuvant enhances a cytokine milieu *in vivo* promoting Ig class switch that induced antigen-specific B cell responses that are able to kill target positive cells.

4.4 Evaluation of isRNA-LPX adjuvant with other protein-based vaccines

Based on the fact that isRNA-LPX adjuvant may improve the efficacy of any protein-based vaccine upon active immunization, we evaluated the adjuvant activities of isRNA-LPX in combination with a vaccine based on peptides conjugated to CRM197 (AT07, AffiRis AG), a genetically detoxified form of diphtheria toxin, for inducing a combined Th1/Th2 immune response [233].

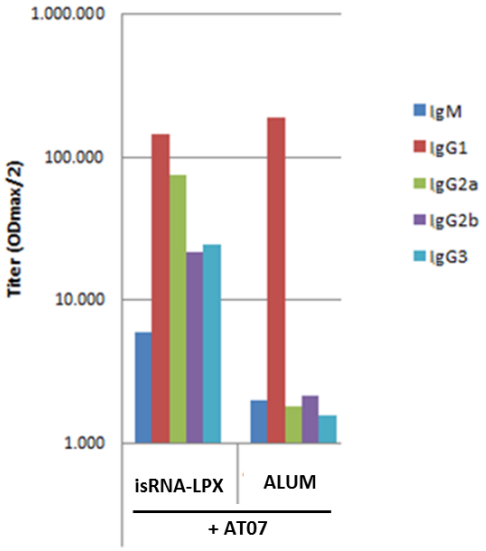

Figure 4.2: isRNA-LPX leads to an induction of Th1 immune responses and a combined Th1/Th2 in combination with an AT07 vaccine. Balb/c mice (n=5 per group) were immunized three times at two-week intervals with AT07 adjuvanted with Alum (s.c.) or isRNA-LPX (i.v.). Ten days after the last immunization the sera were taken and the induced Ig subtypes titers of pooled sera against the target peptide were analyzed by ELISA. ELISA assays and data analysis were performed by AFFiRis AG (Vienna, Austria).

As shown in Figure 4.2, immunization with AT07 adjuvanted 0.2% Alhydrogel adjuvant (Alum) resulted in high IgG1 immune responses and very low IgG2a and IgG2b titers, which indicated an immune response shifted towards the Th2 type response. Actually, several studies revealed that alum induced mainly Th2 responses as confirmed in this experiment and accordingly may not be suited for cancer immunotherapy [120, 234-236]. In contrast, the combination of isRNA-LPX adjuvant and AT07 vaccine triggered the induction of IgG2a, IgG2b and also IgG3, without reducing the IgG1 antibody levels indicating a balanced Th1/Th2 induced immunity. The same observations were also made by Nguyen *et al*. who showed that the co-injection of lipidoid-isRNA nanoparticles and OVA protein resulted in increasing of Th1-biased IgG2c subclass compared to immunization with OVA alone [122]. It needs to be emphasized that the co-administration of OVA and CpG-ODNs have been shown to induce a stong Th1-biased IgG2a responses [122, 237, 238]. In contrast, isRNA-LPX adjuvant enhanced IgG2a titers without decreasing of Th2-associated IgG1 response originated from protein vaccination alone. Indeed, the balanced Th1/Th2 immunity has been shown to be critically important in several induced immune responses, including anti-tumoral immune responses [239]. Whereas Th1 cells secreting IFN-γ are the crucial part for the induction of cellular immunity, Th2 cells secreting IL4 and IL5 play an important role in

humoral immunity [240]. This is in agreement with other observations suggesting that the activation of Th1 dominant immune response may facilitate the induction of anti-tumoral immunity [241]

As a conclusion, the results confirmed our previously generated data (Figure 3.38) that the isRNA-LPX adjuvant was inducing a predominantly Th1 driven immune response making it relevant in cancer immunotherapy as shown also by Heidenreich *et al*. and others [120, 239].

4.4.1 Whole overview of the induced CLDN6 specific immunity

One of the aims of developing chimeric HBcAg-VLPs as a vaccine in combination with formulated isRNA adjuvants was not only to induce a high titer of antigen-specific antibodies but also to induce an antigen-specific T cell response with effector and memory functions. The capability of such vaccines to stimulate both arms of the adaptive immunity, followed by the induction of antigen-specific immune responses are considered to be pivotal for inducing a strong and effective anti-tumoral effect [38]. In particular, the HBcAg-VLP processing by defined APCs can occur rapidly and results in activation of all splenic antigen-specific T cells in a TCR-transgenic mouse model within 24 h [216]. Therefore, a rapid induction of antigen-specific T cell responses after immunization is expected to be effective at priming of anti-tumoral immune responses in wild-type mice.

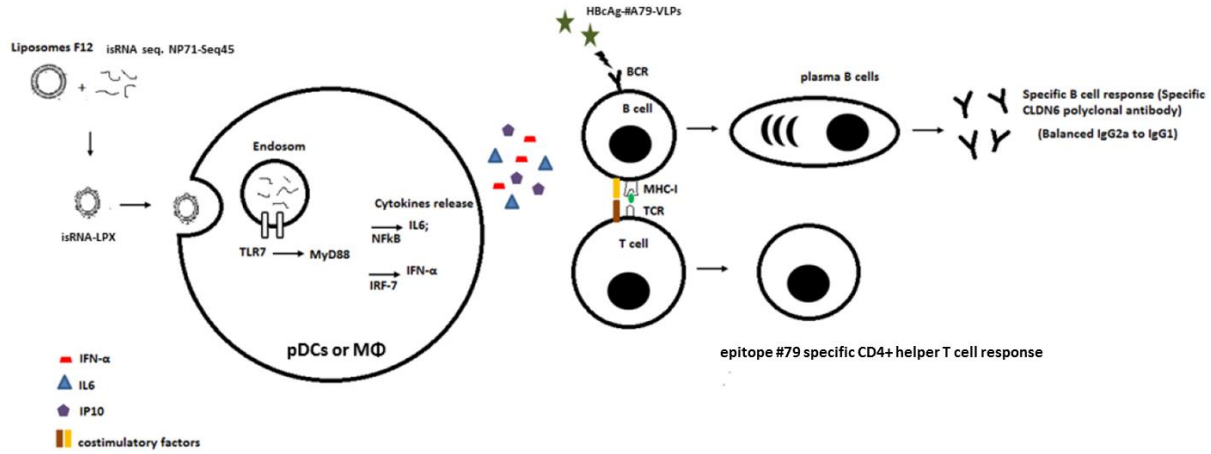

Figure 4.3: Schematic illustration of the induced immune response after i.v. immunization of mice with isRNA-LPX adjuvant and HBcAg-#A79-VLPs. The rational to use the isRNA-LPX adjuvant was to act in combination with HBcAg-VLPs intravenously. Subsequently, the F12 formulation serves for the isRNA protection against the degradation by nucleases in tissue and blood. The isRNA uptake by APCs, mainly by pDCs, results in the stimulation of MYD88-TLR7-IRF7 but also NF-kB signaling pathways. In turn, the activation results in the release of cytokines in particular IFN-α. In parallel, HBcAg-#A79 VLPs are initially bound by B cells. However, the HBcAg-VLPs uptake and processing might be performed in B cells, but also in DCs or macrophages (not illustrated in the figure). The induced cytokine milieu and the antigen presentation by APCs affect the induction of effector adaptive immune cells including antigen-specific B and T cell responses. MyD88: myeloid differentiation primary response gene. NF-kb: nuclear factor kappa-light-chain-enhancer of activated B cells. BCR: B cell receptor. TCR: T cell receptor. IFN-α: interferon alpha. IL-6: interleukin 6. IRF: Interferon regulatory factor. MHC: Major histocompatibility complex. TCR: T cell receptor. MΦ: Macrophage. pDCs: plasmacytoid dendritic cells. HBcAg: Hepatitis B core antigen.

As previously reported, the fusion of an MHC class-I restricted T cell epitope to the C-terminus of HBcAg-VLPs, via a three leucine linking sequence, enhances the antigen-specific T cell responses *in vivo* [216]. Interestingly, DCs and macrophages were the APCs that efficiently processed and cross-presented the epitopes to T cells [216]. However, the performed binding experiments revealed that our chimeric VLPs were primarily bound by B cells (Figure 3.3). Unfortunately, experiments analyzing uptake and processing of our chimeric HBcAg-VLPs by B cells were not yet performed. As already demonstrated, the isRNA-LPX adjuvant primarily targeted pDCs *in vivo* (Figure 3.31.b) and *in vitro* (3.24 and 3.38.c) resulting in an induction of a defined cytokines among others IFN-α (Figure 3.26 and 3.38) that was mainly responsible for the adjuvant effect of isRNA-LPX (Figure 3.31.c). Thus, it remains possible that the chimeric HBcAg-VLPs and the RNA-LPX adjuvant target different immune cells and this point will be the matter of our next investigations. In conclusion, the identified isRNAs administered i.v. in a liposomal formulation can act as an adjuvant to boost the generation of humoral and cellular antigen-specific immune responses *in vivo* when combined with a chimeric HBcAg-based vaccine with defined characteristics (Figure 4.3).

4.5 Anti-tumoral efficacy of isRNA-LPX adjuvant in combination with chimeric HBcAg-based vaccines

Within the presented work, it was demonstrated that, the i.v. co-administration of isRNA-LPX adjuvant and chimeric HBcAg-VLPs induced potent antigen-specific immune responses *in vivo*. Depending on the inserted CLDN6 epitope and the type of the HBcAg-backbone it was possible to provoke either a CLDN6 specific B cell response only or combined CLDN6 specific B and T cell responses in mice (Figure 3.34, 3.35 and 5.4). Using a preventive strategy Chu Xiaojie *et al*. demonstrated the ability of the immunization with chimeric HBcAg-VLPs presenting an HPV 16 E7 epitope in MIR to nearly completely suppress tumor growth in a suitable mouse tumor model [162]. Furthermore, the therapeutic VLP immunization enhanced humoral and cellular specific immunity and showed a significant suppression of tumor progression in mice carrying 2-3 mm tumors [162]. Hence, he reported that the induced specific T cells were responsible for the therapeutic anti-tumoral effect of VLPs [162]. Subsequently, Klamp *et al*. demonstrated the ability of the induced auto-antibodies after prophylactic vaccination with chimeric HBcAg-CLDN18.2 VLPs to trigger anti-tumoral effects [36]. Thus, it seems highly probable that target specific T cells are the main effector cells which are responsible for the anti-tumoral activity of therapeutic vaccination with chimeric HBcAg-VLPs. However, numerous studies revealed the strong association between tumor-infiltrating lymphocytes and clinical benefit in human cancer [242]. Although most studies focus on $CD8^+$ T cells, the roles of $CD20^+$ infiltrating B cells in anti-tumoral efficacy could be demonstrated in favorable outcomes in breast, lung, ovarian and cervical cancer [174, 243].

In this regard, the anti-tumoral activity of the simultaneously induced antigen-specific humoral and cellular immunity after immunization with isRNA-LPX adjuvanted HBcAg#A79

VLPs and the induced antigen-specific humoral immunity after immunization with HBcAg#H88 VLPs were analyzed.

4.5.1 Prophylactic vaccination

As shown by Klamp *et al*., prophylactic vaccination with chimeric HBcAg-VLPs could trigger anti-tumoral effects in established syngeneic mouse tumor models [36]. In line with these observations, we could show that the induced immune responses after co-administration of isRNA-LPX and HBcAg-#A79 VLPs resulted in a complete tumor control against s.c. or i.v. challenge with murine CLDN6-expressing CT26 tumor cells (Figure 3.43 and 3.44). However, no tumor control could be observed in mice that were immunized with isRNA-LPX adjuvanted HBcAg-#H88 VLPs. Convincingly and in agreement with the finding made by Klamp *et al*., the anti-tumoral efficacy may correlate with the induction of antibodies mediating cytotoxic effector functions against cells expressing the native target protein [36]. Whereas vaccination with isRNA-LPX and HBcAg-#A79 VLPs resulted in antigen-specific antibodies mediating cytocidal effector function, antibodies induced after immunization with RNA adjuvanted HBcAg-#H88 VLPs were not capable of exerting this function (Section 3.6.3 and 3.6.5). As already reported, induced antibodies after active vaccination execute their anti-tumoral activity by effector functions including CDC and ADCC [244]. As expected, the induced immune response upon immunization with non-adjuvanted or with isRNA-LPX adjuvanted HBcAg#WT-VLPs was not able to induce anti-tumoral activities in mice. Thus, the co-administration of the both, the correct immunogen and the adjuvant seems to be essential for triggering a prophylactic immune response that was able to control the tumor growth *in vivo.* In fact, non-adjuvanted recombinant protein antigens are not capable of exerting potent immune responses due to low immunogenicity [245, 246]. In addition, it was frequently reported that immunostimulatory adjuvants enhance immunity against the vaccine and contribute to shaping the immune response to the applied antigens [247]. The incapability of adjuvant alone to enhance strong anti-tumoral activity was also shown by Heidenreich *et al*. [120]. This, RNAdjuvant alone could not able to control tumor growth Strikingly, the prophylactic vaccination of isRNA-LPX adjuvant in combination with HBcAg-#H88 VLPs enhanced the humoral immune response that was capable to inhibit the growth of E0771-mmCLDN6 tumors in C57BL/6 mice (Figure 3.51). Indeed, the direct comparison of the induced humoral immune responses revealed that HBcAg-#H88 VLPs vaccination induced a more efficient CLDN6-specific antibody response in C57BL/6 than in Balb/c mice (Figure 3.43). Whether the induced CLDN6 specific antibodies influence the cytocidal effector functions is not yet known. Nevertheless, the titer of the induced CLDN6 antibodies may be attributed to the enhanced anti-tumoral efficacy.

As a conclusion, the induction of potent antigen-specific antibody responses can control tumor growth if they are able to exert cytocidal effector functions such as CDC and ADCC. However, the complete tumor control could be shown only in case of simultaneous induction of antigen-specific B and T cells.

4.5.2 Therapeutic vaccination

The therapeutic activity of vaccination with isRNA-LPX adjuvanted HBcAg-#A79 VLPs against murine CLDN6-expressing tumor cells was evaluated using established syngeneic tumor models (Figure 3.41). The therapeutic efficacy of isRNA-LPX adjuvant and HBcAg-#A79 VLPs could be demonstrated in Balb/c mice bearing syngeneic CT26-mmCLDN6 tumor cells (Figure 3.51 and Figure 3.52). However, no antitumoral activity was seen after therapeutic immunization with isRNA-LPX adjuvanted HBcAg-#H88 VLPs (Figure 3.52). The data revealed that the level of induced B cell responses owning effector function like CDC may be the key factor, which could trigger the therapeutic effect against tumor growth (Figure 3.40 and Figure 3.48). Whether NK cells are also involved should be analyzed in further detail by depletion experiments or by using other mouse strains. Thus, the NK cells could be directly activated by the TLR agonist isRNA-LPX adjuvant. Bourquin et al demonstrated the ability of formulated small isRNA to stimulate NK cells and CTLs which led to control of tumor growth in mice [248]. However, the lack of anti-tumoral efficacy after therapeutic vaccination with isRNA-LPX adjuvant and HBcAg-#WT VLPs demonstrated that NK cells are probably not involved (Figure 3.51). It needs to be emphasized that the target epitope-specific T cell responses were determined by *ex vivo* IFN-γ ELISpot and the conducted *ex vivo* analysis for characterization of T cell phenotype allowed us to uncover that our vaccine induced CLDN6 specific $CD4^+$ helper T cells (Figure 3.37). Interestingly, we found that $CD4^+$ positive T cells against the target epitope are key for initiating class switching towards generation of IgG2a antibodies [249, 250]. Thus, RNA adjuvanted HBcAg-#H88 VLPs without generating target-epitope specific $CD4^+$ T cells induced only weak B cell responses without cytocidal capacities (Figure 3.40 and Figure 3.44). As already reported, $CD4^+$ T cell help is required for the initiation of B-cell differentiation into plasma cells, isotype switching and B cell memory formation [250]. Exploiting the natural mechanism of viral defenses by inducing target specific immunity translating in a beneficial control of tumor growth is our objective by co-administrating isRNA-LPX and HBcAg-#A79 VLP, both RNA/VLP are viral origin. In fact, mAb-based cancer immunotherapies could achieve good clinical results and have entered successfully routine clinical usage [16, 30]. Only a few studies have used VLPs to trigger immune responses in particular antibodies against self-cancer antigens [251, 252]. So far, none therapeutic effect could be seen using active vaccination for inducing antibodies which are capable of binding and killing target positive cells in ADCC or CDC like manner. Critical parameters such as the type of adjuvant and immunization route improved drastically the quality of our immunogen enabling generation of antibodies with cytocidal activities such as CDC in mice. These mode of action are likely to be responsible for the in vivo generated control of the tumor growth. We noted here, that therapeutic vaccination with isRNA-LPX alone may induce a potent anti-tumoral effect in mice. However, the combination with HBcAg-#A79 VLP led to a significant better antitumoral effect (Data not shown). Thus, these same observations were made by Brignole et al. for direct tumor targeting. He revealed that liposomal delivery of CpG ODNs specifically to the tumors triggered potent anti-tumoral effects, whereas CpG ODNs alone were not able to induce such anti-tumoral responses

[253]. Targeting the spleen with immunostimulatory agents like isRNAs or CpG ODNs may be also an alternative to stimulate various immune cells such as macrophages and NK cells and accordingly to manipulate tumor microenvironment when these cells reach the tumor.

In summary, Design of chimeric VLP capable of inducing Target specific CD+4 and B cell responses and adjuvant with high immunostimulatory capacities may play the crucial role to induce therapeutic anti-cancer effect.

4.6 Conclusion and outlook

This thesis describes the development of a novel and highly immunostimulatory adjuvant based on small RNA molecules that is applicable for i.v.application route and referred to as isRNA-LPX. The adjuvant combined a small RNA sequence, called NP71-Seq45 with a defined primary and secondary structure derived from Influenza A NP encoding RNA by using an iterative fragmentation strategy and cationic liposomes F12. The *in vitro* and *in vivo* analysis of isRNA-LPX adjuvant revealed the high TLR7 specificity and a rationally designed cytokine induction profile (high IFN-α and low TNF-α) promoting a Th1-like immune response.
Systemic administration of isRNA-LPX adjuvant was safe and well- tolerated in mice inducing no signs of harmful side effects or splenomegaly. When combined with a suitable protein antigen it was able to bridge the innate and adaptive immunity followed by a potent induction of antigen-specific humoral and cellular immune responses. Using chimeric HBcAg-CLDN6 VLPs as model antigens, we could demonstrate that the newly designed isRNA-LPX adjuvant strongly enhanced titers of antibodies specifically recognizing the native CLDN6 protein on the surface of living cells. Furthermore, the induced CLDN6 antibodies were able to efficiently trigger killing of target positive cells *in vitro* by complement-dependent cytotoxicity (CDC). Depending on the used HBcAg-CLDN6 VLPs, only the isRNA-LPX adjuvant was capable of provoking target-epitope specific CD4 +T cell responses, as determined by *ex vivo* IFN-γ ELISpot.
Complete immune protection against s.c. or i.v. challenge with syngeneic tumor cells could be achieved only by prophylactic vaccination with isRNA-LPX adjuvanted HBcAg-#A79 VLPs in Balb/c mice indicating the strong effect of the induced CLDN6 specific B response. The induced specific #79 epitope CD4+ cells seem to be essential to obtain such type of the induced B cell responses. To confirm these observations, the depletion of B cells before starting prophylactic vaccination using mAbs such as anti-mmCD20 antibodies [138] or anti-CD4 mAbs [138] should be performed in future experiments. Furthermore, we also demonstrated that the prophylactic immunization of tumor-bearing C57BL/6 mice with isRNA-LPX adjuvanted HBcAg-#A79 VLPs led to a highly significant, partial tumor rejection (Figure 3.50). Whether the isRNA-LPX adjuvanted HBcAg-#A79 VLPs vaccine could induce target-specific T cells and B cells (Figure 3.44, Table 3.3) in C57BL/6 has to be determined. Furthermore, the anti-tumoral activity of of isRNA-LPX adjuvanted HBcAg-#A101 VLPs, a

vaccine construct designed at the end of this thesis, should be further investigated. In addition, several points are of outstanding interest for future studies.

First, improvement of anti-tumoral effects of isRNA-LPX and HBcAg-#CLDN6 VLPs in combination with immune checkpoint inhibitors or IL2 cytokine. It is well known that checkpoint inhibition emerges as one of the most successful approaches in cancer immune therapy [254, 255]. Indeed, Lemke *et al*. showed that intratumoral injection of CMP-001 VLPs containing a novel CpG and anti-PD-1 could increase the indcution of a tumor-specific T cell response that can be maintained by anti-PD-1 therapy [256]. Furthemore, IL2 shows to improve the antitumoral effects of mAbs such as anti-EGFR Cetuximab in Advanced colorectal cancers by augmenting theeffector function ADCC [257]. Thus, combination IL2 and isRNA/VLP schould evaluate in preclinical studies using mouse strain.

Second, insertion of T cell epitopes at the C-Terminus of HBcAg to induce potent cellular immunity and accordingly to improve the anti-tumoral activity. Indeed, the C-terminal insertion assures potent induction of T cells as already mentioned elsewhere [216].

Third, optimisation of local application of isRNA-LPX adjuvant varying formulation types and conditions. As already mentioned, the positive charged cationic nanoparticles were better in enhancing innate immunity than the negative charged cationic nanoparticles [122]. Subsequently, another carrier could be tested with our lead isRNA NP71-Seq45 such as in vivo–jetPEI [258] or cationically modified poly(D, L-lactide-co-glycolide) (PLGA) [259].

Our proposed approach using HBcAg-VLPs as antigen and isRNA-LPX as an adjuvant for therapeutic and prophylactic vaccination was illustrated in Figure 4.4.

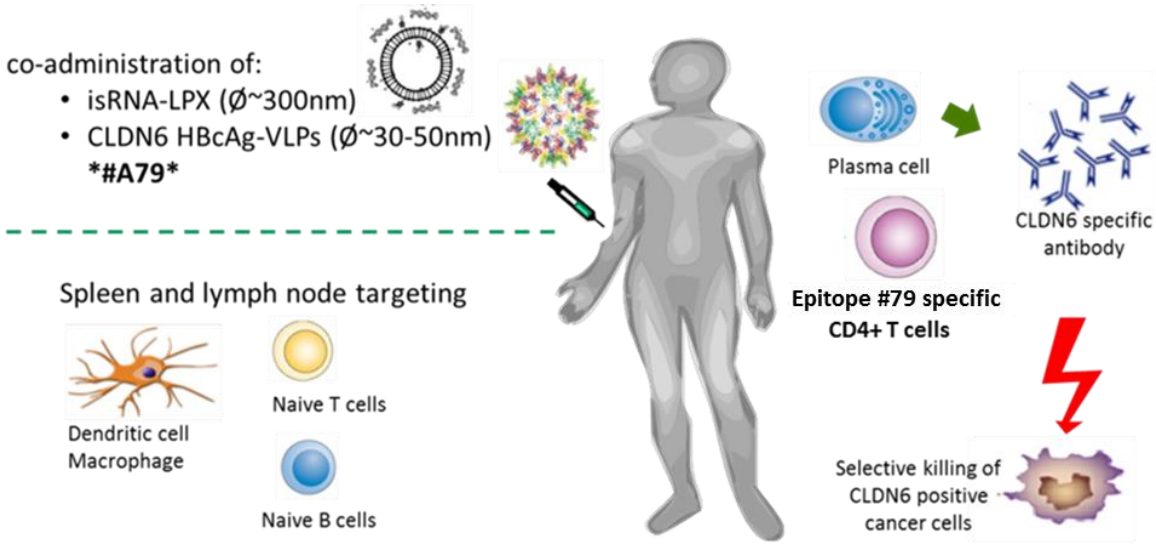

Figure 4.4: The whole overview of the designed vaccine strategy. The i.v. co-administration of the defined isRNA-LPX adjuvant and HBcAg-VLPs which carried a CLDN6 epitope (#A79 as an example)

In this thesis, it was shown that the delivering of isRNA-LPX adjuvant and chimeric HBcAg-CLDN6 VLPs in separate nanoparticles enhance effective antitumoral activities in two different tumor models. These encouraging results laid the foundation for further preclinical

studies and accordingly could be followed with a first-in-human clinical trial of active immunization with isRNA-LPX adjuvanted VLP-based vaccines for the treatment of CLDN6-positive tumor types.

5 Supplementary Information

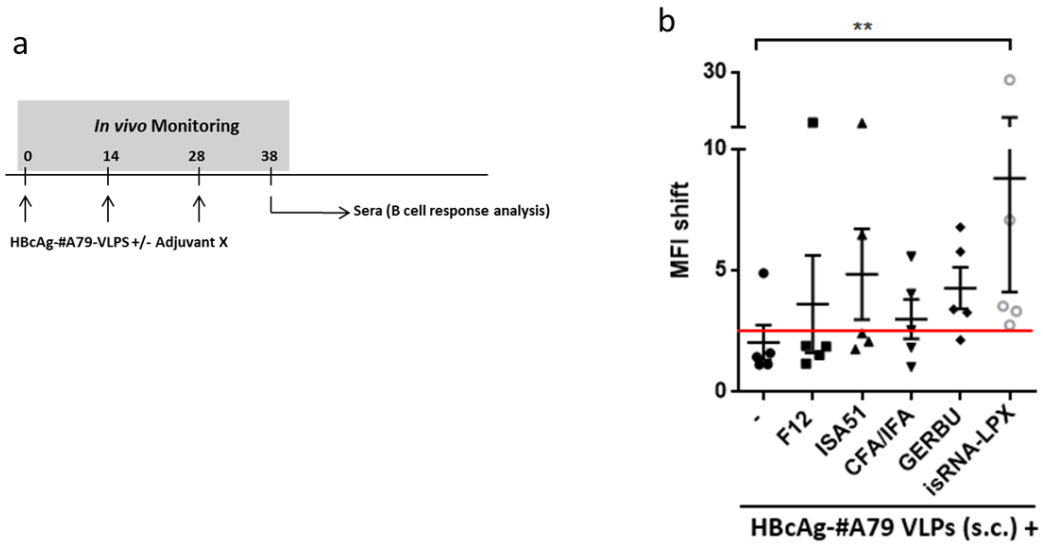

Figure 5.1: Immunostimulatory effect after local administration of isRNA-LPX. BLAB/C mice (n=5) were immunized s.c. three times at two-week intervals with HBcAg-#A79-VLPs alone, or in combination with several classes of adjuvants including isRNA-LPX. Ten days after the last immunization the sera were taken and FACS assay was applied. **b)** Immunization schedule; **C)** FACS analysis of sera using CHO-K1 cells which stably expressed and presented hs CLDN6 protein. Detection of bound antibodies was expressed as x-fold MFI-shift (Final serum vs. Pre-serum). Shown are the mean values +/- SEM. The difference between the groups were considered to be statistically significant at $p<0.05$. ns = not significant; **P<0.01.

6 References

1. Buonaguro, L., et al., *Translating tumor antigens into cancer vaccines.* Clin Vaccine Immunol, 2011. **18**(1): p. 23-34.
2. Pulendran, B. and R. Ahmed, *Immunological mechanisms of vaccination.* Nature immunology, 2011. **12**(6): p. 509-517.
3. Pulendran, B., et al., *Immunity to viruses: learning from successful human vaccines.* Immunological reviews, 2013. **255**(1): p. 243-255.
4. Srivatsan, S., et al., *Allogeneic tumor cell vaccines: the promise and limitations in clinical trials.* Human vaccines & immunotherapeutics, 2014. **10**(1): p. 52-63.
5. Li, J., et al., *Whole tumor cell vaccine with irradiated S180 cells as adjuvant.* Vaccine, 2009. **27**(4): p. 558-564.
6. Moingeon, P., *Cancer vaccines.* Vaccine, 2001. **19**(11-12): p. 1305-26.
7. Deacon, D.H., et al., *The use of gamma-irradiation and ultraviolet-irradiation in the preparation of human melanoma cells for use in autologous whole-cell vaccines.* BMC cancer, 2008. **8**(1): p. 360.
8. Guo, C., et al., *Therapeutic cancer vaccines: past, present and future.* Advances in cancer research, 2013. **119**: p. 421.
9. Reuschenbach, M., M. von Knebel Doeberitz, and N. Wentzensen, *A systematic review of humoral immune responses against tumor antigens.* Cancer immunology, immunotherapy, 2009. **58**(10): p. 1535-1544.
10. Buonaguro, L., et al., *Translating tumor antigens into cancer vaccines.* Clinical and Vaccine Immunology, 2011. **18**(1): p. 23-34.
11. Laheru, D.A. and E.M. Jaffee, *Potential role of tumor vaccines in GI malignancies.* Oncology (Williston Park), 2000. **14**(2): p. 245-56; discussion 259-60, 265.
12. Baxter, D., *Active and passive immunization for cancer.* Human vaccines & immunotherapeutics, 2014. **10**(7): p. 2123-2129.
13. Melero, I., et al., *Therapeutic vaccines for cancer: an overview of clinical trials.* Nature reviews Clinical oncology, 2014. **11**(9): p. 509-524.
14. Zarour, H.M., et al., *Tumor antigens.* Cancer Medicine, 2003. **6**: p. 196-208.
15. Cawood, R., et al., *Recombinant viral vaccines for cancer.* Trends Mol Med, 2012. **18**(9): p. 564-74.
16. Braun, M., et al., *Peptide and protein-based cancer vaccines*, in *Cancer Immunotherapy*. 2013, Springer. p. 111-146.
17. Longo, D.L., *New therapies for castration-resistant prostate cancer*. 2010, Mass Medical Soc.
18. Health, U.N.I.o., *ClinicalTrials. gov*. 2012.
19. Wong, H.H., N.R. Lemoine, and Y. Wang, *Oncolytic viruses for cancer therapy: overcoming the obstacles.* Viruses, 2010. **2**(1): p. 78-106.
20. Scanlan, E.G.M.K.C., A.H.L.B.Y. Benchek, and K.P.P.P.R. Waghmare, *Bioprocessing Technology Trends of RNA-Based Therapeutics and Vaccines.* 2016.
21. Postow, M., M.K. Callahan, and J.D. Wolchok, *Beyond cancer vaccines: a reason for future optimism with immunomodulatory therapy.* Cancer journal (Sudbury, Mass.), 2011. **17**(5): p. 372.
22. Xiao, Y.-F., et al., *Peptide-based treatment: a promising cancer therapy.* Journal of immunology research, 2015. **2015**.
23. Perrie, Y., et al., *Vaccine adjuvant systems: enhancing the efficacy of sub-unit protein antigens.* Int J Pharm, 2008. **364**(2): p. 272-80.
24. Marchand, M., et al., *Tumor regression responses in melanoma patients treated with a peptide encoded by gene MAGE-3.* Int J Cancer, 1995. **63**(6): p. 883-5.

25. Yoshitake, Y., et al., *Phase II clinical trial of multiple peptide vaccination for advanced head and neck cancer patients revealed induction of immune responses and improved OS.* Clin Cancer Res, 2015. **21**(2): p. 312-21.
26. Aruga, A., et al., *Phase I clinical trial of multiple-peptide vaccination for patients with advanced biliary tract cancer.* J Transl Med, 2014. **12**: p. 61.
27. Slingluff, C.L., Jr., *The present and future of peptide vaccines for cancer: single or multiple, long or short, alone or in combination?* Cancer J, 2011. **17**(5): p. 343-50.
28. Reche, P., et al., *Peptide-Based Immunotherapeutics and Vaccines 2015.* J Immunol Res, 2015. **2015**: p. 349049.
29. Riedmann, E.M., *Positive phase 2 results for immatics colorectal cancer vaccine.* Hum Vaccin Immunother, 2012. **8**(3): p. 282.
30. Scott, A.M., J.P. Allison, and J.D. Wolchok, *Monoclonal antibodies in cancer therapy.* Cancer Immunity Archive, 2012. **12**(1): p. 14.
31. Reichert, J.M. *Marketed therapeutic antibodies compendium*. in *MAbs*. 2012. Taylor & Francis.
32. Weiner, L.M., R. Surana, and S. Wang, *Monoclonal antibodies: versatile platforms for cancer immunotherapy.* Nature Reviews Immunology, 2010. **10**(5): p. 317-327.
33. Chames, P., et al., *Therapeutic antibodies: successes, limitations and hopes for the future.* Br J Pharmacol, 2009. **157**(2): p. 220-33.
34. Milich, D.R., et al., *Role of B cells in antigen presentation of the hepatitis B core.* Proc Natl Acad Sci U S A, 1997. **94**(26): p. 14648-53.
35. Spohn, G. and M.F. Bachmann, *Exploiting viral properties for the rational design of modern vaccines.* Expert Rev Vaccines, 2008. **7**(1): p. 43-54.
36. Klamp, T., et al., *Highly specific auto-antibodies against claudin-18 isoform 2 induced by a chimeric HBcAg virus-like particle vaccine kill tumor cells and inhibit the growth of lung metastases.* Cancer Res, 2011. **71**(2): p. 516-27.
37. Rabinovich, G.A., D. Gabrilovich, and E.M. Sotomayor, *Immunosuppressive strategies that are mediated by tumor cells.* Annu. Rev. Immunol., 2007. **25**: p. 267-296.
38. Patel, J.M., et al., *Influenza virus-like particles engineered by protein transfer with tumor-associated antigens induces protective antitumor immunity.* Biotechnol Bioeng, 2015. **112**(6): p. 1102-10.
39. Wang, J.W. and R.B. Roden, *Virus-like particles for the prevention of human papillomavirus-associated malignancies.* Expert Rev Vaccines, 2013. **12**(2): p. 129-41.
40. Chen, Q. and H. Lai, *Plant-derived virus-like particles as vaccines.* Hum Vaccin Immunother, 2013. **9**(1): p. 26-49.
41. van den Ende, C., et al., *The immunogenicity and safety of GSK's recombinant hepatitis B vaccine in adults: a systematic review of 30 years of experience.* Expert review of vaccines, 2017(just-accepted).
42. Ma, B., R. Roden, and T. Wu, *Current status of HPV vaccines.* Journal of the Formosan Medical Association= Taiwan yi zhi, 2010. **109**(7): p. 481.
43. Nascimento, I.P. and L.C. Leite, *Recombinant vaccines and the development of new vaccine strategies.* Braz J Med Biol Res, 2012. **45**(12): p. 1102-11.
44. Huang, X., et al., *Escherichia coli-derived virus-like particles in vaccine development.* npj Vaccines, 2017. **2**(1): p. 3.
45. Meireles, L.C., R.T. Marinho, and P. Van Damme, *Three decades of hepatitis B control with vaccination.* World J Hepatol, 2015. **7**(18): p. 2127-32.
46. Chu, X., et al., *Chimeric HBcAg virus-like particles presenting a HPV 16 E7 epitope significantly suppressed tumor progression through preventive or therapeutic immunization in a TC-1-grafted mouse model.* Int J Nanomedicine, 2016. **11**: p. 2417-29.
47. Wang, J.W. and R.B. Roden, *Virus-like particles for the prevention of human papillomavirus-associated malignancies.* Expert review of vaccines, 2013. **12**(2): p. 129-141.

48. Ruedl, C., et al., *Virus-like particles as carriers for T-cell epitopes: limited inhibition of T-cell priming by carrier-specific antibodies.* J Virol, 2005. **79**(2): p. 717-24.
49. Newman, M., et al., *Stability and morphology comparisons of self-assembled virus-like particles from wild-type and mutant human hepatitis B virus capsid proteins.* J Virol, 2003. **77**(24): p. 12950-60.
50. Crowther, R.A., et al., *Three-dimensional structure of hepatitis B virus core particles determined by electron cryomicroscopy.* Cell, 1994. **77**(6): p. 943-50.
51. Zheng, X. and P.C. Bevilacqua, *Activation of the protein kinase PKR by short double-stranded RNAs with single-stranded tails.* RNA, 2004. **10**(12): p. 1934-45.
52. Wynne, S.A., R.A. Crowther, and A.G. Leslie, *The crystal structure of the human hepatitis B virus capsid.* Mol Cell, 1999. **3**(6): p. 771-80.
53. Zhang, Z., et al., *Structural Analysis Reveals that Toll-like Receptor 7 Is a Dual Receptor for Guanosine and Single-Stranded RNA.* Immunity, 2016. **45**(4): p. 737-748.
54. Newman, M., et al., *Stability and morphology comparisons of self-assembled virus-like particles from wild-type and mutant human hepatitis B virus capsid proteins.* Journal of virology, 2003. **77**(24): p. 12950-12960.
55. Arora, U., et al., *Chimeric Hepatitis B core antigen virus-like particles displaying the envelope domain III of dengue virus type 2.* J Nanobiotechnology, 2012. **10**: p. 30.
56. Kratz, P.A., B. Bottcher, and M. Nassal, *Native display of complete foreign protein domains on the surface of hepatitis B virus capsids.* Proc Natl Acad Sci U S A, 1999. **96**(5): p. 1915-20.
57. McGonigle, R., et al., *An N-terminal extension to the hepatitis B virus core protein forms a poorly ordered trimeric spike in assembled virus-like particles.* J Struct Biol, 2015. **189**(2): p. 73-80.
58. Pumpens, P. and E. Grens, *HBV core particles as a carrier for B cell/T cell epitopes.* Intervirology, 2001. **44**(2-3): p. 98-114.
59. Dishlers, A., et al., *The Hepatitis B Virus Core Variants that Expose Foreign C-Terminal Insertions on the Outer Surface of Virus-Like Particles.* Mol Biotechnol, 2015. **57**(11-12): p. 1038-49.
60. Milich, D.R. and A. McLachlan, *The nucleocapsid of hepatitis B virus is both a T-cell-independent and a T-cell-dependent antigen.* Science, 1986. **234**(4782): p. 1398-401.
61. Stadler, C.R., et al., *Characterization of the first-in-class T-cell-engaging bispecific single-chain antibody for targeted immunotherapy of solid tumors expressing the oncofetal protein claudin 6.* Oncoimmunology, 2016. **5**(3): p. e1091555.
62. Micke, P., et al., *Aberrantly activated claudin 6 and 18.2 as potential therapy targets in non-small-cell lung cancer.* Int J Cancer, 2014. **135**(9): p. 2206-14.
63. Stadler, C.R., et al., *Elimination of large tumors in mice by mRNA-encoded bispecific antibodies.* Nat Med, 2017.
64. Bose, C.K. and A. Mukhopadhyay, *Claudin and ovarian cancer.* Journal of the Turkish German Gynecological Association, 2010. **11**(1): p. 48.
65. Shin, K., V.C. Fogg, and B. Margolis, *Tight junctions and cell polarity.* Annu. Rev. Cell Dev. Biol., 2006. **22**: p. 207-235.
66. Ding, L., et al., *The claudin family of proteins in human malignancy: a clinical perspective.* Cancer Manag Res, 2013. **5**(8): p. 367-375.
67. Günzel, D. and S. Alan, *Claudins and the modulation of tight junction permeability.* Physiological reviews, 2013. **93**(2): p. 525-569.
68. Kwon, M.J., *Emerging roles of claudins in human cancer.* International journal of molecular sciences, 2013. **14**(9): p. 18148-18180.
69. Hashimoto, Y., et al., *Efficacy and safety evaluation of claudin-4-targeted antitumor therapy using a human and mouse cross-reactive monoclonal antibody.* Pharmacol Res Perspect, 2016. **4**(5): p. e00266.
70. Mrsny, R.J., et al., *A key claudin extracellular loop domain is critical for epithelial barrier integrity.* Am J Pathol, 2008. **172**(4): p. 905-15.

71. Ding, L., et al., *The claudin family of proteins in human malignancy: a clinical perspective.* Cancer Manag Res, 2013. **5**: p. 367-75.
72. Ben-David, U., N. Nudel, and N. Benvenisty, *Immunologic and chemical targeting of the tight-junction protein Claudin-6 eliminates tumorigenic human pluripotent stem cells.* Nat Commun, 2013. **4**: p. 1992.
73. Costa, R.H., V.V. Kalinichenko, and L. Lim, *Transcription factors in mouse lung development and function.* Am J Physiol Lung Cell Mol Physiol, 2001. **280**(5): p. L823-38.
74. Lewis, J.B., et al., *Up-Regulation of Claudin-6 in the Distal Lung Impacts Secondhand Smoke-Induced Inflammation.* Int J Environ Res Public Health, 2016. **13**(10).
75. Jimenez, F.R., et al., *Developmental lung expression and transcriptional regulation of claudin-6 by TTF-1, Gata-6, and FoxA2.* Respir Res, 2014. **15**: p. 70.
76. Milich, D.R., et al., *Comparative immunogenicity of hepatitis B virus core and E antigens.* J Immunol, 1988. **141**(10): p. 3617-24.
77. Buchmann, P., et al., *A novel therapeutic hepatitis B vaccine induces cellular and humoral immune responses and breaks tolerance in hepatitis B virus (HBV) transgenic mice.* Vaccine, 2013. **31**(8): p. 1197-203.
78. Modlin, R.L., *Innate immunity: ignored for decades, but not forgotten.* J Invest Dermatol, 2012. **132**(3 Pt 2): p. 882-6.
79. Ramon, G., *Sur l'augmentation anormale de l'antitoxine chez les chevaux producteurs de serum antidiphterique.* Bull Soc Centr Med Vet, 1925. **101**: p. 227-234.
80. Ramon, G., *Procedes pour accroitre la production des antitoxines.* Ann. Inst. Pasteur, 1926. **40**(1).
81. Freund, J. and E.L. Opie, *Sensitization and Antibody Formation with Increased Resistance to Tuberculous Infection Induced by Heat Killed Tubercle Bacilli.* J Exp Med, 1938. **68**(2): p. 273-98.
82. Reed, S.G., M.T. Orr, and C.B. Fox, *Key roles of adjuvants in modern vaccines.* Nat Med, 2013. **19**(12): p. 1597-608.
83. Mills, K.H., *TLR-dependent T cell activation in autoimmunity.* Nat Rev Immunol, 2011. **11**(12): p. 807-22.
84. Gallo, R.L. and T. Nakatsuji, *Microbial symbiosis with the innate immune defense system of the skin.* J Invest Dermatol, 2011. **131**(10): p. 1974-80.
85. Medzhitov, R., *Toll-like receptors and innate immunity.* Nat Rev Immunol, 2001. **1**(2): p. 135-45.
86. Reed, S.G., et al., *New horizons in adjuvants for vaccine development.* Trends in immunology, 2009. **30**(1): p. 23-32.
87. Lee, S. and M.T. Nguyen, *Recent advances of vaccine adjuvants for infectious diseases.* Immune Netw, 2015. **15**(2): p. 51-7.
88. Rakoff-Nahoum, S. and R. Medzhitov, *Toll-like receptors and cancer.* Nat Rev Cancer, 2009. **9**(1): p. 57-63.
89. Cervantes, J.L., et al., *TLR8: the forgotten relative revindicated.* Cell Mol Immunol, 2012. **9**(6): p. 434-8.
90. Volchenkov, R., et al., *The 2011 Nobel Prize in physiology or medicine.* Scandinavian journal of immunology, 2012. **75**(1): p. 1-4.
91. Hornung, V., et al., *Silica crystals and aluminum salts activate the NALP3 inflammasome through phagosomal destabilization.* Nat Immunol, 2008. **9**(8): p. 847-56.
92. Franchi, L. and G. Nunez, *The Nlrp3 inflammasome is critical for aluminium hydroxide-mediated IL-1beta secretion but dispensable for adjuvant activity.* Eur J Immunol, 2008. **38**(8): p. 2085-9.
93. Marichal, T., et al., *DNA released from dying host cells mediates aluminum adjuvant activity.* Nat Med, 2011. **17**(8): p. 996-1002.
94. Liang, F. and K. Lore, *Local innate immune responses in the vaccine adjuvant-injected muscle.* Clin Transl Immunology, 2016. **5**(4): p. e74.

95. Moser, C., et al., *Influenza virosomes as a combined vaccine carrier and adjuvant system for prophylactic and therapeutic immunizations.* Expert Rev Vaccines, 2007. **6**(5): p. 711-21.
96. Cusi, M.G., *Applications of influenza virosomes as a delivery system.* Hum Vaccin, 2006. **2**(1): p. 1-7.
97. Ammi, R., et al., *Poly(I:C) as cancer vaccine adjuvant: knocking on the door of medical breakthroughs.* Pharmacol Ther, 2015. **146**: p. 120-31.
98. Orr, M.T., et al., *Adjuvant formulation structure and composition are critical for the development of an effective vaccine against tuberculosis.* J Control Release, 2013. **172**(1): p. 190-200.
99. Garcon, N. and M. Van Mechelen, *Recent clinical experience with vaccines using MPL- and QS-21-containing adjuvant systems.* Expert Rev Vaccines, 2011. **10**(4): p. 471-86.
100. Leroux-Roels, I., et al., *Improved CD4(+) T cell responses to Mycobacterium tuberculosis in PPD-negative adults by M72/AS01 as compared to the M72/AS02 and Mtb72F/AS02 tuberculosis candidate vaccine formulations: a randomized trial.* Vaccine, 2013. **31**(17): p. 2196-206.
101. Lovgren Bengtsson, K., B. Morein, and A.D. Osterhaus, *ISCOM technology-based Matrix M adjuvant: success in future vaccines relies on formulation.* Expert Rev Vaccines, 2011. **10**(4): p. 401-3.
102. Bigaeva, E., et al., *Meta-Analysis on Randomized Controlled Trials of Vaccines with QS-21 or ISCOMATRIX Adjuvant: Safety and Tolerability.* PLoS One, 2016. **11**(5): p. e0154757.
103. Drane, D., et al., *Priming of CD4+ and CD8+ T cell responses using a HCV core ISCOMATRIX vaccine: a phase I study in healthy volunteers.* Hum Vaccin, 2009. **5**(3): p. 151-7.
104. Clegg, C.H., J.A. Rininger, and S.L. Baldwin, *Clinical vaccine development for H5N1 influenza.* Expert Rev Vaccines, 2013. **12**(7): p. 767-77.
105. Weiss, S.A., S. Chandra, and A.C. Pavlick, *Update on vaccines for high-risk melanoma.* Curr Treat Options Oncol, 2014. **15**(2): p. 269-80.
106. Diebold, S.S., et al., *Innate antiviral responses by means of TLR7-mediated recognition of single-stranded RNA.* Science, 2004. **303**(5663): p. 1529-31.
107. Larange, A., et al., *TLR7 and TLR8 agonists trigger different signaling pathways for human dendritic cell maturation.* J Leukoc Biol, 2009. **85**(4): p. 673-83.
108. Vollmer, J., et al., *Immune stimulation mediated by autoantigen binding sites within small nuclear RNAs involves Toll-like receptors 7 and 8.* J Exp Med, 2005. **202**(11): p. 1575-85.
109. Savarese, E., et al., *U1 small nuclear ribonucleoprotein immune complexes induce type I interferon in plasmacytoid dendritic cells through TLR7.* Blood, 2006. **107**(8): p. 3229-34.
110. Heil, F., et al., *Species-specific recognition of single-stranded RNA via toll-like receptor 7 and 8.* Science, 2004. **303**(5663): p. 1526-9.
111. Hornung, V., et al., *Sequence-specific potent induction of IFN-alpha by short interfering RNA in plasmacytoid dendritic cells through TLR7.* Nat Med, 2005. **11**(3): p. 263-70.
112. Judge, A.D., et al., *Sequence-dependent stimulation of the mammalian innate immune response by synthetic siRNA.* Nat Biotechnol, 2005. **23**(4): p. 457-62.
113. Sioud, M., *Induction of inflammatory cytokines and interferon responses by double-stranded and single-stranded siRNAs is sequence-dependent and requires endosomal localization.* J Mol Biol, 2005. **348**(5): p. 1079-90.
114. Forsbach, A., et al., *Characterization of conserved viral leader RNA sequences that stimulate innate immunity through TLRs.* Oligonucleotides, 2007. **17**(4): p. 405-17.
115. Diebold, S.S., et al., *Nucleic acid agonists for Toll-like receptor 7 are defined by the presence of uridine ribonucleotides.* Eur J Immunol, 2006. **36**(12): p. 3256-67.
116. Ablasser, A., et al., *Selection of molecular structure and delivery of RNA oligonucleotides to activate TLR7 versus TLR8 and to induce high amounts of IL-12p70 in primary human monocytes.* J Immunol, 2009. **182**(11): p. 6824-33.
117. Gantier, M.P., et al., *TLR7 is involved in sequence-specific sensing of single-stranded RNAs in human macrophages.* J Immunol, 2008. **180**(4): p. 2117-24.

118. Kranz, L.M., et al., *Systemic RNA delivery to dendritic cells exploits antiviral defence for cancer immunotherapy.* Nature, 2016. **534**(7607): p. 396-401.
119. Heidenreich, R., et al., *RNAdjuvant®, a novel, highly-potent RNA-based adjuvant, combines strong immunostimulatory capacities with a favorable safety profile.* Journal for immunotherapy of cancer, 2015. **3**(2): p. P163.
120. Heidenreich, R., et al., *A novel RNA-based adjuvant combines strong immunostimulatory capacities with a favorable safety profile.* Int J Cancer, 2015. **137**(2): p. 372-84.
121. Ziegler, A., et al., *A New RNA-Based Adjuvant Enhances Virus-Specific Vaccine Responses by Locally Triggering TLR- and RLH-Dependent Effects.* J Immunol, 2017. **198**(4): p. 1595-1605.
122. Nguyen, D.N., et al., *Lipid-derived nanoparticles for immunostimulatory RNA adjuvant delivery.* Proc Natl Acad Sci U S A, 2012. **109**(14): p. E797-803.
123. Bourquin, C., et al., *Immunostimulatory RNA oligonucleotides trigger an antigen-specific cytotoxic T-cell and IgG2a response.* Blood, 2007. **109**(7): p. 2953-60.
124. Bourquin, C., et al., *Immunostimulatory RNA oligonucleotides induce an effective antitumoral NK cell response through the TLR7.* J Immunol, 2009. **183**(10): p. 6078-86.
125. Hamm, S., et al., *Immunostimulatory RNA is a potent inducer of antigen-specific cytotoxic and humoral immune response in vivo.* Int Immunol, 2007. **19**(3): p. 297-304.
126. Rettig, L., et al., *Particle size and activation threshold: a new dimension of danger signaling.* Blood, 2010. **115**(22): p. 4533-41.
127. Barchet, W., et al., *Accessing the therapeutic potential of immunostimulatory nucleic acids.* Curr Opin Immunol, 2008. **20**(4): p. 389-95.
128. Studier, F.W., et al., *[6] Use of T7 RNA polymerase to direct expression of cloned genes.* Methods in enzymology, 1990. **185**: p. 60-89.
129. Wizemann, H. and A. Von Brunn, *Purification of E. coli-expressed HIS-tagged hepatitis B core antigen by Ni 2+-chelate affinity chromatography.* Journal of virological methods, 1999. **77**(2): p. 189-197.
130. Kuhn, A.N., et al., *Phosphorothioate cap analogs increase stability and translational efficiency of RNA vaccines in immature dendritic cells and induce superior immune responses in vivo.* Gene Ther, 2010. **17**(8): p. 961-71.
131. Saiki, R.K., et al., *Primer-directed enzymatic amplification of DNA with a thermostable DNA polymeraseScience 239, 487–91.* Google Scholar, 1988.
132. Mullis, K.B. and F.A. Faloona, *[21] Specific synthesis of DNA in vitro via a polymerase-catalyzed chain reaction.* Methods in enzymology, 1987. **155**: p. 335-350.
133. Holtkamp, S., et al., *Modification of antigen-encoding RNA increases stability, translational efficacy, and T-cell stimulatory capacity of dendritic cells.* Blood, 2006. **108**(13): p. 4009-4017.
134. Kreiter, S., et al., *Simultaneous ex vivo quantification of antigen-specific CD4+ and CD8+ T cell responses using in vitro transcribed RNA.* Cancer immunology, immunotherapy, 2007. **56**(10): p. 1577-1587.
135. Easton, L.E., Y. Shibata, and P.J. Lukavsky, *Rapid, nondenaturing RNA purification using weak anion-exchange fast performance liquid chromatography.* RNA, 2010. **16**(3): p. 647-653.
136. Strober, W., *Monitoring cell growth.* Current protocols in immunology, 2001: p. A. 3A. 1-A. 3A. 2.
137. Lin, Z., et al., *In vivo antigen-driven plasmablast enrichment in combination with antigen-specific cell sorting to facilitate the isolation of rare monoclonal antibodies from human B cells.* Nature protocols, 2014. **9**(7): p. 1563.
138. Kreiter, S., et al., *Mutant MHC class II epitopes drive therapeutic immune responses to cancer.* Nature, 2015. **520**(7549): p. 692-6.
139. Rammensee, H., et al., *SYFPEITHI: database for MHC ligands and peptide motifs.* Immunogenetics, 1999. **50**(3-4): p. 213-9.
140. Zabel, F., T.M. Kundig, and M.F. Bachmann, *Virus-induced humoral immunity: on how B cell responses are initiated.* Curr Opin Virol, 2013. **3**(3): p. 357-62.

141. Lazdina, U., et al., *Priming of cytotoxic T cell responses to exogenous hepatitis B virus core antigen is B cell dependent.* Journal of general virology, 2003. **84**(1): p. 139-146.
142. Stadler, C.R., et al., *Characterization of the first-in-class T-cell-engaging bispecific single-chain antibody for targeted immunotherapy of solid tumors expressing the oncofetal protein claudin 6.* Oncoimmunology, 2016. **5**(3): p. e1091555.
143. Micke, P., et al., *Aberrantly activated claudin 6 and 18.2 as potential therapy targets in non-small-cell lung cancer.* International journal of cancer, 2014. **135**(9): p. 2206-2214.
144. Rendón-Huerta, E., et al., *Distribution and expression pattern of claudins 6, 7, and 9 in diffuse-and intestinal-type gastric adenocarcinomas.* Journal of gastrointestinal cancer, 2010. **41**(1): p. 52-59.
145. Rammensee, H.-G., et al., *SYFPEITHI: database for MHC ligands and peptide motifs.* Immunogenetics, 1999. **50**(3-4): p. 213-219.
146. Billaud, J.N., et al., *Combinatorial approach to hepadnavirus-like particle vaccine design.* J Virol, 2005. **79**(21): p. 13656-66.
147. Herbert, W.J., *The mode of action of mineral-oil emulsion adjuvants on antibody production in mice.* Immunology, 1968. **14**(3): p. 301-18.
148. Petrovsky, N., *Novel human polysaccharide adjuvants with dual Th1 and Th2 potentiating activity.* Vaccine, 2006. **24 Suppl 2**: p. S2-26-9.
149. Browne, E.P., *Regulation of B-cell responses by Toll-like receptors.* Immunology, 2012. **136**(4): p. 370-379.
150. Imburgio, D., et al., *Studies of promoter recognition and start site selection by T7 RNA polymerase using a comprehensive collection of promoter variants.* Biochemistry, 2000. **39**(34): p. 10419-30.
151. Kochetkov, S.N., E.E. Rusakova, and V.L. Tunitskaya, *Recent studies of T7 RNA polymerase mechanism.* FEBS Lett, 1998. **440**(3): p. 264-7.
152. Easton, L.E., Y. Shibata, and P.J. Lukavsky, *Rapid, nondenaturing RNA purification using weak anion-exchange fast performance liquid chromatography.* RNA, 2010. **16**(3): p. 647-53.
153. Cazenave, C. and O.C. Uhlenbeck, *RNA template-directed RNA synthesis by T7 RNA polymerase.* Proc Natl Acad Sci U S A, 1994. **91**(15): p. 6972-6.
154. Schlee, M., et al., *Recognition of 5' triphosphate by RIG-I helicase requires short blunt double-stranded RNA as contained in panhandle of negative-strand virus.* Immunity, 2009. **31**(1): p. 25-34.
155. Hofacker, I.L., *Vienna RNA secondary structure server.* Nucleic Acids Res, 2003. **31**(13): p. 3429-31.
156. Hornung, V., et al., *RNA recognition via TLR7 and TLR8.* Handb Exp Pharmacol, 2008(183): p. 71-86.
157. Sarvestani, S.T., et al., *Inosine-mediated modulation of RNA sensing by Toll-like receptor 7 (TLR7) and TLR8.* J Virol, 2014. **88**(2): p. 799-810.
158. Bourquin, C., et al., *Systemic cancer therapy with a small molecule agonist of toll-like receptor 7 can be improved by circumventing TLR tolerance.* Cancer Res, 2011. **71**(15): p. 5123-33.
159. Broad, A., D.E. Jones, and J.A. Kirby, *Toll-like receptor (TLR) response tolerance: a key physiological "damage limitation" effect and an important potential opportunity for therapy.* Curr Med Chem, 2006. **13**(21): p. 2487-502.
160. Lappin, M. and J. Campbell, *The Th1-Th2 classification of cellular immune responses: concepts, current thinking and applications in haematological malignancy.* Blood reviews, 2000. **14**(4): p. 228-239.
161. Wu, T.Y.H., *Strategies for designing synthetic immune agonists.* Immunology, 2016. **148**(4): p. 315-325.
162. Chu, X., et al., *Chimeric HBcAg virus-like particles presenting a HPV 16 E7 epitope significantly suppressed tumor progression through preventive or therapeutic immunization in a TC-1-grafted mouse model.* International journal of nanomedicine, 2016. **11**: p. 2417.

163. Malik, I.R., et al., *A bi-functional hepatitis B virus core antigen (HBcAg) chimera activates HBcAg-specific T cells and preS1-specific antibodies.* Scandinavian journal of infectious diseases, 2012. **44**(1): p. 55-59.
164. Buonaguro, F.M., M.L. Tornesello, and L. Buonaguro, *Virus-like particle vaccines and adjuvants: the HPV paradigm.* Expert review of vaccines, 2009. **8**(10): p. 1379-1398.
165. Liu, J.K., *Anti-cancer vaccines - a one-hit wonder?* Yale J Biol Med, 2014. **87**(4): p. 481-9.
166. Lindblad, E.B., *Aluminium compounds for use in vaccines.* Immunology and cell biology, 2004. **82**(5): p. 497.
167. Heidenreich, R., et al., *A novel RNA-based adjuvant combines strong immunostimulatory capacities with a favorable safety profile.* International journal of cancer, 2015. **137**(2): p. 372-384.
168. Adams, S., *Toll-like receptor agonists in cancer therapy.* Immunotherapy, 2009. **1**(6): p. 949-964.
169. Martins, K.A., et al., *Toll-like receptor agonist augments virus-like particle-mediated protection from Ebola virus with transient immune activation.* PLoS One, 2014. **9**(2): p. e89735.
170. Lee, B.O., et al., *Interaction of the hepatitis B core antigen and the innate immune system.* The Journal of Immunology, 2009. **182**(11): p. 6670-6681.
171. Milich, D.R., et al., *Role of B cells in antigen presentation of the hepatitis B core.* Proceedings of the National Academy of Sciences, 1997. **94**(26): p. 14648-14653.
172. Ilyinskii, P.O., et al., *Adjuvant-carrying synthetic vaccine particles augment the immune response to encapsulated antigen and exhibit strong local immune activation without inducing systemic cytokine release.* Vaccine, 2014. **32**(24): p. 2882-2895.
173. Schmidt, S.T., et al., *The administration route is decisive for the ability of the vaccine adjuvant CAF09 to induce antigen-specific CD8+ T-cell responses: The immunological consequences of the biodistribution profile.* Journal of Controlled Release, 2016. **239**: p. 107-117.
174. Nielsen, J.S. and B.H. Nelson, *Tumor-infiltrating B cells and T cells: Working together to promote patient survival.* Oncoimmunology, 2012. **1**(9): p. 1623-1625.
175. Bronte, V. and M.J. Pittet, *The spleen in local and systemic regulation of immunity.* Immunity, 2013. **39**(5): p. 806-818.
176. Link, B.K., et al., *Oligodeoxynucleotide CpG 7909 delivered as intravenous infusion demonstrates immunologic modulation in patients with previously treated non-Hodgkin lymphoma.* Journal of Immunotherapy, 2006. **29**(5): p. 558-568.
177. Dudek, A.Z., et al., *First in human phase I trial of 852A, a novel systemic toll-like receptor 7 agonist, to activate innate immune responses in patients with advanced cancer.* Clinical Cancer Research, 2007. **13**(23): p. 7119-7125.
178. Dummer, R., et al., *An exploratory study of systemic administration of the toll-like receptor-7 agonist 852A in patients with refractory metastatic melanoma.* Clinical Cancer Research, 2008. **14**(3): p. 856-864.
179. Engel, A.L., G.E. Holt, and H. Lu, *The pharmacokinetics of Toll-like receptor agonists and the impact on the immune system.* Expert review of clinical pharmacology, 2011. **4**(2): p. 275-289.
180. Kranz, L.M., et al., *Systemic RNA delivery to dendritic cells exploits antiviral defence for cancer immunotherapy.* Nature, 2016. **534**(7607): p. 396.
181. Wilson, K.D., et al., *Effects of intravenous and subcutaneous administration on the pharmacokinetics, biodistribution, cellular uptake and immunostimulatory activity of CpG ODN encapsulated in liposomal nanoparticles.* International immunopharmacology, 2007. **7**(8): p. 1064-1075.
182. Lan, T., et al., *Stabilized immune modulatory RNA compounds as agonists of Toll-like receptors 7 and 8.* Proceedings of the National Academy of Sciences, 2007. **104**(34): p. 13750-13755.

183. Wilson, K.D., et al., *The combination of stabilized plasmid lipid particles and lipid nanoparticle encapsulated CpG containing oligodeoxynucleotides as a systemic genetic vaccine.* The journal of gene medicine, 2009. **11**(1): p. 14-25.
184. Mohsen, M.O., et al., *Delivering adjuvants and antigens in separate nanoparticles eliminates the need of physical linkage for effective vaccination.* Journal of Controlled Release, 2017. **251**: p. 92-100.
185. van Doorn, E., et al., *Safety and tolerability evaluation of the use of Montanide ISA51 as vaccine adjuvant: A systematic review.* Hum Vaccin Immunother, 2016. **12**(1): p. 159-69.
186. Brunner, R., E. Jensen-Jarolim, and I. Pali-Scholl, *The ABC of clinical and experimental adjuvants--a brief overview.* Immunol Lett, 2010. **128**(1): p. 29-35.
187. Asselin-Paturel, C., et al., *Mouse strain differences in plasmacytoid dendritic cell frequency and function revealed by a novel monoclonal antibody.* J Immunol, 2003. **171**(12): p. 6466-77.
188. Jarrossay, D., et al., *Specialization and complementarity in microbial molecule recognition by human myeloid and plasmacytoid dendritic cells.* Eur J Immunol, 2001. **31**(11): p. 3388-93.
189. Asami, T., et al., *Modulation of murine macrophage TLR7/8-mediated cytokine expression by mesenchymal stem cell-conditioned medium.* Mediators Inflamm, 2013. **2013**: p. 264260.
190. Zhang, Z., et al., *Structural analysis reveals that toll-like receptor 7 is a dual receptor for guanosine and single-stranded RNA.* Immunity, 2016. **45**(4): p. 737-748.
191. Shibata, T., et al., *Guanosine and its modified derivatives are endogenous ligands for TLR7.* International immunology, 2015. **28**(5): p. 211-222.
192. Liu, Z. and P.A. Roche, *Macropinocytosis in phagocytes: regulation of MHC class-II-restricted antigen presentation in dendritic cells.* Front Physiol, 2015. **6**: p. 1.
193. Weber, M. and F. Weber, *Monitoring activation of the antiviral pattern recognition receptors RIG-I and PKR by limited protease digestion and native PAGE.* J Vis Exp, 2014(89): p. e51415.
194. Anchisi, S., J. Guerra, and D. Garcin, *RIG-I ATPase activity and discrimination of self-RNA versus non-self-RNA.* MBio, 2015. **6**(2): p. e02349.
195. Goubau, D., et al., *Antiviral immunity via RIG-I-mediated recognition of RNA bearing 5'-diphosphates.* Nature, 2014. **514**(7522): p. 372-5.
196. Kolakofsky, D., E. Kowalinski, and S. Cusack, *A structure-based model of RIG-I activation.* RNA, 2012. **18**(12): p. 2118-27.
197. Luft, T., et al., *Type I IFNs enhance the terminal differentiation of dendritic cells.* The Journal of Immunology, 1998. **161**(4): p. 1947-1953.
198. Montoya, M., et al., *Type I interferons produced by dendritic cells promote their phenotypic and functional activation.* Blood, 2002. **99**(9): p. 3263-3271.
199. Braun, D., I. Caramalho, and J. Demengeot, *IFN-α/β enhances BCR-dependent B cell responses.* International immunology, 2002. **14**(4): p. 411-419.
200. Hervas-Stubbs, S., et al., *Direct effects of type I interferons on cells of the immune system.* Clinical Cancer Research, 2011. **17**(9): p. 2619-2627.
201. Giordani, L., et al., *IFN-α amplifies human naive B cell TLR-9-mediated activation and Ig production.* Journal of leukocyte biology, 2009. **86**(2): p. 261-271.
202. Le Bon, A., et al., *Cutting edge: enhancement of antibody responses through direct stimulation of B and T cells by type I IFN.* The Journal of Immunology, 2006. **176**(4): p. 2074-2078.
203. Crouse, J., U. Kalinke, and A. Oxenius, *Regulation of antiviral T cell responses by type I interferons.* Nature reviews. Immunology, 2015. **15**(4): p. 231.
204. Ray, J.P., et al., *Transcription factor STAT3 and type I interferons are corepressive insulators for differentiation of follicular helper and T helper 1 cells.* Immunity, 2014. **40**(3): p. 367-377.
205. Oestreich, K.J., S.E. Mohn, and A.S. Weinmann, *Molecular mechanisms that control the expression and activity of Bcl-6 in TH1 cells to regulate flexibility with a TFH-like gene profile.* Nature immunology, 2012. **13**(4): p. 405-411.
206. Chroboczek, J., I. Szurgot, and E. Szolajska, *Virus-like particles as vaccine.* Acta Biochim Pol, 2014. **61**(3): p. 531-9.

207. Monie, A., et al., *Cervarix™: a vaccine for the prevention of HPV 16, 18-associated cervical cancer.* Biologics: targets & therapy, 2008. **2**(1): p. 107.
208. Hung, C.-F., et al., *Therapeutic human papillomavirus vaccines: current clinical trials and future directions.* Expert opinion on biological therapy, 2008. **8**(4): p. 421-439.
209. Pontén, F., K. Jirström, and M. Uhlen, *The Human Protein Atlas—a tool for pathology.* The Journal of pathology, 2008. **216**(4): p. 387-393.
210. Karpenko, L., et al., *Insertion of foreign epitopes in HBcAg: how to make the chimeric particle assemble.* Amino acids, 2000. **18**(4): p. 329-337.
211. Crowther, R., et al., *Three dimensional reconstructions of spherical viruses by Fourier synthesis from electron micrographs.* Nature, 1970. **226**(5244): p. 421-425.
212. Fuller, S., et al., *Three-dimensional reconstruction of icosahedral particles—the uncommon line.* Journal of structural biology, 1996. **116**(1): p. 48-55.
213. Lachmann, S., et al., *Characterization of Potential Insertion Sites in the Core Antigen of Hepatitis B Virus by the Use of a Short-Sized Model Epitope1.* Intervirology, 1999. **42**(1): p. 51-56.
214. Schödel, F., et al., *The position of heterologous epitopes inserted in hepatitis B virus core particles determines their immunogenicity.* Journal of virology, 1992. **66**(1): p. 106-114.
215. Schodel, F., et al., *The position of heterologous epitopes inserted in hepatitis B virus core particles determines their immunogenicity.* J Virol, 1992. **66**(1): p. 106-14.
216. Storni, T., et al., *Critical role for activation of antigen-presenting cells in priming of cytotoxic T cell responses after vaccination with virus-like particles.* J Immunol, 2002. **168**(6): p. 2880-6.
217. Billaud, J.-N., et al., *Combinatorial approach to hepadnavirus-like particle vaccine design.* Journal of virology, 2005. **79**(21): p. 13656-13666.
218. Roseman, A., et al., *Structures of hepatitis B virus cores presenting a model epitope and their complexes with antibodies.* Journal of molecular biology, 2012. **423**(1): p. 63-78.
219. Borisova, G., et al., *Behavior of a short preS1 epitope on the surface of hepatitis B core particles.* Biological chemistry, 1999. **380**(3): p. 315-324.
220. Borisova, G., et al., *Spatial structure and insertion capacity of immunodominant region of hepatitis B core antigen.* Intervirology, 1996. **39**(1-2): p. 16-22.
221. Ruedl, C., et al., *Virus-like particles as carriers for T-cell epitopes: limited inhibition of T-cell priming by carrier-specific antibodies.* Journal of virology, 2005. **79**(2): p. 717-724.
222. Slansky, J.E., et al., *Enhanced antigen-specific antitumor immunity with altered peptide ligands that stabilize the MHC-peptide-TCR complex.* Immunity, 2000. **13**(4): p. 529-38.
223. Brentville, V.A., et al., *Citrullinated Vimentin Presented on MHC-II in Tumor Cells Is a Target for CD4+ T-Cell–Mediated Antitumor Immunity.* Cancer research, 2015.
224. Diken, M., et al., *Discovery and Subtyping of Neo-Epitope Specific T-Cell Responses for Cancer Immunotherapy: Addressing the Mutanome.* Methods Mol Biol, 2017. **1499**: p. 223-236.
225. Vidarsson, G., G. Dekkers, and T. Rispens, *IgG subclasses and allotypes: from structure to effector functions.* Front Immunol, 2014. **5**: p. 520.
226. Imai, K. and A. Takaoka, *Comparing antibody and small-molecule therapies for cancer.* Nat Rev Cancer, 2006. **6**(9): p. 714-27.
227. Ey, P., G. Russell-Jones, and C. Jenkin, *Isotypes of mouse IgG—I. Evidence for 'non-complement-fixing'IgG1 antibodies and characterization of their capacity to interfere with IgG2, sensitization of target red blood cells for lysis by complement.* Molecular immunology, 1980. **17**(6): p. 699-710.
228. Germann, T., et al., *Interleukin-12 profoundly up-regulates the synthesis of antigen-specific complement-fixing IgG2a, IgG2b and IgG3 antibody subclasses in vivo.* European journal of immunology, 1995. **25**(3): p. 823-829.
229. Dvorak, A.M. and H.F. Dvorak, *Structure of Freund's complete and incomplete adjuvants. Relation of adjuvanticity to structure.* Immunology, 1974. **27**(1): p. 99-114.
230. Shibaki, A. and S.I. Katz, *Induction of skewed Th1/Th2 T-cell differentiation via subcutaneous immunization with Freund's adjuvant.* Exp Dermatol, 2002. **11**(2): p. 126-34.

231. Yip, H.C., et al., *Adjuvant-guided type-1 and type-2 immunity: infectious/noninfectious dichotomy defines the class of response.* J Immunol, 1999. **162**(7): p. 3942-9.
232. Griggs, J. and K. Zinkewich-Peotti, *The state of the art: immune-mediated mechanisms of monoclonal antibodies in cancer therapy.* Br J Cancer, 2009. **101**(11): p. 1807-12.
233. Galabova, G., et al., *Peptide-based anti-PCSK9 vaccines - an approach for long-term LDLc management.* PLoS One, 2014. **9**(12): p. e114469.
234. Awate, S., L.A. Babiuk, and G. Mutwiri, *Mechanisms of action of adjuvants.* Frontiers in immunology, 2013. **4**.
235. Brewer, J.M., et al., *Aluminium hydroxide adjuvant initiates strong antigen-specific Th2 responses in the absence of IL-4-or IL-13-mediated signaling.* The Journal of Immunology, 1999. **163**(12): p. 6448-6454.
236. Bungener, L., et al., *Alum boosts TH2-type antibody responses to whole-inactivated virus influenza vaccine in mice but does not confer superior protection.* Vaccine, 2008. **26**(19): p. 2350-2359.
237. Malyala, P., D.T. O'Hagan, and M. Singh, *Enhancing the therapeutic efficacy of CpG oligonucleotides using biodegradable microparticles.* Advanced drug delivery reviews, 2009. **61**(3): p. 218-225.
238. Wilson, K.D., S.D. de Jong, and Y.K. Tam, *Lipid-based delivery of CpG oligonucleotides enhances immunotherapeutic efficacy.* Advanced drug delivery reviews, 2009. **61**(3): p. 233-242.
239. Mosmann, T.R., et al., *Two types of murine helper T cell clone. I. Definition according to profiles of lymphokine activities and secreted proteins.* The Journal of immunology, 1986. **136**(7): p. 2348-2357.
240. Nishimura, T., et al., *Distinct role of antigen-specific T helper type 1 (Th1) and Th2 cells in tumor eradication in vivo.* Journal of Experimental Medicine, 1999. **190**(5): p. 617-628.
241. Mosmann, T.R. and S. Sad, *The expanding universe of T-cell subsets: Th1, Th2 and more.* Immunology today, 1996. **17**(3): p. 138-146.
242. Pages, F., et al., *Immune infiltration in human tumors: a prognostic factor that should not be ignored.* Oncogene, 2010. **29**(8): p. 1093.
243. Nelson, B.H., *CD20+ B cells: the other tumor-infiltrating lymphocytes.* The Journal of Immunology, 2010. **185**(9): p. 4977-4982.
244. Clay, T.M., et al., *Polyclonal immune responses to antigens associated with cancer signaling pathways and new strategies to enhance cancer vaccines.* Immunologic research, 2011. **49**(1-3): p. 235-247.
245. Clausi, A.L., et al., *Influence of protein conformation and adjuvant aggregation on the effectiveness of aluminum hydroxide adjuvant in a model alkaline phosphatase vaccine.* Journal of pharmaceutical sciences, 2009. **98**(1): p. 114-121.
246. Nascimento, I. and L. Leite, *Recombinant vaccines and the development of new vaccine strategies.* Brazilian Journal of Medical and Biological Research, 2012. **45**(12): p. 1102-1111.
247. Carter, D. and S.G. Reed, *Role of adjuvants in modeling the immune response.* Current Opinion in HIV and AIDS, 2010. **5**(5): p. 409.
248. Bourquin, C., et al., *Immunostimulatory RNA oligonucleotides induce an effective antitumoral NK cell response through the TLR7.* The Journal of Immunology, 2009. **183**(10): p. 6078-6086.
249. Stavnezer, J., *Immunoglobulin class switching.* Current opinion in immunology, 1996. **8**(2): p. 199-205.
250. Braun, M., et al., *Virus-like particles induce robust human T-helper cell responses.* European journal of immunology, 2012. **42**(2): p. 330-340.
251. Dorn, D.C., et al., *Cellular and humoral immunogenicity of hamster polyomavirus-derived virus-like particles harboring a mucin 1 cytotoxic T-cell epitope.* Viral immunology, 2008. **21**(1): p. 12-26.
252. Kong, J., et al., *Anti-tumor effects of immunotherapeutic peptide on the treatment of hepatocellular carcinoma with HBc carrier.* Oncology reports, 2007. **18**(1): p. 279-285.

253. Temizoz, B., E. Kuroda, and K.J. Ishii, *Vaccine adjuvants as potential cancer immunotherapeutics.* International immunology, 2016. **28**(7): p. 329-338.
254. Couzin-Frankel, J., *Cancer immunotherapy*. 2013, American Association for the Advancement of Science.
255. Alsaab, H.O., et al., *PD-1 and PD-L1 Checkpoint Signaling Inhibition for Cancer Immunotherapy: Mechanism, Combinations, and Clinical Outcome.* Frontiers in Pharmacology, 2017. **8**.
256. Lemke, C.D., et al., *Combination Lymphoma Immunotherapy Using Checkpoint Blockade and Intratumoral Virus-like Particles Containing CpG TLR9 Agonist*. 2016, Am Soc Hematology.
257. Hara, M., et al., *Interleukin-2 potentiation of cetuximab antitumor activity for epidermal growth factor receptor-overexpressing gastric cancer xenografts through antibody-dependent cellular cytotoxicity.* Cancer science, 2008. **99**(7): p. 1471-1478.
258. Poeck, H., et al., *5'-Triphosphate-siRNA: turning gene silencing and Rig-I activation against melanoma.* Nature medicine, 2008. **14**(11): p. 1256-1263.
259. Nafee, N., et al., *Chitosan-coated PLGA nanoparticles for DNA/RNA delivery: effect of the formulation parameters on complexation and transfection of antisense oligonucleotides.* Nanomedicine: Nanotechnology, Biology and Medicine, 2007. **3**(3): p. 173-183.